Light-Activated Antimicrobial Polymers For Healthcare Applications

This thesis is submitted in partial fulfilment of the requirements for the Degree of Doctor of Engineering (Chemistry)

SACHA M. NOIMARK

2015

Supervised by: Professor Ivan P. Parkin, Dr Elaine Allan and Professor Christopher W. M. Kay

DECLARATION

I, Sacha Noimark confirm that the work presented in this thesis is my own. Where information has been derived from other sources, I confirm that this has been indicated in the thesis.

ABSTRACT

This thesis details the development of potent light-activated antimicrobial silicone polymers for use in healthcare environments. Upon illumination, these polymers induce the lethal photosensitisation of bacteria through the generation of a range of reactive oxygen species at the polymer surface, initiating a non-site specific attack against bacteria in the vicinity. Activation of the antimicrobial technology developed was achieved using laser illumination (635 nm) and UVA illumination for medical device applications, or white hospital lighting conditions for hospital touch surface applications. Moreover, for the first time, some photobactericidal materials developed also demonstrated strong antimicrobial activity through an additional dark-activated mechanism.

Antimicrobial polymers were developed through use of a swell-encapsulation-shrink strategy to incorporate photosensitiser dyes such as methylene blue and crystal violet, in addition to a range of nanoparticles including 2 nm gold nanoparticles, zinc oxide nanoparticles and titania nanoparticles, into medical grade silicone. Specifically, the photobactericidal silicone polymer systems detailed in this thesis are: (i) crystal violet-coated, methylene blue and 2 nm gold nanoparticle-encapsulated silicone for both medical device and hospital touch surface applications, (ii) crystal violet-coated, zinc oxide nanoparticle-encapsulated silicone for hospital touch surface applications and (iii) oleic acid-functionalised titania or gold-doped titania nanoparticle-encapsulated silicone for medical device or hospital touch surface applications (in combination with a suitable light delivery system).

The materials were characterised using techniques including: light microscopy, fluorescence microscopy, transmission electron microscopy, UV-Vis absorbance spectroscopy, X-ray photoelectron spectroscopy, time-resolved electron paramagnetic resonance spectroscopy and

time-resolved detection of near infrared singlet oxygen phosphorescence (~ 1270 nm). Functional testing indicated that these materials were suitable for targeted applications and demonstrated strong material photostability and dye-polymer stability under aqueous conditions. The polymers demonstrated strong light-activated antimicrobial activity when tested against key Gram-positive and Gram-negative bacteria associated with hospital-acquired infections including *Staphylococcus aureus*, *Staphylococcus epidermidis* and *Escherichia coli*, with > 4 log reductions in viable bacterial numbers observed. Significant antimicrobial activity was also noted under dark conditions. It is anticipated that the potent antimicrobial technology detailed in this thesis could ultimately be used in both medical device and hospital touch surface applications, to reduce bacterial surface colonisation and the associated incidence of hospital-acquired infections.

ACKNOWLEDGMENTS

Firstly, I would like to thank my primary supervisor, Professor Ivan Parkin, for all his advice, support, encouragement and inspiration over the years. I would also like to thank my secondary supervisor, Dr Elaine Allan, for her help and invaluable expertise in Microbiology and my tertiary supervisor, Professor Christopher Kay (UCL EPR), for his EPR expertise, guidance and enthusiasm and for his patience in teaching me how to use MATLAB! I would also like to take this opportunity to thank Professor Michael Wilson, my secondary supervisor in my first year of Doctoral Research, for introducing me to the field of Microbiology and for providing me with a strong foundation for future work in this area.

Over the course of my doctorate, I have had the opportunity to work with many people covering a range of academic disciplines. First and foremost, I would like to thank everyone on the 'MRC Catheter Project Team'. Without their diverse range of expertise, I could not have achieved such an inter-disciplinary project. In particular, I would like to thank Professor Sandy MacRobert, Dr Sandy Mosse, Dr Melissa Bovis and Dr Josephine Woodhams at the National Medical Laser Centre for their collaboration, excellent help and continual support over the course of my research. My thanks also goes to Dr Enrico Salvadori (UCL EPR) for his EPR expertise, spectrometer tuning and MATLAB tutorials!

I would also like to thank all my colleagues at the Eastman Dental Institute who have helped and supported me over the years. In particular, I would like to thank Annapaula Correia who gave me a crash course in microbiology, showed me countless useful tricks and kept me company during countless hours of plating up bacteria!

UCL Chemistry has been an incredible and enjoyable environment to work in, and in this friendly, collaborative atmosphere, my research

has flourished. I would like to extend my thanks to the Parkin and Carmalt groups and other colleagues at UCL Chemistry for their help, friendship and support. In particular I would like extend a massive thank you to: Will (nanoparticle synthesis and TEM), Nuru (XPS), Joe (nanoparticle functionalisation), Raul and Carlos (photocatalysis) for all their technical expertise and advice in my project.

I would like to extend a special thank you to a close friend and collaborator, Jonathan Weiner (Imperial College London). I still can't believe it, our crazy idea worked! Thank you for all your help over the years, access to Imperial equipment - including the Titan(!) - and for putting up with me and my countless emails whilst we wrote that paper! I would also like to thank Matthew Allinson (Imperial College London) for his help in running the ICP-OES experiments for us.

Thank you to all my friends, for being there for me throughout and keeping me sane when work piled up! In particular, Jonathan Hoyland, thank you so much for helping me format my thesis in LaTeX- I apologise for crazy code and disorganised labeling systems!

Last but by no means least, I would like to thank my Mum, Dad, Nan, brothers and sister-in-laws for their love and support and for putting up with me over the years! I would especially like to thank my Mum, Gaby and Joel for being my 'presentation practice crew' - I honestly don't know how I would've got through them without you - and my oldest brothers Dr Lee and Dr Dean for their profound patience, despite my millions of questions, and for their help in explaining the more medical aspects of my project.

PUBLICATIONS

List of publications associated with this thesis:

[1] **S. Noimark**, C. W. Dunnill and I. P. Parkin. Shining light on materials - a self-sterilising revolution, *Advanced Drug Delivery Reviews*, **2013**, 65, 570 - 580.

[2] **S. Noimark**, M. Bovis, A. J. MacRobert, A. Correia, E. Allan, M. Wilson and I. P. Parkin. Photobactericidal polymers; the incorporation of crystal violet and nanogold into medical grade silicone, *RSC Advances*, **2013**, 3, 18383 - 18394.

[3] **S. Noimark**, E. Allan and I. P. Parkin. Light-activated antimicrobial surfaces with enhanced efficacy induced by a dark-activated mechanism, *Chemical Science*, **2014**, 5, 2216 - 2223.

[4] **S. Noimark**, J. Weiner, N. Noor, E. Allan, C. K. Williams, M. S. P. Shaffer and I. P. Parkin. Dual mechanism antimicrobial polymer - ZnO nanoparticle and crystal violet encapsulated silicone, *Advanced Functional Materials*, **2015**, 25, 1367 - 1373.

[5] **S. Noimark**, K. Page, J. C. Bear, C. Sotelo-Vazquez, R. Quesada-Cabrera, Y. Lu, E. Allan, J. A. Darr and I. P. Parkin. Functionalised gold and titania nanoparticles and surfaces for use as antimicrobial coatings, *Faraday Discussions*, **2014**, 175, 273 - 287.

[6] **S. Noimark**, E. Salvadori, R. Gomez-Bombarelli, A. J. MacRobert, C. W. M. Kay and I. P. Parkin. Photoexcitation of phenothiazine and triarylmethane photosensitiser dyes, **2015**, (Manuscript in Preparation).

CONTENTS

LIST OF FIGURES

LIST OF TABLES

LIST OF ABBREVIATIONS

Attenuated total reflectance-Fourier transform infrared	ATR-FTIR
Brain-Heart-Infusion	BHI
Charge-coupled device	CCD
Centers for Disease Control and Prevention	CDC
Continuous hydrothermal flow synthesis	CHFS
Di(octyl)phosphinic acid	DOPA-H
Food and Drug Administration	FDA
Hospital-acquired infection	HAI
High resolution-transmission electron microscope	HR-TEM
Inductively coupled plasma-optical emission spectroscopy	ICP-OES
Intensive care unit	ICU
MacConkey agar	MAC
Methicillin resistant-Staphylococcus aureus	MRSA
Mannitol salt agar	MSA
Phosphate buffer saline	PBS
Photodynamic therapy	PDT
Reactive oxygen species	ROS
Room temperature	RT
Singlet oxygen	$^1O_2$
Transmission electron microscope	TEM
Tetrahydrofuran	THF
Time-resolved electron paramagnetic resonance	TR-EPR
Time-resolved near infrared	TRNIR
Urinary tract infection	UTI
Ultraviolet	UV
Ultraviolet-Visible	UV-Vis
X-ray photoelectron spectroscopy	XPS
X-ray diffraction	XRD
Zero-field splitting	ZFS

1

HOSPITAL-ACQUIRED INFECTIONS; STRATEGIES TO REDUCE CATHETER-RELATED INFECTIONS

1.1 INTRODUCTORY REMARKS

This thesis is focused on the development of light-activated antimicrobial polymers for use in medical device and hospital touch surface applications, as a strategy to decrease the incidence of hospital-acquired infections (HAIs). This literature review chapter details the origins of HAIs, the ongoing issue of the emergence of bacterial drug-resistance and infection prevention measures adopted to decrease the prevalence of these infections. This chapter specifically focuses on catheter-related infections and provides an extensive review on current strategies to decrease the incidence of these infections, including the use of antimicrobial locks and flushes, antimicrobial wound dressings and anti-infective catheter devices. The effectiveness of each of these approaches is evaluated and compared and ultimately, this chapter highlights the need for the development of new, more effective infection-prevention strategies. Research detailed in this thesis showcases the development of potent laser-activated photobactericidal polymers for medical device applications, as a strategy to address these issues and reduce the risk of device-related infections. Further work explores how this novel antimicrobial technology can also achieve the lethal photosensitisation of bacteria using white hospital illumination to activate the antimicrobial properties of these materials, for applications in hospital touch surfaces. It is hoped that this surface technology can be used to decrease bacterial surface colonisation in healthcare environments and reduce the incidence of associated infections.

HAIs have been noted as one of the 'major complications' in modern medical treatment and many of these infections are associated with the increased use of invasive medical devices, or inappropriate use of antimicrobial treatments [1]. As exampled in Figure 1 [2], HAIs range from septicaemia to respiratory tract infections and these infections are commonly linked to bacterial colonisation of surfaces of devices commonly used in medical practice, such as indwelling catheters, intravenous cannulas and endotracheal tubing [3–5]. In fact, key HAIs include central line-associated bloodstream infections, catheter-associated urinary tract infections, ventilator-associated pneumonia, in addition to surgical site infections [1, 5]. These infections not only present a taxing financial and resource burden on healthcare institutions, but result in extensive hospitalisation durations, patient discomfort and in some cases, mortality [3, 4, 6].

Educational programmes, hygiene training, antibiotic prophylaxis and implant surface modifications and coatings are just a few examples of strategies adopted to help decrease the risk of infection, however, the incidence of these infections is still significant [4, 7, 8]. Consequently, there remains a need to increase the stringency to which infection-prevention regimes are followed and to introduce

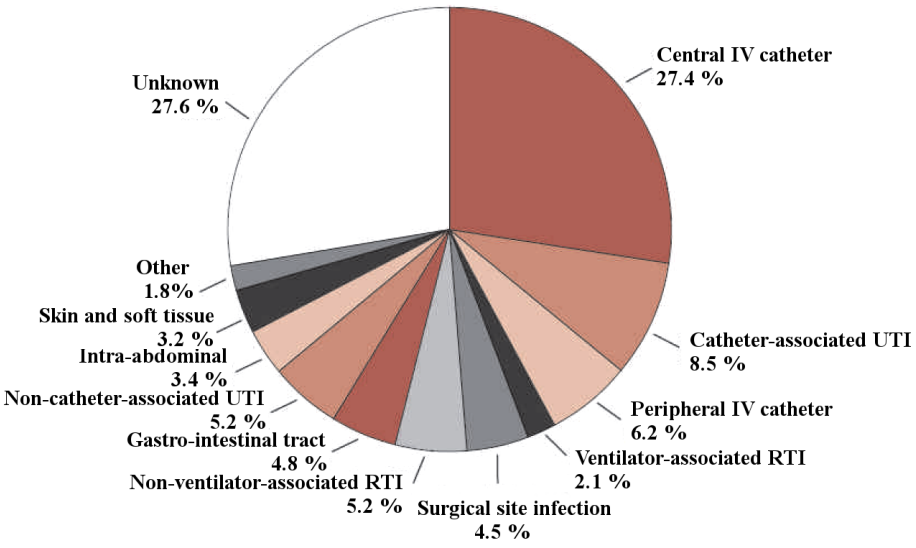

Figure 1: Probable source of hospital-acquired bacteraemia [2]

new, more potent antimicrobial approaches. This chapter explores and evaluates the current prevalence of hospital-infection attributed to the use of catheters, with a particular focus on intravascular devices including peripheral intravenous-devices (such as cannulae) and central-lines and assesses the efficacy of infection-control strategies that have been adopted in medical institutions.

1.2.1 *The escalating burden of bacterial drug-resistance*

The use of antimicrobial agents to combat bacterial infections was developed *ca.* 65 years ago [9]. However, soon after the widespread introduction of antibiotics as a means of managing and treating bacterial infections, the emergence of bacterial resistance was documented and has been acknowledged as an escalating problem [9, 10], posing a serious threat to global healthcare services and the effective prevention and treatment of infection [11]. The Centers for Disease Control and Prevention (CDC, 2013) reported an estimated 2 million patients were affected by antibiotic resistant infections, resulting in at least 23,000 deaths in the U.S. alone, [12, 13] although it has been suggested that these figures are in fact an underestimation [12]. A high proportion of bacteria causing device-associated infection demonstrate drug-resistance and it has been reported that infected patients utilise greater hospital resources than patients infected with the drug-sensitive bacteria [11].

In hospitals, the greatest incidence of bacterial drug-resistance is encountered in intensive care units (ICU) and the increase in resistance over time, particularly in ICUs, can be linked to the systemic use of antimicrobial agents such as antibiotics, as a strategy to treat and prevent bacterial infections [8, 9, 14–16]. Consequently, infection management is proving increasingly challenging, since the number of effective antibiotic treatments is diminishing and few new antimicrobials are entering the market [14, 17]. The correlation between the escalation in the emergence of microbial drug-resistance and bacterial exposure to antimicrobial agents, can be theorised through Darwinian evolutionary concepts and rationalised as follows [3, 15].

Upon contact with antibiotics, the few bacteria that harbour genes encoding antibiotic resistance, will out-compete those bacteria that are sensitive to the antimicrobial agent [3]. Consequently, due to the elimination of drug-sensitive bacteria, conditions are favourable for the remaining bacteria to rapidly grow and reproduce, transferring genes encoding antibiotic resistance, ultimately generating large populations of resistant bacteria. As a result, the prevalence of bacterial drug-resistance increases proportionally to drug exposure [3].

One approach to decrease the incidence of microbial drug-resistance is to target and reduce the over-prescription and misuse of antibiotics in medical practice [10]. Hospital antibiotic stewardship programmes have been implemented to control and optimise the utilisation of antibiotic therapies, as a means to minimise microbial drug resistance [10, 14, 16–19]. With the increasing rate of bacterial drug resistance and the difficulty and cost associated with the development of new antibiotics, the preservation of existing antibiotics is essential and stewardship programmes can assist with achieving this goal [10, 19]. Such programmes have been recommended for up to 20 years in the U.S. and more recently, in Europe [10], however, the fight against bacterial drug resistance must be strengthened and more effective infection control strategies are key.

1.2.2 *Catheter-associated infections; the origins of an acute problem*

Drug-resistant bacterial pathogens and subsequent nosocomial infections have been associated with increased duration of hospitalisation, healthcare expenditure and mortality [20]. Each year in the U.S. there are an estimated 2 million cases of HAIs and 99,000 associated deaths, with hospital-infection costs ranging from $10,500 to $111,000 per case and total associated costs exceeding $33 billion [1, 21]. The British National Audit Office reported that in the U.K., HAIs cause an estimated 5,000 deaths annually, costing the National Health Service (NHS) at least £1 billion and in Europe, approximately 4 - 10 % of all hospital admissions result in an HAI [21], such as a device-associated

bloodstream infection. A Public Health England report indicated that although there has been a decrease in the incidence of both methicillin resistant *Staphylococcus aureus* (MRSA) and *Clostridium difficile* since the survey conducted in 2006, the prevalence of infections attributed to *Escherichia coli* and *Salmonella* sp. is increasing [22, 23].

The utilisation of polymeric medical devices is fundamental in daily medical practice. More than 30 million urinary catheters are inserted annually in the U.S. and their use is associated with high infection rates (10 - 30 %) [24, 25]. Approximately 449,334 cases of catheter-associated urinary tract infections are reported each year in the U.S., costing an additional $749 - $1,007 per hospital admission, with costs increasing up to *ca.* $3,744 in the event of a bloodstream infection [26], however, the attributable mortality rates are low [25]. Moreover, an estimated 5 million central-venous catheters are inserted each year in the U.S. and over 200,000 are inserted in adult patients in the U.K. alone [25, 27]. The associated incidence of central-venous catheter-related bloodstream infections ranges from 80,000 to 400,000 cases annually in the U.S. and the mortality rate is higher than for urinary catheterisation (up to 25 %) [28, 29]. These devices are crucial in the treatment of critically ill patients, however, most cases of infection in this patient category are associated with their use [25]. It has been noted that 95 % of urinary tract infections are related to urinary catheterisation, 86 % of cases of pneumonia are attributed to mechanical ventilation and 87 % of bloodstream infections are caused by indwelling intravascular devices [25].

Prior to insertion, the surface of the medical device, for example, an intravascular catheter, can be described as 'clean' and 'sterile' [30]. However, immediately after device implantation, a conditioning film is deposited on the surface [30] and microbial colonisation and biofilm formation occurs within 24 h [28]. The composition of the conditioning film is highly dependent upon the catheter insertion location and is comprised of adsorbed high molecular-weight proteins present in the fluid in the environs of the implant, for example, intravascular catheters are prone to encrustation by fibronectin and fibrin [3, 30, 31]. The presence of the "mesh-like"

conditioning film is crucial for microbial implant adherence as it obscures the smooth, somewhat inhospitable implant surface that most bacteria are unable to effectively interact with, providing a rough, charged surface to which planktonic bacteria can adhere [30].

Sessile bacteria that attach to the mesh-like conditioning film on the catheter surface rapidly grow and divide, colonising the surface and creating a biofilm through the secretion of an exopolymeric matrix, composed principally of polysaccharides, proteins and nucleic acids [28, 32]. The presence of the biofilm matrix may enable further species of planktonic bacteria to interact with and attach to the implant surface, forming a more diverse microbial community with many different microenvironments within [32]. It has been noted that microbes within a biofilm are less susceptible to antimicrobial agents than their planktonic counterparts [32]. However, bacterial overcrowding can effect challenging conditions within the biofilm community, resulting in shortages of available nutrients required for the sessile, biofilm-embedded bacteria to survive [3, 32]. Consequently, colonised bacteria may become planktonic and detach from the biofilm and it has been suggested that this microbial dissemination may effect the onset of a bloodstream infection, especially if the quantity of planktonic bacteria exceed a certain limit [3, 28].

Microorganisms commonly associated with intravascular catheter-related infections include both Gram-positive and Gram-negative bacteria such as coagulase-negative staphylococci, MRSA, methicillin-sensitive *Staphylococcus aureus*, *E. coli*, *Pseudomonas aeruginosa*, *Enterobacter* species, in addition to the yeast *Candida albicans* and there is a correlation between the microbial species and site of catheterisation [33]. HAIs are commonly caused by bacteria from the patient's skin microbiota, although there may be additional microbes present, originating from the inanimate hospital environment, equipment or staff [5]. These microorganisms usually access the catheter through extraluminal migration down the device from the site of insertion, colonising the catheter-tip and subsequently, effecting the onset of a bloodstream infection [28]. Another frequent cause of catheter-related bloodstream infections is the microbial colonisation

of the catheter-hub [34] and this type of contamination, usually caused by hospital-acquired microorganisms transferred through hub manipulation by healthcare personnel, leads to bacterial migration along the intraluminal catheter surface [35]. More rarely, bloodstream infections can be attributed to the microbial contamination of catheter-infusate such as parenteral nutrition (intravenous feeding lines), during the preparation process [36].

It has been noted that in the case of short-term intravascular catheterisation (< 10 days), for example with intravenous-peripheral or non-tunnelled devices (see section 1.4.2 for definition), the most frequent source of microbial colonisation is the catheter insertion site [28]. However, in patients catheterised for extensive periods, for example with tunnelled, cuffed central-venous catheters, bloodstream infections can often be attributed to hub contamination [28]. The different pathogens responsible for the onset of infection may require the consideration of different antimicrobial therapies and regimens [28]. Although it is often necessary to prescribe antibiotics to treat catheter-related infections, this may escalate the emergence of drug-resistant bacteria, especially due to the more resistant nature of biofilm-embedded microbes colonising medical implants [30]. Reports suggest that the spread of HAIs is frequently attributed to poor staff compliance with hygiene guidelines [37, 38] and therefore, staff training and education programmes are recommended [39].

1.3 The use of antimicrobial agents for infection-prevention

The integration and implementation of evidence-based guidelines through catheter care bundles and the reduction of unnecessary catheterisation, has resulted in a decrease in the incidence of associated infections [6, 26, 39–42]. However, despite interventions reducing the risk of device-associated infection, this tactic alone will not eliminate or decrease entirely, the incidence of catheter-associated infections. Subsequently, additional infection-prevention approaches are required to further decrease the rate of catheter-related infections

and associated mortality [39]. In the following section, the utilisation of antimicrobial catheter lock solutions is described, as a strategy to prevent bacterial intravascular catheter colonisation and decrease the incidence of catheter-related infections.

1.3.1 *Antimicrobial lock therapy*

Pneumonia, urinary tract infections and bloodstream infections are the most prevalent infections in ICUs and are largely associated with the use of biomaterial devices such as catheters [42]. It has been proposed that in the case of long-term catheterisation, bloodstream infections can be attributed to intraluminal, rather than extraluminal bacterial contamination [43]. Central-venous access devices are routinely flushed with a heparin solution to prevent blood clot formation and prolong catheter patency, however, the efficacy of this strategy is inconclusive [44–46]. Moreover, heparin possesses no intrinsic antibacterial properties and as a result, does little to reduce microbial catheter colonisation [47].

Routine antimicrobial lock solutions can be used as a strategy to sterilise the internal catheter lumen and enhance the efficacy of the implementation of catheter care bundles by decreasing intraluminal catheter colonisation [42, 48–50]. The volume of antimicrobial lock solution used, is such that it fills the complete catheter lumen in addition to the extension tubing [43]. The antimicrobial solution is allowed to dwell in the internal lumen for a specified duration, before it is withdrawn and the catheter is flushed with a heparin/saline solution [43]. Multiple investigations have demonstrated the efficacy of antimicrobial lock therapy as an infection-control approach against catheter-related infections, using systemic antibiotic therapy in conjuction with antimicrobial lock solutions including: minocycline-ethylenediaminetetraacetate (EDTA) [47], heparin in combination with vancomycin, gentamicin, cefazolin, ethanol [49] and fusidic acid lock solutions [51].

Guidelines suggest that antimicrobial lock therapy may be particularly beneficial in the case of certain "high-risk" patients, or those that present recurrent intravascular catheter-related infections [48, 52–54]. *Candida* species are associated with 10 - 15 % of catheter-related bloodstream infections and Gram-positive bacteria account for a further 75 % of such infections [47]. Consequently, the antibiotic/anticoagulant combination of vancomycin and heparin is frequently used as a prophylaxis therapy and has demonstrated effective bactericidal activity against catheter-related infections [47, 55, 56]. A meta-analysis of 7 randomised trials evaluated the antimicrobial efficacy of a vancomycin/ heparin lock solution compared to a control heparin lock solution and concluded that vancomycin lock therapy was effective at lowering the risk of catheter-associated bloodstream infections in high-risk patients [42, 57]. However, it should be highlighted that the systemic use of antibiotics in medical regimes may be discouraged due to concerns about the increased risk of microbial drug resistance [3, 9, 14, 15].

It should be noted that in one prospective, randomised double-blind trial, the routine locking of peripheral catheters with a heparin/ vancomycin solution, decreased the incidence of associated bloodstream infections, with no evidence of vancomycin resistance amongst catheter colonising bacteria [43]. The reduced incidence of catheter-related bloodstream infections upon use of the vancomycin/ heparin lock solution, was attributed to impedance of biofilm formation - through the inhibition of bacteria adhering to the catheter walls - rather than a direct, rapid bactericidal activity of the presence of the low-levels of vancomycin (~10 μg) in the catheter lumen [43].

Overall, the use of antimicrobial lock therapy has demonstrated clinical efficacy as a prophylaxis for catheter-related infections [48–50, 54–57], predominantly caused by vancomycin-sensitive Gram-positive bacteria [43, 55–57]. However, it can be suggested that the lock solution efficacy against vancomycin-sensitive bacteria may improve "living conditions" for vancomycin-resistant bacteria through the reduction in bacterial competition within the biofilm community, thereby generating conditions suitable for rapid microbial multiplica-

tion [3, 48]. Moreover, it should be noted that enterococcal infections attributed to vancomycin-resistant *Enterococcus* species correlate with lengthier hospitalisation durations (18 days) and greater healthcare costs compared to vancomycin-sensitive bacteria, in addition to a 29 % risk of morbidity [58]. Vancomycin lock solution use as a strategy for infection-prevention has been termed an "independent risk-factor" for the emergence of vancomycin-resistant *Enterococcus* sp. [59] and CDC guidelines advise control of its use, overshadowing its advantages as a prophylaxis. Although the use of lock solutions comprising of combinations of minocycline/ EDTA have demonstrated clinical efficacy in a small study [47], the associated risk of antibiotic-resistant bacteria is unknown. Consequently, the use of antibiotic lock solutions should be carefully considered and employed only in cases where the catheterised patient is at a high risk of developing an associated infection.

1.3.2 *Ethanol lock therapy*

One alternative 'lock therapy' approach is the use of ethanol lock solutions [49, 60–63]. It has been suggested that contrary to antibiotic-based prophylaxes, bacterial ethanol 'resistance and resilience' is improbable, since the mode of bacterial kill is through a "non-specific" protein deactivation mechanism, deterring catheter colonisation and preventing consequent infection [49, 64]

Anticoagulants such as heparin are frequently used to prevent catheter-attributed thrombosis [48]. However, it has been noted that ethanol-lock therapy should not be used in combination with heparin flushes as precipitate formation may occur [49, 64, 65]. The absence of an anticoagulant in the lock solution however, may result in thrombosis formation, increasing the risk of infection. Nevertheless, *in-vitro* studies have reported the use of ethanol in combination with alternative anticoagulants such as EDTA [66–68]. Moreover, ethanol has inherent anticoagulation properties and therefore may prevent catheter-associated thrombosis without the need for further

anti-coagulants [64].

In-vitro studies indicate that the use of at least a 30 % solution of ethanol-containing lock solutions were effective at achieving bacterial kill on silicone Hickman catheter sections, when tested against *S. aureus* [64, 68]. Moreover, the study indicated that the use of ethanol lock solutions (> 30 % concentration) was more efficacious than lock solutions containing either minocycline, ciprofloxacin, vancomycin, EDTA, minocycline/ rifampin, ciprofloxacin/ rifampin, vancomycin/ rifampin or minocycline/ EDTA, against a range of microorganisms including *Staphylococcus epidermidis*, *P. aeruginosa* and *Candida* species [64, 68]. Further *in-vitro* studies indicated that the use of lock solutions containing ethanol alone, or in combination with antibiotics or anticoagulants, inhibited biofilm formation by both Gram-negative and Gram-positive bacteria in addition to *Candida* species [64, 66, 67].

In clinical studies, the utilisation of ethanol lock therapy has been reported both in terms of the treatment and prevention of catheter-associated bloodstream infections and has demonstrated significant antimicrobial activity [61, 64, 69–72]. However, it has been pointed out that these clinical trials are associated with various limitations including narrow trial patient populations, retrospective design, un-standardised ethanol locking durations, the additional administration of antibiotics intravenously and the use of only one catheter polymer type (silicone) [64]. Moreover, adverse side-effects have been attributed to the utilisation of ethanol-lock therapy such as nausea, light-headedness, unusual taste sensations, dyspnea, chest pain and fatigue [62, 64]. Other potential undesirable clinical side-effects of ethanol-lock therapy include the risk cardiac arrhythmias, especially when used in combination with EDTA if there is leakage into patient blood circulation [49]; 'central nervous system depression'; and local phlebitis [64].

An additional point for consideration with regard to the use of ethanol lock therapy, is the effect of the lock solution on the stability of the polymeric catheter material [49, 64]. Mechanical testing studies indicated that relative to a control, there was a minor decrease in the

elasticity modulus of polyurethane and silicone catheters, as well as a slight swelling of the polyurethane catheter walls, upon exposure to a 70 % ethanol lock solution [49, 64, 73]. However, no other discrepancy in the results of catheter integrity investigations were observed and overall, it was concluded that the use of an ethanol lock solution did not cause any significant change to the mechanical properties of the catheter that would detrimentally affect its suitability in clinical applications [64, 73]

Further *in-vitro* investigations that explored the effect of ethanol lock solutions on the integrity of selected catheter implants included structural damage assessment, in addition to leaching effects. Scanning electron microscopy indicated that the immersion of silicone catheters in a 95 % concentration ethanol solution for 15 days at 37 ^{0}C (to simulate host conditions), caused no structural damage to the internal catheter lumen relative to a control [64, 74]. Conversely, gas chromatography, in addition to further analytical methods, showed that the immersion of the silicone catheter in 95 % ethanol resulted in the leaching of a higher concentration of cyclic polydimethylsiloxanes, compared to catheters immersed in 0.9 % sodium chloride or 60 % ethanol solutions [64, 74]. The greatest leaching effects were noted within the first 4 h of immersion in the 95 % ethanol solution, although no significant difference in the subsequent release of polydimethylsiloxanes was noted, between immersion in 60 % ethanol or 0.9 % sodium chloride solution [64, 74]. The adverse effects associated with the dissemination of polydimethylsiloxanes and other chemicals into the patient circulatory system are unknown [64] and it is advised that this is further investigated to ensure safety for application in clinical practice.

1.3.3 *Antimicrobial flushes*

Many different approaches have been tested in an attempt to decrease the incidence of catheter-related infections, including the use of systemic antibiotics [29, 75, 76]. Similar to antimicrobial lock therapy, another method of reducing microbial catheter colonisation and asso-

ciated infections is the use of antimicrobial flushes; the sterilisation of the internal catheter lumen, by flushing antibacterial solutions through the catheter. Flush solutions containing the anticoagulant heparin [75], antibiotics such as vancomycin [76], in addition to solutions containing antibiotics and anticoagulant combinations such as minocycline/ EDTA or vancomycin/ ciprofloxacin/ heparin have been investigated [77, 78].

It has been reported that the administration of a vancomycin flush immediately post catheter insertion results in a decrease in the prevalence of catheter-related infections, suggesting that this was the best prophylactic strategy in terms of both benefit and cost, in high-risk patients [76]. In a different study, a significant reduction in the rate of catheter-related bloodstream infections caused by vancomycin-sensitive bacteria was reported, when antibiotic/ heparin flush solutions (vancomycin/ ciprofloxacin/ heparin or vancomycin/ heparin) were used, compared to when a heparin flush solution was used [78]. However, conflicting findings were reported in another clinical study, where no significant difference in the rate of central-venous catheter-related infections was documented in paediatric patients, when vancomycin/ heparin lock solutions were used, compared to heparin lock solutions [79]. Moreover, due to fears concerning the potential development of vancomycin-resistant *Enterococcus* sp. [59, 80], the vancomycin flush strategy is recommended only in the case of high-risk patients, for example adult and paediatric oncology patients [75, 76]. Likewise, although the use of a minocycline/ EDTA catheter flush solution eradicated the incidence of associated infection in a small-scale clinical trial of adult patients who had previously collectively presented 40 cases of intravascular catheter-related infections, CDC guidelines only recommend the use of an antimicrobial treatment strategy in the case of high-risk catheterised patients, for example those that present recurrent infections [24, 48, 77].

1.3.4 *Evaluation of Antimicrobial Locks and Flushes*

The clinical data reviewed in this chapter shows some effectiveness of antimicrobial catheter flushes as a prophylaxis for catheter-related infections [61, 64, 69–72, 76, 78], however, this approach requires more investigation. The use of an antimicrobial catheter lock, rather than flushing the catheter, has also demonstrated greater antimicrobial efficacy [39, 57] and therefore, may be presented as a more effective prophylactic strategy against catheter-associated infections. Nevertheless, recommendation of such therapies are only encouraged in the case of 'high-risk' patients, such as those that present recurring infections [53]. This is due to concerns regarding an increased risk of bacterial resistance upon exposure to antibiotics, in addition to the potential for systemic toxicity from leakage of the lock solution into the patient bloodstream [53]. The use of ethanol as an alternative lock treatment method was also associated with significant drawbacks [49].

Overall, the utilisation of antimicrobial locks or flushes as a prophylaxis against catheter-associated infections have demonstrated efficacy, but each approach is encumbered with significant problems and in general, are recommended for use in the case of high-risk patients only. Consequently, the examination of alternative infection-prevention strategies for example, the use of antimicrobial catheter devices or wound-dressings is necessary to impact on the rate of catheter-related bloodstream infections.

1.4 Antimicrobial medical devices as an infection-prevention strategy

The incorporation of antimicrobial therapies, such as catheter locks and flushes into catheter-care regimes, have impacted on the incidence of catheter-related bloodstream infections. However, the use of these therapies to enhance standard evidence-based catheter-care bundles has been widely recommended only in the case of high-risk patients. An alternative tactic to reduce the risk of associated

infections in catheterised patients, is the use of anti-infective medical devices and wound-dressings to decrease bacterial contamination at the insertion site or on the device itself.

1.4.1 *Antiseptic wound-dressings*

The enhanced risk of bloodstream infections associated with the use of catheter devices has resulted in the implementation of educational training regarding asepsis for clinical personnel, in addition to extensive guidelines concerning device insertion, manipulation and care [81]. Emphasis on clinical asepsis upon catheter insertion is imperative, since bacterial contamination due to the migration of host skin microbiota down the external catheter surface, has been noted as the most prevalent cause of infection in short-term central-venous catheterisation [81]. Subsequently, the insertion and manipulation of central-venous catheter devices is accomplished with stringent adherence to aseptic technique protocols, including cutaneous anti-sepsis prior to device insertion, using a > 0.5 % chlorhexidine-based agent unless contraindicated, as well as maximum sterile-barrier precautions [39, 48] to decrease bacterial extraluminal colonisation and reduce the risk of associated infection.

Post catheter implantation, CDC guidelines advise the covering of the insertion site with a sterile wound-dressing [39, 48], to prevent subsequent extrinsic microbial contamination and it has been documented that the frequency that the wound-dressing should be changed, is dependent on the catheter type and duration of catheterisation [39]. It has been suggested, though not evidenced, that the permeability of the site dressing is linked to the incidence of infection, for example, non-permeable dressings that trap moisture create optimal conditions for microbial proliferation [81]. Consequently, the two types of sterile wound-dressings that are frequently employed in medical practice; transparent, adhesive polyurethane dressings or 'gauze-and-tape' dressings, are both semi-permeable [39, 48, 81].

Polyurethane dressings are often preferred as their application is straightforward, patients can bathe and shower without saturating the dressing and the material is transparent, which facilitates continuous, unobtrusive surveillance of the insertion site [81, 83]. These dressings also require less frequent changes than 'gauze-and-tape dressings' [81]. However, in one meta-analysis comparing different dressing types for peripheral and central catheters, the use of polyurethane wound-dressings was linked to an increased risk of catheter tip colonisation compared to 'gauze-and-tape' dressings and it was speculated that this may be due to insufficient "moisture-vapour" permeability of the polyurethane, creating a favourable environment for microbial growth and multiplication [83, 84]. A Cochrane review on the subject provides a more extensive comparison between the use of polyurethane and 'gauze-and-tape' dressings and concluded from the available evidence, that the use of polyurethane dressing results in a four-fold increase in the risk of catheter-associated bloodstream infections [85]. However, it was reported that larger, better quality studies are crucial, to confirm these findings [85]. Although current guidelines specifically advise the use of standard 'gauze-and-tape' dressings in cases where the insertion site is bleeding or oozing, otherwise, they recommend the use of either 'gauze-and-tape' or 'semi-permeable' dressings to cover the catheter insertion site [39, 54].

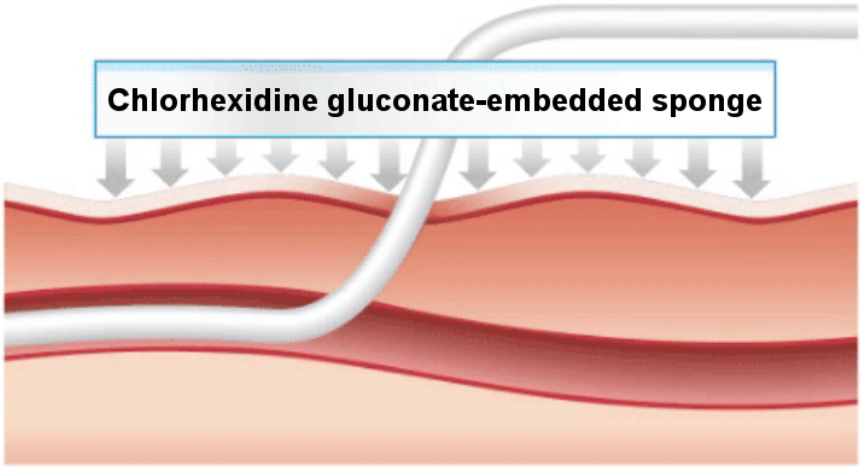

Figure 2: Diagram to show the antimicrobial action of BIOPATCH® wound dressings, through a chlorhexidine gluconate release mechanism, adapted from [82]

The use of an anti-infective wound dressing, Biopatch®, as a strategy to decrease the incidence of catheter-associated infections, has been investigated in clinical studies [86–90]. Biopatch® is an antiseptic chlorhexidine-gluconate impregnated sponge (2.5 cm) that can be placed over the catheter insertion site (Figure 2) and is subsequently covered with a transparent polyurethane wound-dressing [88, 91]. The Biopatch® dressing continuously delivers the antimicrobial agent chlorhexidine gluconate to the insertion site, for a period of up to 7 days [88, 91, 92]. Since external bacterial catheter colonisation is a principal mechanism of central-venous catheter-related infections [87], the application of these dressings is relevant. However, it is anticipated that the use of antimicrobial wound dressings such as Biopatch® may not impact on the rates of infection caused by bacterial hub contamination or the migration of microbes along the intraluminal catheter surface.

Several clinical studies have investigated the efficacy of chlorhexidine-impregnated wound-dressings as a strategy to decrease the risk of catheter contamination and associated infection, with varying results [91]. A small study reported that the use of the chlorhexidine-containing dressings did not result in a statistically significant difference in either microbial catheter-tip contamination or, skin exit-site contamination, however, it was reported that a larger randomised controlled trial is crucial to evaluate the efficacy of this device [88]. In another study, the use of Biopatch® did not result in a statistically significant decrease in the incidence of bacteraemia/ septicemia in patients with tunneled, cuffed central venous catheters, however, there was a statistically significant reduction in the prevalence of local exit-site infections [90]. The use of Biopatch® did not decrease the incidence of catheter-related bloodstream infections among hemodialysis patients with tunneled central venous catheters and it was speculated that in this patient population, contamination of the catheter hub, rather than the catheter exit site, plays a larger role in the pathogenesis of associated bloodstream infections [89].

Numerous large clinical trials have demonstrated the effective antimicrobial activity of chlorhexidine-gluconate impregnated catheter-site

wound-dressings [86, 87, 93]. A meta-analysis of 8 randomised trials examining the efficacy of the use of Biopatch® as a prophylaxis for catheter-related infections, indicated that the use of the antimicrobial wound-dressing resulted in a substantial reduction in vascular and epidural catheter colonisation [94]. This however was only associated with a 'trend' towards a decrease in episodes of vascular and epidural catheter-related infections [94]. The authors of the meta-analysis subsequently published a further comment concluding that upon the incorporation of the results of 2 large European trials, conducted post-publication of the initial meta-analysis, evidence suggested that the use of a chlorhexidine-impregnated wound dressing was an efficacious preventative measure against catheter-related bloodstream infections and recommended its use with vascular catheters in adult patients [87, 93, 95]. More recently, a meta-analysis of 9 randomised controlled trials concluded that the use of chlorhexidine-impregnated dressings was effective at preventing microbial catheter contamination and also, effected a decrease in the incidence of associated bloodstream infections [96]. The authors of this meta-analysis also recommended routine use of chlorhexidine-impregnated dressings, in patients with central venous or arterial catheters at a high-risk of catheter-associated bloodstream infection [96].

In conclusion, evidence suggests that the incorporation of chlorhexidine-impregnated dressings is beneficial in preventing microbial catheter contamination and the onset of associated bloodstream infections [95, 96]. However, although usually well-tolerated by patients [87, 93], it has been reported that the use of chlorhexidine as an antimicrobial agent in medical devices has caused adverse events such as hypersensitivity reactions [97–102], including an incident involving the use of the Biopatch® in low birth-weight neonatal patients [99]. In addition, localised contact dermatitis has been reported when Biopatch® has been used in low-birth weight neonatal patients [48, 98, 103]. A further 7 cases of erosive irritant contact dermatitis were reported - in six cases, the patients were children aged 4 months to 2 years and in one case, the patient was a critically ill 62-year-old man - and it was suggested that care should be taken in using chlorhexidine-impregnated dressings

in immunosuppressed or critically ill patients, since they may be more sensitive to irritant effects [104]. Overall, although reports have suggested that in some cases it may be beneficial to use chlorhexidine-gluconate impregnated wound-dressings to prevent microbial catheter contamination and the onset of infection, and the use of the antiseptic-dressing is recommended in the case of high-risk patients over 2 months in age [94, 95, 105], the associated risk of hypersensitivity and skin reactions, diminishes the efficiency of this strategy as a wide spectrum catheter-infection control strategy.

1.4.2 *Antimicrobial catheter cuffs*

Intravascular catheters can be classified into two categories; tunnelled and non-tunnelled devices. Non-tunnelled catheters are percutaneously inserted into the jugular or subclavian vein under local anaesthesia and are used for short-term catheterisation [91]. For long-term catheterisation, catheters that are surgically tunnelled under the skin for several inches to a cannulated vein are used and a subcutaneous Dacron cuff secures the device in place, as it becomes entangled with fibrous host tissue [91, 106].

One of the frequently noted complications associated with intravascular-catheter devices is the contraction of bloodstream infections caused by host skin microbiota contamination of the catheter-insertion site and this highlights the importance of cutaneous antisepsis prior to catheter insertion [48, 106]. Nevertheless, even after skin disinfection, repressed microbial levels can escalate, especially after the application of a wound-dressing, resulting in bacterial contamination of the exit site [81, 106] and subsequent migration and colonisation along the catheter length. However, as aforementioned, tunnelled catheters, used in long-term catheterisation, have a subcutaneous cuff placed 0.25 cm to 0.75 cm below the surface of the skin and this acts as a barrier to bacteria tracking and colonising the catheter, hindering the onset of infection [106, 107].

Studies have investigated the clinical efficacy of the impregnation of a subcutaneous collagen catheter cuff with antimicrobial agents, as a means to enhance its infection-prevention properties, through presenting both a chemical and mechanical barrier to microorganisms [39, 48, 106]. The cuff (VitaCuff®), comprises of a biodegradable collagen matrix - in which subcutaneous tissue can grow, anchoring the catheter - with chelated silver ions [106]. However, the enhanced anti-infection efficacy of catheters with an antimicrobial subcutaneous cuff is controversial. In an early (1988) multi-centre, randomised trial, consisting of 234 catheters, it was found that the use of the silver-impregnated catheter cuff resulted in a three-fold decrease in the risk of microbial catheter colonisation and an even greater reduction in bacteraemia, relative to a control group consisting of 'non-cuffed' catheterised patients [106]. However, later trials reported that the anti-infective catheter cuff did not effect a statistically significant reduction in microbial catheter colonisation or the risk of associated infection, in either short-term or long-term catheterised patients [107–112]. Moreover, since the catheter cuff is biodegradable, concerns were expressed regarding the loss of the chemical and physical antibacterial attributes of the cuff over time in cases of long-term catheterisation [108]. Overall, there is limited evidence demonstrating that the use of a silver-impregnated cuff is an effective strategy in preventing bacterial catheter contamination and associated infection.

1.4.3 *Antibiotic-coated catheters*

An alternative anti-infection strategy is the use of antimicrobial catheter-devices to prevent microbial catheter contamination and the subsequent onset of infection. Pre-clinical trials have demonstrated that the treatment of commercial catheters with the antibiotic ciprofloxacin, effected potent antimicrobial activity against *P. aeruginosa* and hindered bacterial catheter adhesion [113]. It was reported that the modification of commercial catheters to enable antimicrobial activity can be achieved using a simple dip-coating method and further pre-clinical trials evaluated the antimicrobial

efficacy of catheters coated with antibiotics including gentamicin and norfloxacin, indicating promising results [114–116]. Moreover, the antibiotic nitrofurazone has been used to coat urinary catheters and both *in-vitro* and *in-vivo* trials have established that these antibiotic catheters demonstrate an anti-infective efficacy and show promise in reducing the incidence of urinary tract infections in short-term catheterised patients, within the constraints of the studies performed [116–123]. The use of combination antibiotic-coated catheters also demonstrated antimicrobial efficacy compared to standard catheters, in short-term urinary catheterised patients [122]. Minocycline and rifampin-coated catheters resulted in reduced rates of asymptomatic bacteriuria compared to control catheters, in patients catheterised for less than one week, however, no statistically significant reduction was noted in patients catheterised for more than one week [122].

The use of a combination of antibiotics to coat the inner and outer catheter lumens, has also been explored as a prophylactic strategy to decrease the incidence of intravascular-catheter associated infection. The two broad spectrum antibiotics, minocycline and rifampin, effective against a wide range of bacteria including MRSA, were coated onto commercial catheters pre-treated with a tridodecylmethylammonium chloride surfactant [124, 125]. The synergistic combination of the two antibiotics, minocycline and rifampin, exhibited enhanced efficacy compared to other combinations of antibiotics including vancomycin/ rifampin, inhibiting bacterial catheter colonisation, in particular by slime-producing *S. aureus* and *S. epidermidis* [125, 126] - slime is bacterial exopolymer associated with biofilms. These dual antibiotic-coated catheters also demonstrated antimicrobial efficacy in a multi-institutional, double-blind randomised trial in the U.S. [125]. The study indicated that the use of minocycline/ rifampin (MR) coated central-venous catheters (Cook Critical Care, Indiana) effected a substantial decrease in the prevalence of microbial catheter colonisation when compared to a control group (8 % and 26 % of cases respectively), with no reported cases of catheter-related infection in patients catheterised with the MR-coated device [125]. A meta-analysis of eight randomised controlled trials indicated MR-coated catheters are effective at reducing the risk of bacterial

catheter colonisation and associated infection [127]. It has also been suggested that the use of these catheters may be a cost-effective preventative strategy [124, 125, 127].

These catheters are approved by the U.S. Food and Drug Administration (FDA), commercially available in the U.S. and in addition to standard catheter care protocol, guidelines recommend the integration of these antibiotic catheters into medical practice in the case of high-risk patients requiring extensive catheterisation [39, 54, 128]. A meta-analysis of eight-randomised controlled trials indicated that the use of these catheters decreased catheter colonisation and the incidence of associated catheter-related bloodstream infections [127]. However, it was noted that in all trials reviewed, cutaneous antisepsis was executed using povidone-iodine, rather than a chlorhexidine-based preparation; the antisepsis approach strongly recommended in catheter-care guidelines [48, 105, 127]. Consequently, it is disputable whether the antimicrobial efficacy exhibited by the MR-coated catheters would be significant compared with the effective prophylaxis against infection demonstrated by the use of chlorhexidine-based skin antisepsis, as both approaches prevent infection from similar microorganisms [127]. Some trials also indicated that the use of an MR-coated catheter impacted on the type of microorganism colonising the catheter, with a marked increase in the proportion of *Candida* species documented on MR-coated catheters [127, 129–131].

The incorporation of this antibiotic anti-infective strategy into medical regimes, especially at sub-optimal antibiotic dosage levels, has raised concerns about the potential escalation in the development of drug-resistant bacteria [125, 132, 133]. In particular, a chief concern regarding the widespread use of these antibiotic central-venous catheters, is the development of resistance against rifampin [132]. This antibiotic is used to treat tuberculosis infections caused by *Mycobacterium tuberculosis*, which infects *ca.* 40 % of the population in India [132]. Rifampin-resistance in MRSA has been reported in units treating tuberculosis patients and hence, the emergence of rifampin-resistance in *M. tuberculosis* is possible when the antibiotic

is used as a treatment against MRSA [132, 134]. Moreover, some cases of rifampin-resistance in *M. tuberculosis* in France have been reported and there are fears that this may be a precursor to multi-drug resistance [135]. It can also be speculated that the potential issue of the development of genes encoding rifampin resistance in *M. tuberculosis* may also present a problem in the U.K., since recent findings suggest that there are nearly 8,000 reported cases each year [136, 137]. Moreover, it has been remarked that nearly 40 % of tuberculosis infections in the U.K. are diagnosed in London, where the prevalence of infection has risen by more than 50 % since 1999 [136, 137]. In response to these reports, it can be commented that the more widespread use of antibiotic catheters coated with rifampin as a prophylaxis against catheter-related infections, may effect detrimental outcomes with regard to infection-control and minimising the escalation in bacterial drug-resistance.

Despite these concerns, as yet, clinical studies have demonstrated no evidence of the emergence of bacterial resistance associated with the use of MR-coated catheters and the incidence of this occurring is reported as 'unlikely' [125, 132, 138]. This is since the two antibiotics, minocycline and rifampin, have different modes of action, the former inhibiting bacterial protein synthesis, whereas rifampin inhibits DNA-dependent RNA polymerase required for transcription [132]. Therefore, it can be suggested that even if bacteria develop resistance against one type of antibiotic, they are likely to be susceptible to the attack mechanism of the second, thus rendering the Darwinian selection of a resistant sub-population unlikely. Moreover, the antibiotics used to coat the catheters, minocycline and rifampin, are not systemically used to treat bloodstream infections and both antibiotics exhibit a broad-spectrum of bactericidal activity against both Gram-negative and Gram-positive bacteria, in addition to *Candida* species, deeming the subsequent development of drug-resistance unlikely [125, 139].

Overall, the utilisation of antibiotic catheters such as the MR-coated catheters have demonstrated significant antimicrobial activity, hindering bacterial catheter colonisation and reducing the risk of associated bloodstream infections [125, 132, 140]. Relative to an uncoated but oth-

erwise identical device, the additional cost of an MR-coated catheter is $14 per catheter device, compared to the estimated cost of each episode of catheter-related bloodstream infection, which is approximately $740 [125]. Consequently, it is clear that the use of antibiotic catheters is a valuable and cost-effective infection-prevention strategy. However, guidelines only recommend their use in cases where the risk of catheter-related bloodstream infection is unacceptably high, despite the implementation of basic infection-control strategies [54].

1.4.4 *Silver-coated anti-infective catheters*

The efficacy of antibiotic-coated medical devices as a novel prophylaxis against catheter-related infections has been established through clinical trials. However, the use of these catheters has received a varied response as a result of drawbacks regarding its suitability, including the associated risk of potential escalation in the emergence of drug-resistance amongst bacteria and limitations in broader device applications due to its greater efficacy at preventing infections caused by Gram-positive, rather than Gram-negative bacteria [141]. An alternative catheter-related infection prevention strategy that involves the coating or impregnating of catheters with silver-based antiseptic agents, has been reported in the literature and commercialised products are available in the U.S. [128].

The intrinsic antimicrobial properties of silver has been utilised for countless applications including the treatment of infections, burns and wounds [142]. Modern technology has harnessed the anti-infective properties of silver and silver ions and its incorporation into medical implants results in materials that show efficacious antimicrobial activity, even at low silver concentrations [97, 143], with lower toxicity to human cells, relative to other heavy metals [97, 143]. Metallic silver is 'inert', however, it reacts with moisture for example, on a patient's skin and rapidly ionises, generating highly reactive species [97, 142]. These silver ions can bind to DNA and RNA in microbial cells and tissue-proteins, ultimately effecting cell deformation and death, subsequent to impeding cellular replication and causing structural changes in bacterial cell walls and nuclear membranes

[142–144]. Silver-based antimicrobials have been developed using metallic silver, nanoparticulate silver, silver sulfadiazine and silver zeolites and it has been commented that the antimicrobial activity demonstrated is proportional to both the amount of silver and the rate it is released from its host [142].

Although the complete mechanistic detail of its bactericidal activity is not fully understood, silver-compounds have been employed as an antimicrobial coating in medical devices including catheters [143, 145–148], to prevent bacterial surface colonisation and reduce the risk of associated infection. The use of urinary catheters impregnated with silver alloy resulted in a statistically significant reduction in bacteriuria, in patients catheterised for both less than and more than one week [122]. However, no similar effect was noted when silver oxide impregnated catheters were used [122], or in patients catheterised with silver alloy impregnated devices for long-term bladder drainage [149]. The use of silver alloy intravascular catheters has not been reported in the literature. However, intravascular catheters have been modified such that they exhibit antimicrobial properties through the incorporation of anti-infective agents, such as the combination of chlorhexidine and silver sulfadiazine and these catheters have been reported as an efficacious and prospectively cost-effective approach [124, 148, 150].

1.4.5 *Chlorhexidine and silver sulfadiazine-coated catheters*

'First-generation' antiseptic catheters were coated with chlorhexidine/silver sulfadiazine (CSS) on the external surface only and gradually release the antimicrobial agents into the host tissue in the environs of the implanted catheter, demonstrating antimicrobal activity against a range of pathogens causing nosocomial vascular catheter-related bloodstream infections [148]. In a multi-centre randomised trial it was observed that in comparison to a control group, the use of these CSS anti-infective catheters achieved a sevenfold decrease in microbial cutaneous colonisation of the catheter insertion site, in addition to a fivefold reduction in the incidence of associated

bloodstream infections, especially those caused by Gram-negative bacilli, enterococci, *S. aureus* and *Candida* species [148]. More than 16 randomised clinical studies have investigated the antibacterial efficacy of 'first generation' CSS catheters and these trials indicate that the use of these devices decreases bacterial catheter colonisation [91]. However, only two studies showed a statistically significant reduction in the incidence of catheter-associated bloodstream infection [91].

A blind, multi-institutional comparative study inferred that central-venous catheters coated on both surfaces with an antibiotic combination of MR achieved a greater decrease in the incidence of bloodstream infection than CSS-catheters coated with the antiseptic agent on the external lumen only [151]. Bacterial catheter colonisation was 1/3 as likely on MR-coated catheters as CSS-coated catheters and the associated incidence of bloodstream infection was 1/12 as probable on MR-coated catheters [151]. In addition, it was found that the silver antiseptic catheters demonstrated only a short term antimicrobial activity (3 - 7 days), whereas the MR-catheters exhibited efficacious antimicrobial activity over a longer duration (4 weeks) [152].

It can be speculated that the discrepancy in the duration of antimicrobial efficacy of the two catheters may at least in part, be consequent to the difference in the number of surfaces coated with the antimicrobial agents. To be exact, the MR-catheter had the antimicrobial agent present on both the internal and external catheter surfaces, whereas the CSS-catheter had the antiseptic agent present on the external surface only [148]. Although both the outer and inner catheter surfaces are key routes of central venous catheter-related infection, extraluminal bacterial contamination caused by microbial migration from the insertion site, is a frequent cause of infection in patients undergoing short-term catheterisation [153]. Therefore, an antimicrobial coating on the external catheter may help prevent microbial colonisation and the onset of infection. Conversely, the incidence of infection in patients catheterised for extensive time lengths can be predominantly attributed to intraluminal bacterial colonisation caused by catheter-hub or infusate contamination

[153] and subsequently, the incorporation of antiseptic agents on both the internal and external catheter surfaces may help decrease the incidence of microbial catheter colonisation irrespective of the catheterisation duration.

'Second-generation' CSS-catheters were developed and both the internal and external surfaces of these catheters were coated with the antiseptic agent [91]. Moreover, the concentration of the antimicrobial agent on the external surface of the 'second-generation' CSS catheters was three times higher than the concentration used to coat the same surface in the 'first-generation' CSS catheters [154]. The antibacterial efficacy of these 'second-generation' anti-infective catheters was investigated in three multi-institutional, randomised clinical trials [91, 154–156]. It was reported that although the antiseptic catheters significantly decreased bacterial catheter contamination, there was no statistically significant reduction in the prevalence of associated bloodstream infection [154–156]. However, these studies were underpowered to show a statistically significant decrease in the rate of catheter-related infections [39, 91]. In a more recent study, the use of 'second-generation' CSS catheters reduced the prevalence of catheter-related bloodstream infections in patients catheterised using internal jugular venous access [157]. Moreover, it was found that the use of these catheters reduced immediate intravascular catheter related costs [157] and may be a cost-effective strategy in settings where there is a high risk of catheter-related bloodstream infections [39, 158]. Nevertheless, several disadvantages have been noted regarding the utilisation of these catheters, including the use of sulfadiazine resulting in bacterial cross-resistance with the frequently used antibiotic trimethaprim-sulfamethoxazole, chlorhexidine resistance in Gram-negative bacteria, in addition to possible anaphylaxis attributed to chlorhexidine sensitivity [91, 152, 157].

Hypersensitivity reactions caused by CSS catheters have been observed in Japan and in 1997, they were withdrawn from the Japanese market after 13 incidents of catheter-associated hypersensitivity responses were reported [128, 159, 160]. It can be suggested that the anaphylactic response is triggered by the presence of chlorhexidine-

based antiseptics in the catheter coating, which have reportedly been associated with inducing hypersensitivity reactions in other medical applications [97, 161], in many countries including the U.S. [98], U.K. [99, 100], Switzerland [101] and Japan [102]. In catheter applications, the concentration of chlorhexidine employed for antisepsis is below the documented threshold for cytotoxicity, however, hypersensitivity reactions caused by drugs can be dose-independent and a reaction can potentially be induced by even minimal leaching of the chlorhexidine into host tissue in the environs of the catheter [97, 159, 162]. In addition to prior findings indicating chlorhexidine sensitivity in medical applications [98, 99, 128, 163], recently, there have been an increasing number of reported cases regarding anaphylaxis associated with the utilisation of the CSS catheters in the U.S. [164], U.K. [165–167] and Australia [168]. Nevertheless, catheters coated with a combination of chlorhexidine and silver sulfadiazine have been approved for use by the FDA and are commercially available in the U.S., where sales of these catheters have exceeded 2.5 million units [128]. CDC guidelines (2011) 'strongly recommend' the use of antiseptic catheters such as the CSS- or MR-coated catheters, in patients with an expected catheterisation duration of > 5 days, where adherence to standard catheter care strategies (maximal sterile barrier precautions, healthcare personnel education and cutaneous antisepsis using > 0.5 % chlorhexidine/ alcohol) has not effectively reduced the rate of associated bloodstream infection [39, 128].

Overall, the CSS-coated central-venous catheters have demonstrated antimicrobial efficacy and cost-effectiveness, reducing bacterial catheter colonisation and decreasing the incidence of associated infection in high-risk patients [124, 150, 169]. However, the estimated additional cost of the CSS-coated catheter ($25) in comparison to uncoated catheters, exceeds that of the MR-coated catheters ($14), despite the reduced antibacterial activity demonstrated [125, 148, 151]. Moreover, although no evidence of bacterial resistance was exhibited in clinical studies [148], the emergence of microbial resistance to a chlorhexidine-based compound was demonstrated in an *in-vitro* investigation [164, 170], raising concerns that the introduction of these antiseptic catheters in routine healthcare practice, could

effect the development of bacterial resistance to anti-infective agents. Consequently, although these catheters are FDA approved and recommended for use in high-risk patients, the considerable concerns associated with their use, indicates that an alternative antimicrobial strategy to reduce the risk of catheter-related bloodstream infections is necessary.

1.4.6 *Oligon catheters*

Intravascular catheters coated with antimicrobial agents, for example MR-coated catheters or CSS-coated catheters, have been associated with a decreased incidence of microbial catheter colonisation and a reduced risk of catheter-related bloodstream infections [125, 148, 152]. However, the antimicrobial activity demonstrated by these catheters can be attributed to a coating on the catheter surface, rather than the incorporation of the antimicrobial agents throughout the catheter material bulk, perhaps limiting the bactericidal efficacy. A novel catheter composed of an antibacterial material, oligon, consisting of a polyurethane host matrix impregnated with carbon, platinum and silver, was developed [171]. The silver antiseptic agent was impregnated throughout the catheter material, resulting in a controlled and sustainable release of antibacterial silver ions from both the intra- and extraluminal surfaces, through an iontophoretic reaction [172], hindering microbial catheter colonisation [171].

In-vitro investigations indicate that when placed in a "conductive fluid medium" such as saline solution or blood, oligon effects a continual release of silver ions down the 'electrochemical gradient' to the surface of the catheter and this ion release mechanism continues over a period of nine months [172]. Moreover, *in-vitro* studies demonstrated that oligon exhibits strong antimicrobial activity against a range of Gram-positive and Gram-negative bacteria notorious for catheter-colonisation, including *S. epidermidis*, *S. aureus*, *E. coli*, *P. aeruginosa* and *Candida* species [97, 172]. Clinical studies, including a multi-institutional investigation, showed that the use of an oligon catheter reduced the incidence of microbial catheter colonisation in

intravascular-catheterised patients and may decrease the incidence of associated infection [130, 171, 173]. Conversely, other trials have concluded that oligon catheters are not effective in reducing bacterial catheter colonisation or the risk of associated bloodstream infections [172, 174].

A recent *in-vitro* study investigated the comparative antimicrobial activity, in addition to the anti-adherence efficacy, of a range commercial anti-infective catheters such as MR-coated, CSS-coated and silver-impregnated (oligon) devices, against multi-drug resistant bacteria commonly associated with catheter-related infections [175]. The relative bactericidal activity against catheter-associated Gram-negative and Gram-positive bacteria, including vancomycin-, rifampin- and methicillin-resistant *S. aureus* was evaluated and it was observed that the most potent and enduring antimicrobial and anti-adherence properties were demonstrated by the MR-coated catheters [175]. Moreover, it was noted that the silver impregnated (oligon) catheters exhibited comparatively inferior bactericidal and anti-adherence activity, relative to the MR- and CSS-coated catheters [175]. These *in-vitro* results were supported by the findings of a comparative clinical study, which demonstrated that the MR-coated catheters superseded that of the oligon catheters, in terms of the prevention of bacterial catheter colonisation [130]. Overall, the results of the *in-vitro* studies and the inconsistencies in the findings of clinical studies, casts doubt on the efficacy of the antimicrobial properties of the oligon catheters and its strength as a strategy to decrease the risk of catheter-associated infection.

1.4.7 *Silver/ hydrogel-coated catheters*

An alternative method to control microbial device colonisation, is the use of catheters with extremely hydrophilic surfaces. This can be achieved using a hydrogel coating which helps to prevent microorganisms from adhering to the device surface. Hydrogels are macromolecular cross-linked polymers capable of absorbing substantial volumes of fluid within their structures, resulting in the formation of a thin 'sheet' of water on the surface which facilitates an inherent 'self-cleaning' action [116, 176, 177]. Catheters modified

with a hydrogel coating would present an extremely smooth, hydrophilic surface that is unfavourable for microbial attachment and colonisation, hindering biofilm formation and potentially reducing the likelihood of the incidence of associated infection [97, 116]. In addition, the thin film of water at the hydrogel-coated catheter surface, increases lubricity and this may prove beneficial in clinical applications, by enhancing patient comfort through relieving irritation to host membranes [97, 116].

There are many commercially available hydrogel-coated (urinary) catheters and although they may demonstrate antimicrobial adhesion properties, these catheters have no intrinsic anti-infective capabilities. Attempts have been made to incorporate antiseptic silver ions into the hydrogel-coated catheters and *in-vitro* studies confirmed the efficacy of silver/ hydrogel-coated catheters, at repressing both Gram-positive and Gram-negative bacterial surface adhesion, compared to both hydrogel-coated and uncoated control catheters [116, 178, 179]. The suppression of microbial silver/ hydrogel-coated catheter adhesion may prove advantageous in clinical applications, particularly in preventing or delaying the onset of urinary tract infections in catheterised patients [178]. Conversely, an *in-vitro* investigation indicated that hydrogel coatings assist bacterial migration across catheter surfaces and it was found that the additional incorporation of antiseptic silver into the hydrogel coating, did not impede microbial migration across the catheter surface [116, 180]. Moreover, clinical studies, including one multi-institutional investigation, reported conflicting findings regarding the efficacy of the bactericidal activity of the silver/ hydrogel-coated catheters [116].

A double-blind clinical study demonstrated that the use of silver/ hydrogel-coated catheters was an adequate prophylaxis against catheter-related urinary tract infections caused by *Candida* species and Gram-positive bacteria that generally frequent the extraluminal catheter surface [121, 181]. Furthermore, a multicentre randomised trial indicated that the use of hydrogel catheters coated on both the intra- and extraluminal surfaces with a monolayer of metallic silver, effected a "trend" towards a decrease in the prevalence of

catheter-related infections [182]. However, in most cases this trend was deemed "statistically insignificant", although the use of these catheters was still categorised as a cost-effective approach in one centre [182]. Further clinical trials reported that the utilisation of silver/ hydrogel-coated catheters resulted in a noticeable decrease in the incidence of urinary tract infections in catheterised patients [183, 184]. Due to the insufficient evidence that the use of silver/ hydrogel-coated catheters reduces the risk of catheter-related infections, the use of these catheters is not recommended [185, 186].

Overall, the efficacy of the bactericidal activity of silver/ hydrogel-coated catheters is inconclusive and their use as a prophylaxis for catheter-related infections is currently not acknowledged in urinary-catheter care recommendations [116, 187]. Moreover, to date, antiseptic hydrogel technology has not been used for applications in intravascular catheterisation and clinical studies have focused on the prevention of urinary tract infections in catheterised patients. Consequently, due to the inconclusive antimicrobial efficacy of the antiseptic hydrogel catheters, in addition to their limited applicability, it can be suggested that this is not an effective preventative strategy against catheter-associated infections.

1.4.8 *Problems associated with the use of silver as an infection-prevention strategy*

The use of silver as an antiseptic agent in clinical applications has raised concerns about the development of argyria, where the most dramatic symptoms are the accumulation of silver in the host skin tissue due to leaching of silver ions from the polymeric host, resulting in a grey skin hue [97, 141, 188]. An additional concern is that genes encoding silver-ion resistance, are often selected for upon bacterial exposure to silver salts in hospital antiseptics and it has been reported that more than 10 % of an arbitrary selection of enteric bacteria in a hospital in Chicago, demonstrated genes for silver-ion resistance [189, 190]. Silver-resistance has also been documented in bacteria colonising the urinary tract, including strains of *Proteus mirabilis*,

Klebsiella pneumoniae [191] and *E. coli* [189] and therefore, it can be suggested that widespread silver exposure, for example, through the integration of silver-coated catheters into daily medical care, may impact on the prevalence of silver-resistant bacteria [97, 190].

Overall, the use of catheters incorporated with silver, for example, in silver/ hydrogel and oligon devices, has demonstrated inconclusive evidence in reducing the risk of catheter-associated infection. Catheters coated with CSS have exhibited efficacious antimicrobial activity, reducing microbial catheter colonisation, however, clinical studies have indicated that these catheters are not as effective as the antibiotic MR-coated devices [130, 150, 175].

1.4.9 *Heparin-coated catheters*

Heparin, a polysaccharide anticoagulant with no inherent antimicrobial properties, has been used by itself or in combination with other antimicrobials, as a catheter rinse or lock [192–195]. The anticoagulant properties of heparin stem from its ability to bind to antithrombin, forming antithrombin-thrombin complexes, thus inactivating it and preventing the conversion of fibrinogen to fibrin [195]. It has been documented that catheter-related bloodstream infections can be caused by thrombosis formation in catheterised patients [192] and therefore heparin is systemically used to reduce the risk of blood clots in central-vascular catheterised patients, to decrease the risk of infection [196].

Protein constituents of a thrombus such as fibrinogen, fibrin and fibronectin, can assist catheter surface adherence of key causative pathogens for nosocomial infection, including *S. epidermidis*, *S. aureus* and *Candida* species [192, 197–199]. Consequently, heparin-coating or -bonding on catheters has been used as a strategy to help decrease the risk of device-associated infection [195, 200–203] since the 1980s [200]. Although the mechanism of infection-prevention activity has not been entirely rationalised, it can be suggested that the presence of heparin decreases the accrual of fibronectin, hindering bacterial

surface adherence and subsequent catheter colonisation [200, 203]. A heparin-coated polyurethane catheter for haemodialysis applications has been approved for use by the FDA and the heparin is covalently bound to both catheter surfaces through an 'end-point linkage mechanism' [195]. The advantage of this strategy for heparin attachment is that it does not impinge on the site at which the molecule binds to antithrombin (enabling complexation with and deactivation of thrombin) [195]. After complexation with antithrombin, the antithrombin-thrombin complex 'detaches' from the polyurethane-bound heparin molecule, enabling continual anticoagulant catheter activity [195] and potentially, a prolonged efficacy at reducing the risk of associated infection.

Results across three clinical studies demonstrated that the use of heparin-bonded catheters resulted in a significant decrease in the incidence of associated bloodstream infection compared to standard, uncoated central-venous catheters [200, 202–204]. A further trial demonstrated that the use of a heparin-bonded haemodialysis catheter reduced the risk of catheter-related bacteremia, however, it was noted that it did not impact on the incidence of catheter malfunction [205]. The lack of improvement on catheter patency was also observed in a different trial [195]. Moreover, the use of heparin can also trigger antibody-mediated thrombocytopenia (condition where platelet count is low) and several cases have been reported in the early use of pulmonary-artery catheterised patients with heparin-associated antiplatelet antibodies [206, 207]. If heparin-induced thrombocytopenia occurs, removal of the catheter is necessary to reverse thrombocytopenia and avoid complications [207]. However, according to the catheter manufacturer (Cook, Indiana, U.S.A.), no cases have been associated with the use of their catheters [200].

Various clinical studies have directly compared the antimicrobial activity of different types of antiseptic catheters. One trial evaluated the antimicrobial efficacy of heparin-coated central-venous catheters inserted in the subclavian vein under operating room conditions, relative to that demonstrated by CSS-coated central-venous catheters inserted under identical conditions [208]. It was observed that the

incidence of catheter-related infection was only marginally higher in the heparin-catheter arm of the study than in the CSS-catheter arm and the chief causative pathogens for infection were coagulase-negative staphylococci, *S. aureus*, *Candida* species and *P. aeruginosa* [208]. Interestingly, there was a similar incidence of central-venous catheter associated thrombosis in both study arms [208]. Another clinical study comparing the antimicrobial efficacy of the heparin-bonded catheter and CSS-catheter confirmed these findings and reported that the use of CSS-catheters did not reduce the incidence of catheter-related infections, compared to heparin-coated catheters [209]. However, the prevalence of catheter colonisation was lower in the CSS-catheter group [209].

A recent "network meta-analysis" indicated that the use of heparin-bonded catheters decreased the prevalence of catheter-related blood-stream infections and demonstrated a similar infection-prevention efficacy as MR-coated catheters [210]. Moreover, a further systematic review commented that currently, the strongest line of defence in reducing the incidence of catheter-related bloodstream infections are heparin-coated or MR-coated catheters [200]. Nevertheless, no reduction in microbial catheter colonisation was noted for heparin-bonded devices and it was commented that this may decrease the reliability of the infection-prevention efficacy of these catheters [210]. The network meta-analysis cautiously concluded that compared to the other antiseptic catheters reviewed (including CSS, silver alloy, oligon and heparin), MR-catheters can be considered as a superior anti-infective catheter in clinical applications, as a prophylaxis against catheter-related infection [210], although a high-quality, large, randomised controlled trial is necessary to conclusively determine which is more effective [200].

1.4.10 *Are anti-infective devices the way forward?*

The prevalence of catheter-related bloodstream infections has generated much interest amongst the scientific community and hundreds of different prophylactic strategies have been investigated and eval-

uated over the decades. The modification of commercial catheters such that they incorporate antiseptic agents as a means to prevent microbial catheter colonisation and subsequent bloodstream infection, has been thoroughly examined and several of these products have been commercialised, including oligon catheters, CSS-catheters, heparin-bonded catheters and MR-catheters. It has been suggested that MR-coated catheters demonstrate the most efficacious infection-prevention activity, nevertheless, the effectiveness of heparin-coated catheters is also significant [200, 210]

The use of antimicrobial catheters as a cost-effective strategy has been evaluated in the literature [124, 150, 211–213]. It has been commented that the cost of heparin-coated or antibiotic-coated catheters (Cook Inc., U.K.) is almost double that of standard uncoated catheters, but CSS-catheters are less expensive [200]. However, the financial burden associated with the incidence and treatment of catheter-related bloodstream infections is heavy and therefore, the use of anti-infective catheters is recommended as a cost-effective approach in ICU patients, even when the risk of infection is relatively low [200, 211–213]. Comparing MR-catheters and CSS-catheters, the former device has been reported to perform better 'financially' and is a more economically attractive strategy for the prevention of catheter-associated bloodstream infections [212]. However, there are disadvantages and concerns associated with the use of antimicrobial devices. It has been noted that in many of the clinical trials conducted that cutaneous antisepsis was accomplished using the povidone-iodine antiseptic, rather than the recommended chlorhexidine-based preparation [125, 127, 129, 171, 173, 202, 209]. Consequently, it is unclear whether the use of the antimicrobial catheter would result in a significantly enhanced effect against catheter-related infections, if the recommended cutaneous antisepsis protocols had been executed. Moreover, there are fears that the use of antibiotic-based strategies may escalate the prevalence of bacterial resistance [125, 132, 133, 135]. Consequently, although the use of antiseptic catheters such as MR-coated or heparin-coated devices may be a cost-effective strategy and impact on the incidence of catheter-associated infections, these antimicrobial devices are associated with significant shortcomings

and therefore, research into an alternative infection-prevention strategy, in particular, one in which the emergence of bacterial resistance is improbable, is key.

Antimicrobial medical devices have demonstrated efficacy in reducing the risk of catheter-related infections. However, the development of alternative antimicrobial surface technologies for use in healthcare applications with a reduced associated risk of the emergence of bacterial resistance are sought after, to decrease the incidence of HAIs without compromising current antibiotic approaches. The next chapter introduces a novel surface disinfection strategy, that through light-activation, generates cytotoxic species that initiate a multi-site attack against bacteria in the vicinity, so killing them. This chapter also provides a foundation for the research strategy detailed in this thesis.

REFERENCES

[1] J. A. Al-Tawfiq and P. A. Tambyah. "Healthcare associated infections (HAI) perspectives." In: *Journal of Infection and Public Health* 7 (2014), pp. 339–344.

[2] *Report for the National Audit Office: Trend in rates of Healthcare Associated Infection in England, 2004 to 2008*. http://www.nao.org.uk/wp-content/uploads/2009/06/0809560_MDA_Trends.pdf. Accessed: 2014-09-18.

[3] S. Noimark, C. W. Dunnill, M. Wilson, and I. P. Parkin. "The role of surfaces in catheter-associated infections." In: *Chem Soc Rev* 38 (2009), pp. 3435–48.

[4] M. Merchan, J. Sedlarikova, V. Sedlarik, M. Machovsky, J. Svobodova, and P. Saha. "Antibacterial Polyvinyl Chloride/Antibiotic Films: The Effect of Solvent on Morphology, Antibacterial Activity, and Release Kinetics." In: *Journal of Applied Polymer Science* 118 (2010), pp. 2369–2378.

[5] D. W. Spelman. "2: Hospital-acquired infections." In: *Med J Aust* 176 (2002), pp. 286–91.

[6] K. Blot, J. Bergs, D. Vogelaers, S. Blot, and D. Vandijck. "Prevention of Central Line-Associated Bloodstream Infections Through Quality Improvement Interventions: A Systematic Review and Meta-analysis." In: *Clin Infect Dis* 59 (2014), pp. 96–105.

[7] D. K. Warren, J. E. Zack, J. L. Mayfield, A. Chen, D. Prentice, V. J. Fraser, and M. H. Kollef. "The effect of an education program on the incidence of central venous catheter-associated bloodstream infection in a medical ICU." In: *Chest* 126 (2004), pp. 1612–8.

[8] C. Landelle, K. Marimuthu, and S. Harbarth. "Infection control measures to decrease the burden of antimicrobial resistance in the critical care setting." In: *Current opinion in critical care* 20 (2014), pp. 499–506.

[9] P. M. Hawkey. "The growing burden of antimicrobial resistance." In: *J Antimicrob Chemother* 62 Suppl 1 (2008), pp. i1–9.

[10] P. Lesprit and C. Brun-Buisson. "Hospital antibiotic stewardship." In: *Curr Opin Infect Dis* 21 (2008), pp. 344–9.

[11] *World Health Organisation - Antimicrobial Resistance*. http://www.who.int/mediacentre/factsheets/fs194/en/. Accessed: 2014-09-18.

[12] M. Metz and D. M. Shlaes. "Eight more ways to deal with antibiotic resistance." In: *Antimicrobial Agents and Chemotherapy* 58 (2014), pp. 4253 –4256.

[13] "Antibiotic resistance threats in the United States, 2013. Centers for Disease Control and Prevention, US Department of Health and Human Services, Atlanta, GA." In: *Centers for Disease Control and Prevention* (2013).

[14] T. N. Gandhi, D. D. DePestel, C. D. Collins, J. Nagel, and L. L. Washer. "Managing antimicrobial resistance in intensive care units." In: *Crit Care Med* 38 (2010), S315–23.

[15] I. M. Gould. "Antibiotic policies to control hospital-acquired infection." In: *J Antimicrob Chemother* 61 (2008), pp. 763–5.

[16] I. Martin-Loeches, E. Diaz, and J. Valles. "Risks for multidrug-resistant pathogens in the ICU." In: *Current opinion in critical care* 20 (2014), pp. 516–24.

[17] J. Cooke, P. Stephens, D. Ashiru-Oredope, A. P. Johnson, D. M. Livermore, and M. Sharland. "Antibacterial usage in English NHS hospitals as part of a national Antimicrobial Stewardship Programme." In: *Public Health* 128 (2014), pp. 693–697.

[18] T. H. Dellit, R. C. Owens, J. McGowan J. E., D. N. Gerding, R. A. Weinstein, J. P. Burke, W. C. Huskins, D. L. Paterson, N. O. Fishman, C. F. Carpenter, P. J. Brennan, M. Billeter, T. M. Hooton, I. D. S. of America, and S. for Healthcare Epidemiology of America. "Infectious Diseases Society of America and the Society for Healthcare Epidemiology of America guidelines for developing an institutional program to enhance antimicrobial stewardship." In: *Clin Infect Dis* 44 (2007), pp. 159–77.

[19] P. D. Tamma, A. Holmes, and E. Dodds-Ashley. "Antimicrobial stewardship: another focus for patient safety?" In: *Current Opinion in Infectious Diseases* 27 (2014), pp. 348 –355.

[20] A. M. Milstone, K. A. Bryant, W. C. Huskins, and D. M. Zerr. "The past, present, and future of healthcare-associated infection prevention in pediatrics: multidrug-resistant organisms." In: *Infect Control Hosp Epidemiol* 31 Suppl 1 (2010), S18–21.

[21] A. Bhutta, C. Gilliam, M. Honeycutt, S. Schexnayder, J. Green, M. Moss, and K. J. Anand. "Reduction of bloodstream infections associated with catheters in paediatric intensive care unit: stepwise approach." In: *BMJ* 334 (2007), pp. 362–5.

[22] *MRSA rates slashed, but other bugs a threat*. http://www.nhs.uk/news/2012/05may/Pages/mrsa-hospital-acquired-infection-rates.aspx. Accessed: 2014-09-18.

[23] "Health Protection Agency (HPA), Healthcare-Associated Infection and Antimicrobial Resistance: 2010/11." In: (2012).

[24] B. W. Trautner and R. O. Darouiche. "Catheter-associated infections: pathogenesis affects prevention." In: *Arch Intern Med* 164 (2004), pp. 842–50.

[25] R. O. Darouiche. "Device-associated infections: a macroproblem that starts with microadherence." In: *Clin Infect Dis* 33 (2001), pp. 1567–72.

[26] J. Meddings, M. A. M. Rogers, S. L. Krein, M. G. Fakih, R. N. Olmsted, and S. Saint. "Reducing unnecessary urinary catheter use and other strategies to prevent catheter-associated urinary tract infection: an integrative review." In: *Bmj Quality & Safety* 23 (2014), pp. 277–289.

[27] J. C. Hockenhull, K. M. Dwan, G. W. Smith, C. L. Gamble, A. Boland, T. J. Walley, and R. C. Dickson. "The clinical effectiveness of central venous catheters treated with anti-infective agents in preventing catheter-related bloodstream infections: a systematic review." In: *Crit Care Med* 37 (2009), pp. 702–12.

[28] I. Raad. "Intravascular-catheter-related infections." In: *Lancet* 351 (1998), pp. 893–8.

[29] L. A. Mermel. "Prevention of intravascular catheter-related infections." In: *Ann Intern Med* 132 (2000), pp. 391–402.

[30] M. Habash and G. Reid. "Microbial biofilms: their development and significance for medical device-related infections." In: *J Clin Pharmacol* 39 (1999), pp. 887–98.

[31] P. Appelgren, U. Ransjo, L. Bindslev, F. Espersen, and O. Larm. "Surface heparinization of central venous catheters reduces microbial colonization in vitro and in vivo: results from a prospective, randomized trial." In: *Crit Care Med* 24 (1996), pp. 1482–9.

[32] P. Watnick and R. Kolter. "Biofilm, city of microbes." In: *J Bacteriol* 182 (2000), pp. 2675–9.

[33] L. Lorente, A. Jimenez, J. L. Iribarren, J. J. Jimenez, M. M. Martin, and M. L. Mora. "The micro-organism responsible for central venous catheter related bloodstream infection depends on catheter site." In: *Intensive Care Med* 32 (2006), pp. 1449–50.

[34] M. B. Salzman, H. D. Isenberg, J. F. Shapiro, P. J. Lipsitz, and L. G. Rubin. "A prospective study of the catheter hub as the portal of entry for microorganisms causing catheter-related sepsis in neonates." In: *J Infect Dis* 167 (1993), pp. 487–90.

[35] I. Raad and H. A. Hanna. "Intravascular catheter-related infections: new horizons and recent advances." In: *Arch Intern Med* 162 (2002), pp. 871–8.

[36] I. Raad and G. P. Bodey. "Infectious complications of indwelling vascular catheters." In: *Clin Infect Dis* 15 (1992), pp. 197–208.

[37] E. Larson. "A causal link between handwashing and risk of infection? Examination of the evidence." In: *Infect Control Hosp Epidemiol* 9 (1988), pp. 28–36.

[38] K. Page, M. Wilson, and I. P. Parkin. "Antimicrobial surfaces and their potential in reducing the role of the inanimate environment in the incidence of hospital-acquired infections." In: *J Mater Chem* 19 (2009), pp. 3819–31.

[39] N. P. O. Grady, M. Alexander, L. A. Burns, P. Dellinger, J. Garland, S. O. Heard, P. A. Lipsett, H. Masur, L. A. Mermel, M. L. Pearson, I. I. Raad, A. Randolph, M. E. Rupp, and S. Saint. "Guidelines for the Prevention of Intravascular Catheter-Related Infections, 2011." In: *CDC* (2011).

[40] P. Pronovost, D. Needham, S. Berenholtz, D. Sinopoli, H. Chu, S. Cosgrove, B. Sexton, R. Hyzy, R. Welsh, G. Roth, J. Bander, J. Kepros, and C. Goeschel. "An intervention to decrease catheter-related bloodstream infections in the ICU." In: *N Engl J Med* 355 (2006), pp. 2725–32.

[41] D. Frasca, C. Dahyot-Fizelier, and O. Mimoz. "Prevention of central venous catheter-related infection in the intensive care unit." In: *Crit Care* 14 (2010), p. 212.

[42] M. Kollef. "SMART approaches for reducing nosocomial infections in the ICU." In: *Chest* 134 (2008), pp. 447–56.

[43] J. S. Garland, C. P. Alex, K. J. Henrickson, T. L. McAuliffe, and D. G. Maki. "A vancomycin-heparin lock solution for prevention of nosocomial bloodstream infection in critically ill neonates with peripherally inserted central venous catheters: a prospective, randomized trial." In: *Pediatrics* 116 (2005), e198–205.

[44] *Flush volumes for central venous access devices (CVADs)*. http://www.gosh.nhs.uk/health-professionals/clinical-guidelines/flush-volumes-for-central-venous-access-devices-cvads/. Accessed: 2014-09-18.

[45] R. J. Pratt, C. M. Pellowe, J. A. Wilson, H. P. Loveday, P. J. Harper, S. R. Jones, C. McDougall, and M. H. Wilcox. "epic2: National evidence-based guidelines for preventing healthcare-associated infections in NHS hospitals in England." In: *J Hosp Infect* 65 Suppl 1 (2007), S1–64.

[46] L. Bishop, L. Dougherty, A. Bodenham, J. Mansi, P. Crowe, C. Kibbler, M. Shannon, and J. Treleaven. "Guidelines on the insertion and management of central venous access devices in adults." In: *Int J Lab Hematol* 29 (2007), pp. 261–78.

[47] I. Chatzinikolaou, T. F. Zipf, H. Hanna, J. Umphrey, W. M. Roberts, R. Sherertz, R. Hachem, and I. Raad. "Minocycline-ethylenediaminetetraacetate lock solution for the prevention of implantable port infections in children with cancer." In: *Clin Infect Dis* 36 (2003), pp. 116–9.

[48] N. P. O'Grady, M. Alexander, E. P. Dellinger, J. L. Gerberding, S. O. Heard, D. G. Maki, H. Masur, R. D. McCormick, L. A. Mermel, M. L. Pearson, I. I. Raad, A. Randolph, and R. A. Weinstein. "Guidelines for the Prevention of Intravascular Catheter-Related Infections." In: *Clinical Infectious Diseases* 35 (2002), pp. 1281 –1307.

[49] E. Y. Kim, P. Saunders, and N. Yousefzadeh. "Usefulness of anti-infective lock solutions for catheter-related bloodstream infections." In: *Mt Sinai J Med* 77 (2010), pp. 549–58.

[50] D. Yahav, B. Rozen-Zvi, A. Gafter-Gvili, L. Leibovici, U. Gafter, and M. Paul. "Antimicrobial Lock Solutions for the Prevention of Infections Associated with Intravascular Catheters in Patients Undergoing Hemodialysis: Systematic Review and Meta-analysis of Randomized, Controlled Trials." In: *Clinical Infectious Diseases* 47 (2008), pp. 83–93.

[51] L. Filippi, M. Pezzati, S. Di Amario, C. Poggi, and P. Pecile. "Fusidic acid and heparin lock solution for the prevention of catheter-related bloodstream infections in critically ill neonates: a retrospective study and a prospective, randomized trial." In: *Pediatr Crit Care Med* 8 (2007), pp. 556–62.

[52] B. H. Stover, S. T. Shulman, D. F. Bratcher, M. T. Brady, G. L. Levine, W. R. Jarvis, and N. Pediatric Prevention. "Nosocomial infection rates in US children's hospitals' neonatal and pediatric intensive care units." In: *Am J Infect Control* 29 (2001), pp. 152–7.

[53] J. Marschall et al. "Strategies to prevent central line-associated bloodstream infections in acute care hospitals." In: *Infect Control Hosp Epidemiol* 29 Suppl 1 (2008), S22–30.

[54] J. Marschall, L. A. Mermel, M. Fakih, L. Hadaway, A. Kallen, N. P. O'Grady, A. M. Pettis, M. E. Rupp, T. Sandora, L. L. Maragakis, and D. S. Yokoe. "Strategies to Prevent Central Line–Associated Bloodstream Infections in Acute Care Hospitals: 2014 Update." In: *Infection Control and Hospital Epidemiology* 35 (2014), pp. 753–771.

[55] J. Carratala, J. Niubo, A. Fernandez-Sevilla, E. Juve, X. Castellsague, J. Berlanga, J. Linares, and F. Gudiol. "Randomized, double-blind trial of an antibiotic-lock technique for prevention of gram-positive central venous catheter-related infection in neutropenic patients with cancer." In: *Antimicrob Agents Chemother* 43 (1999), pp. 2200–4.

[56] C. Schwartz, K. J. Henrickson, K. Roghmann, and K. Powell. "Prevention of bacteremia attributed to luminal colonization of tunneled central venous catheters with vancomycin-susceptible organisms." In: *J Clin Oncol* 8 (1990), pp. 1591–7.

[57] N. Safdar and D. G. Maki. "Use of vancomycin-containing lock or flush solutions for prevention of bloodstream infection associated with central venous access devices: a meta-analysis of prospective, randomized trials." In: *Clin Infect Dis* 43 (2006), pp. 474–84.

[58] D. M. Borschel, C. E. Chenoweth, S. R. Kaufman, K. V. Hyde, K. A. VanDerElzen, T. E. Raghunathan, C. D. Collins, and S. Saint. "Are antiseptic-coated central venous catheters effective in a real-world setting?" In: *Am J Infect Control* 34 (2006), pp. 388–93.

[59] A. K. Zaas, X. Song, P. Tucker, and T. M. Perl. "Risk factors for development of vancomycin-resistant enterococcal bloodstream infection in patients with cancer who are colonized with vancomycin-resistant enterococci." In: *Clin Infect Dis* 35 (2002), pp. 1139–46.

[60] K. A. Bryant, D. M. Zerr, W. C. Huskins, and A. M. Milstone. "The past, present, and future of healthcare-associated infection prevention in pediatrics: catheter-associated bloodstream infections." In: *Infect Control Hosp Epidemiol* 31 Suppl 1 (2010), S27–31.

[61] L. Slobbe, J. K. Doorduijn, P. J. Lugtenburg, A. el Barzouhi, E. Boersma, W. B. van Leeuwen, and B. J. A. Rijnders. "Prevention of Catheter-Related Bacteremia with a Daily Ethanol Lock in Patients with Tunnelled Catheters: A Randomized, Placebo-Controlled Trial." In: *PLoS ONE* 5 (2010), e10840.

[62] J. K. Broom, R. Krishnasamy, C. M. Hawley, E. G. Playford, and D. W. Johnson. "A randomised controlled trial of Heparin versus EthAnol Lock THerapY for the prevention of Catheter Associated infecTion in Haemodialysis patients–the HEALTHY-CATH trial." In: *BMC Nephrol* 13 (2012), p. 146.

[63] M. J. Pérez-Granda, J. M. Barrio, P. Muñoz, J. Hortal, C. Rincón, P. M. Rabadán, M. S. Pernia, and E. Bouza. "Ethanol Lock Therapy (E-Lock) in the Prevention of Catheter-Related Bloodstream Infections (CR-BSI) after Major Heart Surgery (MHS): A Randomized Clinical Trial." In: *PLoS ONE* 9 (2014), e91838.

[64] M. Maiefski, M. E. Rupp, and E. D. Hermsen. "Ethanol lock technique: review of the literature." In: *Infect Control Hosp Epidemiol* 30 (2009), pp. 1096–108.

[65] J. Laird, R. Soutar, and I. Butcher. "Complications of the ethanol-lock technique in the treatment of central venous catheter sepsis." In: *Journal of Infection* 51 (2005), pp. 338–.

[66] T. A. Takla, S. A. Zelenitsky, and L. M. Vercaigne. "Effectiveness of a 30% ethanol/4% trisodium citrate locking solution in preventing biofilm formation by organisms causing haemodialysis catheter-related infections." In: *J Antimicrob Chemother* 62 (2008), pp. 1024–6.

[67] I. Raad, H. Hanna, T. Dvorak, G. Chaiban, and R. Hachem. "Optimal antimicrobial catheter lock solution, using different combinations of minocycline, EDTA, and 25-percent ethanol, rapidly eradicates organisms embedded in biofilm." In: *Antimicrob Agents Chemother* 51 (2007), pp. 78–83.

[68] R. J. Sherertz, M. S. Boger, C. A. Collins, L. Mason, and I. Raad. "Comparative in vitro efficacies of various catheter lock solutions." In: *Antimicrob Agents Chemother* 50 (2006), pp. 1865–8.

[69] M. T. Opilla, D. F. Kirby, and M. B. Edmond. "Use of ethanol lock therapy to reduce the incidence of catheter-related bloodstream infections in home parenteral nutrition patients." In: *J Parenter Enteral Nutr* 31 (2007), pp. 302–5.

[70] E. Mouw, K. Chessman, A. Lesher, and E. Tagge. "Use of an ethanol lock to prevent catheter-related infections in children with short bowel syndrome." In: *J Pediatr Surg* 43 (2008), pp. 1025–9.

[71] W. Onland, C. E. Shin, S. Fustar, T. Rushing, and W. Y. Wong. "Ethanol-lock technique for persistent bacteremia of long-term intravascular devices in pediatric patients." In: *Arch Pediatr Adolesc Med* 160 (2006), pp. 1049–53.

[72] J. Broom, M. Woods, A. Allworth, J. McCarthy, J. Faoagali, S. Macdonald, and A. Pithie. "Ethanol lock therapy to treat tunnelled central venous catheter-associated blood stream infections: results from a prospective trial." In: *Scand J Infect Dis* 40 (2008), pp. 399–406.

[73] C. J. Crnich, J. A. Halfmann, W. C. Crone, and D. G. Maki. "The effects of prolonged ethanol exposure on the mechanical properties of polyurethane and silicone catheters used for intravascular access." In: *Infect Control Hosp Epidemiol* 26 (2005), pp. 708–14.

[74] S. Guenu, A. E. Heng, F. Charbonne, M. J. Galmier, F. Charles, P. Deteix, B. Souweine, and C. Lartigue. "Mass spectrometry and scanning electron microscopy study of silicone tunneled dialysis catheter integrity after an exposure of 15 days to 60% ethanol solution." In: *Rapid Commun Mass Spectrom* 21 (2007), pp. 229–36.

[75] M. D. van de Wetering and J. B. M. van Woensel. "Prophylactic antibiotics for preventing early central venous catheter Gram positive infections in oncology patients." In: *Cochrane Database of Systematic Reviews* (2007), p. CD003295.

[76] N. Penel and Y. Yazdanpanah. "Vancomycin flush as antibiotic prophylaxis for early catheter-related infections: a cost-effectiveness analysis." In: *Support Care Cancer* 17 (2009), pp. 285–93.

[77] I. Raad, A. Buzaid, J. Rhyne, R. Hachem, R. Darouiche, H. Safar, M. Albitar, and R. J. Sherertz. "Minocycline and ethylenediaminetetraacetate for the prevention of recurrent vascular catheter infections." In: *Clin Infect Dis* 25 (1997), pp. 149–51.

[78] K. J. Henrickson, R. A. Axtell, S. M. Hoover, S. M. Kuhn, J. Pritchett, S. C. Kehl, and J. P. Klein. "Prevention of central venous catheter-related infections and thrombotic events in immunocompromised children by the use of vancomycin/-ciprofloxacin/heparin flush solution: A randomized, multicenter, double-blind trial." In: *J Clin Oncol* 18 (2000), pp. 1269–78.

[79] W. R. Rackoff, M. Weiman, D. Jakobowski, R. Hirschl, V. Stallings, J. Bilodeau, P. Danz, L. Bell, and B. Lange. "A randomized, controlled trial of the efficacy of a heparin and vancomycin solution in preventing central venous catheter infections in children." In: *J Pediatr* 127 (1995), pp. 147–51.

[80] S. Kachroo, T. Dao, F. Zabaneh, M. Reiter, M. T. Larocco, L. O. Gentry, and K. W. Garey. "Tolerance of vancomycin for surgical prophylaxis in patients undergoing cardiac surgery and incidence of vancomycin-resistant enterococcus colonization." In: *Ann Pharmacother* 40 (2006), pp. 381–5.

[81] D Frasca, C Dahyot-Fizelier, and O Mimoz. "Prevention of central venous catheter-related infection in the intensive care unit." In: *Critical Care* 14 (2010), pp. 212–19.

[82] *BIOPATCH® Protective Disk with CHG is the Solution to Reducing Risk of Catheter-Related BSIs*. http://www.biopatch.com/solution-chg. Accessed: 2014-12-25.

[83] P Eggimann, H Sax, and D Pittet. "Catheter-related infections." In: *Microbes and Infection* 6 (2004), pp. 1033 –42.

[84] K. Hoffmann, D. Weber, G. Samsa, and W. Rutala. "Transparent polyurethane film as an intravenous catheter dressing. A metaanalysis of the infection risks." In: *JAMA* 267 (1992), pp. 2072 –76.

[85] J. Webster, D. Gillies, E. O'Riordan, K. L. Sherriff, and C. M. Rickard. "Gauze and tape and transparent polyurethane dress-

ings for central venous catheters." In: *Cochrane Database of Systematic Reviews* (2011).

[86] D. Maki, L. Mermel, D Kluger, L Narans, V Knasinski, S Parenteau, and P Covington. "The efficacy of a chlorhexidine-impregnated sponge (Biopatch) for the prevention of intravascular catheter-related infection: a prospective, randomized, controlled, multicenter study." In: *40th Interscience conference on Antimicrobial Agents and Chemotherapy* 40 (2000), p. 422.

[87] H. Ruschulte, M. Franke, P. Gastmeier, S. Zenz, K. H. Mahr, S. Buchholz, B. Hertenstein, H. Hecker, and S. Piepenbrock. "Prevention of central venous catheter related infections with chlorhexidine gluconate impregnated wound dressings: a randomized controlled trial." In: *Annals of Hematology* 88 (2008), pp. 267–272.

[88] B. Roberts. "Biopatch^{TM} - a new concept in antimicrobial dressings for invasive devices." In: *Australian Critical Care* 11 (1998), pp. 16–19.

[89] B. C. Camins, A. M. Richmond, K. L. Dyer, H. N. Zimmerman, D. W. Coyne, M. Rothstein, and V. J. Fraser. "A Crossover Intervention Trial Evaluating the Efficacy of a Chlorhexidine-Impregnated Sponge (BIOPATCH®) to Reduce Catheter-Related Bloodstream Infections in Hemodialysis Patients." In: *Infection control and hospital epidemiology : the official journal of the Society of Hospital Epidemiologists of America* 31 (2010), pp. 1118–1123.

[90] S. K. O'Horo, D. Corson, and R. A. Baum. "Efficacy of Biopatch™ in reducing catheter related infections in cuffed, tunneled central venous catheters." In: *Journal of Vascular and Interventional Radiology* 24 (2013), S127.

[91] I Raad, H Hanna, and D Maki. "Intravascular catheter-related infections: advances in diagnosis, prevention, and management." In: *The Lancet Infectious Diseases* 7 (2007), pp. 645 –57.

[92] J Edgeworth. "Intravascular catheter infections." In: *Journal of Hospital Infection* 73 (2009), pp. 323 –330.

[93] J. Timsit et al. "Chlorhexidine-impregnated sponges and less frequent dressing changes for prevention of catheter-related infections in critically ill adults: a randomized controlled trial." In: *JAMA* 301 (2009), pp. 1231 –41.

[94] K. M. Ho. "Use of chlorhexidine-impregnated dressing to prevent vascular and epidural catheter colonization and infection: a meta-analysis." In: *Journal of Antimicrobial Chemotherapy* 58 (2006), pp. 281–287.

[95] K. Ho. "Comment on: Use of chlorhexidine impregnated dressing to prevent vascular and epidural catheter colonization and infection: a meta-analysis." In: *Journal of Antimicrobial Chemotherapy* 65 (2010), pp. 811 –14.

[96] N. Safdar, J. C. O'Horo, A. Ghufran, A. Bearden, M. E. Didier, D. Chateau, and D. G. Maki. "Chlorhexidine-Impregnated Dressing for Prevention of Catheter-Related Bloodstream Infection: A Meta-Analysis." In: *Critical Care Medicine* 42 (2014), pp. 1703–1713.

[97] S. Noimark, C. W. Dunnill, M. Wilson, and I. P. Parkin. "The role of surfaces in catheter-associated infections." In: *Chemical Society Reviews* 38 (2009), pp. 3435–3448.

[98] J. Garland, C Alex, C. Mueller, and L. Cisler-Kahill. "Local reactions to a chlorhexidine gluconate-impregnated antimicrobial dressing in very low birth weight infants." In: *The Pediatric Infectious Disease Journal* 15 (1996), pp. 912 –14.

[99] H Karwowska, M Nesin, and P. Auld. "Safety and effectiveness of Biopatch™ in the reduction of catheter related sepsis in low birth weight neonates." In: *Pediatric Research* 37 (1995), p. 293.

[100] R. Evans. "Acute anaphylaxis due to topical chlorhexidine acetate." In: *Bmj* 304 (1992), p. 686.

[101] R Torricelli and Wuthrich. "Life-threatening anaphylactic shock due to skin application of Chlorhexidine." In: *Clinical and Experimental Allergy* 26 (1996), p. 112.

[102] T Ohtoshi, N Yamauchi, K Tadokoro, S Miyachi, S Suzuki, T Miyamoto, and M Muranaka. "IgE antibody-mediated shock reaction caused by topical application of chlorhexidine." In: *Clinical Allergy* 16 (1986), pp. 155–61.

[103] J. Garland, C Alex, C. Mueller, D Otten, S Shivpuri, M. Harris, M Naples, J Pellegrini, R. Buck, L McAuliffe, D. Goldmann, and D. Maki. "A randomized trial comparing povidone-iodine to a chlorhexidine gluconate-impregnated dressing for prevention of central venous catheter infections in neonates." In: *Pediatrics* 107 (2001), pp. 1431 –36.

[104] W. NA, L. CT, W. JA, and et al. "Chlorhexidine gluconate-impregnated central access catheter dressings as a cause of erosive contact dermatitis: A report of 7 cases." In: *JAMA Dermatology* 149 (2013), pp. 195–199.

[105] J. Marschall et al. "Strategies to Prevent Central Line-Associated Bloodstream Infections in Acute Care Hospitals." In: *Infection Control and Hospital Epidemiology* 29 (2008), S22–S30.

[106] D. Maki, L Cobb, J. Garman, J. Shapiro, R. M, and R. Helgerson. "An Attachable Silver-Impregnated Cuff for Prevention of Infection with Central Venous Catheters: A. Prospective Randomized Multicenter Trial." In: *The American Journal of Medicine* 85 (1988), pp. 307 –14.

[107] J. Groeger, A. Lucas, D Coit, M LaQuaglia, A. Brown, A Turnball, and P Exelby. "A prospective, randomized evaluation of the effect of silver impregnated subcutaneous cuffs for preventing tunneled chronic venous access catheter infections in cancer patients." In: *Annals of Surgery* 218 (1993), pp. 206 –10.

[108] P. Dahlberg, W. Agger, J. Singer, W. Yutuc, K. Newcomer, A Schaper, and B. Rooney. "Subclavian hemodialysis catheter infections: a prospective, randomized trial of an attachable silver-impregnated cuff for prevention of catheter-related infections." In: *Infection Control and Hospital Epidemiology* 16 (1995), pp. 506–511.

[109] C. Babycos, A Barrocas, and W. Webb. "A prospective randomised trial comparing the silver-impregnated collagen cuff with the bedside tunneled subclavian catheter." In: *Journal of Parenteral and Enteral Nutrition* 17 (1993), pp. 61–63.

[110] S. Bonawitz, E. Hammell, and J. Kirkpatrick. "Prevention of central venous catheter sepsis: a prospective randomized trial." In: *American Surgeon* 57 (1991), pp. 618 –23.

[111] N. Hasaniya, M Angelis, M. Brown, and M Yu. "Efficacy of Subcutaneous Silver-Impregnated Cuffs in Preventing Central Venous Catheter Infections." In: *Chest* 109 (1996), pp. 1030 –32.

[112] B Walder, D Pittet, and M. Tramer. "Prevention of bloodstream infections with central venous catheters treated with anti-infective agents depends on catheter type and insertion time: evidence from a meta-analysis." In: *Infection Control and Hospital Epidemiology* (2002), pp. 748 –56.

[113] G Reid, S Sharma, K Advikolanu, C Tieszer, R. Martin, and A. Bruce. "Effects of ciprofloxacin, norfloxacin, and ofloxacin on in vitro adhesion and survival of Pseudomonas aeruginosa AK1 on urinary catheters." In: *Antimicrobial Agents and Chemotherapy* 38 (1994), pp. 1490 –95.

[114] Y. Cho, J. Park, S. Kim, Y. Cho, J. Choi, H. Shin, Y. Bae, H Chung, S. Jeong, and I. Kwon. "Gentamicin-releasing urethral catheter for short-term catheterization, Journal of Biomaterials Science." In: *Polymer Edition* 14 (2003), pp. 963 –72.

[115] J. Park, Y. Cho, Y. Cho, J. Choi, H. Shin, Y. Bae, H Chung, S. Jeong, and I. Kwon. "Norfloxacin-releasing urethral catheter for long-term catheterization." In: *Journal of Biomaterials Science, Polymer Edition* 14 (2003), pp. 951 –62.

[116] U. Ha and Y. Cho. "Catheter-associated urinary tract infections: new aspects of novel urinary catheters." In: *International Journal of Antimicrobial Agents* 28 (2006), pp. 485 –90.

[117] I Al-Habdan, M Sadat-Ali, J. Corea, A Al-Othman, B. Kamal, and D. Shriyan. "Assessment of nosocomial urinary tract infections in orthopaedic patients: a prospective and comparative

study using two different catheters." In: *International Surgery* 88 (2003), pp. 152–54.

[118] J. Johnson, P Delavari, and M Azar. "Activities of a nitrofurazone containing urinary catheter and a silver hydrogel catheter against urinary tract infection." In: *Antimicrobial Agents and Chemotherapy* 43 (1999), pp. 2990 –95.

[119] S. Lee, S. Kim, Y. Cho, W. Shin, S. Lee, C. Kim, S. Hong, B. Chung, J. Kim, and M. Yoon. "A comparative multicentre study on the incidence of catheter-associated urinary tract infection between nitrofurazone-coated and silicone catheters." In: *International Journal of Antimicrobial Agents* 24 (2004), S65 – 69.

[120] D. Maki, V Knasinski, and P. Tambyah. "A prospective investigator blinded trial of a novel nitrofurazone-impregnated urinary catheter." In: *Infection Control and Hospital Epidemiology* 18 (1997), pp. 50, M49.

[121] D. Maki and P. Tambyah. "Engineering out the risk of infection with urinary catheters." In: *Emerging Infectious Diseases* 7 (2001), pp. 1–6.

[122] L Schumm and T. B. L. Lam. "Types of urethral catheters for management of short-term voiding problems in hospitalised adults." In: *Cochrane Database of Systematic Reviews* (2008), p. CD004013.

[123] R Pickard, T Lam, G Maclennan, K Starr, M Kilonzo, G McPherson, K Gillies, A McDonald, K Walton, B Buckley, C Glazener, C Boachie, J Burr, J Norrie, L Vale, A Grant, and J N'dow. "Types of urethral catheter for reducing symptomatic urinary tract infections in hospitalised adults requiring short-term catheterisation: multicentre randomised controlled trial and economic evaluation of antimicrobial- and antiseptic-impregnated urethral catheters (the CATHETER trial)." In: *Health Technol Assess* 16 (2012), pp. 1–197.

[124] J. O' Leary and T. Jacome. "Solutions for Central Line Infections: Yes or No?" In: *Current Surgery* 58 (2001), pp. 547 –50.

[125] I Raad, R. Darouiche, J Dupuis, D Abi-Said, A Gabrielli, R Hachem, M Wall, R Harris, J Jones, A Buzaid, C Robertson, S Shenaq, P Curling, T Burke, and C Ericsson. "Central Venous Catheters Coated with Minocycline and Rifampin for the Prevention of Catheter-Related Colonization and Bloodstream Infections; A Randomized, Double-Blind Trial." In: *Annals of Internal Medicine* 127 (1997), pp. 267 –74.

[126] I Raad, R Darouiche, R Hachem, M Sacilowski, and G. Bodey. "Antibiotics and prevention of microbial colonization of catheters." In: *Antimicrobial Agents and Chemotherapy* 39 (1995), pp. 2397 –400.

[127] M. Falagas, K Fragoulis, I. Bliziotis, and I Chatzinikolaou. "Rifampicin-impregnated central venous catheters: a meta-analysis of randomized controlled trials." In: *Antimicrobial Chemotherapy* 59 (2007), pp. 359 –69.

[128] B. Trautner and R. Darouiche. "Catheter-Associated Infections; Pathogenesis Affects Prevention." In: *Archives of Internal Medicine* 164 (2004), pp. 842 –50.

[129] C Leon, S Ruiz-Santana, J Rello, M. de la Torre, J Valles, F Alvarez-Lerma, R Sierra, P Saavedra, and F Alvarez-Salgado. "Benefits of minocycline and rifampin-impregnated central venous catheters. A prospective, randomized, double-blind, controlled, multicenter trial." In: *Journal of Intensive Care Medicine* 30 (2004), pp. 1891 –99.

[130] D Fraenkel, C. Rickard, P. Thomas, J Faoagali, N George, and R Ware. "A prospective, randomized trial of rifampicin-minocycline-coated and silver-platinum carbon-impregnated central venous catheters." In: *Critical Care Medicine* 34 (2006), pp. 668–75.

[131] R. O. Darouiche, D. H. Berger, N. Khardori, C. S. Robertson, M. J. J. Wall, M. H. Metzler, S. Shah, M. D. Mansouri, C. Cerra-Stewart, J. Versalovic, M. J. Reardon, and I. I. Raad. "Comparison of antimicrobial impregnation with tunneling of long-term central venous catheters: a randomized controlled trial." In: *Ann Surg* 242 (2005), pp. 193–200.

[132] R. Darouiche. "In Vivo Efficacy of Antimicrobial-Coated Devices." In: *The Journal of Bone and Joint Surgery* 90 (2008), pp. 1785 –86.

[133] I Chatzinikolaou, H Hanna, L Graviss, G Chaiban, C Perego, R Arbuckle, R Champlin, R Darouiche, G Samonis, and I Raad. "Clinical experience with minocycline and rifampin-impregnated central venous catheters in bone marrow transplantation recipients: efficacy and low risk of developing staphylococcal resistance." In: *Infection Control and Hospital Epidemiology* 24 (2003), pp. 961 –63.

[134] J Sekiguchi, T Fujino, M Araake, E Toyota, K Kudo, K Saruta, H Yoshikura, T Kuratsuji, and T Kirikae. "Emergence of rifampicin resistance in methicillin resistant Staphylococcus aureus in tuberculosis wards." In: *Journal of Infection and Chemotherapy* 12 (2006), pp. 47 –50.

[135] V. Meyssonnier, T. V. Bui, N. Veziris, V. Jarlier, and J. Robert. "Rifampicin mono-resistant tuberculosis in France: a 2005-2010 retrospective cohort analysis." In: *BMC Infect Dis* 14 (2014), p. 18.

[136] *London - the tuberculosis capital of Europe.* http://www.ucl.ac.uk/news/news-articles/1012/10121603. Accessed: 2011-02-22.

[137] *Public Health England: Tubercolosis in the U.K. 2014 report*. https://www.gov.uk/government/uploads/system/uploads/attachment_data/file/360335/TB_Annual_report__4_0_300914.pdf. Accessed: 2015-01-04.

[138] E. R. Ramos, R. Reitzel, Y. Jiang, R. Y. Hachem, A. M. Chaftari, R. F. Chemaly, B. Hackett, S. E. Pravinkumar, J. Nates, J. J. Tarrand, and I. I. Raad. "Clinical effectiveness and risk of emerging resistance associated with prolonged use of antibiotic-impregnated catheters: more than 0.5 million catheter days and 7 years of clinical experience." In: *Crit Care Med* 39 (2011), pp. 245–251.

[139] I Raad, R Darouiche, R Hachem, M Mansouri, and G. Bodey. "The broad-spectrum activity and efficacy of catheters coated with minocycline and rifampin." In: *The Journal of Infectious Diseases* 173 (1996), pp. 418 –24.

[140] P. Marik, G Abraham, P Careau, J Varon, and R. Fromm. "The ex vivo antimicrobial activity and colonization rate of two antimicrobial-bonded central venous catheters." In: *Critical Care Medicine* 27 (1999), pp. 1128–31.

[141] P. Tambyah. "Catheter-associated urinary tract infections: diagnosis and prophylaxis*." In: *International Journal of Antimicrobial Agents* 24 (2004), pp. 44–48.

[142] M Rai, A Yadav, and A Gade. "Silver nanoparticles as a new generation of antimicrobials." In: *Biotechnology advances* 27 (2009), pp. 76–83.

[143] B. Kwakye-Awuah, C. Williams, M. A. Kenward, and I. Radecka. "Antimicrobial action and efficiency of silver-loaded zeolite X." In: *Journal of Applied Microbiology* 104 (2008), pp. 1516–1524.

[144] A. Lansdown. "Silver I: its antibacterial properties and mechanism of action." In: *Journal of Wound Care* 11 (2002), pp. 125 –38.

[145] A Bach, H Schmidt, B Bottiger, B Schreiber, H Böhrer, J Motsch, E Martin, and H. Sonntag. "Retention of antibacterial activity and bacterial colonization of antiseptic-bonded central venous catheters." In: *Journal of Antimicrobial Chemotherapy* 37 (1996), pp. 315 –22.

[146] D. Riley, D. Classen, L. Stevens, and J. Burke. "A large randomised clinical trial of a silver-impregnated urinary catheter: lack of efficacy and staphylococcal superinfection." In: *The American Journal of Medicine* 98 (1995), pp. 349 –56.

[147] A Bach, H Eberhardt, A Frick, H Schmidt, B. Bottiger, and E Martin. "Efficacy of silver-coating central venous catheters in reducing bacterial colonization." In: *Critical Care Medicine* 27 (1999), pp. 515 –21.

[148] D. Maki, S. Stolz, S Wheeler, and L. Mermel. "Prevention of central venous catheter-related bloodstream infection by use of an antiseptic-impregnated catheter: a randomised, controlled trial." In: *Annals of Internal Medicine* 127 (1997), pp. 257–66.

[149] P. Jahn, M. Preuss, A. Kernig, G. Langer, and A. Seifert-Huehmer. "Types of indwelling urinary catheters for long-term bladder drainage in adults." In: *Cochrane Database of Systematic Reviews* (2007), p. CD004997.

[150] D. Veenstra, S Saint, S Saha, T Lumley, and S. Sullivan. "Efficacy of antiseptic-impregnated central venous catheters in preventing catheter related bloodstream infection: a meta-analysis." In: *JAMA* 281 (1999), pp. 261–67.

[151] R. Darouiche, I. Raad, S. Heard, J. Thornby, O. Wenker, A Gabrielli, J Berg, N Khardori, H Hanna, R Hachem, R. Harris, and G Mayhall. "A comparison of two antimicrobial-impregnated central venous catheters." In: *New England Journal of Medicine* 340 (1999), pp. 1–8.

[152] I Raad and H Hanna. "Intravascular catheters impregnated with antimicrobial agents: a milestone in the prevention of bloodstream infections." In: *Support Care Cancer* 7 (1999), pp. 386 –390.

[153] L. A. Mermel. "What is the predominant source of intravascular catheter infections?" In: *Clin Infect Dis* 52 (2011), pp. 211–212.

[154] C. Brun-Buisson, F. Doyon, J.-P. Sollet, J.-F. Cochard, Y. Cohen, and G. Nitenberg. "Prevention of intravascular catheter-related infection with newer chlorhexidine-silver sulfadiazine-coated catheters: a randomized controlled trial." In: *Intensive Care Medicine* 30 (2004), pp. 837–843.

[155] T Ostendorf, A Meinhold, C Harter, H Salwender, G Egerer, H. Geiss, A. Ho, and H Goldschmidt. "Chlorhexidine and silver-sulfadiazine coated central venous catheters in haematological patients - a double-blind, randomised, prospective, controlled trial." In: *Support Care Cancer* 13 (2005), pp. 993–1000.

[156] M. Rupp, S. Lisco, P. Lipsett, T. Perl, K Keating, J. Civetta, L. Mermel, D Lee, E. Dellinger, M Donahoe, D Giles, M. Pfaller, D. Maki, and R Sherertz. "Effect of a Second-Generation Venous Catheter Impregnated with Chlorhexidine and Silver Sulfadiazine on Central Catheter-Related Infections; A Ran-

domized, Controlled Trial." In: *Annals of Internal Medicine* 143 (2005), pp. 570 –80.

[157] L. Lorente, M. Lecuona, A. Jiménez, R. Santacreu, L. Raja, O. Gonzalez, and M. L. Mora. "Chlorhexidine-silver sulfadiazine-impregnated venous catheters save costs." In: *American Journal of Infection Control* 42 (2014), pp. 321 –324.

[158] D. L. Veenstra, S. Saint, and S. D. Sullivan. "Cost-effectiveness of antiseptic-impregnated central venous catheters for the prevention of catheter-related bloodstream infection." In: *JAMA* 282 (1999), pp. 554–60.

[159] T Oda, J Hamasaki, N Kanda, and K Mikami. "Anaphylactic shock induced by an antiseptic-coated central nervous catheter." In: *Anesthesiology* 87 (1997), pp. 1242 –44.

[160] E Terazawa, H Shimonaka, K Nagase, T Masue, and i. S. Doh. "Severe anaphylactic reaction due to a chlorhexidine-impregnated central venous catheter." In: *Anesthesiology* 89 (1998), pp. 1296 –8.

[161] *Centers for Devices and Radiological Health, US Food and Drug Administration. FDA public health notice: potential hypersensitivity reactions to chlorhexidine-impregnated medical devices; 1998*. http://www.fda.gov/medicaldevices/safety/alertsandnotices/publichealthnotifications/ucm062306.htm. Accessed: 2011-02-22.

[162] R. DeSwarte. "Drug allergy - Problems and strategies." In: *The Journal of Allergy and Clinical Immunology* 74 (1984), pp. 209 –24.

[163] G. F. Calogiuri, E. Di Leo, A. Trautmann, E. Nettis, A. Ferrannini, and A. Vacca. "Chlorhexidine Hypersensitivity: A Critical and Updated Review." In: *Journal of Allergy & Therapy* 4 (2013), pp. 1–7.

[164] L. Mermel. "New Technologies to Prevent Intravascular Catheter-Related Bloodstream Infections." In: *Emerging Infectious Diseases* 7 (2001), pp. 197 –99.

[165] R Jee, L Nel, G Gnanakumaran, A Williams, and E Eren. "Four cases of anaphylaxis to chlorhexidine impregnated central venous catheters: a case cluster or the tip of the iceberg?" In: *British Journal of Anaesthesia* 103 (2009), pp. 614 –15.

[166] A Pittaway and S Ford. "Allergy to chlorhexidine-coated central venous catheters revisited." In: *British Journal of Anaesthesia* 88 (2002), pp. 304 –5.

[167] R Stephens, M Mythen, P Kallis, D. Davies, W Egner, and A Rickards. "Two episodes of life-threatening anaphylaxis in the same patient to a chlorhexidine-sulphadiazine-coated central venous catheter." In: *British Journal of Anaesthesia* 87 (2001), pp. 306 –8.

[168] A Khoo and P Oziemski. "Chlorhexidine impregnated central venous catheter inducing an anaphylatic shock in the Intensive Care Unit," in: *Heart, Lung and Circulation* (2010), pp. 1–2.

[169] D. Borschel, C. Chenoweth, S. Kaufman, K. Hyde, K. Vanderelzen, T. Raghunathan, C. Collins, and S. Saint. "Are antiseptic-coated central venous catheters effective in a real-world setting?" In: *American Journal of Infection Control* 34 (2006), pp. 388–393.

[170] U Tattawasart, J. Maillard, J. Furr, and A. Russell. "Development of resistance to chlorhexidine diacetate and cetylpyridimium chloride in Pseudomonas stutzeri and changes in antibiotic susceptibility." In: *Journal of Hospital Infection* 42 (1999), pp. 219 –29.

[171] M Ranucci, G Isgro, P. Giomarelli, M Pavesi, A Luzzani, I Cattabriga, M Carli, P Paolo Giomi, A Compostella, A Digito, V Mangani, V Silvestri, and E Mondelli. "Impact of oligon central venous catheters on catheter colonisation and catheter-related bloodstream infection." In: *Critical Care Medicine* 31 (2003), pp. 52–59.

[172] J. J. Bong. "Prevention of catheter related bloodstream infection by silver iontophoretic central venous catheters: a randomised controlled trial." In: *Journal of Clinical Pathology* 56 (2003), pp. 731–735.

[173] L Corral, M Nolla-Salas, J Ibañez Nolla, M. León, R. Díaz, M Cruz Martín, R Iglesia, and R Catalan. "A prospective, randomised study in critically ill patients using the Oligon Vantex catheter." In: *Journal of Hospital Infection* 55 (2003), pp. 212–19.

[174] E. Moretti, C. Ofstead, R. Kristy, and H. Wetzler. "Impact of central venous catheter type and methods on catheter-related colonization and bacteraemia." In: *Journal of Hospital Infection* 61 (2005), pp. 139–145.

[175] I. Raad, R. Reitzel, Y. Jiang, R. F. Chemaly, T. Dvorak, and R. Hachem. "Anti-adherence activity and antimicrobial durability of anti-infective-coated catheters against multidrug-resistant bacteria." In: *Journal of Antimicrobial Chemotherapy* 62 (2008), pp. 746–750.

[176] N Nakagawa, N Yashiro, Y Nakajima, W. Barnhart, and M Wakabayashi. "Hydrogel-coated glide catheter: experimental studies and initial clinical experience." In: *American Journal of Roentgenology* 163 (1994), pp. 1227 –29.

[177] I. Parkin and R. Palgrave. "Self-cleaning coatings." In: *Journal of Materials Chemistry* 15 (2005), pp. 1689 –95.

[178] D. G. Ahearn, D. T. Grace, M. J. Jennings, R. N. Borazjani, K. J. Boles, L. J. Rose, R. B. Simmons, and E. N. Ahanotu. "Effects of Hydrogel/Silver Coatings on In Vitro Adhesion to Catheters of Bacteria Associated with Urinary Tract Infections." In: *Current Microbiology* 41 (2000), pp. 120–125.

[179] M. Gabriel, M. Mayo, L. May, R. Simmons, and D. Ahearn. "In-vitro evaluation of the efficacy of a silver-coated catheter." In: *Current Microbiology* 33 (1996), pp. 1–5.

[180] N Sabbuba, G Hughes, and D. Stickler. "The migration of Proteus mirabilis and other urinary tract pathogens over Foley catheters." In: *British Journal of Urology International* 89 (2002), pp. 55 –60.

[181] D. Maki, V Knasinski, K. Halvorson, and P. Tambyah. "A novel silver-hydrogel urinary catheter reduces catheter-associated urinary tract infections: a prospective, randomized, double

blind study." In: *Abstracts of the Interscience Conference on Antimicrobial Agents and Chemotherapy* 38 (1998), p. 534.

[182] R. Bologna, L. Tu, M Polansky, H. Fraimow, D. Gordon, and K. Whitmore. "Hydrogel/silver ion-coated urinary catheter reduces nosocomial urinary tract infection rates in intensive care unit patients: a multicenter study." In: *Urology* 54 (1999), pp. 982 –87.

[183] R Ramirez, A Dobin, E Britten, and S Wadman. "A silver opportunity for reducing nosocomial urinary tract infections." In: *Infection Control and Hospital Epidemiology* 19 (1998), S28.

[184] T. Karchmer, E. Giannetta, C. Muto, B. Strain, and B. Farr. "A Randomized Crossover Study of Silver-Coated Urinary Catheters in Hospitalized Patients." In: *Archives of Internal Medicine* 160 (2000), pp. 3294 –98.

[185] P. Thibon. "Randomized multi-centre trial of the effects of a catheter coated with hydrogel and silver salts on the incidence of hospital-acquired urinary tract infections." In: *Journal of Hospital Infection* 45 (2000), pp. 117–124.

[186] A Srinivasan, T Karchmer, A Richards, X Song, and T. Perl. "A prospective trial of a novel, silicone-based, silver-coated foley catheter for the prevention of nosocomial urinary tract infections." In: *Infection Control and Hospital Epidemiology* 27 (2006), pp. 38 –43.

[187] B. W. Trautner. "Management of catheter-associated urinary tract infection." In: *Current Opinion in Infectious Diseases* 23 (2010), pp. 76–82.

[188] "Concise Medical Dictionary." In: *4th Edition, Oxford University Press* (1994).

[189] S. Silver, L. T. Phung, and G. Silver. "Silver as biocides in burn and wound dressings and bacterial resistance to silver compounds." In: *Journal of Industrial Microbiology & Biotechnology* 33 (2006), pp. 627–634.

[190] S Silver. "Bacterial silver resistance: molecular biology and uses and misuses of silver compounds." In: *FEMS Microbiology Reviews* 27 (2003), pp. 341 –53.

[191] J. Guggenbichler, M Böswald, S Lugauer, and T Krall. "A new technology of microdispersed silver in polyurethane induces antimicrobial activity in central venous catheters." In: *Infection* 27 (1999), S16–S23.

[192] L. Mermel. "Prevention of Intravascular Catheter-Related Infections." In: *Annals of Internal Medicine* 132 (2000), pp. 391 – 402.

[193] L. Filippi, M. Pezzati, S. Di Amario, C. Poggi, and P. Pecile. "Fusidic acid and heparin lock solution for the prevention of catheter-related bloodstream infections in critically ill neonates: A retrospective study and a prospective, randomized trial*." In: *Pediatric Critical Care Medicine* 8 (2007), pp. 556–562.

[194] J. S. Garland, C. Alex, K. Henrickson, T. McAuliffe, and D. Maki. "A Vancomycin-Heparin Lock Solution for Prevention of Nosocomial Bloodstream Infection in Critically Ill Neonates With Peripherally Inserted Central Venous Catheters: A Prospective, Randomized Trial." In: *Pediatrics* 116 (2005), e198 –e205.

[195] T. W. I. Clark, D. Jacobs, H. W. Charles, S. Kovacs, T. Aquino, J. Erinjeri, and J. A. Benstein. "Comparison of Heparin-Coated and Conventional Split-Tip Hemodialysis Catheters." In: *CardioVascular and Interventional Radiology* 32 (2009), pp. 703–706.

[196] J Meyer. "A Broad-Spectrum Look at Catheter-Related Bloodstream Infections." In: *Journal of Infusion Nursing* 32 (2009), pp. 80–86.

[197] M Herrmann, Q. Lai, R. Albrecht, D. Mosher, and R. Proctor. "Adhesion of Staphylococcus aureus to surface-bound platelets: role of fibrinogen/fibrin and platelet integrins." In: *The Journal of Infectious Diseases* 167 (1993), pp. 312 –22.

[198] M Nilsson, L Frykberg, J. Flock, L Pei, M Lindberg, and B Guss. "A fibrinogen-binding protein of Staphylococcus epidermidis." In: *Infection and Immunity* 66 (1998), pp. 2666 –73.

[199] G. DeMuri and M. Hostetter. "Evidence for a β1 integrin fibronectin receptor in Candida tropicalis." In: *The Journal of Infectious Diseases* 174 (1996), pp. 127–32.

[200] R. Gilbert and M Harden. "Effectiveness of impregnated central venous catheters for catheter related blood stream infection: a systematic review." In: *Current Opinion in Infectious Diseases* 21 (2008), pp. 235 –45.

[201] D. Long and M. Coulthard. "Effect of heparin-bonded central venous catheters on the incidence of catheter-related thrombosis and infection in children and adults." In: *Anaesthesia and Intensive Care* 34 (2006), pp. 481 –84.

[202] A Abdelkefi, W Achour, O. T. Ben, S Ladeb, L Torjman, A Lakhal, H. A. Ben, M Hsairi, and A. A. Ben. "Use of heparin-coated central venous lines to prevent catheter-related bloodstream infection." In: *The Journal of Supportive Oncology* 5 (2007), pp. 273 –78.

[203] C. Pierce, A Wade, and Q Mok. "Heparin-bonded central venous lines reduce thrombotic and infective complications in critically ill children." In: *Journal of Intensive Care Medicine* 26 (2000), pp. 967 –72.

[204] P Appelgren, U Ransjo, and L Bindslev. "Surface heparinization of central venous catheters reduces microbial colonization in vitro and in vivo: results from a prospective, randomized trial." In: *Critical Care Medicine* 24 (1996), pp. 1482 –89.

[205] G. Jain, M. Allon, S. Saddekni, J.-F. Barker, and I. D. Maya. "Does Heparin Coating Improve Patency or Reduce Infection of Tunneled Dialysis Catheters?" In: *Clinical Journal of the American Society of Nephrology* 4 (2009), pp. 1787–1790.

[206] J. L. Laster, W. K. Nichols, and D Silver. "Thrombocytopenia associated with heparin-coated catheters in patients with heparin-associated antiplatelet antibodies." In: *Arch Intern Med* 149 (1989), pp. 2285–2287.

[207] J. Laster and D. Silver. "Heparin-coated catheters and heparin-induced thrombocytopenia." In: *Journal of Vascular Surgery* 7 (1988), pp. 667 –672.

[208] A Abdelkefi, M Chelli, W Achour, N Romdhane, L Torjman, S Ladeb, A Lakhal, M Hsairi, H Kallel, F Ladeb, A. Hassen, and T. Othman. "Catheter Related Bloodstream Infection in Haema-

tological Patients: A Prospective, Randomized Study Comparing Heparin-Coated with Chlorhexidine and Silver Sulfadiazine Impregnated Central Venous Catheters." In: *Acute and Chronic GVHD, Infectious Complications, and Immune Reconstitution Poster I (abstract)* ().

[209] M. Carrasco, A Bueno, C de las Cuevas, S Jimenez, I Salinas, A Sartorius, T Recio, M Generelo, and F Ruiz-Ocaña. "Evaluation of a triple-lumen central venous heparin-coated catheter versus a catheter coated with chlorhexidine and silver sulfadiazine in critically ill patients." In: *Journal of Intensive Care Medicine* 30 (2004), pp. 633 –38.

[210] H. Wang, T. Huang, J. Jing, J. Jin, P. Wang, M. Yang, W. Cui, Y. Zheng, and H. Shen. "Effectiveness of different central venous catheters for catheter-related infections: a network meta-analysis." In: *Journal of Hospital Infection* 76 (2010), pp. 1–11.

[211] K. Marciante. "Which antimicrobial impregnated central venous catheter should we use? Modeling the costs and outcomes of antimicrobial catheter use." In: *American Journal of Infection Control* 31 (2003), pp. 1–8.

[212] A. F. Shorr. "New Choices for Central Venous Catheters: Potential Financial Implications." In: *Chest* 124 (2003), pp. 275–284.

[213] S Saint, D. Veenstra, and B. Lipsky. "The clinical and economic consequences of nosocomial central venous catheter-related infection: are antimicrobial catheters useful?" In: *Infection Control and Hospital Epidemiology* 21 (2000), pp. 375–80.

2

PHOTODISINFECTION OF SURFACES

2.1 PHOTODYNAMIC THERAPY APPROACH

The previous chapter reviewed strategies to decrease the risk of HAIs associated with the use of catheter devices and highlighted that current infection-prevention approaches demonstrate varying efficacies in terms of their antimicrobial activity and impact on associated infection rates. The chapter also detailed further concerns including the potential increase in bacterial resistance where antibiotics are used in prophylaxis approaches and the incidence of severe adverse reactions to infection-prevention strategies using the antiseptic 'chlorhexidine'. Consequently, there is a dire need for the development of new, efficacious antimicrobial surfaces for use in medical device and hospital touch surface applications, with the aim of reducing the risk of hospital-acquired infections.

This chapter details the development of antimicrobial surfaces that kill bacteria through a novel light-activated mechanism. The chapter details the origins of the 'photodynamic reaction' exploited in this antimicrobial strategy, the photophysical processes involved and reviews the development of photosensitiser-based photobactericidal polymers. This chapter provides a foundation for the research detailed in this thesis, which exploits the 'photodynamic reaction' in the development of light-activated antimicrobial polymers with incorporated photosensitiser dyes and nanoparticles, that kill bacteria through the photo-generation of cytotoxic species.

2.1.1 *Photodynamic Therapy; A Brief History*

In the beginning of the 20th century, a lethal, light-activated bactericidal technique; photodynamic therapy (PDT), was pioneered [1]. Oskar Raab first observed the phototoxicity of acridine hydrochloride

against *Paramecia caudatum* [1–3] and further investigation into this phenomenon by his supervisor, Hermann von Tappeiner, confirmed that the deactivation of bacteria was not a consequence of heat, but rather a light-activated effect, a "photodynamic reaction" [1, 4, 5]. Since the discovery of this photodynamic reaction, much research effort has been invested into the utilisation of PDT, particularly in applications related to tumour detection [2, 6–10] and tumour photodestruction [2, 11–16]. However, until recently, photodynamic antimicrobial therapy has been less well studied [17].

The use of PDT as a powerful antimicrobial tool was abandoned upon the discovery of antibiotics such as penicillins around 60 years ago, as antibiotics were found to possess antibacterial therapeutic effectiveness [1, 18–20]. However, with the accelerating rise in bacterial drug resistance [19], recently there has been much research

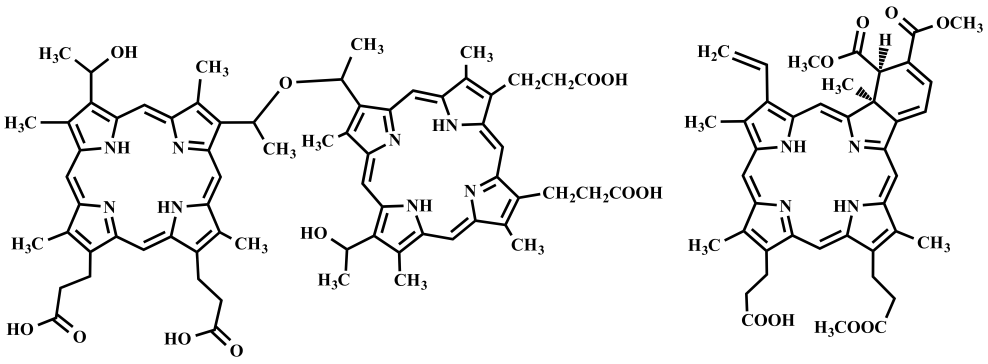

Figure 3: Chemical structures of examples of tetrapyrrole-based and non-tetrapyrrole based photosensitiser molecules

into the development of alternative anti-infective strategies. These include the use of organic photosensitisers or inorganic nanoparticles (TiO_2) in PDT [21] to treat localised infection [22] and to effect the photocatalytic destruction of bacteria for example on glass surfaces [23, 24], polymer surfaces [25–33] and titania surfaces [34–36], to reduce the prevalence of microbial contamination.

2.1.2 *The Use of Photosensitiser Molecules in PDT*

Photosensitisers used in PDT are commonly heterocyclic ring type structures, as exampled in Figure 3, that demonstrate low toxicity in the dark, but which generate cytotoxic species upon photo-activation in the presence of oxygen [37, 38]. These photosensitive compounds can be sub-categorised under (i) porphyrin-based and (ii) chlorophyll-based structures, in addition to (iii) dye molecules [38].

The photoprocesses that occur upon excitation of photosensitiser dye molecules, shown in Figure 4, are as follows. Upon illumination, typically with laser light of a wavelength correlating to the absorbance peak maximum, the photosensitiser molecule is promoted to an excited singlet state, after which it undergoes a radiationless process, an intersystem crossing, to a lower energy, longer lifetime triplet state [2]. This triplet state can undergo one of two photochemical processes namely, a Type I (electron transfer) or a Type II (energy transfer) photoprocess [2, 37]. The Type I photochemical pathway involves the interaction of the triplet state with substrate molecules, for example biomolecules, generating a wide range of reactive oxygen species (ROS) such as superoxide anions and hydroxyl radicals, in addition to other radicals [1, 2]. The triplet state can also undergo a Type II photoprocess in which it is quenched through collision with molecular oxygen in the environs, generating the highly reactive, transient species, singlet oxygen, which subsequently forms adducts with organic substrate molecules [1, 2]. The triplet state species of the excited photosensitiser can interact with molecular oxygen, since it has a triplet state ground state and low lying excited states and this interaction between the two triplet states results in the production of

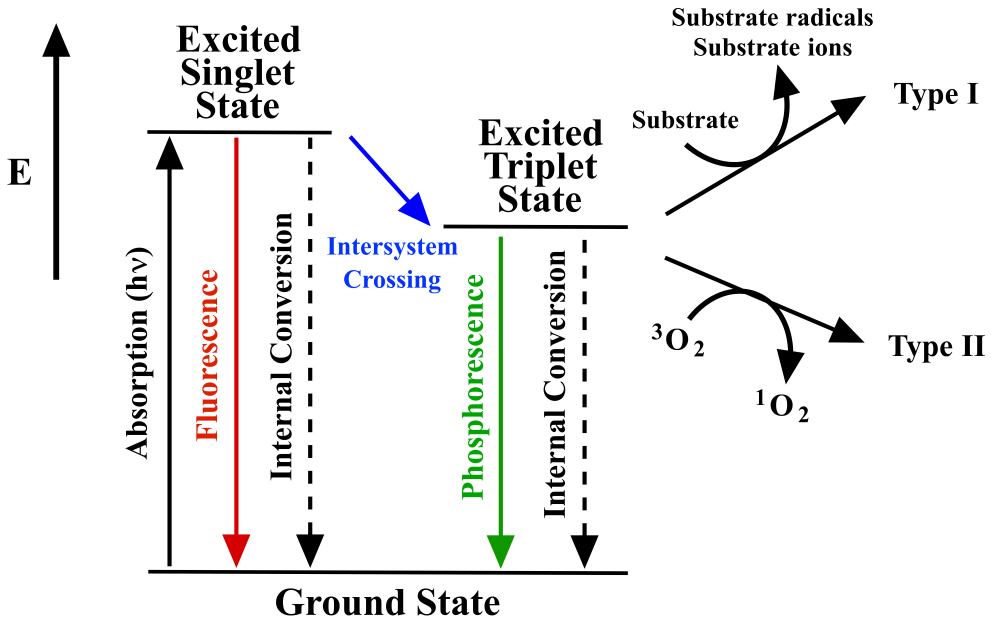

Figure 4: Jablonski diagram representing processes involved in photodynamic therapy. The ground state photosensitiser molecule absorbs a photon of energy and is promoted to an excited singlet state. The excited singlet state molecule can release energy radiatively (fluorescence), via internal conversion or can undergo an intersystem crossing to the excited triplet state. The triplet state molecule can release energy as radiation (phosphorescence) or transfer its energy to surrounding molecules by either Type I or Type II photoprocesses and return to the ground state. A Type I photoprocess involves the interaction of the triplet state dye with substrate molecules in the vicinity, resulting in their oxidation and a Type II photoprocess involves the quenching of the triplet state by molecular oxygen

singlet oxygen, a low energy triplet-singlet transition in oxygen of ~ 22 kcal mol^{-1} [2]. The ROS generated upon the irradiation of the photosensitiser molecule can subsequently initiate a multi-site attack mechanism against cellular membranes, intracellular proteins and DNA of bacteria in the vicinity, rendering the likelihood of the incidence of resistance, improbable [18, 28, 39]. Multi-site attack reduces the likelihood of resistance as multiple mechanisms of resistance will have to occur simultaneously in the same microorganism.

The generation of ROS such as the cytotoxic singlet oxygen species, gives rise to the potential for the utilisation of photosensitisers in antimicrobial PDT applications. However, an important factor for consideration is the selectivity of the photosensitising agent towards bacterial cells. Studies demonstrated that antimicrobial PDT regimes

sufficient to cause the efficacious photosensitisation of the bacteria tested, did not result in a similar cytotoxicity towards mammalian cells [40–43]. It was found that photosensitiser concentrations and illumination time-periods that effectively reduced bacterial levels, did not damage mammalian cells [40, 41, 43]. Moreover, the photo-kill rates of human keratinocyte cells was on average 200-fold slower than cutaneous prokaryotic bacteria and 18-fold lower than *Candida* species tested previously, using the same irradiation conditions [42, 44]. However, it was noted that exposure to higher photosensitiser concentrations did impact on the survival rate of human fibroblasts and keratinocytes [41]. In addition, lengthier irradiation times (> 90 minutes) affected the ability of mammalian cell recovery (48 %), implying a greater likelihood of irreversible keratinocyte cell damage [42]. Nevertheless, these more rigorous conditions far surpass those required for the effective photosensitisation of the bacteria tested and thus, it can be suggested that PDT conditions that efficaciously eradicate bacteria are not expected to cause irreversible damage to surrounding host cells.

Although the discovery of the "photodynamic reaction" was associated with bacterial photoinactivation [1], initial intensive research relating to PDT used this technique for tumour detection and photodestruction [2]. Many of the photosensitisers examined for the treatment of tissue disease and cancers, such as the porphyrin-based Photofrin^{TM}, chlorophyll-based chlorins and bacteriochlorins and so forth, are based on a tetrapyrrole nucleus type structure [37, 38]. The use of PDT can result in the rapid destruction of tumours, however, damaged healthy tissue efficiently recovers over the course of 6 - 8 weeks after treatment [45]. It has also been noted that some photosensitisers preferentially accumulate in tumour tissues as opposed to normal surrounding tissues and this can be used to help deliver a sufficient concentration of photosensitiser to target cells for PDT, without causing unnecessary photodamage to normal tissue [16, 45]. PDT has also been considered for and utilised in many other medical applications, including as a strategy to treat Barrett's oesophagus [37, 46], a treatment for age-related macular degeneration [37, 47, 48] and also as a potential therapeutic measure for psoriasis, although

adverse associated side effects such as burning sensations and pain have been reported [1, 37, 49, 50].

Many of the photosensitiser molecules used in PDT cancer therapies are porphyrin- or chlorin- based structures, however, there are many photosensitisers with different molecular structures, for example, photosensitiser dyes which are used in antimicrobial PDT for the lethal photosensitisation of microorganisms [37]. Numerous studies have examined the use of planar tri-heterocyclic photosensitiser dye molecules, including phenothiazines such as toluidine blue O [51, 52], halogenated xanthenes such as rose bengal [53] or acridines [20, 54], to effect the lethal photosensitisation of bacteria [37]. Trials investigating the use of PDT to treat bacterial wound infections caused by both Gram-positive and Gram-negative bacteria have proven successful in animal models [1, 22, 55–61]. Moreover, although in one study it was reported that a strain of *Candida glabrata* was insensitive to PDT under the conditions used [62], overall, the results of *in-vitro* investigations demonstrated that some *Candida* sp. are susceptible to photosensitisation and the use of PDT may be a promising alternative to current fungicidal strategies to treat infections [62–65]. The use of methylene blue-mediated PDT has also shown promising results in an *in-vivo* study using mice models, in the treatment of oral candidiasis [63].

PDT has been exploited for dentistry related applications including oral cancer therapies, in addition to the treatment of bacterial and fungal oral infections [1, 22, 66]. Toluidine blue-mediated PDT resulted in the photo-inactivation of *Porphyromonas gingivalis*, a bacteria considered to be a leading cause of periodontitis in adults, in a rat model [67]. Further *in-vivo* studies employing rat models [68–72] or a beagle dog model [73] of periodontal disease, demonstrated the therapeutic efficacy of PDT in the treatment of periodontitis, both alone [70, 71, 73] and as an adjuvant treatment to mechanical scaling and root planing methods [68, 69, 72]. Pre-clinical trials have indicated potential advantages in the utilisation of PDT to treat periodontal disease and recently there have been some small-scale clinical trials ($\leqslant$ 24 patients) [22, 74–77], to determine whether this

beneficial effect is demonstrated in actual clinical applications.

Clinical trials indicated conflicting results with regard to the overall benefit of using PDT in combination with mechanical scaling and root planing methods to treat periodontal disease [74–77]. In two trials it was found that as an adjunctive method, a single episode of PDT failed to enhance the effects of scaling and root planing strategies in patients with chronic periodontitis in terms of "probing depth" reduction and "clinical attachment level" gain, however, it was noted that there was a statistically substantial reduction in "bleeding scores" [74, 75]. Conversely, a different study indicated that the use of adjunctive PDT proved efficacious in the treatment of patients with chronic periodontitis [76]. Although PDT was reported to be well tolerated in patients and is a less time consuming treatment strategy than implemented scaling and root planing methods, further clinical trials are vital in order to determine whether the use of adjunctive PDT is beneficial in the clinical treatment of periodontal disease [77].

Despite the inconsistencies in the small-scale clinical trials conducted, currently there is much industry research interest into the use of antimicrobial PDT to treat dental infections. Three companies: Ondine Biopharma (North America), HELBO Photodynamic Systems (Austria) and Denfotex (United Kingdom), are involved in clinical trials and the commercialisation of PDT therapies, including those for the treatment of periodontitis [22]. Ondine Biopharma have developed Periowave^{TM}, a system to be used in conjunction with scaling and root planing methods, for the photodestruction of remaining oral bacteria [78]. Ondine Biopharma have instigated 5 clinical trials to evaluate the validity and safety of this antimicrobial strategy and the system, which utilised the photosensitiser methylene blue in combination with a 660 nm laser device, has been used in over 75,000 treatments and is currently available in Canada, Korea, Mexico and the U.K. [22, 78, 79]. Ondine Biopharma have also invested research power into the development of PDT systems for chronic sinusitis (Sinuwave^{TM}), nasal bacterial decolonisation (MRSAid^{TM}), the photo-sterilisation of endotracheal tubes in mechanically ventilated patients (Exelume^{TM}) and the decolonisation of the birth

canal to prevent transmission of HIV and other pathogens in third world countries (Vitalwave^{TM}) [78]. HELBO Photodynamic Systems and Denfotex have also developed light-activated oral disinfection systems employing another phenothiazine dye toluidine blue O, in combination with a 635 nm red laser light system, for the potential treatment of periodontitis and endodontic infections [22, 80, 81].

Overall, PDT utilising photosensitiser molecules has exhibited a promising efficacy in *in-vitro* and *in-vivo* investigations for the lethal photosensitisation of pathogenic microorganisms. The demonstrated antimicrobial efficacy can be further exploited through the fixation of these molecules in polymeric materials, such that the resultant modified materials are theoretically self-sterilising.

2.2 SELF-STERILISING POLYMERS

2.2.1 *The Role of Surfaces in Hospital-Acquired Infection*

It has been estimated that in ICUs of U.S. hospitals, the endogenous microbiota of patients is a key source of pathogens, associated with approximately 40 - 60 % of nosocomial infection [82, 83]. Surfaces in healthcare environments have been acknowledged as potential reservoirs of bacteria associated with the incidence of HAIs [84] and it is likely that hands of healthcare workers become contaminated from direct patient contact, or from exposure to colonised hospital surfaces. These surfaces act as reservoirs of bacteria and constant contact by healthcare personnel between these surfaces and patients aid the transfer of bacteria and facilitate the spread of infection within healthcare institutions [84, 85]. The transmission of bacteria such as MRSA *via* person-person contact may not cause serious health complications outside a clinical environment, but in a healthcare setting in which there are immunocompromised patients, this simple transmission of bacteria between healthcare personnel and patients, may result in morbidity [86]. Although rigorous cleaning regimes are enforced, it is difficult to prevent the contamination of touch surfaces in hospitals and despite promotion of healthcare worker

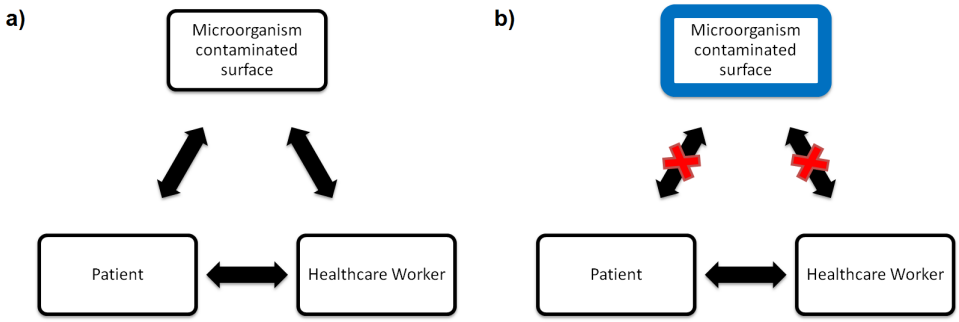

Figure 5: The role of surfaces in the transmission of hospital infection. (a) Cycle of bacterial transfer from surfaces to patients. (b) Disruption of cycle due to the use of an antimicrobial surface

hygiene protocols, in heavily contaminated areas, hand washing may be ineffectual [84]. Studies have demonstrated bacterial colonisation of a variety of hospital surfaces including: X-ray cassettes, door handles, mops, telephones, computers and keyboards, taps, pens, stethoscopes, sterile packaging and so forth [84, 87–94]. Evidence also suggests that the resilient spores of *C. difficile* contaminate hospital surfaces and medical equipment, with contamination persisting for extensive durations of up to 5 months, in an unused hospital room [85, 95, 96]. Similarly, both methicillin-susceptible *S. aureus* and MRSA have demonstrated longevity despite desiccation, under varying experimental conditions [84, 85, 97]. Bacterial contamination of hospital touch surfaces is extremely prevalent and can cause potentially avoidable infections. One strategy to reduce hospital contamination is the use of self-sterilising surfaces (Figure 5). By utilising an antimicrobial surface, the transmission of bacteria from surfaces to patients and from surfaces to healthcare workers is disrupted and may result in a decrease in the spread of associated infection in healthcare environments.

To prevent the spread of HAIs through direct contact, these microbial reservoirs need to be targeted. Consequently, the development of antimicrobial coatings for surfaces, or the modification of materials such that they demonstrate bactericidal properties, may play an important role in decreasing the incidence of HAIs, through inhibiting the cycle of the transference of microorganisms from patient to healthcare worker to surface and so forth, acting to enhance routine

cleaning regimes [84].

2.2.2 *Porphyrin-Based Light-Activated Antimicrobial Polymers*

One approach by which this can be achieved is through the development of light-activated antimicrobial surfaces incorporating photosensitisers, that continually and effectively self-clean [98–102]. The utilisation of photosensitisers is advantageous since they effect a non site-specific, multi-site attack against microorganisms in the vicinity, hence rendering the development of bacterial resistance unlikely [37, 103]. Porphyrin-based compounds have demonstrated the photosensitisation of pathogenic microorganisms upon visible light irradiation [102] and although the photochemical activity can effect changes in the structure of the photosensitiser, it has been noted that the predominant photodegradation products are stable with respect to subsequent "self-sensitised photooxygenation" and exhibit a good Type II photochemical activity [102, 104]. Porphyrin-based photobactericidal materials have been developed by grafting porphyrin-based compounds onto nylon fibres [102] and alkylated cellulose [105].

Protoporphyrin IX and zinc protoporphyrin IX were grafted on to nylon fibres to form light-activated antimicrobial materials which effected the photo-inactivation of *S. aureus*, although it should be noted that the zinc protoporphyrin IX sample showed a more potent antimicrobial efficacy [102]. Moreover, the zinc protoporphyrin IX grafted nylon sample exhibited some antimicrobial activity against *E. coli*, but only upon irradiation with light intensities of greater than 60,000 lux [102]. These porphyrins have also been grafted on to nylon films, although the resultant photo-activated antimicrobial activity was not reported [106]. In a different study, the covalent attachment of porphyrin compounds to cellulose polymers via a "one-pot, two-step" esterification reaction to form photo-activated bactericidal films, was reported [105]. The photobactericidal films synthesised demonstrated antimicrobial activity against both Gram-positive bacteria (*S. aureus*) and Gram-negative bacteria (*E. coli*), upon illumination with a visible

light source and it was speculated that the photochemical activity proceeded via a Type II pathway [105]. The potential use of these photoactive bactericidal materials in healthcare institutions, may help decrease the prevalence of microbial surface contamination, particularly by Gram-positive bacteria [102].

2.2.3 *Phenothiazine-Based Photobactericidal Polymers to Coat Surfaces*

Phenothiazine photosensitiser dyes such as methylene blue, toluidine blue O and rose bengal have also been used to develop photo-activated bactericidal materials [25, 26, 28, 29, 98–101]. New methylene blue, which has been documented to effect cell death as well as the photodestruction of a *P. aeruginosa* biofilm on silicone tubing [107], was incorporated into polymer resins and the antimicrobial activity of the resultant copolymer films was tested against both Gram-positive and Gram-negative bacteria [101]. It was found that the antimicrobial activity was dependent upon the composition of the copolymer films, the concentration of the photosensitiser present, in addition to the light dose received [101]. The photo-activated antimicrobial activity of methylene blue-containing styrene-butadiene films was greater than that observed for the corresponding polyacrylic ester films and overall, higher concentrations of photosensitiser and greater light dose energy led to greater lethal photosensitisation of bacteria [101]. Moreover, in all cases, the demonstrated antimicrobial activity of the photobactericidal films was more effective against the Gram-positive bacterium *S. epidermidis*, than the Gram-negative bacterium *E. coli* [101].

Toluidine blue O was incorporated into cellulose acetate, for use as an antimicrobial paint on surfaces [33, 98–100]. Toluidine blue O incorporated cellulose acetate demonstrated promising light-activated antimicrobial activity against MRSA and *P. aeruginosa*, with bacterial kills of the order 10^5 cfu /cm^2 over a 24 hour period of white light illumination (60-W domestic lamp bulb); adequate to maintain low levels of microbial contamination on surfaces in occupied hospital rooms [98]. Subsequent studies involved the incorporation of a com-

bination of photosensitiser dyes, rose bengal and toluidine O, into cellulose acetate, to maximise the absorption of light over the visible spectral range [33, 99, 100] and enhance the lethal photosensitisation of bacteria.

When illuminated with a white light source (28-W fluorescent lamp) for periods ranging from 2 hours to 16 hours, the cellulose acetate coating incorporated with rose bengal and toluidine blue O achieved the photoinactivation of a range of microorganisms including *S. aureus*, MRSA, *C. difficile*, *E. coli* and *C. albicans* under laboratory conditions [99]. *C. albicans* was found to be the least susceptible to photosensitisation using this system, with an 88 % reduction in viable yeast after 16 hours irradiation [99]. It was also noted that the Gram-negative bacterium *E. coli* was less sensitive to photosensitisation than the Gram-positive bacteria tested, however, 100 % kills were achieved upon exposure to the dye-incorporated surface irradiated with white light for 16 hours [99].

When irradiated with a white light source for 6 hours, there was a significant reduction in the viable count of *S. aureus* deposited on the photosensitiser-incorporated cellulose acetate coating, although the efficacy of bacterial photoinactivation was found to be dependent on the fluid the bacteria was suspended in [100]. The reduction in viable bacterial counts was greatest when the *S. aureus* was suspended in PBS (99.8 % kill), with decreased activity demonstrated when aerosols in human saliva and horse serum were used (97.6 % and 78.9 % kill respectively) [100]. Significant kills were also observed when photosensitiser-free cellulose acetate coatings inoculated with *S. aureus* were illuminated, although the photoinactivation of bacteria on these surfaces was less potent than in the presence of the photosensitiser dye [100, 108]. This interesting finding may be accounted for by the reported presence of an endogenous photosensitiser in *S. aureus*, which is activated when irradiated by light with a wavelength of 632 nm [33].

The antimicrobial activity of toluidine blue O and rose bengal incorporated cellulose acetate coatings under the settings of a clinical

environment was evaluated, to determine whether they effected any reduction in surface contamination [33]. The study was conducted over a period of 24 hours and a compact fluorescent lamp was used to irradiate the dye incorporated coatings [100]. Despite demonstrating a lesser antimicrobial efficacy than in previous laboratory investigations [33], the toluidine blue O and rose bengal incorporated cellulose acetate coatings induced the lethal photosensitisation of bacteria prevalent in the clinical environment [33]. Moreover, due to the negligible leaching of the photosensitiser dyes once incorporated in the coatings, concerns relating to photosensitiser phototoxicity should not arise, in potential applications to reduce surface contamination in clinical environments [33].

2.2.4 *Incorporation of Photosensitiser Dyes into Medical Grade Polymers*

A simple dipping method was used to coat medical devices such as endotracheal tubes and catheters with the antiseptic chlorhexidine, in combination with triarylmethane dyes for example, gentian violet and brilliant green [109–113]. Although the light-activated antimicrobial properties of these materials were not explored, *in-vitro* investigations highlighted the inherent bactericidal properties of the medical devices coated with the broad-spectrum antiseptic combination [109–111]. These coated samples demonstrated non-photoactivated anti-adherence properties against *Candida* species [109–111], as well as against a range of bacteria including MRSA [110], *P. aeruginosa* strains, vancomycin-resistant *Enterococcus* and *E. coli* strains [110, 111]. The gentian violet/ chlorhexidine-coated surfaces also helped prevent biofilm formation [111]. A further study demonstrated that endotracheal tubes coated with either the brilliant green/ chlorhexidine combination or the gentian violet/ chlorhexidine combination prevented device biofilm formation of *P. aeruginosa*, MRSA, *Enterobacter cloacae*, *K. pneumoniae* and *Acinetobacter baumannii*, in addition to *C. albicans*, demonstrating superiority in terms of their efficacy at inhibiting biofilm formation, in comparison to commercially available silver catheters [112]. Recent research has also shown that the use of gentian violet/ chlorhexidine antimicrobial cuffed

endotracheal tubes effectively prevented microbial proliferation and transmission, in an *in-vitro* model [114]. However, concerns regarding potential chlorhexidine irritation need to be further investigated in *in-vivo* studies [114].

Much research effort has been invested into the use of a simple solvent-facilitated dipping technique, a "swell-encapsulation-shrink" approach, to incorporate a range of photosensitiser dyes into medical grade polymers [25, 26, 28–31]. This strategy exploits the finding that biomaterials such as silicone, swell when exposed to certain solvents [25, 26, 28–31]. Consequently, polymers immersed in solutions of solvated photosensitisers swell enabling the diffusion of the dye molecules throughout the polymeric matrix [25, 26, 28–31]. After removal from the swelling solution, any trapped residue solvent within the swollen polymer evaporates and it shrinks to its original size, resulting in strongly coloured dye-encapsulated polymer sections [25, 26, 28–31].

The dye-encapsulated polymers prepared using this "swell-encapsulation-shrink" technique induced the lethal photosensitisation of both planktonic Gram-positive and Gram-negative bacteria, when illuminated with either white light [31] or a laser light source of an appropriate wavelength [25, 26, 28–30]. Reports suggested that methylene blue solutions also demonstrated a dark toxicity against some tested *S. aureus* and MRSA strains [27, 115, 116]. However, dye-encapsulated polymers kept in the dark demonstrated no bactericidal activity against either the Gram-positive or Gram-negative bacteria tested [25, 26, 28–31]. This discrepancy can be attributed to the far greater concentrations of dye that were used in solution studies, compared to the dye concentrations that were encapsulated into the polymeric materials investigated [27, 115, 116]. These studies also showed that despite the fact that the gold nanoparticles used had no intrinsic antimicrobial properties when in aqueous solution, the presence of gold nanoparticles significantly enhanced the photosensitisation of bacteria by toluidine blue O [117].

In contrast to the results of solution studies [117], the additional incorporation of 2 nm gold nanoparticles did not enhance the light-activated antimicrobial activity demonstrated by the toluidine blue O encapsulated polymers when tested against *E. coli* and in fact, the presence of gold nanoparticles reduced the potency of the photosensitisation effects of the material [28]. However, some minimal enhancement in the photo-activity of toluidine blue O was noted when toluidine blue O and gold nanoparticle encapsulated polymers were tested against *S. aureus* [28]. It was also noted that toluidine blue O encapsulated polyurethane (with and without gold nanoparticles) exhibited a more efficacious bactericidal activity than corresponding silicone samples [28]. This can be attributed to a greater uptake of the photosensitiser dye into the polyurethane, resulting in a larger yield of cytotoxic singlet oxygen species upon photoactivation [28]. When tested against MRSA, all viable bacterial counts decreased below the detection limit upon irradiation of the samples with red laser light for < 2.5 minutes, whether nanogold was present or not [28]. However, in a similar study in which a white light source was used to activate the dye, a 0.5 log enhancement in the bacterial kill was noted when polyurethane samples were encapsulated with toluidine blue O in addition to 2 nm gold nanoparticles, when the samples were tested against *S. aureus* [31].

Studies showed that polymers encapsulated with another phenothiazine dye, methylene blue, in addition to 2 nm gold nanoparticles, demonstrated an enhanced light-activated antimicrobial activity against Gram-positive and Gram-negative bacteria, compared to those encapsulated with methylene blue only [25, 26, 31]. The properties of gold nanoparticles are size dependent and particles greater than 4 nm demonstrate a phenomena termed 'surface plasmon resonance', which results in strong nanoparticle colouration [25]. Therefore, the effect of the varying the diameter of the gold nanoparticles on the photobactericidal activity of the methylene blue/ nanogold-encapsulated silicone sample was investigated [26]. It was found that the incorporation of 20 nm gold nanoparticles reduced the light-activated antimicrobial activity of the methylene blue embedded silicone polymer, when tested against both the Gram-

positive bacterium and Gram-negative bacterium *S. epidermidis* and *E. coli* respectively [26]. The presence of 5 nm gold nanoparticles did not dramatically improve the light-activated antimicrobial activity of methylene blue encapsulated silicone polymers when tested against *E. coli* [26]. However, a significant enhancement was observed when tested against *S. epidermidis* [26]. Conversely, the incorporation of 2 nm gold nanoparticles - below the size limit for the occurrence of surface plasmon resonance - significantly enhanced the bactericidal activity of methylene blue embedded silicone against MRSA, *S. epidermidis* and *E. coli*, when irradiated with red laser light [25, 26].

Silicone encapsulated with 2 nm gold nanoparticles only, did not demonstrate any antimicrobial activity against *E. coli* or MRSA [25]. This indicates that the 2 nm gold nanoparticles embedded in the silicone polymer do not exhibit any direct toxicity against either the Gram-positive or the Gram-negative bacteria tested [25]. It has been speculated that the enhancement in photobactericidal activity may be dependent upon the wavelength of light used to activate the dye, as this may affect the interaction of the nanoparticle and photosensitiser [28]. Alternatively, the dye-nanoparticle interaction may influence the photochemical pathway the dye undergoes, impacting on the distributions of ROS generated [28, 31]. In addition, fluorescence studies have indicated that dye fluorescence is suppressed when nanogold is present [117, 118], which correlates with time-resolved electron paramagnetic resonance spectroscopy studies, which showed that the presence of nanogold results in increased dye triplet state production in methylene blue encapsulated PVC catheters [30]. This enhancement in dye triplet state production may ultimately lead to the generation of a greater concentration of ROS. However, as yet, there is no definite explanation as to why the presence of 2 nm gold nanoparticles effects a synergistic enhancement in the photosensitisation of bacteria on methylene blue- and toluidine blue O- embedded polymers.

This chemistry has been geared towards the development of self-sterilising polymers for medical devices such as catheters (Figure 6) [27, 30], although the potent lethal photosensitisation demonstrated

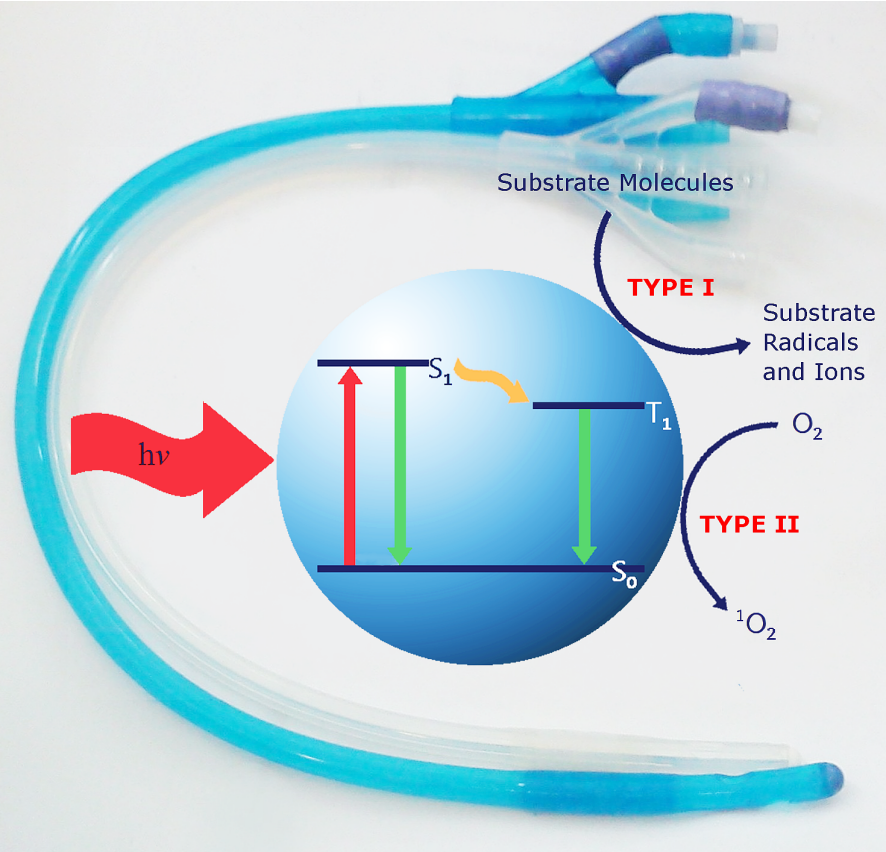

Figure 6: Methylene blue-encapsulated silicone catheter prepared using a swell-encapsulation shrink approach, compared to standard untreated silicone catheter, with a diagrammatic representation of the mechanism of antimicrobial activity upon light-activation

upon white light activation indicates that this technology is not limited to device-related applications. Pre-clinical studies indicated that silicone encapsulated with methylene blue and 2 nm gold nanoparticles effectively reduced *S. epidermidis* biofilm formation under specific laser irradiation regimes [27]. The experiments were performed using a flow cell and polymer samples received a constant energy dose of laser irradiation in situ, with varying irradiation times and frequency [27]. Irradiation conditions were preliminarily optimised to maximise the efficacy of the photocatalytic prevention of *S. epidermidis* biofilm formation on the modified polymer sample [27]. It was found that hourly 10 minute laser irradiation of the methylene blue and 2 nm gold nanoparticle embedded polymer resulted in a more than 50 % decrease in surface biofilm coverage, compared to untreated silicone elastomer control samples [27]. Live-dead staining indicated that in both the control and treated samples,

nearly all the bacterial cells attached to the polymeric surface were alive, irrespective of the laser irradiation, although laser irradiation significantly reduced biofilm coverage on the treated surface [27]. Consequently, it can be speculated that the ROS produced on the irradiated methylene blue-nanogold embedded surface damage the external structures such as the adhesion proteins and pili on the bacterial cells, impacting on their ability to maintain attachment to the polymer surface [27]. This may contribute to the reduction of bacterial surface contamination and efficacious prevention of *S. epidermidis* biofilm formation exhibited by the irradiated methylene blue-nanogold embedded silicone in this study [27].

The tribological performance of untreated polymers (exposed to the solvent treatment used in the swell-encapsulation-shrink process) and polymers encapsulated with toluidine blue O and 2 nm gold nanoparticles, was evaluated using the surfaces of both the vena cava and the inner part of the aorta of a sheep [119]. These further studies demonstrated that neither solvent exposure, nor the encapsulation of toluidine blue O and 2 nm gold nanoparticles, changed the static and kinetic friction coefficients of polyurethane and silicone polymers [119]. This finding holds promise for the potential use of this antimicrobial technology in medical applications, since patient comfort during catheter manipulation and catheterisation, in addition to potential tissue damage caused by friction, is a key concern with regard to the suitability of the material in clinical applications [119].

Reports indicated a change in the Young's modulus of both the silicone and polyurethane polymers upon exposure to the solvent treatment, although there was no significant further change upon encapsulation of the dye or the dye and nanogold combination [25, 28]. However, an investigation into the effect of laser light on the methylene blue and 2 nm gold nanoparticle embedded silicone polymeric surfaces demonstrated that there is no change in the elasticity of the material upon irradiation [27]. Moreover, although the experimental set-up only facilitated relative polymer deformations no greater than five times its initial length, it is unlikely that polymer stretching of this magnitude occurs during normal catheter use and

manipulation [27]. Thus, since no change in the breaking point was noted within the experimental constraints, it can be concluded that even if the polymer becomes more brittle upon laser irradiation, it should not affect its function in medical applications [27].

A further potential concern regarding the use of implanted medical devices embedded with photosensitiser dyes, is the toxicity of generated ROS towards host cells upon photoactivation. Despite its cytotoxicity, in a physiological environment, the half-life of the ROS singlet oxygen is shorter than 1 μs, with a reported diffusion distance of 10 - 100 nm [25]. Therefore, it is unlikely that the singlet oxygen will diffuse far enough to reach host tissue cells near the catheter device [25]. In addition, epithelial tissue in the vicinity of the implanted device is a continually shedding surface and hence, if in the unlikely event, singlet oxygen effected damage to surrounding epithelium cells, this would be a short-term effect as the cells would merely be "shed" and "replaced" [25]. Consequently, the toxicity of ROS towards host cells should not be problematic in the potential use of photosensitiser encapsulated devices in clinical applications.

It is hoped that this novel antimicrobial material in combination with a simple laser system can be utilised in the development of a range of photobactericidal polymeric medical devices including catheters, endotracheal tubes, stents and so forth. Ultimately, this may help decrease the prevalence of infection associated with their use, through the photosensitisation of bacteria contaminating the device surfaces and the subsequent prevention of biofilm accumulation.

2.3 RESEARCH AIMS

This thesis focuses on the photoinactivation of bacteria on surfaces, primarily through the use of organic photosensitiser dye molecules. The development of coatings synthesised through the incorporation of photosensitiser dye molecules and nanoparticles into polymeric materials, will be examined and their antimicrobial efficacy will be evaluated. Ultimately, the focus of this thesis is geared towards

the introduction of light-activated antimicrobial agents into medical grade polymers, for example silicone, such that these modified polymeric surfaces demonstrate efficacious photo-activated self-sterilising properties. An exploration into the mechanistic detail of the photochemical activity will be achieved, with the aim to shed light on the interaction between the polymer immobilised photosensitiser dyes and nanoparticles. It is hopeful that these surfaces can be used in healthcare applications, to reduce microbial surface contamination and subsequently, decrease the risk of healthcare-associated infections.

REFERENCES

[1] T. Maisch. "Anti-microbial photodynamic therapy: useful in the future?" In: *Lasers in Medical Science* 22 (2007), pp. 83–91.

[2] I. J. MacDonald and T. J. Dougherty. "Basic principles of photodynamic therapy." In: *Journal of Porphyrins and Phthalocyanines* 5 (2001), pp. 105–129.

[3] O. Raab. "Ueber die Wirkung fluorizierender Stoffe auf Infusorien." In: *Z Biol* 39 (1900), pp. 524–546.

[4] H. von Tappeiner. "Zur Kenntnis der lichtwirkenden (fluoreszierenden) stoffe." In: *Dtsch Med Wochenschr* 1 (1904), pp. 579–580.

[5] H. von Tappeiner and A Jodlbauer. "Uber die wirkung der photodynamischen (fluoreszierenden) stoffe auf infusorien." In: *Dtsch Arch Klin Med* 80 (1904), pp. 427–487.

[6] A. Policard. "Etudes sur les aspects offerts par des tumeurs experimentales examinee a la lumiere de Woods." In: *Compt. Rend. Soc. Biol.* 91 (1924), pp. 1423 –1424.

[7] F. Ronchese. "The fluorescence of cancer under the Wood light." In: *Oral Surgery Oral Medicine Oral Pathology Oral Radiology and Endodontics* 7 (1954), pp. 967–971.

[8] F. H. J. Figge, G. S. Weiland, and L. O. J. Manganiello. "Cancer detection and therapy - affinity of neoplastics, embryonic, and traumatized tissues for porphyrins and metalloporphyrins." In: *Proceedings of the Society for Experimental Biology and Medicine* 68 (1948), pp. 640–641.

[9] D. S. Rasmussen-Taxdal, G. E. Ward, and F. H. Figge. "Fluorescence of human lymphatic and cancer tissues following high doses of intravenous hematoporphyrin." In: *Surgical forum* 5 (1955), pp. 619–24.

[10] J. Winkelman. "The distribution of tetraphenylporphinesulfonate in the tumor-bearing rat." In: *Cancer Research* 22 (1962), pp. 589–596.

[11] T. J. Dougherty. "Activated dyes as antitumor agents." In: *Journal of the National Cancer Institute* 52 (1974), pp. 1333–1336.

[12] K. R. Weishaupt, C. J. Gomer, and T. J. Dougherty. "Identification of singlet oxygen as the cytotoxic agent in photoinactivation of a murine tumor." In: *Cancer Research* 36 (1976), pp. 2326–2329.

[13] T. J. Dougherty. "A brief history of clinical photodynamic therapy development at Roswell Park Cancer Institute." In: *Journal of clinical laser medicine & surgery* 14 (1996), pp. 219–21.

[14] T. J. Dougherty, J. E. Kaufman, A. Goldfarb, K. R. Weishaupt, D. Boyle, and A. Mittleman. "Photoradiation therapy for treatment of malignant-tumors." In: *Cancer Research* 38 (1978), pp. 2628–2635.

[15] T. Dougherty, G. Grindey, R. Fiel, K. Weishaupt, and D. Boyle. "Photoradiation therapy II. Cure of animal tumors with hematoporphyrin and light." In: *J. Nati. Cancer Inst.* 55 (1975), pp. 115 –121.

[16] R. Allison, K. Moghissi, G. Downie, and K. Dixon. "Photodynamic therapy (PDT) for lung cancer." In: *Photodiagnosis and Photodynamic Therapy* 8 (2011), pp. 231–239.

[17] M. Wainwright. "Photodynamic antimicrobial chemotherapy (PACT)." In: *Journal of Antimicrobial Chemotherapy* 42 (1998), pp. 13–28.

[18] S. Noimark, C. W. Dunnill, M. Wilson, and I. P. Parkin. "The role of surfaces in catheter-associated infections." In: *Chemical Society Reviews* 38 (2009), pp. 3435–3448.

[19] P. M. Hawkey. "The growing burden of antimicrobial resistance." In: *Journal of Antimicrobial Chemotherapy* 62 (2008), pp. i1–i9.

[20] M. Wainwright. "Acridine - a neglected antibacterial chromophore." In: *Journal of Antimicrobial Chemotherapy* 47 (2001), pp. 1–13.

[21] S. Perni, P. Prokopovich, J. Pratten, I. P. Parkin, and M. Wilson. "Nanoparticles: their potential use in antibacterial photodynamic therapy." In: *Photochemical & Photobiological Sciences* 10 (2011), pp. 712–720.

[22] T. Dai, Y.-Y. Huang, and M. R. Hamblin. "Photodynamic therapy for localized infections-State of the art." In: *Photodiagnosis and Photodynamic Therapy* 6 (2009), pp. 170–188.

[23] C. W. Dunnill, K. Page, Z. A. Aiken, S. Noimark, G. Hyett, A. Kafizas, J. Pratten, M. Wilson, and I. P. Parkin. "Nanoparticulate silver coated-titania thin films-Photo-oxidative destruction of stearic acid under different light sources and antimicrobial effects under hospital lighting conditions." In: *Journal of Photochemistry and Photobiology a-Chemistry* 220 (2011), pp. 113–123.

[24] Z. A. Aiken, G. Hyett, C. W. Dunnill, M. Wilson, J. Pratten, and I. P. Parkin. "Antimicrobial Activity in Thin Films of Pseudobrookite-Structured Titanium Oxynitride under UV Irradiation Observed for Escherichia coli." In: *Chemical Vapor Deposition* 16 (2010), pp. 19–22.

[25] S. Perni, C. Piccirillo, J. Pratten, P. Prokopovich, W. Chrzanowski, I. P. Parkin, and M. Wilson. "The antimicrobial properties of light-activated polymers containing methylene blue and gold nanoparticles." In: *Biomaterials* 30 (2009), pp. 89–93.

[26] S. Perni, C. Piccirillo, A. Kafizas, M. Uppal, J. Pratten, M. Wilson, and I. P. Parkin. "Antibacterial Activity of Light-Activated Silicone Containing Methylene Blue and Gold Nanoparticles of Different Sizes." In: *Journal of Cluster Science* 21 (2010), pp. 427–438.

[27] S. Perni, P. Prokopovich, I. P. Parkin, M. Wilson, and J. Pratten. "Prevention of biofilm accumulation on a light-activated antimicrobial catheter material." In: *Journal of Materials Chemistry* 20 (2010), pp. 8668–8673.

[28] S. Perni, P. Prokopovich, C. Piccirillo, J. Pratten, I. P. Parkin, and M. Wilson. "Toluidine blue-containing polymers exhibit potent bactericidal activity when irradiated with red laser

light." In: *Journal of Materials Chemistry* 19 (2009), pp. 2715–2723.

[29] S. Perni, J. Pratten, M. Wilson, C. Piccirillo, I. P. Parkin, and P. Prokopovich. "Antimicrobial Properties of Light-activated Polyurethane Containing Indocyanine Green." In: *Journal of Biomaterials Applications* 25 (2011), pp. 387–400.

[30] S. Noimark, C. W. Dunnill, C. W. M. Kay, S. Perni, P. Prokopovich, S. Ismail, M. Wilson, and I. P. Parkin. "Incorporation of methylene blue and nanogold into polyvinyl chloride catheters; a new approach for light-activated disinfection of surfaces." In: *Journal of Materials Chemistry* 22 (2012), pp. 15388–15396.

[31] A. J. T. Naik, S. Ismail, C. Kay, M. Wilson, and I. P. Parkin. "Antimicrobial activity of polyurethane embedded with methylene blue, toluidene blue and gold nanoparticles against Staphylococcus aureus; illuminated with white light." In: *Materials Chemistry and Physics* 129 (2011), pp. 446–450.

[32] C. Piccirillo, S. Perni, J. Gil-Thomas, P. Prokopovich, M. Wilson, J. Pratten, and I. P. Parkin. "Antimicrobial activity of methylene blue and toluidine blue O covalently bound to a modified silicone polymer surface." In: *Journal of Materials Chemistry* 19 (2009), pp. 6167–6171.

[33] V. Decraene, J. Pratten, and M. Wilson. "Assessment of the Activity of a Novel Light-Activated Antimicrobial Coating in a Clinical Environment." In: *Infection Control and Hospital Epidemiology* 29 (2008), pp. 1181–1184.

[34] Y. Sekiguchi, Y. Yao, Y. Ohko, K. Tanaka, T. Ishido, A. Fujishima, and Y. Kubota. "Self-sterilizing catheters with titanium dioxide photocatalyst thin films for clean intermittent catheterization: Basis and study of clinical use." In: *International Journal of Urology* 14 (2007), pp. 426–430.

[35] Y. Yao, Y. Ohko, Y. Sekiguchi, A. Fujishima, and Y. Kubota. "Self-sterilization using silicone catheters coated with Ag and TiO2 nanocomposite thin film." In: *Journal of Biomedical Materials Research Part B-Applied Biomaterials* 85B (2008), pp. 453–460.

[36] Y. Ohko, Y. Utsumi, C. Niwa, T. Tatsuma, K. Kobayakawa, Y. Satoh, Y. Kubota, and A. Fujishima. "Self-sterilizing and self-cleaning of silicone catheters coated with TiO2 photocatalyst thin films: A preclinical work." In: *Journal of Biomedical Materials Research* 58 (2001), pp. 97–101.

[37] M. R. Hamblin and T. Hasan. "Photodynamic therapy: a new antimicrobial approach to infectious disease?" In: *Photochemical & Photobiological Sciences* 3 (2004), pp. 436–450.

[38] Z. Huang. "A review of progress in clinical photodynamic therapy." In: *Technology in Cancer Research & Treatment* 4 (2005), pp. 283–293.

[39] M. A. Kohanski, D. J. Dwyer, B. Hayete, C. A. Lawrence, and J. J. Collins. "A common mechanism of cellular death induced by bactericidal antibiotics." In: *Cell* 130 (2007), pp. 797–810.

[40] T. Maisch, C. Bosl, R. M. Szeimies, N. Lehn, and C. Abels. "Photodynamic effects of novel XF porphyrin derivatives on prokaryotic and eukaryotic cells." In: *Antimicrobial Agents and Chemotherapy* 49 (2005), pp. 1542–1552.

[41] M. Soncin, C. Fabris, A. Busetti, D. Dei, D. Nistri, G. Roncucci, and G. Jori. "Approaches to selectivity in the Zn(ii)-phthalocyanine-photosensitized inactivation of wild-type and antibiotic-resistant Staphylococcus aureus." In: *Photochemical & Photobiological Sciences* 1 (2002), pp. 815–819.

[42] B. Zeina, J. Greenman, D. Corry, and W. M. Purcell. "Cytotoxic effects of antimicrobial photodynamic therapy on keratinocytes in vitro." In: *British Journal of Dermatology* 146 (2002), pp. 568–573.

[43] B. Zeina, J. Greenman, D. Corry, and W. M. Purcell. "Antimicrobial photodynamic therapy: assessment of genotoxic effects on keratinocytes in vitro." In: *British Journal of Dermatology* 148 (2003), pp. 229–232.

[44] B. Zeina, J. Greenman, W. M. Purcell, and B. Das. "Killing of cutaneous microbial species by photodynamic therapy." In: *British Journal of Dermatology* 144 (2001), pp. 274–278.

[45] S. B. Brown, E. A. Brown, and I. Walker. "The present and future role of photodynamic therapy in cancer treatment." In: *The Lancet Oncology* 5 (2004), pp. 497–508.

[46] In: *Photodynamic therapy for Barrett's oesophagus: National Institute for Health and Clinical Excellence (NICE)* (2010).

[47] M. S. Blumenkranz, N. M. Bressler, M. J. Potter, S. B. Bressler, J. M. Mones, P. Harvey, L. J. Singerman, E. S. Gragoudas, J. W. Miller, and U. Schmidt-Erfurth. "Photodynamic therapy of subfoveal choroidal neovascularization in age-related macular degeneration with verteporfin - Two-year results of 2 randomized clinical trials - TAP report 2." In: *Archives of Ophthalmology* 119 (2001), pp. 198–207.

[48] N. M. Bressler and S. B. Bressler. "Photodynamic therapy with verteporfin (visudyne): Impact on ophthalmology and visual sciences." In: *Investigative Ophthalmology & Visual Science* 41 (2000), pp. 624–628.

[49] W. H. Boehncke, T. Elshorst-Schmidt, and R. Kaufmann. "Systemic photodynamic therapy is a safe and effective treatment for psoriasis." In: *Archives of Dermatology* 136 (2000), pp. 271–272.

[50] Y. K. Tandon, M. F. Yang, and E. D. Baron. "Role of photodynamic therapy in psoriasis: a brief review." In: *Photodermatology Photoimmunology & Photomedicine* 24 (2008), pp. 222–230.

[51] J. Gil-Tomas, S. Tubby, I. P. Parkin, N. Narband, L. Dekker, S. P. Nair, M. Wilson, and C. Street. "Lethal photosensitisation of Staphylococcus aureus using a toluidine blue O-tiopronin-gold nanoparticle conjugate." In: *Journal of Materials Chemistry* 17 (2007), pp. 3739–3746.

[52] M. Bhatti, A. MacRobert, S. Meghji, B. Henderson, and M. Wilson. "A study of the uptake of toluidine blue O by Porphyromonas gingivalis and the mechanism of lethal photosensitization." In: *Photochemistry and Photobiology* 68 (1998), pp. 370–376.

[53] M. Schafer, C. Schmitz, R. Facius, G. Horneck, B. Milow, K. H. Funken, and J. Ortner. "Systematic study of parameters influencing the action of Rose Bengal with visible light on bacterial cells: Comparison between the biological effect and singlet-oxygen production." In: *Photochemistry and Photobiology* 71 (2000), pp. 514–523.

[54] B. S. Hass and R. B. Webb. "Photodynamic effects of dyes on bacteria. 4. Lethal effects of acridine-orange and -nm or 500-nm monochromatic light in strains of Escherichia-coli that differ in repair capability." In: *Mutation Research* 81 (1981), pp. 277–285.

[55] M. R. Hamblin, D. A. O'Donnell, N. Murthy, C. H. Contag, and T. Hasan. "Rapid control of wound infections by targeted photodynamic therapy monitored by in vivo bioluminescence imaging." In: *Photochemistry and Photobiology* 75 (2002), pp. 51–57.

[56] T. Dai, G. P. Tegos, T. Zhiyentayev, E. Mylonakis, and M. R. Hamblin. "Photodynamic Therapy for Methicillin-Resistant Staphylococcus aureus Infection in a Mouse Skin Abrasion Model." In: *Lasers in Surgery and Medicine* 42 (2010), pp. 38–44.

[57] T. W. Wong, Y. Y. Wang, H. M. Sheu, and Y. C. Chuang. "Bactericidal effiects of toluidine blue-mediated photodynamic action on Vibrio vulnificus." In: *Antimicrobial Agents and Chemotherapy* 49 (2005), pp. 895–902.

[58] P. Zolfaghari, S. Packer, M. Singer, S. P. Nair, J. Bennett, C. Street, and M. Wilson. "In vivo killing of Staphylococcus aureus using a light-activated antimicrobial agent." In: *Bmc Microbiology* 9 (2009).

[59] S. A. G. Lambrechts, T. N. Demidova, M. Aalders, T. Hasan, and M. R. Hamblin. "Photodynamic therapy for Staphylococcus aureus infected burn wounds in mice." In: *Photochemical & Photobiological Sciences* 4 (2005), pp. 503–509.

[60] T. Dai, G. P. Tegos, Z. Lu, L. Huang, T. Zhiyentayev, M. J. Franklin, D. G. Baer, and M. R. Hambline. "Photodynamic Therapy for Acinetobacter baumannii Burn Infections in Mice."

In: *Antimicrobial Agents and Chemotherapy* 53 (2009), pp. 503–509.

[61] X. X. Ragas, T. Dai, G. P. Tegos, M. Agut, S. Nonell, and M. R. Hamblin. "Photodynamic Inactivation of Acinetobacter baumannii Using Phenothiazinium Dyes: In Vitro and In Vivo Studies." In: *Lasers in Surgery and Medicine* 42 (2010), pp. 384–390.

[62] J. M. Bliss, C. E. Bigelow, T. H. Foster, and C. G. Haidaris. "Susceptibility of Candida species to photodynamic effects of photofrin." In: *Antimicrobial Agents and Chemotherapy* 48 (2004), pp. 2000–2006.

[63] M. C. Teichert, J. W. Jones, M. N. Usacheva, and M. A. Biel. "Treatment of oral candidiasis with methylene blue-mediated photodynamic therapy in an immunodeficient murine model." In: *Oral Surgery Oral Medicine Oral Pathology Oral Radiology and Endodontics* 93 (2002), pp. 155–160.

[64] M. Wilson and N. Mia. "Sensitisation of Candida albicans to killing by low-power laser light." In: *J. Oral Pathol. Med* 22 (1993), pp. 354–357.

[65] P. G. Calzavara-Pinton, M. Venturini, and R. Sala. "A comprehensive overview of photodynamic therapy in the treatment of superficial fungal infections of the skin." In: *Journal of Photochemistry and Photobiology B-Biology* 78 (2005), pp. 1–6.

[66] K. Konopka and T. Goslinski. "Photodynamic Therapy in Dentistry." In: *Journal of Dental Research* 86 (2007), pp. 694–707.

[67] N. Komerik, H. Nakanishi, A. J. MacRobert, B. Henderson, P. Speight, and M. Wilson. "In vivo killing of Porphyromonas gingivalis by toluidine blue-mediated photosensitization in an animal model." In: *Antimicrobial Agents and Chemotherapy* 47 (2003), pp. 932–940.

[68] P. E. Bottura, J. Milanezi, L. A. Femandes, H. C. Caldas, M. Abbud-Filho, V. G. Garcia, and M. A. S. F. Baptista. "Non-surgical Periodontal Therapy Combined with Laser and Photodynamic Therapies for Periodontal Disease in Immuno-

suppressed Rats." In: *Transplantation Proceedings* 43 (2011), pp. 2009–2016.

[69] J. M. de Almeida, L. H. Theodoro, A. F. Bosco, M. J. Hitomi Nagata, S. Bonfante, and V. G. Garcia. "Treatment of Experimental Periodontal Disease by Photodynamic Therapy in Rats With Diabetes." In: *Journal of Periodontology* 79 (2008), pp. 2156–2165.

[70] J. M. de Almeida, L. H. Theodoro, A. F. Bosco, M. J. Hitomi Nagata, M. Oshiiwa, and V. G. Garcia. "Influence of photodynamic therapy on the development of ligature-induced periodontitis in rats." In: *Journal of Periodontology* 78 (2007), pp. 566–575.

[71] Y. L. Qin, X. L. Luan, L. J. Bi, Y. Q. Sheng, C. N. Zhou, and Z. G. Zhang. "Comparison of toluidine blue-mediated photodynamic therapy and conventional scaling treatment for periodontitis in rats." In: *Journal of Periodontal Research* 43 (2008), pp. 162–167.

[72] L. A. Fernandes, J. M. de Almeida, L. H. Theodoro, A. F. Bosco, M. J. Hitomi Nagata, T. M. Martins, T. Okamoto, and V. G. Garcia. "Treatment of experimental periodontal disease by photodynamic therapy in immunosuppressed rats." In: *Journal of Clinical Periodontology* 36 (2009), pp. 219–228.

[73] B. W. Sigusch, A. Pfitzner, V. Albrecht, and E. Glockmann. "Efficacy of photodynamic therapy on inflammatory signs and two selected periodontopathogenic species in a beagle dog model." In: *Journal of Periodontology* 76 (2005), pp. 1100–1105.

[74] P. Chondros, D. Nikolidakis, N. Christodoulides, R. Roessler, N. Gutknecht, and A. Sculean. "Photodynamic therapy as adjunct to non-surgical periodontal treatment in patients on periodontal maintenance: a randomized controlled clinical trial." In: *Lasers in Medical Science* 24 (2009), pp. 681–688.

[75] N. Christodoulides, D. Nikolidakis, P. Chondros, J. Becker, F. Schwarz, R. Roessler, and A. Sculean. "Photodynamic therapy as an adjunct to non-surgical periodontal treatment: A randomized, controlled clinical trial." In: *Journal of Periodontology* 79 (2008), pp. 1638–1644.

[76] A. Braun, C. Dehn, F. Krause, and S. Jepsen. "Short-term clinical effects of adjunctive antimicrobial photodynamic therapy in periodontal treatment: a randomized clinical trial." In: *Journal of Clinical Periodontology* 35 (2008), pp. 877–884.

[77] R. R. de Oliveira, H. O. Schwartz-Filho, J. Novaes Arthur Belem, G. P. Garlet, R. F. de Souza, J. Taba Mario, S. L. S. de Souza, and F. J. Ribeiro. "Antimicrobial Photodynamic Therapy in the Non-Surgical Treatment of Aggressive Periodontitis: Cytokine Profile in Gingival Crevicular Fluid, Preliminary Results." In: *Journal of Periodontology* 80 (2009), pp. 98–105.

[78] http://www.ondinebio.com. Accessed: 2015-01-27.

[79] http://www.periowave.com. Accessed: 2015-01-27.

[80] *Photoactivated disinfection*. http://www.denfotexresearch.com/index3.htm. Accessed: 2015-01-27.

[81] http://www.helbo.de/en/home.html. Accessed: 2015-01-27.

[82] D. J. Weber, D. Anderson, and W. A. Rutala. "The role of the surface environment in healthcare-associated infections." In: *Current Opinion in Infectious Diseases* 26 (2013), pp. 338–44.

[83] R. A. Weinstein. "Epidemiology and control of nosocomial infections in adult intensive care units." In: *The American Journal of Medicine* 91 (1991), S179–S184.

[84] K. Page, M. Wilson, and I. P. Parkin. "Antimicrobial surfaces and their potential in reducing the role of the inanimate environment in the incidence of hospital-acquired infections." In: *Journal of Materials Chemistry* 19 (2009), pp. 3819–3831.

[85] B. Hota. "Contamination, disinfection, and cross-colonization: Are hospital surfaces reservoirs for nosocomial infection?" In: *Clinical Infectious Diseases* 39 (2004), pp. 1182–1189.

[86] M. Wainwright and K. B. Crossley. "Photosensitising agents - circumventing resistance and breaking down biofilms: a review." In: *International Biodeterioration & Biodegradation* 53 (2004), pp. 119–126.

[87] J.-S. Kim, H.-S. Kim, J.-Y. Park, H.-S. Koo, C.-S. Choi, W. Song, H. C. Cho, and K. M. Lee. "Contamination of X-ray Cassettes with Methicillin-resistant Staphylococcus aureus and Methicillin-resistant Staphylococcus haemolyticus in a Radiology Department." In: *Annals of Laboratory Medicine* 32 (2012), pp. 206–209.

[88] S. Oie, I. Hosokawa, and A. Kamiya. "Contamination of room door handles by methicillin-sensitive/methicillin-resistant Staphylococcus aureus." In: *Journal of Hospital Infection* 51 (2002), pp. 140–143.

[89] S. Oie and A. Kamiya. "Survival of methicillin-resistant Staphylococcus aureus (MRSA) on naturally contaminated dry mops." In: *Journal of Hospital Infection* 34 (1996), pp. 145–149.

[90] P. Ciragil, M. Gul, and M. Aral. "Bacterial contamination of computers and telephones in a university hospital in Turkey." In: *Journal of Hospital Infection* 62 (2006), pp. 247–248.

[91] S. Bures, J. T. Fishbain, C. F. T. Uyehara, J. M. Parker, and B. W. Berg. "Computer keyboards and faucet handles as reservoirs of nosocomial pathogens in the intensive care unit." In: *American Journal of Infection Control* 28 (2000), pp. 465–471.

[92] D. Banerjee, A. Fraise, and K. Chana. "Writing pens are an unlikely vector of cross-infection with methicillin resistant Staphylococcus aureus (MRSA)." In: *Journal of Hospital Infection* 43 (1999), pp. 73–75.

[93] H. A. Cohen, J. Amir, A. Matalon, R. Mayan, S. Beni, and A. Barzilai. "Stethoscopes and otoscopes - a potential vector of infection?" In: *Family Practice* 14 (1997), pp. 446–449.

[94] B. Dietze, A. Rath, C. Wendt, and H. Martiny. "Survival of MRSA on sterile goods packaging." In: *Journal of Hospital Infection* 49 (2001), pp. 255–261.

[95] R. Fekety, K. H. Kim, D. Brown, D. H. Batts, M. Cudmore, and J. Silva. "Epidemiology of antibiotic-associated colitis: Isolation of clostridium difficile from the hospital environment." In: *American Journal of Medicine* 70 (1981), pp. 906–908.

[96] K. H. Kim, R. Fekety, D. H. Batts, D. Brown, M. Cudmore, J. Silva, and D. Waters. "Isolation of Clostridium difficile from the Environment and Contacts of Patients with Antibiotic-Associated Colitis." In: *Journal of Infectious Diseases* 143 (1981), pp. 42–50.

[97] P. M. Rountree. "The effect of desiccation on the viability of Staphylococcus aureus." In: *Journal of Hygiene* 61 (1963), pp. 265–272.

[98] M. Wilson. "Light Activated Antimicrobial Coating for the Continuous Disinfection of Surfaces." In: *Infection Control and Hospital Epidemiology* 24 (2003), pp. 782–784.

[99] V. Decraene, J. Pratten, and M. Wilson. "Cellulose acetate containing toluidine blue and rose bengal is an effective antimicrobial coating when exposed to white light." In: *Applied and Environmental Microbiology* 72 (2006), pp. 4436–4439.

[100] V. Decraene, J. Pratten, and M. Wilson. "Novel light-activated antimicrobial coatings are effective against surface-deposited Staphylococcus aureus." In: *Current Microbiology* 57 (2008), pp. 269–273.

[101] M. Wainwright, M. N. Byrne, and M. A. Gattrell. "Phenothiazinium-based photobactericidal materials." In: *Journal of Photochemistry and Photobiology B: Biology* 84 (2006), pp. 227–230.

[102] J. Bozja, J. Sherrill, S. Michielsen, and I. Stojiljkovic. "Porphyrin-based, light-activated antimicrobial materials." In: *Journal of Polymer Science Part a-Polymer Chemistry* 41 (2003), pp. 2297–2303.

[103] M. Wainwright. "Photoantimicrobials-So what's stopping us?" In: *Photodiagnosis and Photodynamic Therapy* 6 (2009), pp. 167–169.

[104] G. S. Cox, C. Bobillier, and D. G. Whitten. "Photo-oxidation and singlet oxygen sensitization by protoporphyrin-IX and its photo-oxidation products." In: *Photochemistry and Photobiology* 36 (1982), pp. 401–407.

[105] M. Krouit, R. Granet, and P. Krausz. "Photobactericidal films from porphyrins grafted to alkylated cellulose - synthesis and bactericidal properties." In: *European Polymer Journal* 45 (2009), pp. 1250–1259.

[106] J. Sherrill, S. Michielsen, and I. Stojiljkovic. "Grafting of light-activated antimicrobial materials to nylon films." In: *J. Polym. Sci. Pol. Chem.* 41 (2003), pp. 41–47.

[107] M. Wainwright, D. A. Phoenix, P. B. Nickson, and G. Morton. "The use of new methylene blue in Pseudomonas aeruginosa biofilm destruction." In: *Biofouling* 18 (2002), pp. 247–249.

[108] M. Wilson and J. Pratten. "Lethal photosensitization of staphylococcus-aureus." In: *Microbios* 78 (1994), pp. 163–168.

[109] D. P. Camacho, A. Gasparetto, and T. I. E. Svidzinski. "The effect of chlorhexidine and gentian violet on the adherence of Candida spp. to urinary catheters." In: *Mycopathologia* 163 (2007), pp. 261–266.

[110] G. Chaiban, H. Hanna, T. Dvorak, and I. Raad. "A rapid method of impregnating endotracheal tubes and urinary catheters with gendine: a novel antiseptic agent." In: *Journal of Antimicrobial Chemotherapy* 55 (2005), pp. 51–56.

[111] R. Hachem, R. Reitzel, A. Borne, Y. Jiang, P. Tinkey, R. Uthamanthil, J. Chandra, M. Ghannoum, and I. Raad. "Novel Antiseptic Urinary Catheters for Prevention of Urinary Tract Infections: Correlation of In Vivo and In Vitro Test Results." In: *Antimicrobial Agents and Chemotherapy* 53 (2009), pp. 5145–5149.

[112] I. I. Raad, J. A. Mohamed, R. A. Reitzel, Y. Jiang, T. L. Dvorak, M. A. Ghannoum, R. Y. Hachem, and A.-M. Chaftari. "The prevention of biofilm colonization by multidrug-resistant pathogens that cause ventilator-associated pneumonia with antimicrobial-coated endotracheal tubes." In: *Biomaterials* 32 (2011), pp. 2689–2694.

[113] I. Raad, H. Hanna, and K. Nabulsi. *Novel antiseptic derivatives with broad spectrum antimicrobial activity for the impregnation of surfaces*. 2003.

[114] J. Rosenblatt, R. Reitzel, Y. Jiang, R. Hachem, and I. Raad. "Insights on the Role of Antimicrobial Cuffed Endotracheal Tubes in Preventing Transtracheal Transmission of VAP Pathogens from an In Vitro Model of Microaspiration and Microbial Proliferation." In: *BioMed Research International* 2014 (2014), p. 11.

[115] M. Wainwright, D. A. Phoenix, S. L. Laycock, D. R. A. Wareing, and P. A. Wright. "Photobactericidal activity of phenothiazinium dyes against methicillin-resistant strains of Staphylococcus aureus." In: *FEMS Microbiology Letters* 160 (1998), pp. 177–181.

[116] M. Wainwright, D. A. Phoenix, J. Marland, D. R. A. Wareing, and F. J. Bolton. "A study of photobactericidal activity in the phenothiazinium series." In: *FEMS Immunology & Medical Microbiology* 19 (1997), pp. 75–80.

[117] N. Narband, S. Tubby, I. P. Parkin, J. Gil-Tomas, D. Ready, S. P. Nair, and M. Wilson. "Gold Nanoparticles Enhance the Toluidine Blue-Induced Lethal Photosensitisation of Staphylococcus aureus." In: *Current Nanoscience* 4 (2008), pp. 409–414.

[118] N. Narband, M. Uppal, C. W. Dunnill, G. Hyett, M. Wilson, and I. P. Parkin. "The interaction between gold nanoparticles and cationic and anionic dyes: enhanced UV-visible absorption." In: *Physical Chemistry Chemical Physics* 11 (2009), pp. 10513–10518.

[119] P. Prokopovich, S. Perni, C. Piccirillo, J. Pratten, I. P. Parkin, and M. Wilson. "Frictional properties of light-activated antimicrobial polymers in blood vessels." In: *Journal of Materials Science - Materials in Medicine* 21 (2010), pp. 815–821.

3

LASER-ACTIVATED ANTIMICROBIAL POLYMERS; CRYSTAL VIOLET, METHYLENE BLUE AND GOLD NANOPARTICLE-ENCAPSULATED SILICONE

3.1 INTRODUCTION

HAIs, a worldwide problem, not only results in severe financial implications for healthcare institutions, but causes patient discomfort, the extensive use of antibiotics and prolonged hospital stays. Unfortunately, in some cases, HAIs can result in patient death. The U.K. Department of Health (2004) estimated that each year there are 300,000 incidents of HAI in the U.K. [1, 2], translating to a financial burden of *ca.* £1 billion on NHS hospitals and an additional 3.6 million patient hospitalisation days [1, 3].

Indwelling polymeric medical devices, for example, endotracheal tubes, intravascular devices and urinary catheters, are crucial in the treatment of critically ill patients. However, many HAIs are associated with their use [4]. Urinary catheters are one of the most frequently used medical devices and in the U.S. alone, more than 30 million urinary catheters are inserted each year [4]. Recent figures suggest that urinary tract infections (UTIs) account for *ca.* 20 % of all HAIs in England and 80 % of UTIs are associated with urinary catheterisation [1]. Although the treatment of an individual UTI is normally relatively inexpensive, due the prevalence of these infections, they were noted as the most costly single site infection in the U.K. [3].

Clinical trials focused on decreasing the incidence of UTIs and other complications have been extensively reviewed, to determine the efficacy of catheter policies for long-term and short-term bladder drainage and to continuously update guidelines for clinical practice [5–10]. Attempts to reduce the risk of UTIs include the use of

antibiotic prophylaxis, catheter flushes and antibiotic and antiseptic devices [5–10]. It has been noted that many trials were small or of poor quality and provided inadequate data to draw reliable conclusions on the efficacy of the approaches, in terms of reducing the incidence of UTIs. However, the use of silver alloy catheters and antibiotic catheters (minocycline/ rifampicin- or nitrofurazone-coated) have demonstrated a statistically significant reduction in asymptomatic bacteriuria (the presence of bacteria in urine), in hospitalised patients catheterised for durations of both less than and more than one week when a silver alloy catheter was used and less than one week when an antibiotic catheter was used [10]. No significant reductions in bacteriuria were reported for cases of long-term catheterised patients with anti-infective indwelling urinary catheters [6]. Moreover, despite a decrease in the risk of bacteriuria with silver alloy or antibiotic-coated catheters in short-term catheterised patients, their impact on the overall risk of UTIs was inconclusive [10]. Overall, there is limited evidence that current infection-prevention strategies help significantly decrease the incidence of UTIs. Moreover, the use of antibiotic-coated catheters may be detrimental, as exposure of bacterial populations to antibiotics is likely to increase the prevalence of drug resistance [11].

Recently, alternative infection prevention strategies have been developed. One such approach is to use a modified form of PDT - used in the treatment of tumours, skin infections and conditions [12–16] - to reduce the risk of device-associated infection. Photosensitisers can demonstrate bactericidal activity through the generation of cytotoxic ROS upon photo-activation [12]. Absorption of a photon of a wavelength within the photosensitiser absorbance range promotes the dye molecule to an excited singlet state [12, 17]. The molecule in the excited singlet state can then undergo an intersystem crossing, a radiationless photochemical process, to a longer lived, lower energy excited triplet state [12, 17]. This triplet state can undergo two major photochemical pathways, termed a “type I” or “type II” photo-process and ultimately both pathways result in the generation of a range of ROS [12]. The “type I” photochemical pathway involves the interaction of the triplet state species with surrounding substrate

molecules, generating radical species [12, 14, 17]. The "type II" photochemical pathway occurs when the triplet state species interacts with molecular oxygen in the vicinity, forming the highly reactive, transient singlet oxygen species [12, 14, 17]. ROS can rapidly kill bacteria in the vicinity by multiple mechanisms, including oxidative damage to cellular membranes, intracellular proteins and DNA, such that the emergence of bacterial resistance is extremely unlikely [12, 18, 19]. Furthermore, mammalian cells show significantly greater resistance to ROS than bacteria, offering a potential window for treatment [20].

Photosensitiser dyes such as methylene blue, toluidine blue O and indocyanine green have been immobilised in medical grade polymers using a simple "swell-encapsulation-shrink" method and these materials exhibit photo-activated antimicrobial activity [19, 21–26]. Moreover, despite possessing no inherent antimicrobial properties, it has been found that the encapsulation of 2 nm gold nanoparticles in combination with the photosensitiser dye methylene blue into medical grade polymers, effects a synergistic enhancement in the light-activated antimicrobial activity of the dye [19, 21, 26]. An electron paramagnetic resonance spectroscopy investigation indicated that the basis of this enhancement in the photobactericidal activity is increased generation of methylene blue triplet state, in the presence of 2 nm gold nanoparticles [25]. An increase in triplet state production may correlate with an increase in the generation of ROS, resulting in greater photobactericidal activity [25].

Although research is still in the 'laboratory investigations' phase, results to date have been promising. Studies indicated that these modified polymeric materials induce the lethal photosensitisation of both Gram-positive and Gram-negative bacteria upon activation with short-term laser light irradiation [19, 21–23], or against Gram-positive bacteria upon activation with longer-term white light illumination [26]. A study also showed that methylene blue/nanogold-encapsulated silicone demonstrated efficacy in the reduction of *S. epidermidis* biofilm formation under specific laser irradiation regimes [22]. It is hopeful that these light-activated antimicrobial dye/

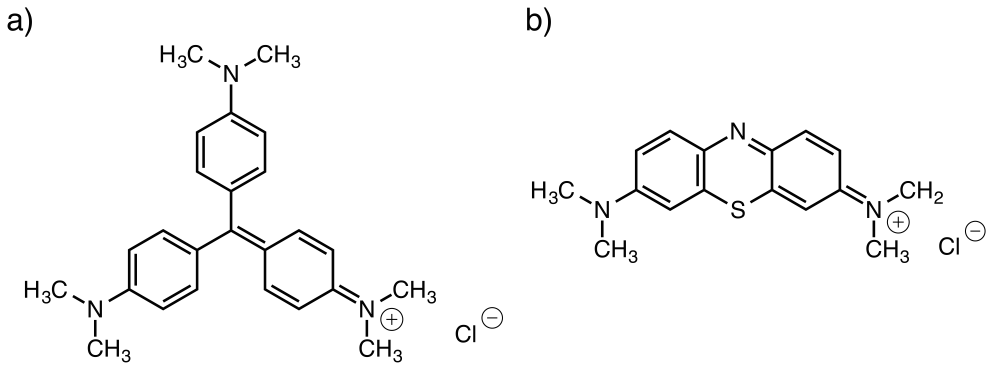

Figure 7: Chemical structures of (a) the triarylmethane photosensitiser dye crystal violet and (b) the phenothiazine photosensitiser dye methylene blue

nanogold combinations can potentially be incorporated into silicone catheters for use in medical applications, in which the bactericidal properties will be activated by laser illumination delivered using an optical fibre down the device lumen.

This chapter reports on the synergistic enhancement in the light-activated antimicrobial activity of medical grade silicone coated with crystal violet in the presence of 2 nm gold nanoparticles and methylene blue. The crystal violet-coated, methylene blue and nanogold-encapsulated samples were prepared using a novel two stage dipping process and the material was characterised using UV-Vis absorbance spectroscopy, light microscopy and fluorescence microscopy. Microbiological testing of the crystal violet, methylene blue and nanogold incorporated silicone was performed using both Gram-positive and Gram-negative bacteria and a low power 635 nm laser to activate the antimicrobial properties. Surprisingly, notable dark kill was seen and this dye-nanogold polymer combination was shown to be a potent photobactericidal polymer for the destruction of *E. coli*.

3.2 EXPERIMENTAL

3.2.1 *Chemicals and Substrates*

The reagents used in materials synthesis were as follows: Methylene blue hydrate (Riedel-de Haën, U.K.), crystal violet (Sigma, U.K.), 2 nm gold nanoparticles (2.49 x 10^{-7} mol L^{-1}, BBI Solutions, U.K.) and acetone (VWR, U.K.). In all synthetic work carried out, the water used was deionised (resistivity 15 MΩcm) and the substrate was medical grade flat silicone sheets (NuSil, Polymer Systems Technology Ltd., U.K.). For the extended microbiological testing, the substrate was commercially available 100 % silicone Foley catheters: 2 way, 30 cc silicone catheter with an opposed eye, (22 Fr, 7.3 mm diameter, Rüsch).

3.2.2 *Materials Synthesis*

3.2.2.1 *System Optimisation - Organic Solvent*

Silicone polymer squares (1 cm^2) were immersed in crystal violet - organic solvent solutions (100 ppm crystal violet, 100 % organic solvent) prepared using the following organic solvents: tetrahydrofuran (THF), toluene, ethyl acetate, hexane, isopropanol, acetone, acetyl acetone, acetonitrile, methanol, ethanol and butanol. The silicone sections were allowed to swell under dark conditions for either 24 h or 72 h. The samples were subsequently removed and allowed to air dry overnight, after which they were washed (distilled water) and towel-dried.

3.2.2.2 *System Optimisation - Solvent Concentration*

Silicone polymer squares (1 cm^2) were immersed in crystal violet solutions (18 ppm crystal violet) made up to the following acetone : water ratios - 1:0, 8:2, 6:4, 4:6, 2:8 and 0:1 and allowed to swell under dark conditions for a period of 3 days. The samples were subsequently removed and allowed to air dry overnight, after which

they were washed and towel-dried.

3.2.2.3 *System Optimisation - Dye Concentration*

Silicone polymer squares (1 cm^2) were immersed in crystal violet solutions (in water) made up to the following concentrations, for a period of 3 days: 1 x 10^{-1} mol dm^{-3}, 5 x 10^{-2} mol dm^{-3}, 1 x 10^{-2} mol dm^{-3}, 5 x 10^{-1} mol dm^{-3}, 1 x 10^{-3} mol dm^{-3}, 5 x 10^{-4} mol dm^{-3}, 1 x 10^{-4} mol dm^{-3}, 5 x 10^{-5} mol dm^{-3}, 1 x 10^{-5} mol dm^{-3} and 5 x 10^{-6} mol dm^{-3} crystal violet. The samples were subsequently removed and allowed to air dry overnight, after which they were washed and towel-dried.

3.2.2.4 *System Optimisation - Immersion Duration*

Silicone polymer squares (1 cm^2) were immersed in a crystal violet solution (0.001 mol dm^{-3}) for varying dipping times extending to 96 h. After each set time period, the corresponding sample was removed from the dipping solution and allowed to air dry overnight, after which it was washed (distilled water) and towel-dried.

3.2.2.5 *Preparation of Materials for Antimicrobial Testing*

A series of samples including the relevant controls, were prepared for antimicrobial testing:

a) Control samples: Silicone polymer squares (1 cm^2) were immersed in a 9:1 acetone : water swelling solution (72 h, dark conditions). The polymer sections were subsequently air-dried (24 h), washed and towel dried.

b) Methylene blue and 2 nm gold nanoparticle encapsulated silicone: Silicone polymer squares (1 cm^2) were immersed in a 9:1 acetone : nanogold swelling solution saturated with methylene blue (700 mg /L) for 72 h under dark conditions. The polymer sections were subsequently air-dried (24 h), washed and towel dried.

c) Crystal violet-coated silicone: Silicone polymer squares (1 cm^2) were immersed in a crystal violet solution (0.001 mol dm^{-3}) for 72

h under dark conditions. The polymer sections were subsequently air-dried (24 h), washed and towel dried.

d) Crystal violet-coated, nanogold-encapsulated silicone: Silicone polymer squares (1 cm^2) were immersed in a 9:1 acetone : nanogold swelling solution (72 h, dark conditions). The polymer sections were subsequently air-dried (24 h), washed and towel dried, after which they were immersed in a crystal violet solution (see c for protocol).

e) Crystal violet-coated, nanogold-encapsulated catheters: Silicone catheter sections (1 cm length, 7.3 mm diamater) were cut along the length such that 2 flat internal surfaces were exposed. The sections were immersed in a 9:1 acetone : nanogold swelling solution (72 h, dark conditions). The catheter sections were subsequently air-dried (24 h), washed and towel dried, after which they were immersed in a crystal violet solution (40 ^0C, 6 hours) that was continuously stirred using a gyro-rotator. The catheter sections were subsequently air-dried (24 h), washed and towel dried.

3.2.3 *Materials Characterisation*

A PerkinElmer Lambda 25 UV-Vis Spectrometer was used to measure the UV-Vis absorption spectra of the modified silicone polymers used for microbiology, within the range 400 - 750 nm. A Bruker Platinum attenuated total reflectance-Fourier transform infrared (ATR-FTIR) was used to measure the infrared transmittance spectra of the samples within the range 4000 - 400 cm^{-1}, with an accumulation of 15 scans per sample. Methylene blue and crystal violet were dissolved in industrial methylated spirits (IMS) and the infrared transmittance spectra were measured within the range 4000 - 400 cm^{-1}, with an accumulation of 15 scans per sample.

Flat silicone polymers prepared by immersion in varying concentrations of crystal violet solutions, were embedded vertically in paraffin blocks. 10 μm sections were cut using a microtome and sections were mounted on Vectabond (Vecta Laboratories, U.K.)

treated slides for fluorescence imaging. On average, 10 sections were taken from each of the 10 silicone sheets dipped in increasing concentrations of crystal violet solution. The sections were imaged at 10x magnification, using a light microscope (Olympus U.K. Ltd., model BH2) with a colour charge-coupled device (CCD) digital camera (Lumenera, model Infinity 1) and Infinity Capture software was used for analysis. Fluorescence microscopy was performed on the thinly sliced crystal violet-coated silicone sections. The samples were imaged using a cooled scientific-grade 16-bit digital CCD camera (Princeton Instruments Ltd., Model PIXIS 512) operated by Win-Spec software, coupled to an inverted fluorescence microscope (Olympus U.K. Ltd., Model IMT-2). The crystal violet present in the silicone sections was detected using fluorescence excitation with a 635 nm laser and the samples were imaged using a 10x objective. Fluorescence was detected using a bandpass filter centred at 660 nm (Omega Optical Inc., model 660DF30). The use of red wavelength excitation minimized the background autofluorescence detected from the polymer itself and is very close to the wavelength used for irradiation (635 nm). The images were subsequently analysed using Roper Scientific Software (WinSpec/32) and ImageJ software (National Institutes of Health, U.S.A.).

3.2.4 *Functional Testing*

3.2.4.1 *Transmission Measurements*

A Gentec-EO TPM-300 power meter was used to estimate the transmision of laser power through unmodified and modified medical grade silicone. A 635 nm laser set to 314 mW was used in the transmission testing and produced a uniform spot size of 2 cm diameter, corresponding to a fluence rate of 100 mW cm^{-2}. The laser power was measured before and after placement of a 1.21 cm^{-2} silicone section at the detector and the percentage transmission through the polymer was calculated.

3.2.4.2 *Water Contact Angle Measurements*

Equilibrium water contact angle measurements (~9 μL) on: untreated silicone, solvent treated (control) silicone, crystal violet-coated silicone, methylene blue and 2 nm gold nanoparticle-encapsulated silicone and crystal violet-coated nanogold-encapsulated silicone, were obtained using an FTA 1000 Drop Shape Instrument. The contact angle measurement for each sample type was taken to be the average value over $\geqslant$10 measurements, using a droplet of deionised water dispensed by gravity from a gauge 27 needle and the samples were photographed side on. The data was analysed using FTA32 software.

3.2.4.3 *Leaching Test*

The stability of the crystal violet-coated silicone polymers in phosphate buffer saline (PBS, Dulbecco A) at 37 °C, was investigated. Crystal violet-coated silicone sections (1 cm^2, as prepared for microbiology) were immersed in PBS (2.5 mL, 37 °C) for an extended period of time. The UV-Vis absorbance of the PBS (596 nm, Pharmacia Biotech Ultrospec 2000) was measured periodically to monitor any leaching of the crystal violet from the polymer, into the surrounding solution. A comparison of the absorbance at 596 nm of the PBS with a crystal violet calibration curve, enabled the determination of the concentration of crystal violet that was released from the silicone into the surrounding solution.

3.2.5 *Microbiological Investigation*

3.2.5.1 *Antimicrobial Testing - Flat Polymer Sheets*

The following medical grade silicone elastomer samples (1 cm^2) were used in the microbiology experiments: (i) solvent treated silicone (control), (ii) crystal violet-coated silicone, (iii) crystal violet-coated, 2 nm gold nanoparticle-encapsulated silicone, (iv) methylene blue and 2 nm gold nanoparticle-encapsulated silicone and (v) crystal violet-coated, methylene blue and 2 nm gold nanoparticle-encapsulated

silicone. The samples were left for a period of 3 days prior to use in the microbiological testing, to 'sterilise'. The microorganisms tested were *S. epidermidis* RP62a and *E. coli* ATCC 25922. These organisms were stored at -70 °C in Brain-Heart-Infusion broth (BHI, Oxoid) containing 20 % (v/v) glycerol and propagated onto either Mannitol Salt agar (MSA, Oxoid) in the case of *S. epidermidis* or MacConkey agar (MAC, Oxoid Ltd.) in the case of *E. coli*, for a maximum of 2 sub-cultures at intervals of 2 weeks.

BHI broth was inoculated with 1 bacterial colony and cultured in air at 37 °C for 18 h. The bacterial pellet was recovered by centrifugation (21 °C, 1771 x*g*, 4 min), washed in PBS (10 mL) and centrifuged again to recover the bacteria, which were finally re-suspended in PBS (10 mL). The washed suspension was diluted 1000-fold to obtain the inoculum (~10^6 cfu /mL). The inoculum in each experiment was confirmed by plating ten-fold serial dilutions on agar for viable counts. Triplicates of each polymer sample type were inoculated with 25 µL of the inoculum and covered with a sterile cover slip (22 mm x 22 mm). The samples were then irradiated for ~13.5 minutes using a 635 nm diode laser (see 3.2.5.2). A further set of samples (in triplicate) was maintained in the dark for the duration of the irradiation time.

Post irradiation, the inoculated samples and cover slips were added to PBS (225 µL) in a 50 mL tube and vortexed. The neat suspension and ten-fold serial dilutions were plated onto the appropriate agar for viable counts. The plates were incubated aerobically at 37 °C for 24 h (*E. coli*) or 48 h (*S. epidermidis*). Each experiment contained 3 technical replicates and the experiment was reproduced three times. The data was analysed using the Mann-Whitney U test.

3.2.5.2 *Laser Specifications for Activation of Antimicrobial Activity*

A 635 nm 1.0 W laser (Changchun New Industries Optoelectronics Technology Co. Ltd., China) coupled to a 1 m long liquid light guide was used for the microbiological testing and produced a uniform spot size of 2 cm diameter, corresponding to a fluence rate of 55.7 mW cm^{-2}. Over the ~13.5 minutes irradiation duration, the total

incident fluence at the sample was 45 J cm^{-2}.

3.2.5.3 *Antimicrobial Testing - Commercial Catheter Sections*

Crystal violet-coated, methylene blue and 2 nm gold nanoparticle-encapsulated (CVMBAu) catheter sections were used in the microbiological testing. The samples were left for a period of 3 days, prior to antimicrobial testing. The microorganisms tested were *E. coli* ATCC 25922, *S. epidermidis* RP62a, MRSA-15, *P. mirabilis* (clinical strain), *Enterococcus faecalis* JH-2 and *P. aeruginosa* PAO1. These organisms were stored at -70 °C in BHI broth containing 20 % (v/v) glycerol and propagated onto BHI Agar (Oxoid Ltd.) for a maximum of 2 sub-cultures at intervals of 2 weeks.

BHI broth was inoculated with 1 bacterial colony and cultured in air at 37 °C for 18 h. The bacterial pellet was recovered by centrifugation, washed in PBS (10 mL) and centrifuged again to recover the bacteria, which were finally re-suspended in the same volume of PBS. The washed suspension was diluted 1000-fold to obtain the inoculum (~10^6 cfu /mL). The inoculum in each experiment was confirmed by plating ten-fold serial dilutions on agar for viable counts. Triplicates of the CVMBAu catheter sections were inoculated with 12.5 µL of the inoculum and covered with a sterile cover slip (22 mm x 22 mm). The samples were then irradiated for ~18 minutes using a 635 nm laser (see 3.2.5.4). A further set of samples (in triplicate) was maintained in the dark for the duration of the irradiation time.

Post irradiation, the inoculated samples and cover slips were added to PBS (112.5 µL) in a 50 mL tube and vortexed. The neat suspension and ten-fold serial dilutions were plated onto either MSA (*S. epidermidis*, MRSA, *E. faecalis*) or MAC agar (*E. coli*, *P. mirabilis*, *P. aeruginosa*) agar for viable counts. The plates were incubated aerobically at 37 °C for 24 h. Each experiment contained 3 technical replicates and the experiment was reproduced three times. The data was analysed using the Mann-Whitney U test.

3.2.5.4 *Laser Specifications for Further Antimicrobial Testing*

A 635 nm laser (Biomed Ltd, U.K.) set to 130 mW power was used for the microbiological testing and produced a uniform spot size of 2 cm diameter, corresponding to a fluence rate of 41.4 mW cm^{-2}. Over the ~18 minutes irradiation duration, the total incident fluence at the sample was 45 J cm^{-2}.

3.3.1 *Materials Synthesis*

A modified "swell-encapsulation-shrink" strategy was developed to incorporate photosensitiser dyes and 2 nm gold nanoparticles into a medical grade silicone polymer. Previous studies have indicated that varying dye-polymer combinations require different swelling conditions [19, 24, 25] and so, in this study, the dipping conditions were optimised to determine conditions that facilitated a good uptake of the dye into the silicone polymer. Silicone polymer coupons were exposed to solutions containing crystal violet under varying conditions to optimise the incorporation procedure. Silicone samples were immersed in crystal violet/ organic solvent swelling solutions prepared using a range of organic solvents, for up to 72 h. Shown in Figure 8(a) are samples prepared by immersion in crystal violet/ organic solvent swelling

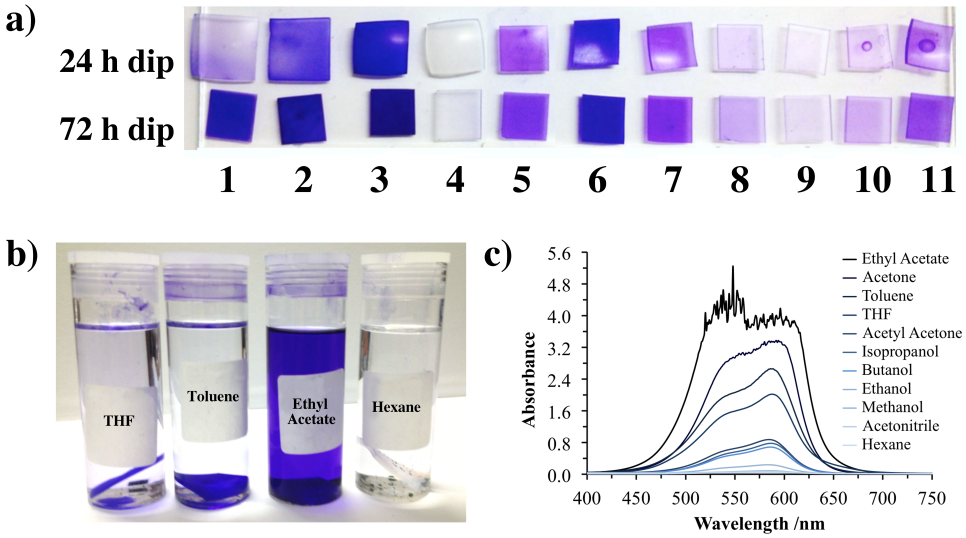

Figure 8: (a) Crystal violet-incorporated silicone sections prepared by immersion in crystal violet/ organic solvent swelling solutions for either 24 h (immediately post-removal from swelling solution) or 72 h. (air-dried overnight). Organic solvents used are as follows: 1. THF, 2. toluene, 3. ethyl acetate, 4. hexane, 5. isopropanol, 6. acetone, 7. acetyl acetone, 8. acetonitrile, 9. methanol, 10. ethanol and 11. butanol. (b) Silicone sections immersed in different crystal violet/ organic solvent swelling solutions (100 % solvent) and (c) UV-Vis absorbance spectra of crystal violet-encapsulated silicone sections prepared by immersion in crystal violet/ organic solvent swelling solutions for 72 h. Note that the spectra are ordered as specified in the legend

solutions either immediately post-immersion (24 h dip samples), or after air-drying (72 h dip samples). It is clear that solvents such as THF, toluene, ethyl acetate and hexane induce significant polymer swelling. Due to the insolubility of crystal violet in hexane (Figure 8(b), no visible encapsulation of the dye is evident despite extreme polymer swelling. However, although the dye demonstrates very limited solubility in both THF and toluene, a significant uptake of dye is achieved. The study indicated that ethanol, methanol and acetonitrile solutions resulted in poor uptake of the dye, whereas the use of ethyl acetate and acetone swelling solutions achieved strong polymer crystal violet colouration, indicative of the most efficacious uptake of the dye. Since the use of acetone as a swelling agent for incorporation of photosensitiser dyes into medical grade polymers has been well established, with functional testing investigations demonstrating little resultant effect on the polymeric material [19, 21–25], it was selected as the preferred solvent for further investigation.

Silicone samples were immersed in solutions comprising of varying water/ acetone ratios and crystal violet concentrations to explore that which facilitated the best uptake of the dye. Immersion of the silicone into either 100 % acetone or 100 % water crystal violet solutions for a period of 72 hours resulted in bright purple coloured silicone squares, correlating to an efficacious uptake of the dye. As the volumes of the acetone and water components of the dipping solution equalised, the polymer uptake of the dye was less efficient (Figure 9(a)).

The concentration of crystal violet in the dipping solution was optimised using water as the solvent, since it was found that this facilitated a good uptake of the dye. Silicone squares were immersed in crystal violet solutions varying in crystal violet concentration from 1×10^{-1} mol dm^{-3} to 5×10^{-6} mol dm^{-3}. The uptake of the dye onto the polymer increased with crystal violet concentration up to 10^{-3} mol dm^{-3}, after which, the uptake of dye onto the polymer decreased (Figure 9(b)).

A solution of 1×10^{-3} mol dm^{-3} crystal violet (in water) was selected and the silicone was exposed to the chosen crystal violet solution

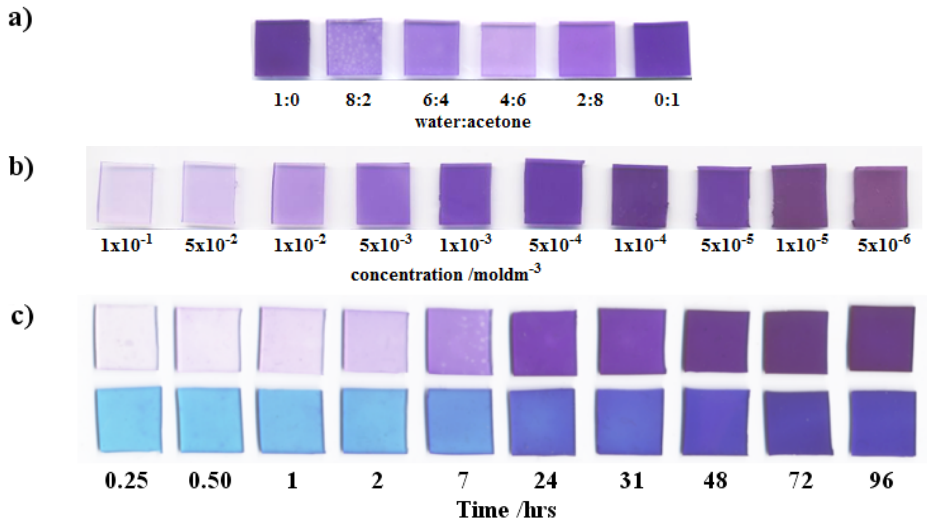

Figure 9: Silicone polymer sections prepared by immersion in: (a) Crystal violet dipping solutions of varying water : acetone ratios for a period of 72 h, (b) 100 % water crystal violet dipping solutions of varying crystal violet concentrations for a period of 72 h and (c) 1 x 10^{-3} mol dm^{-3} crystal violet dipping solutions for increasing immersion time lengths up to a period of 96 h. Methylene blue and 2 nm gold nanoparticle-encapsulated silicone polymers prepared by immersion in crystal violet dipping solutions for increasing immersion time lengths up to a period of 96 h are also shown

for a range of dipping times to further refine the process. A parallel investigation in which methylene blue-silicone sections were exposed to the aqueous crystal violet dipping solution (1 x 10^{-3} mol dm^{-3}) for a range of dipping times, was also carried out. In both studies, it was found that the uptake of the dye into the polymer increased with the immersion duration and a significant uptake of the dye occurred after as little as 7 h at room temperature (Figure 9(c)). Moreover, as demonstrated in the cross sectional photograph Figure 10, the uptake of the crystal violet dye under these conditions was a predominantly surface process, with no visible dye diffusion through the bulk of the silicone.

A further set of polymers were prepared for antimicrobial testing. The methylene blue and 2 nm gold nanoparticle-encapsulated silicone polymer samples were prepared by immersing the silicone polymer squares into a 9:1 acetone : nanogold swelling solution saturated with methylene blue, for a period of 72 h. The crystal violet-coated silicone samples were prepared as described above, by dipping the silicone into a 1 x 10^{-3} mol dm^{-3} crystal violet solution for 72 h. The crystal

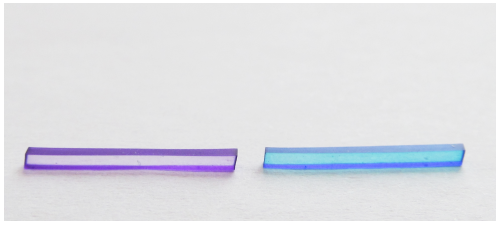

Figure 10: A cross section of the untreated- and methylene blue and 2 nm gold nanoparticle-encapsulated silicone sections coated with crystal violet by immersion in a 1 x 10^{-3} mol dm^{-3} crystal violet dipping solution for 72 h

violet-coated, nanogold-encapsulated samples were prepared using a novel two-step process. The first step involved the encapsulation of 2 nm gold nanoparticles into the silicone by immersion of the polymer in a 9:1 acetone : nanogold swelling solution, for a period of 72 h. The nanogold-encapsulated silicone was subsequently coated with crystal violet, using the protocol detailed above. It is thought that this synthetic route achieves the uniform encapsulation of 2 nm gold nanoparticles throughout the polymer bulk, with visible concentrated bands of crystal violet dye at the polymer surfaces. A similar protocol was used to prepare crystal violet-coated, methylene blue and nanogold-encapsulated samples. However, in the initial dipping step, the 9:1 acetone : nanogold swelling solution was saturated with methylene blue, resulting in the uniform encapsulation of dye through the polymer bulk, with concentrated crystal violet bands at the polymer surfaces (Figure 10).

3.3.2 *Materials Characterisation*

3.3.2.1 *UV-Visible Absorbance Spectroscopy*

The UV-Vis absorbance spectra of crystal violet-encapsulated silicone samples prepared by immersion in a range of crystal violet/ organic solvent swelling solutions, was measured within the range 400 - 750 nm (Figure 8(c)). The spectra indicate that the use of different organic solvents to encapsulate the dye within a silicone polymer, does not affect the main absorption peak position ($\lambda \approx 588$ nm), or the shoulder peak position ($\lambda \approx 546$ nm). However, varying the organic solvent impacts on the efficacy of dye uptake into the

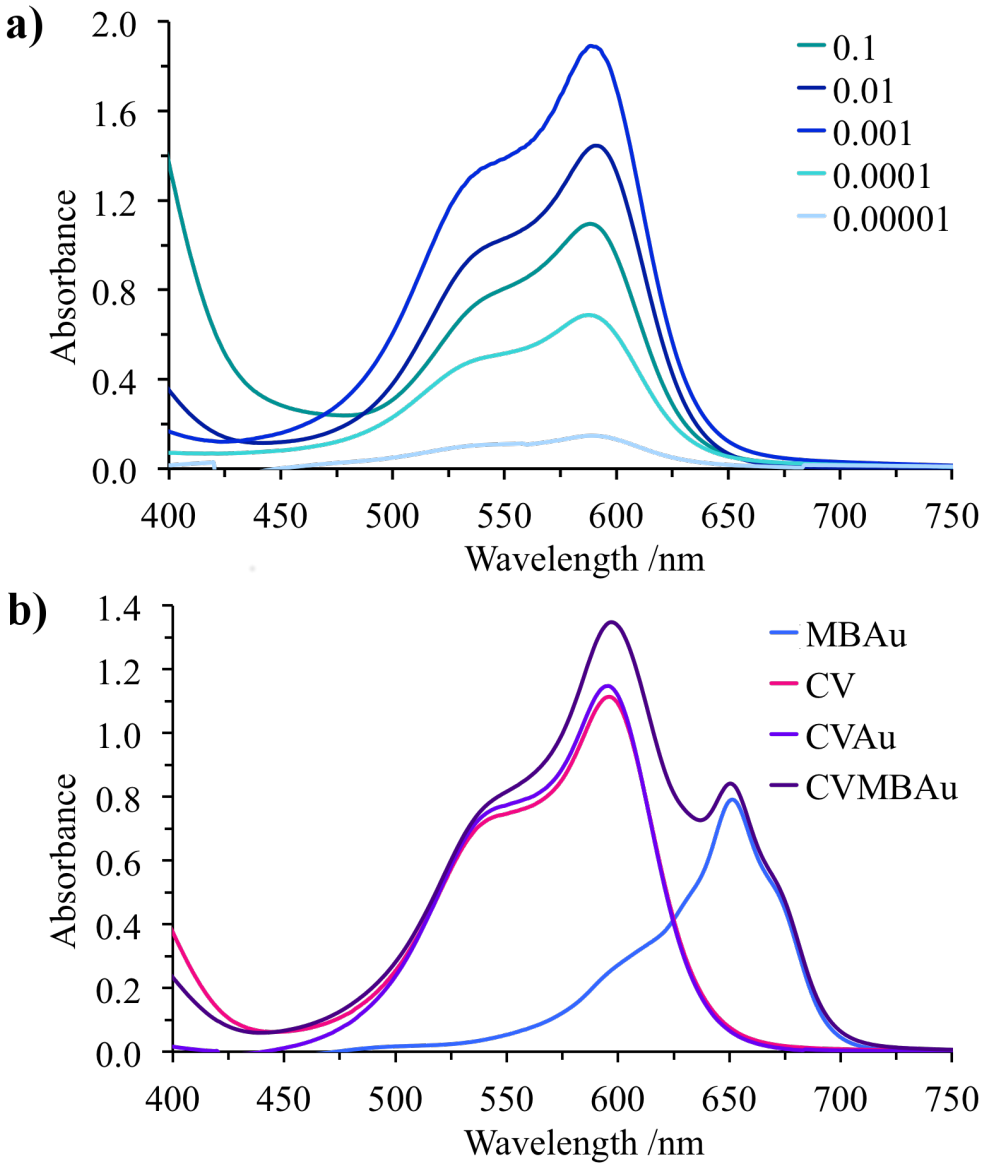

Figure 11: (a) UV-Vis absorbance spectra measured in the range 400 - 750 nm of crystal violet-coated silicone polymers prepared using a simple dipping method. The silicone polymers were immersed in crystal violet solutions of varying concentrations: 1 x 10^{-1} mol dm^{-3}, 1 x 10^{-2} mol dm^{-3}, 1 x 10^{-3} mol dm^{-3}, 1 x 10^{-4} mol dm^{-3} and 1 x 10^{-5} mol dm^{-3}. (b) UV-Vis absorbance spectra measured in the range 400 - 750 nm of samples used for microbiological testing: Methylene blue and nanogold-encapsulated silicone, crystal violet-coated silicone, crystal violet-coated, nanogold-encapsulated silicone, crystal violet-coated, methylene blue and nanogold-encapsulated silicone

polymer. It is clear from the absorbance spectra that the use of ethyl acetate-, acetone- and toluene-crystal violet swelling solutions result in efficient dye uptake, whereas methanol-, acetonitrile- and hexane-crystal violet swelling solutions achieve extremely limited

encapsulation of the dye, within the same dipping time period. This can be attributed to a combination of two key factors: (i) the degree to which the solvent induces polymer swelling and (ii) the solubility of the crystal violet dye in the organic solvent. As shown in Figures 8(a) and 8(b), although hexane induces significant polymer swelling, the dye is largely insoluble in the solvent and thus, limited/ no visible encapsulation of the dye is achieved. Interestingly despite the poor solubility of crystal violet in both THF and toluene, due to extreme polymer swelling, significant uptake of the dye is achieved. However, it is a combination of both good dye-solvent solubility and sufficient polymer swelling that results in the best uptake of dye, as achieved using either ethyl acetate or acetone as swelling solvents.

The UV-Vis absorbance spectra of silicone samples immersed for 3 days in crystal violet solutions of varying concentrations, were measured within the range 400 - 750 nm (Figure 11(a)). When immobilised in the silicone substrate, the main absorption peak of crystal violet is at $\lambda \approx 590$ nm and a shoulder peak at $\lambda \approx 548$ nm is also present. Furthermore, the spectra also indicate a slight variation in the peak maxima with dye concentration. As is clear from Figure 11(a), increasing the concentration of crystal violet in solution results in an increased uptake of dye, up to a concentration of ~5 x 10^{-3} mol dm^{-3} crystal violet (not shown on spectra). Surprisingly, further increase in crystal violet concentration effects a reversal of this trend, with increasing crystal violet concentrations correlating to a decreasing uptake of the dye.

The UV-Vis absorbance spectra of silicone samples used in microbiological testing were also recorded. Figure 11(b) shows the spectra of the crystal violet-coated silicone and the crystal violet-coated, nanogold-encapsulated silicone and crystal violet-coated, methylene blue and nanogold-encapsulated silicone. It is clear from the spectra that the crystal violet peaks across the sample range are similar in peak intensity and peak form, with both absorption maxima and shoulder peaks in the same wavelength region. This indicates that the presence of the nanogold does not change the spectral features. The figure also shows the absorbance spectra of the methylene

blue and nanogold-encapsulated silicone. Methylene blue has an absorption maxima of $\lambda \approx 652$ nm when encapsulated in the silicone polymer, with a shoulder peak at ~610 nm. The spectrum also suggests a second shoulder peak at ~670 nm. It should be noted that the UV-Vis absorbance spectra for both the crystal violet-coated, nanogold-encapsulated silicone sample and the methylene blue/ nanogold-encapsulated silicone sample show no detectable absorption corresponding to the presence of the gold nanoparticles, in the visible region of the spectrum. This can be attributed to the small diameter of the gold nanoparticles used (2 nm), which is below the limit for surface plasmon resonance for nanoparticle colouration (~4 nm) [21]. It was also noted that the absorbance maxima of the two crystal violet samples were comparable, indicating that the coating procedure is reproducible and the incorporation of the 2 nm gold nanoparticles does not hinder the uptake of the dye. The absorbance intensity of the crystal violet-coated, methylene blue and nanogold-encapsulated silicone differs from the other samples, but this can be attributed to the incorporation of multiple dyes within the polymer that demonstrate strong absorbance at similar wavelengths.

3.3.2.2 *ATR-FTIR Spectroscopy*

The infrared transmittance spectra of the photosensitiser dyes and dye-encapsulated silicone samples were obtained by ATR. The photosensitiser dyes methylene blue and crystal violet, were dissolved in industrial methylated spirits and the solutions were deposited onto the ATR crystal. The residual solvent was allowed to evaporate, leaving a thin film of photosensitiser dye. The infrared spectra of methylene blue showed absorbance bands in the region 1600, 1500 and 1400 cm^{-1}, characteristic of aromatic carbon-carbon bonds (Figure 12(a)). The infrared transmittance spectra of crystal violet also shows peaks correlating to aromatic carbon-carbon bonds in this region, although the absorption is much sharper (Figure 12(b)). The broad band evident on both the spectra for methylene blue and crystal violet at around 3400 cm^{-1} can at least in part, be attributed to the presence of residual IMS.

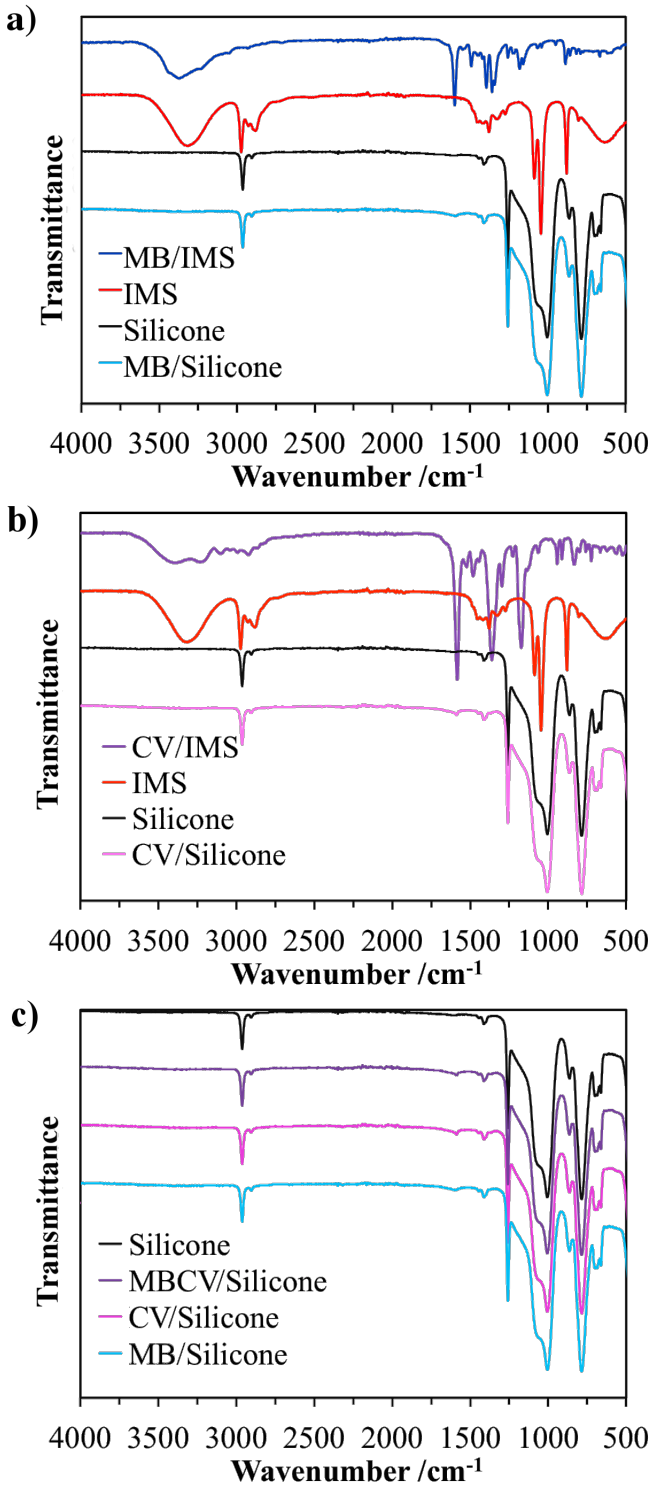

Figure 12: ATR-FTIR transmittance spectra measured within the range 4000 - 400 cm^{-1} of: (a) Methylene blue in industrial methylated spirits (IMS), methylene blue-encapsulated silicone (72 h dipping time) and untreated silicone, (b) crystal violet in IMS, crystal violet-coated silicone (96 h dipping time) and untreated silicone and (c) dye-modified and untreated silicone samples

The infrared-transmittance spectra of methylene blue-encapsulated silicone, crystal violet-coated-silicone, methylene blue encapsulated, crystal violet-coated-silicone and untreated silicone, were obtained by ATR. No significant difference in the measured spectra was evident across the sample range analysed and no peaks correlating to the presence of either dye was observed (Figure 12(c)). This can be attributed to the strong absorbance bands of the silicone substrate, which presumably masks any weak signals from the dye. The absorbance patterns obtained were expected, due to the relatively low dye concentrations present in the polymers. The sharp infrared absorption bands at 2965 cm^{-1} and 1260 cm^{-1} can be attributed to the silicone polymer. It can be suggested that the former indicates that the silicone polymer is functionalised with sp^3-carbon R groups. This is confirmed by the latter peak at 1260 cm^{-1}, which corresponds to the Si-CH_3 bond infrared absorption. The similarity between the spectra of all samples analysed - characteristic of that of the untreated silicone sample - indicated that the solvent treatment did not detrimentally affect the polymer substrate, in terms of effecting a chemical change in the silicone polymer.

3.3.2.3 *Microscopy*

Light microscopy and fluorescence microscopy were used to analyse the effects of exposing the silicone to varying concentrations of crystal violet solution, to determine whether the dye concentration in the dipping solutions can be exploited to adjust the extent of dye diffusion through the polymer bulk. The silicone samples prepared by immersion in varying concentrations of crystal violet solution were analysed using a light microscope with an attached CCD camera (Figure 13(a)). The concentration dependency on the efficacy of the uptake of the dye, in addition to the dye distribution within the polymer, is clearly demonstrated. Immersion of the silicone polymer into solutions of higher crystal violet concentration resulted in the distribution of the dye throughout the polymer bulk, with a less defined dye surface concentration. The dye diffusion through the polymer bulk decreased with crystal violet concentration. Conversely, the dye polymer surface concentration increased with the crystal

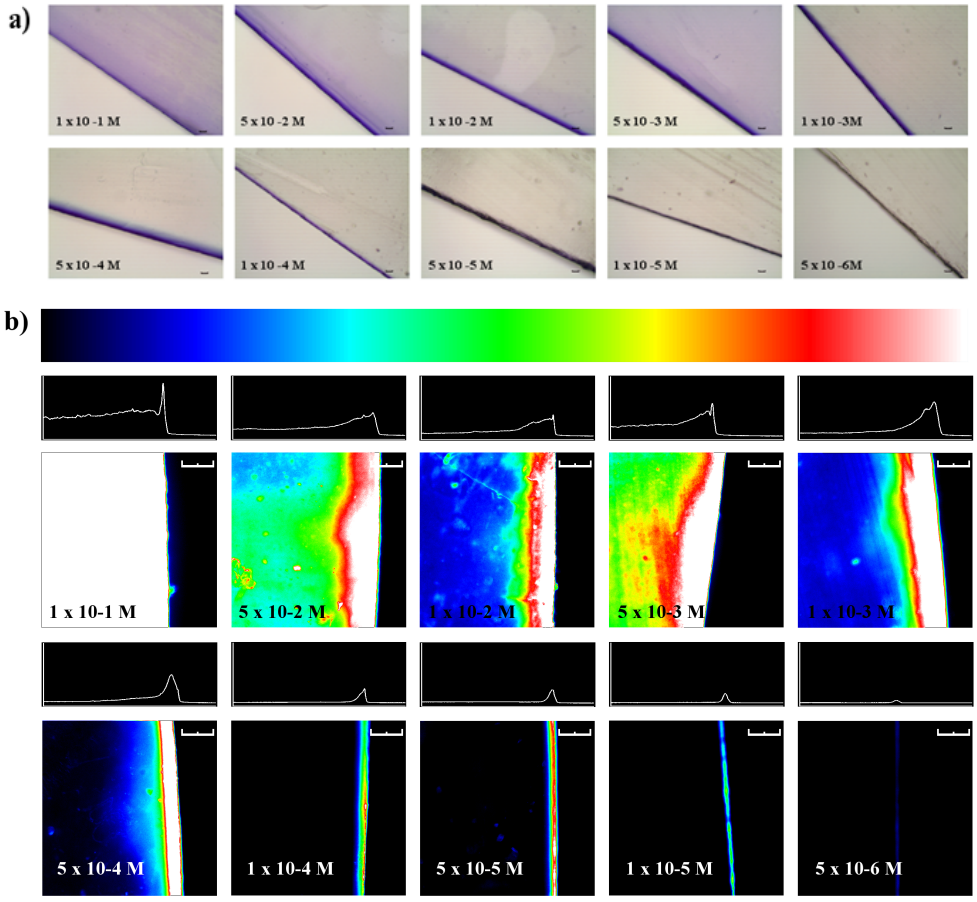

Figure 13: (a) Images of thin sections of crystal violet-coated silicone prepared by immersing the polymer in varying crystal violet dipping solution concentrations. The polymer section imaged is positioned on the upper-right hand corner of the image and is at an incline. The images were recorded using a 10x objective and the bar on each image corresponds to 100 μm. Actual polymer wall-width, 1 mm. (b) CCD false coloured fluorescence microscopy images of 10 micron thick crystal violet-coated silicone sections, prepared from polymer samples immersed in increasing concentrations of crystal violet dipping solution. The polymer analysed is shown on the left hand side of the images with a 100 micron scale bar on each image and the fluorescence intensity scale, top, increases from black (background/no fluorescence) through to white (max. fluorescence). The trace above each fluorescence image indicates the fluorescence distribution through the silicone sample, with peak intensity localised at the outer edge. The image resolution is 512 x 512 pixels, corresponding to 557 x 557 microns

violet dipping solution concentration up to a solution concentration of ~5 x 10^{-4} mol dm^{-3}, after which the uptake of the dye decreased with the dipping solution concentration. Immersion of the silicone into dipping solutions of low crystal violet concentrations such as 5 x 10^{-6} mol dm^{-3}, resulted in extremely poor uptake of the dye over the

3 day immersion period.

These polymer samples of varying crystal violet concentration were subsequently analysed using fluorescence microscopy. The crystal violet embedded in the thinly sliced silicone sections was excited using a 635 nm laser and a bandpass filter centred at 660 nm was used to detect dye fluorescence. The crystal violet fluorescence was imaged using a CCD and the acquired digital images were used to analyse the extent of the diffusion of dye through the polymer. Figure 13(b) shows examples of images obtained using fluorescence microscopy, displayed in false colour. The silicone sections were imaged such that roughly one half of the polymer examined is shown on the left hand side of each image, providing an overview of the dye diffusion gradient through the polymer. The false colour scale corresponds to low fluorescence (shown as black) to high fluorescence (shown as white). Profile plots were also obtained using ImageJ software and correlated to a graphical representation of the fluorescence distribution through the silicone polymer, shown in false colour.

The trend established using light microscopy was confirmed from the fluorescence measurements as it was found that silicone exposed to solutions of higher crystal violet concentrations, resulted in encapsulation of the dye throughout the polymer bulk. The extent of the diffusion of dye through the polymer decreased with dye concentration, such that at lower crystal violet solution concentrations, the uptake of the dye was predominantly a surface process (Figure 13(b)). It should be noted that the sample prepared for microbiological testing (1×10^{-3} mol dm^{-3}) demonstrates a substantial band of dye at the polymer surface, indicated by strong fluorescence, with a decreasing dye concentration gradient through the polymer, as shown by the 3D surface plot of the dye fluorescence distribution through the silicone (Figure 14).

The predominant cause of catheter-associated UTIs in hospitalised catheterised patients, responsible for two-thirds of reported cases, is the bacterial contamination of the extraluminal catheter surface caused by the ascension of bacteria up the urinary tract, along the

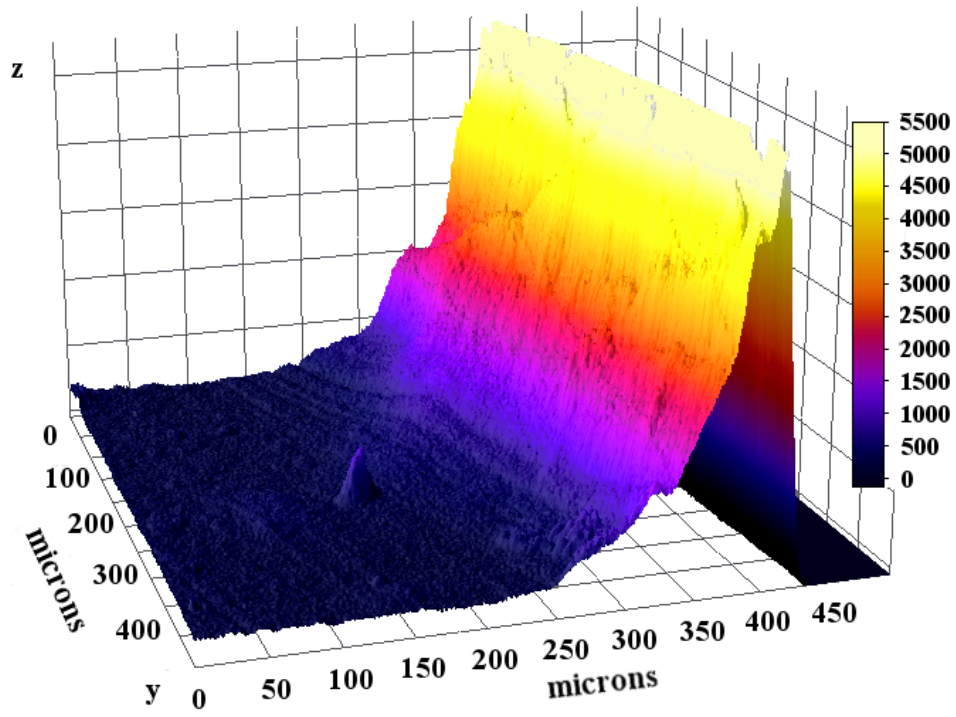

Figure 14: 3D surface plot of the fluorescence distribution through the silicone sample immersed in a 1 x 10^{-3} mol dm^{-3} crystal violet dipping solution (72 h), obtained using CCD false coloured fluorescence microscopy at 10x magnification

catheter-urethra interface [6, 27]. Estimations suggest that only one-third of these infections are attributed to microbial contamination of the intraluminal catheter surface [6, 27], with Gram-negative bacteria such as *E.coli* noted as key causative pathogens for these infections [1]. In potential applications in medical devices such as catheters, the antimicrobial activity of these modified polymers will be activated by irradiation down the catheter lumen using an optical fibre, with the fibre remaining in place for the duration of catheterisation [25]. The antimicrobial properties of the polymer can then be activated by illuminating the catheter at specific time intervals to kill bacteria in contact with the catheter surface, to prevent biofilm accumulation. Consequently, it is key that the polymer used has a substantial surface dye concentration and low dye bulk concentration to enable efficacious light delivery through the polymer for activation of the antimicrobial properties of both the internal and external device surfaces, thereby increasing the suitability of the system for potential clinical applications. Light microscopy and fluorescence microscopy

showed that the desired polymer configuration was achieved by immersing the silicone samples in a 1 x 10^{-3} mol dm^{-3} crystal violet dipping solution for a period of 72 hours. However, it should be noted that for potential commercial applications, the lengthy coating process can be shortened to a few hours by gently heating the dipping solution to 40 - 50 °C, without compromising the strong polymer surface dye uptake.

3.3.3 *Functional Testing*

3.3.3.1 *Transmission Measurements*

A power meter was used to estimate the laser power transmission through modified and unmodified silicone sections, to determine whether sufficient irradiation was received at the outer polymer surface. Results showed that 93 % transmission of laser illumination was obtained through the unmodified silicone polymer, reducing upon polymer crystal violet-coating to 69 %. The encapsulation of 2 nm gold nanoparticles within the polymeric matrix did not further decrease the transmission of laser light through the polymer. However, silicone samples encapsulated with methylene blue and gold nanoparticles, post-coated with crystal violet, showed a significantly reduced transmission of light through the polymer (43 %). This can be attributed to the methylene blue dye which is encapsulated through the polymer bulk, dissimilar to the crystal violet which is predominantly coated at the polymer surface, therefore decreasing laser transmission through the polymer bulk. Nevertheless, in all cases significant transmission through the polymer was achieved. It can be suggested that these polymeric materials are suitable for application in medical devices, as sufficient laser power is transmitted through the polymer, for light-activation of the antimicrobial properties of the outer polymer surface.

Table 1: Average contact angle measurements (°) ± standard deviation of water on the following silicone polymer surfaces: untreated, solvent treated (control), methylene blue and 2 nm gold nanoparticle encapsulated (MBAu), crystal violet-coated (CV), crystal violet-coated, 2 nm gold nanoparticle encapsulated (CVAu) and crystal violet-coated, methylene blue and 2 nm gold nanoparticle encapsulated (CVMBAu)

Silicone Sample	**Contact Angle (°)**	±	**Standard Deviation**
Untreated	102	±	1.0
Control	101	±	1.5
MBAu	100	±	0.3
CV	100	±	0.5
CVAu	100	±	0.5
CVMBAu	102	±	0.8

3.3.3.2 *Water Contact Angle Measurements*

The water contact angles of the untreated silicone, in addition to the treated silicones were measured under laboratory temperature and lighting conditions. The water contact angle measurements indicated that the untreated silicone presents a hydrophobic surface (Table 1). Moreover, it was found that there was there was negligible difference between the wetting properties of the untreated silicone, when compared to the treated silicones, whether the treatment involved solvent exposure, dye encapsulation or, encapsulation with a combination of both dye and gold nanoparticles.

3.3.3.3 *Leaching Study*

The release of crystal violet from the crystal violet-coated silicone samples into a pre-heated aqueous solution, was measured spectroscopically as a function of time. By comparing the optical density of the surrounding aqueous solution at 596 nm with a crystal violet calibration curve, the concentration of crystal violet that leached from the polymer was established (Figure 15). The figure indicates that the sample released some crystal violet into solution upon immersion, although the leaching of dye from the polymer plateaued quickly. Over a period of more than 300 hours, the leaching of crystal violet

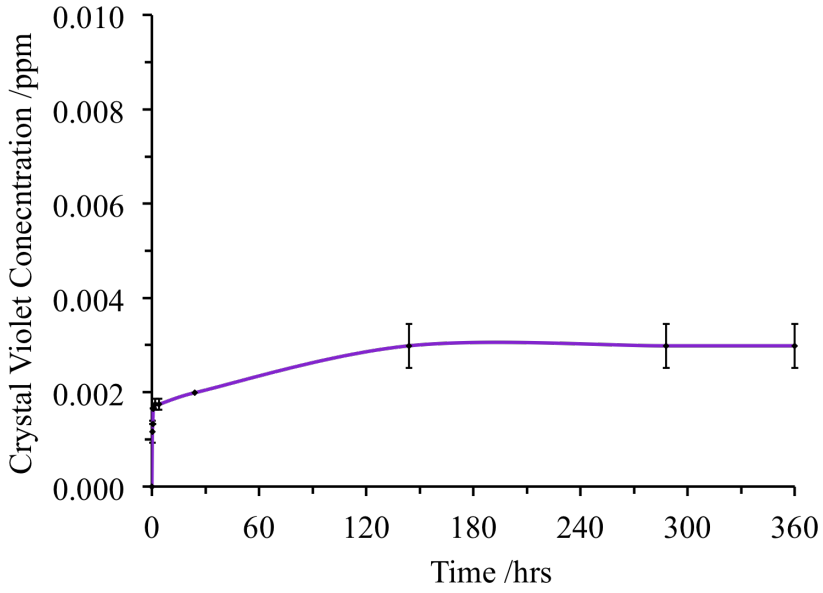

Figure 15: Leaching of crystal violet dye (ppm) from a crystal violet-coated silicone polymer into PBS solution at 37 °C, was measured as function of time (hours)

from the crystal violet-coated silicone into the surrounding PBS solution (which was maintained at 37 °C), was < 0.004 ppm, which is at the detection limit of the spectrometer.

It is anticipated that this technology can be applied to medical implants such as catheter devices, where the dye-coated catheter would be illuminated by pulsing a laser through an optical fibre. Therefore, it is important that the antimicrobial agent, the photosensitiser dye, does not leach from the polymer under aqueous conditions at 37 °C, since if significant concentrations of the photosensitiser leach from the polymer under these conditions, this may reduce the antimicrobial efficacy, in addition to causing concerns for use in potential clinical applications. The leaching studies carried out, demonstrated the stability and suitability of these materials for use in future healthcare applications.

3.3.4 *Microbiological Testing*

3.3.4.1 *Flat Polymer Sections*

In this study, a range of dye-nanogold-embedded polymers were developed and their photobactericidal properties - activated by a low power red laser (635 nm) - were investigated, to determine their antimicrobial efficacy for use in potential applications in indwelling medical devices. Medical grade silicone polymers were incorporated with both crystal violet and 2 nm gold nanoparticles to determine whether similar to the case of methylene blue [19, 21, 26], the 2 nm gold nanoparticles enhance the photochemical activity of the crystal violet. Moreover, samples encapsulated with crystal violet, methylene blue and 2 nm gold nanoparticles were synthesised, to establish whether the use of multi-dye-nanogold combinations can improve bacterial kills.

The light-activated antimicrobial activity of a range of modified silicone samples was tested against a Gram-positive bacterium and a Gram-negative bacterium, *S. epidermidis* and *E. coli*, respectively. The antimicrobial activity was activated by irradiating the samples using a 635 nm laser, such that the samples were exposed to an energy dose corresponding to 45 J cm^{-2}. A control set of samples were stored under dark conditions for the duration of laser irradiation. The photobactericidal activity of the following samples were tested: (i) solvent-treated silicone (control), (ii) crystal violet-coated silicone (CV), (iii) crystal violet-coated, 2 nm gold nanoparticle-encapsulated silicone (CVAu), (iv) methylene blue and 2 nm gold nanoparticle-encapsulated silicone (MBAu) and (v) crystal violet-coated, methylene blue and 2 nm gold nanoparticle-encapsulated silicone (CVMBAu). It should be noted that silicone samples encapsulated with 2 nm gold nanoparticles were not tested as controls, as these were previously shown to lack bactericidal activity [19].

Figure 16 shows the extent of the antimicrobial activity of the treated silicone polymers when tested against both Gram-positive and Gram-negative bacteria. Under dark conditions (~13.5 minutes incubation at room temperature), the control sample, MBAu sample and CV sample

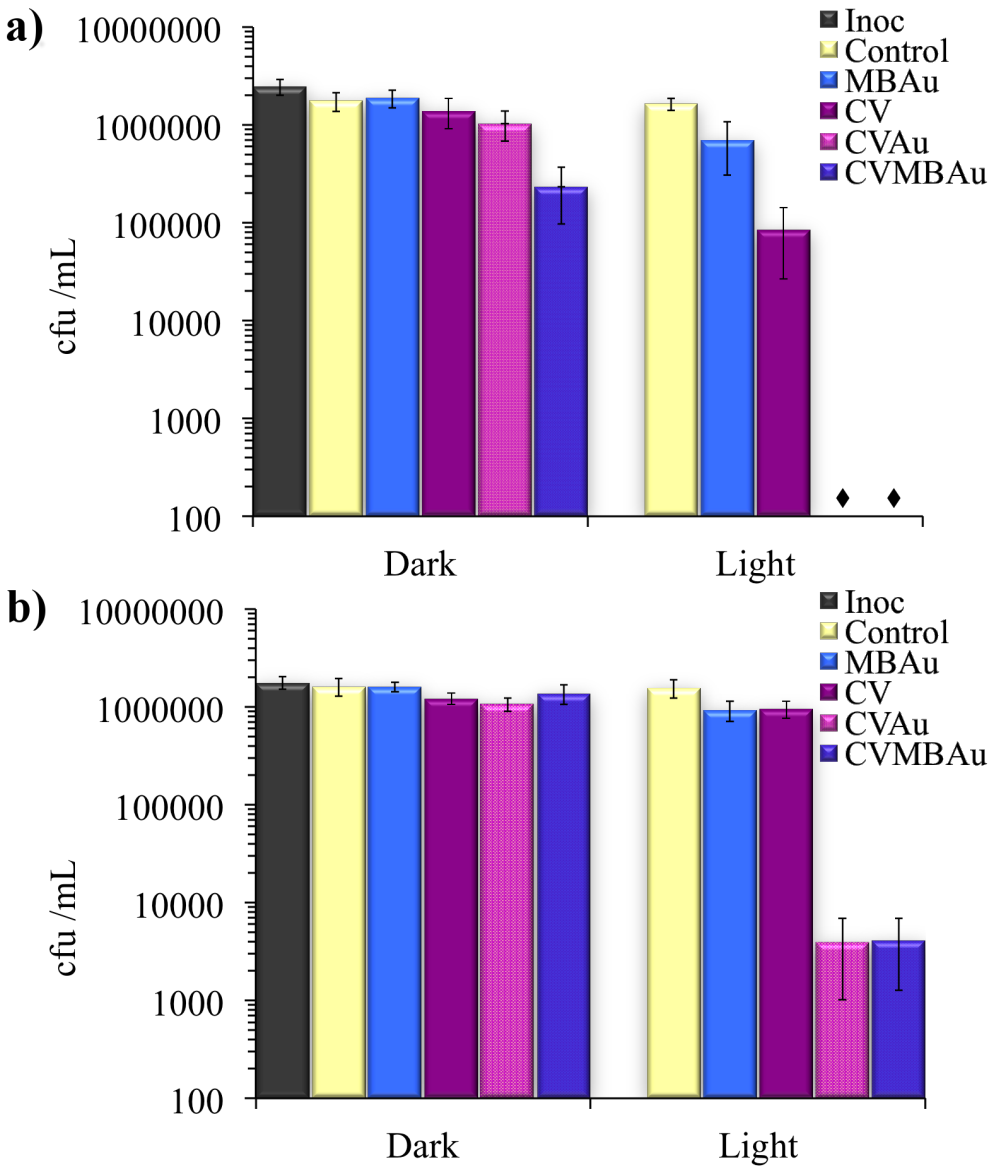

Figure 16: Graph to show the lethal photosensitisation of (a) *Staphylococcus epidermidis* and (b) *Escherichia coli* upon irradiation with a 635 nm laser (45 J cm^{-2} energy dose, ~13.5 minutes laser irradiation). Bars on the graphs represent the: initial inoculum (inoc), control silicone (control), methylene blue and 2 nm gold nanoparticle-encapsulated silicone (MBAu), crystal violet-coated silicone (CV) and crystal violet-coated silicone encapsulated with 2 nm gold nanoparticles (CVAu). The ♦ indicates where the bacterial counts are below the detection limit of 400 cfu/ mL

demonstrated no significant antimicrobial activity against *S. epidermidis*. However, some antimicrobial activity was observed in the dark on the CVAu sample and CVMBAu samples, when tested against the Gram-positive bacterium ($P < 0.01$ and $P < 0.001$ respectively). The enhanced kill achieved in the dark on the CVMBAu sample was

statistically significant compared to the CVAu sample ($P < 0.001$). Crystal violet is a well-known antiseptic agent and its use for medical treatments was described as early as 1890 when Stilling noted the antimicrobial efficacy of aniline dyes and slightly later, in the beginning of the 1900s when Churchman noted its effectiveness in the treatment of superficial skin infections [28–33]. In this experiment however, such short incubation times were used, that it was impossible to establish the full extent of the inherent bactericidal activity of the dye.

Importantly, when irradiated with laser light, efficacious antimicrobial activity was demonstrated by some samples against both Gram-positive and Gram-negative bacteria. Irradiation of the CV sample with a 635 nm laser (~13.5 min, 55.7 mW cm^{-2}) resulted in a highly significant lethal photosensitisation of *S. epidermidis* (1.46 log kill, $P < 0.001$). Moreover, a substantial enhancement in the photobactericidal activity of the crystal violet was noted when 2 nm gold nanoparticles were present ($P < 0.001$), with bacterial levels reduced below the detection limit after ~13.5 minutes of irradiation (> 4 log reduction). The methylene blue and 2 nm gold nanoparticles-encapsulated silicone samples demonstrated a reduced light-activated antimicrobial activity compared to the polymers containing crystal violet, although the kill was still statistically significant compared to the control silicone ($P < 0.001$). The ineffective photobactericidal activity of the MBAu samples compared to previous studies [19, 21, 25], may in part be attributed to the wavelength of laser light used. Previously, the antimicrobial activity of MBAu samples was activated using a 660 nm laser, whereas in this investigation, a 635 nm laser was used and the wavelength of laser light did not correlate directly to the absorption maximum of the dye. Interestingly though, as shown in Figure 11(b), the use of a 635 nm laser is a 'better match' with the methylene blue-nanogold samples than the crystal violet-nanogold samples.

In common with the experiments using *S. epidermidis*, we observed a small but statistically significant reduction in bacterial numbers with CVAu samples in the dark when tested against *E. coli* ($P < 0.001$), but no kill in either the control silicone or MBAu samples. A small but statistically significant reduction in bacterial numbers was also noted

with the CV samples in the dark ($P < 0.01$). Upon irradiation with red laser light, there was negligible kill on the control samples, whereas the MBAu samples and CV samples exhibited some photobactericidal activity against *E. coli* ($P < 0.001$). The lesser susceptibility of Gram-negative bacteria to PDT is unsurprising, given the increased complexity of the Gram-negative cell wall [13, 25, 34].

Importantly, a statistically significant enhancement in the antimicrobial activity of the crystal violet samples was observed when 2 nm gold nanoparticles were present ($P < 0.001$). Both the CVAu samples and CVMBAu samples induced the greatest lethal photosensitisation of *S. epidermidis* and *E. coli*. These samples exhibited comparable antimicrobial efficacy, with bacterial numbers reduced to below the detection limit when tested against *S. epidermidis* and a *ca.* 2.6 log reduction in bacterial numbers when tested against *E. coli*, upon irradiation with a 635 nm laser for ~13.5 min (55.7 mW cm^{-2}). It should be noted that the presence of methylene blue did not achieve a further increase in the photo-activated antimicrobial efficacy compared to the crystal violet-coated, nanogold-encapsulated sample. This can be attributed to the poor photobactericidal efficacy of the methylene blue dye at the irradiation wavelength used in this study.

It is clear that despite no intrinsic antimicrobial activity [19], the presence of the 2 nm gold nanoparticles enhances the photoactivated antimicrobial activity of the triarylmethane dye, crystal violet. This effect has been reported previously, although only with phenothiazine dyes [19, 21, 26, 35]. Both CVAu and CVMBAu samples exhibited comparable exceptional photobactericidal activity, with kills against *E. coli* at least 0.4 log greater than previously reported kills for dye-incoporated silicone polymers prepared using a simple dipping technique [19, 21]. One study reports a similarly outstanding photosensitisation of both Gram-positive and Gram-negative bacteria on toluidine blue O and nanogold incorporated polyurethane polymers, using very short irradiation times [23]. Nevertheless, it should be noted that in this current investigation, the laser power was reduced from 1 W as used previously [23], in order to deliver a lower energy dose over a longer time such that the system is more suitable for

potential use in medical devices, since a 1 W laser would be too expensive and potentially dangerous for use in patients.

It is interesting to note that although the wavelength of laser irradiation does not correspond to the absorption maximum wavelength of either dye, the efficacy of the photobactericidal activity of the CVAu sample and CVMBAu sample far surpasses that of the MBAu samples tested. The antimicrobial activity exhibited by these modified polymers stems from the photogeneration of ROS such as singlet oxygen upon excitation of the photosensitiser molecules and a consideration of the diffusion of these species may shed light onto the substantial differences in polymer photosensitisation of bacteria. To roughly approximate the diffusion distance of the singlet oxygen species within the polymer, 'Einstein's equation for Brownian motion' for the diffusion of atoms and ions in 1 dimension (Equation 1) can be used.

$$\tau \approx \frac{l^2}{2D} \tag{1}$$

Where 'l' is the mean distance travelled by the diffusing species singlet oxygen, 'D' is the diffusion coefficient approximated as that for molecular oxygen in a PDMS polymer (5.4×10^{-10} m^2 s^{-1} [36]) and 'τ' is the lifetime of singlet oxygen generated by the excitation at 532 nm of crystal violet embedded in the silicone polymer (40 μs). The diffusion distance of the singlet oxygen species can be estimated as 0.2 microns. This very short diffusion distance perhaps indicates why under the same irradiation conditions, the crystal violet-coated, nanogold-encapsulated silicone polymer and crystal violet-coated, methylene blue and nanogold-encapsulated silicone polymer are more effective than the methylene blue and nanogold-encapsulated polymer, in terms of their photobactericidal activity (assuming a Type 2 photochemical mechanism). Fluorescence microscopy demonstrates that the crystal violet polymers have concentrated bands of dye very close to the polymer surface. This theoretically correlates to high concentrations of ROS produced at the polymer surface, in close proximity to the bacterial species. Conversely, the methylene blue and nanogold-encapsulated polymer has a uniform distribution of dye

throughout the polymeric matrix, but does not present concentrated bands of methylene blue at the polymer surface. Hence, contrary to the case of the crystal violet/ nanogold incorporated silicone, the ROS produced upon irradiation of these polymers may not be sufficiently close to the polymer surface to initiate an 'attack' against colonising bacteria, subsequently leading to its inefficacious antimicrobial activity under these irradiation conditions.

3.3.4.2 *Commercial Catheter Sections*

Further microbiological studies were carried out on commercial catheters modified to incorporate the photosensitiser dyes, crystal violet and methylene blue, in addition to 2 nm gold nanoparticles.[i] The light-activated antimicrobial activity of these samples was tested against a range of Gram-positive and Gram-negative bacteria, including those noted as key causative pathogens for UTIs [37]. The samples were tested against the following bacteria: *E. coli*, *S. epidermidis*, MRSA, *P. mirabilis*, *E. faecalis* and *P. aeruginosa*. The antimicrobial activity was activated by irradiating the samples using a 635 nm laser, such that the samples were exposed to an energy dose corresponding to 45 J cm^{-2} over an irradiation time period of *ca.* 18 minutes. A control set of CVMBAu samples were stored in the dark for the duration of laser irradiation.

The extended microbiological testing was carried out to determine whether the efficacious photobactericidal efficacy activity demonstrated by the crystal violet-coated, methylene blue and gold nanoparticle-encapsulated flat medical grade silicone, was reproducible when the dye-nanogold combination was encapsulated into commercially available 100 % silicone catheters. Note that further sample controls were not used in this investigation, since the principal experimental aim was to confirm the efficacy of the antimicrobial activity of these samples.

i This study was kindly carried out by Miss Annapaula Correia at the UCL Eastman Dental Institute, Division of Microbial Diseases

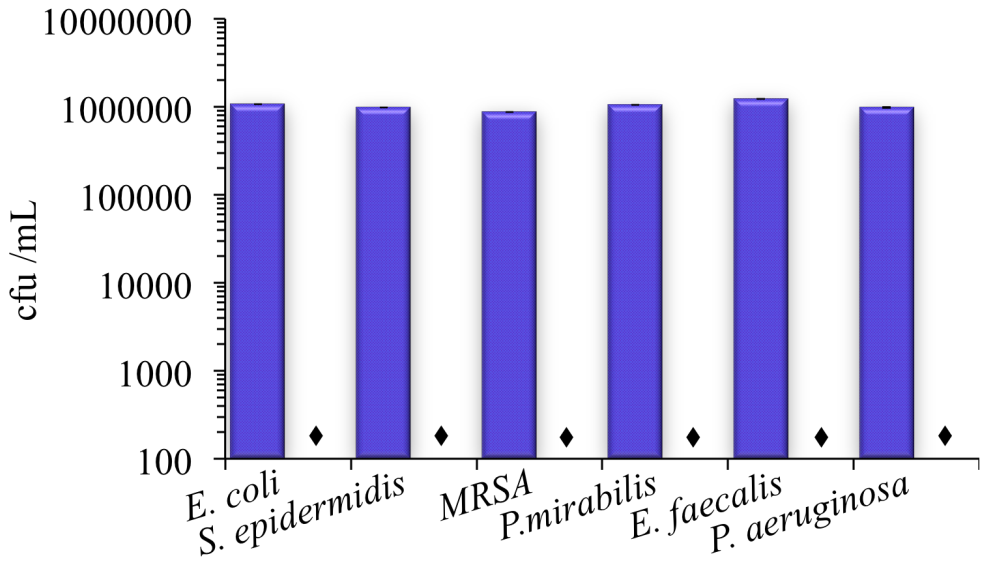

Figure 17: Lethal photosensitisation of key causative agents of urinary tract infections by crystal violet-coated, methylene blue and gold nanoparticle-encapsulated (CVMBAu) commercial catheter surfaces. The antimicrobial activity of the materials was activated using a 635 nm laser (45 J cm^{-2} energy dose, ~18 minutes laser irradiation). Bars on the graphs represent the CVMBAu catheter sections when stored under dark conditions (purple bar). The ♦ represents the irradiated CVMBAu catheter sections and indicates where the bacterial counts are below the detection limit of 400 cfu/ mL. *This work was carried out by Miss Annapaula Correia, Division of Microbial Diseases, UCL Eastman Dental Institute*

Control CVMBAu samples maintained under dark conditions did not exhibit significant antimicrobial activity, with bacterial numbers of the order ~10^6 cfu /mL (Figure 17). However, upon irradiation with a low power red laser (*ca.* 18 minutes), the numbers of all the bacterial species tested were reduced to below the detection limit ($P < 0.001$). The efficacy of this antimicrobial technology when incorporated into commercially available catheters against a wide range of bacteria associated with hospital-acquired infection is extremely promising. Over exposure to antibiotics has been associated with the rise of bacterial drug-resistance [11], and infections such as UTIs, are becoming increasingly difficult to treat. Consequently, it is vital that an infection-prevention strategy, effective against a wide range of bacteria, is developed. Due to the non-site specific mechanism by which the lethal photosensitisation of bacteria occurs, this strategy circumvents the issue of bacterial resistance to the antimicrobial

agent [13, 19]. It is also anticipated that in clinical applications, the possible emergence of crystal violet resistant Gram-positive bacteria is unlikely, since these microorganisms are extremely susceptible to PDT. Consequently, the incorporation of this antimicrobial photosensitiser should not add to the ever-increasing problem of bacterial drug-resistance.

A further cause for concern is the possible effect of the photosensitiser and photogenerated products on host cell tissue, when regarding potential applications in urinary catheter devices. Leaching studies have demonstrated stability of the crystal violet under aqueous conditions at body temperature and thus, release of the dye upon use of the device is improbable, reducing the likelihood of subsequent adverse effects. In addition, it is important that the PDT conditions used to induce the lethal photosensitisation of bacteria on dye incorporated polymers, do not induce a similar phototoxic effect against host cells in the vicinity [25]. Although only a few *in-vitro* studies comparing the effects of antimicrobial PDT conditions on mammalian cells have been conducted, these have indicated the existence of a therapeutic window in which bacterial cells can be targeted, without compromising mammalian cells [38]. Both the irradiation time and photosensitiser concentration sufficient to cause bacterial cell death, does not effect similar damage to mammalian cells [20, 25, 38–42]. Moreover, due to the short half life (< 1 μs) and diffusion distance (10 - 100 nm) of ROS such as singlet oxygen in a physiological environment, it is unlikely to cause significant long-term damage to the 'shedding' nature of the host epithelium cells in the environment of the catheter device [19]. In spite of this, further investigations into the *in-vivo* safety and photobactericidal efficacy of modified silicone need to be accomplished, prior to a clinical evaluation into its suitability for use in medical practice.

3.4 CONCLUSIONS

This chapter details the successful incorporation of 2 nm gold nanoparticles, methylene blue and crystal violet dye into medical

grade silicone, using an innovative two step synthetic route. Efficacious uptake of the crystal violet dye was achieved without the use of an organic solvent, resulting in a polymer with even, concentrated bands of crystal violet on both polymer surfaces, but no dye distributed in the bulk. This non-uniform dye distribution is beneficial for potential clinical applications in catheter devices, since it allows more laser light to pass through the polymer bulk to activate the photobactericidal properties of the outer surface. Spectroscopic analysis showed that the presence of 2 nm gold nanoparticles did not impact on the spectroscopic signature pattern of the crystal violet dye. Moreover, the modification of the silicone to incorporate the antimicrobial agents did not significantly change the wetting properties of the polymer and the dye incorporated polymers were stable under aqueous conditions at 37 °C.

Crystal violet-coated silicone demonstrated significant light-activated antimicrobial activity against Gram-positive bacteria, although this effect was more limited when tested against Gram-negative bacteria. However, the presence of 2 nm gold nanoparticles in combination with crystal violet was found to dramatically enhance the lethal photosensitisation of bacteria, such that a > 2.6 log kill was achieved against Gram-negative bacteria and bacterial numbers were reduced to below the detection limit, when tested against *S. epidermidis*. Comparably efficacious antimicrobial activity was exhibited by crystal violet-coated, methylene blue and gold nanoparticle encapsulated silicone. Both samples demonstrated exceedingly efficacious antimicrobial activity against both Gram-positive and Gram-negative bacteria upon irradiation with a low power laser for short time periods. Indeed, to our knowledge this is the most potent laser-activated polymer developed to date, for use in medical devices. This is even more exciting as it was shown that the crystal violet-nanogold silicone combination has statistically significant dark kill of bacteria, even over the short time period (13.5 minutes) of the experiment. This is the first time that light-activated antimicrobial polymer combinations have shown dark kill, presumably due to the intrinsic bactericidal properties of the crystal violet. This opens up

wider and simple methods of clinical use.

For the first time, significant kill against a wide range of bacteria noted as causative pathogens for UTIs was accomplished for a light-activated antimicrobial polymer. Commercial catheters incorporated with the novel antimicrobial technology, reduced bacterial numbers to below the detection limit, when irradiated with a low power red laser for 18 minutes. It is hoped that this novel system may potentially help reduce the impact of catheter-associated UTIs in clinical practice. In the next chapter, these crystal violet and nanogold- and crystal violet, methylene blue and nanogold-incorporated silicone polymers are tested using a white light source to activate the antimicrobial properties, to determine whether this potent antimicrobial technology can also be used in hospital touch surface applications, to help maintain low surface microbial contamination levels in healthcare environments.

REFERENCES

[1] "National Audit Office: Reducing Healthcare Associated Infections in Hospitals in England." In: *Report by the Controller and Auditor General, HC 560 Session 2008-2009* (12 June 2009).

[2] "Twenty-fourth Report 2004-05: Improving patient care by reducing the risks of hospital acquired infection: A progress report." In: *House of Commons Committee of Public Accounts* (2005).

[3] R. Plowman. "The Socioeconomic Burden of Hospital Acquired Infection." In: *Eurosurveillance* 5 (2000), Article 5.

[4] R. O. Darouiche. "Device-associated infections: A macroproblem that starts with microadherence." In: *Clinical Infectious Diseases* 33 (2001), pp. 1567–1572.

[5] S. Hagen, L. Sinclair, and S. Cross. "Washout policies in long-term indwelling urinary catheterisation in adults." In: *Cochrane Database of Systematic Reviews* (2010).

[6] P. Jahn, M. Preuss, A. Kernig, G. Langer, and A. Seifert-Huehmer. "Types of indwelling urinary catheters for long-term bladder drainage in adults." In: *Cochrane Database of Systematic Reviews* (2007).

[7] B. Niel-Weise and P. van den Broek. "Urinary catheter policies for short-term bladder drainage in adults." In: *Cochrane Database of Systematic Reviews* (2005).

[8] B. S. Niel-Weise and P. J. van den Broek. "Antibiotic policies for short-term catheter bladder drainage in adults." In: *Cochrane Database of Systematic Reviews* (2005).

[9] B. Niel-Weise and P. J. van den Broek. "Urinary catheter policies for long-term bladder drainage." In: *Cochrane Database of Systematic Reviews* (2005).

[10] K. Schumm and T. B. L. Lam. "Types of urethral catheters for management of short-term voiding problems in hospitalised adults." In: *Cochrane Database of Systematic Reviews* (2008).

[11] S. Noimark, C. W. Dunnill, M. Wilson, and I. P. Parkin. "The role of surfaces in catheter-associated infections." In: *Chemical Society Reviews* 38 (2009), pp. 3435–3448.

[12] S. Noimark, C. W. Dunnill, and I. P. Parkin. "Shining light on materials - A self-sterilising revolution." In: *Advanced Drug Delivery Reviews* 65 (2013), pp. 570–580.

[13] M. R. Hamblin and T. Hasan. "Photodynamic therapy: a new antimicrobial approach to infectious disease?" In: *Photochemical & Photobiological Sciences* 3 (2004), pp. 436–450.

[14] T. Maisch. "Anti-microbial photodynamic therapy: useful in the future?" In: *Lasers in Medical Science* 22 (2007), pp. 83–91.

[15] T. Maisch, S. Hackbarth, J. Regensburger, A. Felgentraeger, W. Baeumler, M. Landthaler, and B. Roeder. "Photodynamic inactivation of multi-resistant bacteria (PIB) - a new approach to treat superficial infections in the 21st century." In: *Journal Der Deutschen Dermatologischen Gesellschaft* 9 (2011), pp. 360–366.

[16] S. Perni, P. Prokopovich, J. Pratten, I. P. Parkin, and M. Wilson. "Nanoparticles: their potential use in antibacterial photodynamic therapy." In: *Photochemical & Photobiological Sciences* 10 (2011), pp. 712–720.

[17] I. J. MacDonald and T. J. Dougherty. "Basic principles of photodynamic therapy." In: *Journal of Porphyrins and Phthalocyanines* 5 (2001), pp. 105–129.

[18] M. A. Kohanski, D. J. Dwyer, B. Hayete, C. A. Lawrence, and J. J. Collins. "A common mechanism of cellular death induced by bactericidal antibiotics." In: *Cell* 130 (2007), pp. 797–810.

[19] S. Perni, C. Piccirillo, J. Pratten, P. Prokopovich, W. Chrzanowski, I. P. Parkin, and M. Wilson. "The antimicrobial properties of light-activated polymers containing methylene blue and gold nanoparticles." In: *Biomaterials* 30 (2009), pp. 89–93.

[20] B. Zeina, J. Greenman, D. Corry, and W. M. Purcell. "Cytotoxic effects of antimicrobial photodynamic therapy on keratinocytes in vitro." In: *British Journal of Dermatology* 146 (2002), pp. 568–573.

[21] S. Perni, C. Piccirillo, A. Kafizas, M. Uppal, J. Pratten, M. Wilson, and I. P. Parkin. "Antibacterial Activity of Light-Activated Silicone Containing Methylene Blue and Gold Nanoparticles of Different Sizes." In: *Journal of Cluster Science* 21 (2010), pp. 427–438.

[22] S. Perni, P. Prokopovich, I. P. Parkin, M. Wilson, and J. Pratten. "Prevention of biofilm accumulation on a light-activated antimicrobial catheter material." In: *Journal of Materials Chemistry* 20 (2010), pp. 8668–8673.

[23] S. Perni, P. Prokopovich, C. Piccirillo, J. Pratten, I. P. Parkin, and M. Wilson. "Toluidine blue-containing polymers exhibit potent bactericidal activity when irradiated with red laser light." In: *Journal of Materials Chemistry* 19 (2009), pp. 2715–2723.

[24] S. Perni, J. Pratten, M. Wilson, C. Piccirillo, I. P. Parkin, and P. Prokopovich. "Antimicrobial Properties of Light-activated Polyurethane Containing Indocyanine Green." In: *Journal of Biomaterials Applications* 25 (2011), pp. 387–400.

[25] S. Noimark, C. W. Dunnill, C. W. M. Kay, S. Perni, P. Prokopovich, S. Ismail, M. Wilson, and I. P. Parkin. "Incorporation of methylene blue and nanogold into polyvinyl chloride catheters; a new approach for light-activated disinfection of surfaces." In: *Journal of Materials Chemistry* 22 (2012), pp. 15388–15396.

[26] A. J. T. Naik, S. Ismail, C. Kay, M. Wilson, and I. P. Parkin. "Antimicrobial activity of polyurethane embedded with methylene blue, toluidene blue and gold nanoparticles against Staphylococcus aureus; illuminated with white light." In: *Materials Chemistry and Physics* 129 (2011), pp. 446–450.

[27] P. A. Tambyah, K. T. Halvorson, and D. G. Maki. "A prospective study of pathogenesis of catheter-associated urinary tract infections." In: *Mayo Clinic Proceedings* 74 (1999), pp. 131–136.

[28] L. P. Garrod. "The Selective Bacteriostatic Action of Gentian Violet." In: *British Medical Journal* 1 (1942), pp. 290–1.

[29] P. Bakker, H. V. Doorne, V. Gooskens, and N. F. Wieringa. "Activity of gentian violet and brilliant green against some skin microorganisms associated with skin infections." In: *International Journal of Dermatology* 31 (1992), pp. 210–213.

[30] J. W. Churchman and W. H. Michael. "The selective action of gentian violet on closely related bacterial strains." In: *Journal of Experimental Medicine* 16 (1912), pp. 822–831.

[31] J. W. Churchman. "The selective bactericidal action of gentian violet." In: *Journal of Experimental Medicine* 16 (1912), 221–U50.

[32] J. Stilling. "The aniline dyes as antiseptics, and their use in practice." In: *The Lancet* 136 (1890), pp. 965–966.

[33] J. Stilling. "The aniline dyes as antiseptics." In: *The Lancet* 137 (1891), pp. 872–873.

[34] S. George, M. R. Hamblin, and A. Kishen. "Uptake pathways of anionic and cationic photosensitizers into bacteria." In: *Photochemical & Photobiological Sciences* 8 (2009), pp. 788–795.

[35] J. Gil-Tomas, S. Tubby, I. P. Parkin, N. Narband, L. Dekker, S. P. Nair, M. Wilson, and C. Street. "Lethal photosensitisation of Staphylococcus aureus using a toluidine blue O-tiopronin-gold nanoparticle conjugate." In: *Journal of Materials Chemistry* 17 (2007), pp. 3739–3746.

[36] S. Chowdhury, V. R. Bhethanabotla, and R. Sen. "Measurement of diffusion coefficient of oxygen in FRP using luminescence quenching." In: *Composites & Polycon 2007, American Composites Manufacturers Association*. Tampa, FL.

[37] *The Merck Manual: Bacterial Urinary Tract Infections*. http://www.merckmanuals.com/professional/genitourinary_disorders/urinary_tract_infections_uti/bacterial_urinary_tract_infections.html. Accessed: 2014-06-11.

[38] Y. Xu, M. J. Young, R. A. Battaglino, L. R. Morse, C. R. Fontana, T. C. Pagonis, R. Kent, and N. S. Soukos. "Endodontic Antimicrobial Photodynamic Therapy: Safety Assessment in Mammalian Cell Cultures." In: *Journal of endodontics* 35 (2009), pp. 1567–1572.

[39] T. Maisch, C. Bosl, R. M. Szeimies, N. Lehn, and C. Abels. "Photodynamic effects of novel XF porphyrin derivatives on prokaryotic and eukaryotic cells." In: *Antimicrobial Agents and Chemotherapy* 49 (2005), pp. 1542–1552.

[40] M. Soncin, C. Fabris, A. Busetti, D. Dei, D. Nistri, G. Roncucci, and G. Jori. "Approaches to selectivity in the Zn(ii)-phthalocyanine-photosensitized inactivation of wild-type and antibiotic-resistant Staphylococcus aureus." In: *Photochemical & Photobiological Sciences* 1 (2002), pp. 815–819.

[41] B. Zeina, J. Greenman, D. Corry, and W. M. Purcell. "Antimicrobial photodynamic therapy: assessment of genotoxic effects on keratinocytes in vitro." In: *British Journal of Dermatology* 148 (2003), pp. 229–232.

[42] S. George and A. Kishen. "Advanced Noninvasive Light-activated Disinfection: Assessment of Cytotoxicity on Fibroblast Versus Antimicrobial Activity Against Enterococcus faecalis." In: *Journal of Endodontics* 33 (2007), pp. 599–602.

4

WHITE LIGHT-ACTIVATED ANTIMICROBIAL POLYMERS; CRYSTAL VIOLET, METHYLENE BLUE AND GOLD NANOPARTICLE-ENCAPSULATED SILICONE

4.1 INTRODUCTION

Much research has focused on employing a range of synthetic strategies to develop both hard and soft antimicrobial surfaces [1–3]. Examples include: deposition of TiO_2 or doped-TiO_2 films onto hard surfaces [4–9], silver ion technology [10, 11], copper coated or incorporated surfaces [12–15], the covalent attachment of quaternary ammonium salts to polymeric surfaces [16, 17], microbicide-releasing surfaces [18, 19], in addition to the incorporation of photosensitiser dyes into polymers [20–32]. The latter, as detailed in Chapter 3, is a particularly interesting approach since photosensitisers can inactivate micro-organisms via multiple, conserved targets giving a broad spectrum of activity and low risk of resistance development.

The previous chapter describes the synthesis, characterisation and testing of multi-dye-nanogold incorporated antimicrobial polymers for use in indwelling medical devices such as urinary catheters. The materials were strategically developed such that concentrated bands of crystal violet were present on both polymer surfaces, with 2 nm gold nanoparticles and methylene blue embedded throughout the polymer bulk. It is thought that the high surface concentration of dye maximises the antimicrobial activity of these materials, since the diffusion distance of ROS such as singlet oxygen is very short (estimated as < 1 micron). The antimicrobial activity of these surfaces was activated used a low power red laser light and it is anticipated that in clinical applications an optical fibre can be used to irradiate the indwelling medical device.

A two-step synthetic strategy was used to develop the photobactericidal polymers: a simple dipping step for surface uptake of crystal violet and a 'swell-encapsulation-shrink' technique for encapsulation of the light-activated antimicrobial combination, methylene blue and 2 nm gold nanoparticles, into the medical grade silicone. The literature details the antimicrobial potency of photosensitiser dye-based photobactericidal polymers developed using this synthetic strategy, with resultant materials inducing the lethal photosensitisation of both Gram-positive and Gram-negative bacteria upon either short-term illumination using a laser light source (order of minutes), or over a slightly longer-term irradiation duration, using a standard hospital light source to activate the antimicrobial properties of the surfaces (order of hours) [20–23, 25, 27–32]. Recent research has primarily been targeted towards the development of potent light-activated antimicrobial materials for use in medical devices, that require laser-irradiation to activate the bactericidal properties [20–25, 27]. However, some research on the incorporation of photosensitiser dyes into polymers for use as a material for touch surfaces in a clinical environment has been achieved [29–32].

The antimicrobial activity of the crystal violet-methylene blue-nanogold-incorporated silicone developed in the previous chapter can also be activated using a standard white hospital light source, as the light-activated antimicrobial agents present, absorb light across the visible region of the electromagnetic spectrum. This chapter reports on the efficacious bactericidal activity of crystal violet-coated, methylene blue and 2 nm gold nanoparticle incorporated silicone under both white light illumination and in the dark. The modified polymers were prepared by use of the two-step dipping process as detailed in the previous chapter and the materials were characterised using UV-Vis absorbance spectroscopy. Functional testing of the material included an examination of the wetting properties, in addition to an extensive photostability investigation. Microbiological testing of the material involved a comparison with previously synthesised photosensitiser-incorporated silicones against both a Gram-positive and a Gram-negative bacterium, using a white light source comparable to standard hospital lighting conditions

to activate the antimicrobial properties of the polymers. The multi-dye-nanogold incorporated polymer demonstrated the most potent photobactericidal activity upon white light illumination reported to this point, for dye-embedded polymers and surprisingly for the first time, significant dark kill of both *S. epidermidis* and *E. coli* was observed. This latter fact is a significant step-forward for dye-based antimicrobial surfaces, as it indicates that they can be efficacious under any lighting conditions.

4.2 EXPERIMENTAL

4.2.1 *Chemicals and Substrates*

The reagents used in materials synthesis were as follows: Methylene blue hydrate (Riedel-de Haën), crystal violet (Sigma, U.K.), L-glutathione (Sigma, U.K.), HPLC grade water (Sigma, U.K.), 2 nm gold nanoparticles (2.49 x 10^{-7} mol L^{-1}, BBI Solutions, U.K.), $HAuCl_4.3H_2O$ (Alfa Aesar, U.K.) and acetone (VWR, U.K.). Unless otherwise specified, in all synthetic work carried out, the water used was deionised (resistivity 15 MΩcm) and the substrate was medical grade flat silicone sheets (NuSil, Polymer Systems Technology Ltd., U.K.).

4.2.2 *Synthesis of Gold Nanoparticles*

Gold nanoparticles were kindly provided by Mr William Peveler (University College London) and synthesised using a method adapted from Luo *et al* [33]. $HAuCl_4.3H_2O$ aqueous solution (2 mL, 20 mM) and L-glutathione (reduced) aqueous solution (0.6 mL, 100 mM) were added sequentially to HPLC grade (18 MΩ) water (17.4 mL) and stirred at 500 rpm for 22 hours at 70 °C. The addition of the reagents resulted in the formation of an orange colour, which faded over time to a pale yellow.

4.2.3 *Materials Synthesis*

A series of samples were prepared for microbiological testing and materials characterisation using a simple two-step dipping method (Figure 18). NuSil silicone polymer squares (1.21 cm^2) were immersed in a swelling solution for 72 h as described in Table 2. After air-drying (24 h), the samples were washed and towel-dried, after which selected samples (see Table 2) were subsequently immersed in a crystal violet dipping solution (72 h). These samples were then air-dried again, washed and towel-dried. Gold nanoparticles used in this materials

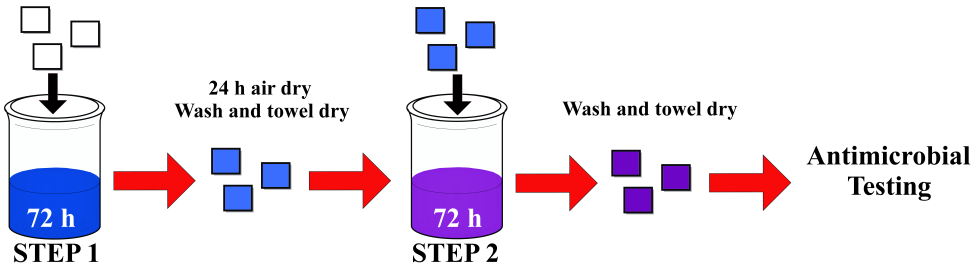

Figure 18: Schematic to show preparation of crystal violet-coated, methylene blue and 2 nm gold nanoparticle-encapsulated sample

Table 2: Dipping conditions for material preparation. Where possible the samples were maintained under dark conditions

Dipping Solution	Control	MBAu	CV	CVAu	CVMBAu
9:1 acetone:water	y	-	-	-	-
9:1 acetone:nanogold		y*	-	y	y*
0.001 M CV solution	-	-	y	y	y

* dipping solution saturated with methylene blue (700 mg L^{-1})

synthesis were purchased from BBI Solutions.

Samples were prepared for further microbiological testing to compare the use of commercially purchased 2 nm gold nanoparticles from BBI Solutions, with laboratory synthesised gold nanoparticles (see Section 4.2.2). A 9:1 acetone : nanogold swelling solution was prepared using the laboratory synthesised gold colloid. Addition of the acetone resulted in the formation of a pale yellow precipitate. The 9:1 acetone : nanogold swelling solution was decanted off and the swelling solution was saturated with methylene blue dye (700 mg/ L), after which silicone polymer squares (1.21 cm^2) were immersed in it for 72 h under dark conditions. The dye/ nanogold incorporated samples were then air-dried (24 h), washed and towel dried. The dye-nanogold embedded polymers were subsequently immersed in a crystal violet solution (0.001 mol dm^{-3}) for 72 h under dark conditions, after which they were air-dried (24 h), washed and towel dried.

4.2.4 *Materials Characterisation*

The UV-Vis absorption spectra of the treated silicone polymers prepared for microbiological testing were measured using a PerkinElmer Lambda 25 UV-Vis Spectrometer, within the range 380 - 800 nm. The infrared absorbance spectra of the same polymers were measured within the range 4000 - 400 cm^{-1} with an accumulation of 15 scans per sample, using a Bruker Platinum ATR-FTIR spectrometer.

Untreated and modified silicone samples were imaged at 40x magnification using a Brunel light microscope (NLSD-120) with a CCD camera attached and Scope Image Advanced software was used for analysis. A transmission electron microscope (TEM) was used to image the 2 nm gold nanoparticle colloid and silicone-embedded with 2 nm gold nanoparticles. 2 nm gold nanoparticles suspended in an aqueous solution were drop cast onto lacey carbon films on 300 Mesh Copper Grids (Agar Scientific Ltd.). Grids were cleaned under an O_2/H_2 plasma stream for 10 s in a Solarus (Model 950) Advanced Plasma Cleaning System (Gatan) prior to imaging. High resolution-TEM (HR-TEM) images were acquired using a Titan 80-300 (FEI) microscope equipped with a monochromator and image corrector and operated with an accelarating voltage of 300 kV and FEG of 4.5 kV. Particle size analysis was carried out using ImageJ software (version 1.40 g, National Institutes of Health, U.S.A.). 5 micron sections of 2 nm gold nanoparticle-encapsulated silicone polymer were secured onto a 400 Cu mesh lacy carbon film coated Cu TEM grid (Agar Scientific Ltd.) and imaged using a Jeol 2100 high resolution transmission electron microcope (HR-TEM) with a LaB_6 source operating at an acceleration voltage of 200 kV. Micrographs were taken on a Gatan Orius CCD with DigitalMicrograph software.

4.2.5 *Dye Adherence Testing*

The crystal violet-coated and crystal violet-coated, methylene blue and nanogold-encapsulated silicone samples were wiped rigorously with a 70% isopropyl alcohol wipe (AZOwipe^{TM}, Synergy Health)

to determine whether the dye adhered to the sample surface under standard cleaning regimes.

4.2.6 *Sample Photostability Testing*

Treated polymer samples were stored in a white light box for an extended duration. The samples were exposed to intense white lighting conditions using a white light source (General Electric 28 W Watt Miser^{TM} T5 2D compact fluorescent lamp) emitting an average light intensity of 12,500 $\pm$ 250 lux at a distance of 16 cm from the samples.

4.2.7 *Wetting Properties*

Equilibrium water contact angle measurements (~9 μL) on: untreated silicone, solvent treated (control) silicone, crystal violet-coated silicone, methylene blue and 2 nm gold nanoparticle-encapsulated silicone and crystal violet-coated nanogold encapsulated silicone, were also obtained. The contact angle measurement for each sample type was taken to be the average value over $\geqslant$ 10 measurements, using a droplet of deionised water dispensed by gravity from a gauge 27 needle and the samples were photographed side on. The data was analysed using FTA32 software.

4.2.8 *Microbiological Testing*

4.2.8.1 *Antimicrobial Activity of a Range of Photobactericidal Polymers*

A range of medical grade silicone elastomer samples (1.1 cm x 1.1 cm) were used in the microbiology experiments: (i) solvent treated silicone (control), (ii) crystal violet-coated silicone, (iii) methylene blue and 2 nm gold nanoparticle-encapsulated silicone, (iv) crystal violet-coated, nanogold-encapsulated silicone and (v) crystal violet-coated, methylene blue and nanogold-encapsulated silicone. These

samples were tested against *S. epidermidis* RP62a and *E. coli* ATCC 25922. These organisms were stored at -70 °C in BHI containing 20 % (v/v) glycerol and propagated on either MSA or MAC agar for a maximum of two sub-cultures at intervals of two weeks.

BHI broth (10 mL) was inoculated with 1 bacterial colony and cultured in air at 37 °C for 18 h with shaking, at 200 rpm. The bacterial pellet was recovered by centrifugation (21 °C, 1771 x*g*, 5 min), washed in PBS and centrifuged again to recover the bacteria, which were finally re-suspended in PBS (10 mL). The washed suspension was diluted 1000-fold to obtain the inoculum ($\sim 10^6$ cfu /mL). The inoculum in each experiment was confirmed by plating ten-fold serial dilutions on agar for viable counts. Triplicates of each polymer sample type were inoculated with 25 μL of the inoculum and covered with a sterile cover slip (22 mm x 22 mm). The samples were then irradiated for up to ~6 hours using a white light source (General Electric 28 W Watt Miser^{TM} T5 2D compact fluorescent lamp) emitting an average light intensity of 3,750 ± 250 lux at a distance of 30 cm from the samples. A further set of samples (in triplicate) was maintained in the dark for the duration of the irradiation time, whilst an additional sample set was maintained under dark conditions for up 18 hours.

Post irradiation, the inoculated samples and cover slips were added to PBS (225 μL) and vortexed. The neat suspension and ten-fold serial dilutions were plated on the appropriate agar for viable counts. The plates were incubated aerobically at 37 °C for 24 h (*E. coli*) or 48 h (*S. epidermidis*). Each experiment contained 3 technical replicates and the experiment was reproduced three times. The Mann-Whitney U test was used to determine the significance of the following comparisons: (i) the activity of each of the modified polymers compared to the control silicone sample when both were incubated in the dark and (ii) the activity of each of the irradiated modified polymers compared to the same material incubated in the dark.

4.2.8.2 *Comparison of Use of Two Different Gold Nanoparticles*

A range of silicone elastomer samples (1.1 cm x 1.1 cm) were used in the microbiology experiments: (i) solvent treated silicone (control), (ii) crystal violet-coated, methylene blue and commercial 2 nm gold nanoparticle-encapsulated silicone (CVMBAu@BBI) and (iii) crystal violet-coated, methylene blue and lab synthesised gold nanoparticle-encapsulated silicone (CVMBAu@Lab). These samples were tested against *S. epidermidis* RP62a and *E. coli* ATCC 25922. These organisms were stored at -70 °C in BHI containing 20 % (v/v) glycerol and propagated on either MSA or MAC agar for a maximum of two sub-cultures at intervals of two weeks.

BHI broth (10 mL) was inoculated with 1 bacterial colony and cultured in air at 37 °C for 18 h with shaking, at 200 rpm. The bacterial pellet was recovered by centrifugation (21 °C, 1771 x*g*, 5 min), washed in PBS and centrifuged again to recover the bacteria, which were finally re-suspended in PBS (10 mL). The washed suspension was diluted 1000-fold to obtain the inoculum (~10^6 cfu /mL). The inoculum in each experiment was confirmed by plating ten-fold serial dilutions on agar for viable counts. Triplicates of each polymer sample type were inoculated with 25 μL of the inoculum and covered with a sterile cover slip (22 mm x 22 mm). The samples were then irradiated for up to ~6 hours using a white light source (General Electric 28 W Watt Miser™ T5 2D compact fluorescent lamp) emitting an average light intensity of 3,750 ± 250 lux at a distance of 30 cm from the samples. A further set of samples (in triplicate) was maintained in the dark for the duration of the irradiation time.

Post irradiation, the inoculated samples and cover slips were added to PBS (225 μL) and vortexed. The neat suspension and ten-fold serial dilutions were plated on the appropriate agar for viable counts. The plates were incubated aerobically at 37 °C for 24 h (*E. coli*) or 48 h (*S. epidermidis*). Each experiment contained 3 technical replicates and the experiment was reproduced three times. The Mann-Whitney U test was used to determine the significance of the following comparisons: (i) the activity of each of the modified polymers compared to the control silicone sample when both were incubated in the dark and (ii)

the activity of each of the irradiated modified polymers compared to the same material incubated in the dark.

4.3 RESULTS AND DISCUSSION

4.3.1 *Materials Synthesis and Characterisation*

4.3.1.1 *Synthesis of Gold Nanoparticles*

Luminescent gold-thiolate nanoparticles were synthesised using a method adapted from the literature [33]. When irradiated with UV light (365 nm), the yellow gold nanoparticle suspension gave an orange emission, correlating to an emission peak of 636 nm. To prepare the swelling solution for polymer nanoparticle encapsulation, nine parts acetone was added to 1 part gold colloid. The addition of acetone to the nanoparticle suspension resulted in the formation of a pale yellow precipitate which fluoresced orange under UV-irradiation (365 nm). It is likely that the fluorescent pale yellow precipate is the gold-thiolate capping agent and the gold nanoparticles remain dispersed in solution.

4.3.1.2 *Materials Synthesis*

The use of a 'one-step' or 'two-step' dipping strategy to incorporate photosensitiser dyes and 2 nm gold nanoparticles into medical grade polymers, has been detailed in the literature [21–23, 25, 27, 29]. As described in the previous chapter, a 'two-step' method was used to develop a polymer encapsulated with a dual photosensitiser dye combination, in addition to 2 nm gold nanoparticles. In the first step, the silicone samples were immersed in a 9:1 acetone : nanogold swelling solution saturated with methylene blue dye. Upon exposure to the solvent, the polymer swells enabling the dye molecules to diffuse through the polymer. When the silicone is removed from the swelling solution, the residual solvent evaporates resulting in a dye-incorporated polymer. In the subsequent step, the treated polymer sections were immersed in a 1 x 10^{-3} mol dm^{-3} crystal violet solution for 72 hours such that the resultant polymer is coated with a thin layer of crystal violet dye at the polymer surface. Although the mechanistic details are unclear, it is clear that the crystal violet dye strongly attaches to the polymer surface under aqueous dipping

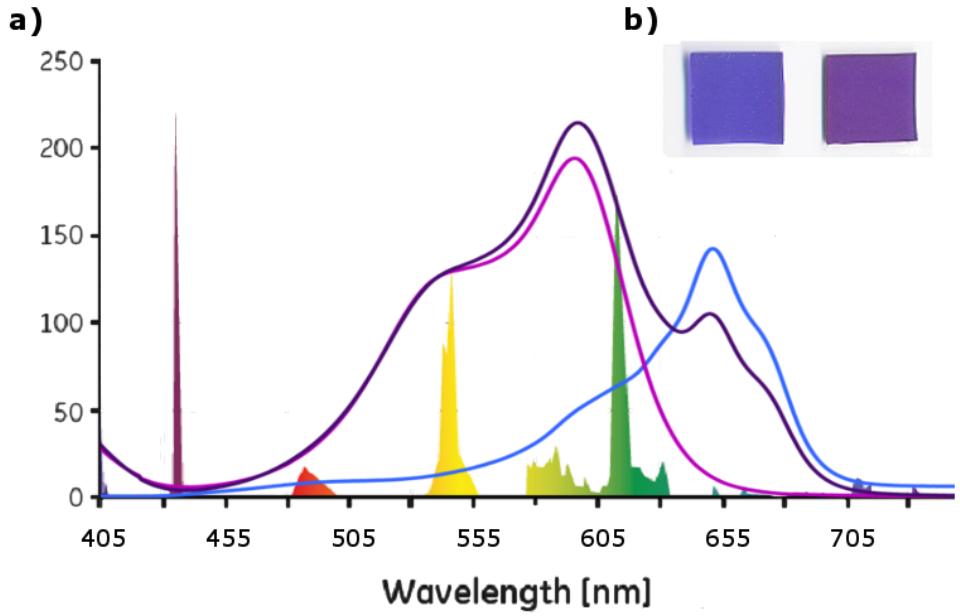

Figure 19: (a) Hospital lighting emission spectrum of a 28-W fluorescent lamp [34] with UV-Vis spectra of a series of treated silicone polymers overlayed. The UV-Vis absorbance spectra of methylene blue and nanogold encapsulated silicone (blue line), crystal violet-coated, nanogold-encapsulated silicone (violet line) and crystal violet coated, methylene blue and nanogold encapsulated silicone (purple line) were measured within the range 380 - 800 nm. The absorbance spectra were scaled to fit the emission spectrum of the hospital lighting source (y-axis units: mW /nm /1 lm). (b) Crystal violet-coated nanogold and methylene blue-encapsulated silicone and nanogold encapsulated silicone samples, prepared using a novel 2-step dipping protocol

conditions, as the polymer sections showed no detectable leaching of crystal violet. Samples incorporated with methylene blue in addition to crystal violet were a blue-purple colour, whereas those exposed to just the crystal violet were a more purple hue (Figure 19(b)). It should be noted that the presence of 2 nm gold nanoparticles did not affect the sample colouration.

4.3.1.3 *UV-Vis Absorbance Spectroscopy*

The dye-incorporated samples were analysed using UV-Vis spectroscopy within the range 380 - 800 nm and their absorbance spectra were compared to that of a hospital lighting emission spectrum similar to that used in the microbiological testing (Figure 19(a)). From the spectra it is clear that the crystal violet-coated, nanogold-

encapsulated silicone sample absorbed strongly at 594 nm with a shoulder peak at 548 nm, whereas the methylene blue encapsulated in the silicone sample demonstrated a maximum absorption at 651 nm with small shoulder peaks at ~610 nm and ~670 nm. The UV-Vis absorbance signal of the crystal violet-coated, methylene blue and nanogold encapsulated sample exhibited key peaks from both the individual samples, with peak maxima in the same wavelength region at 594 nm and 651 nm and shoulder peaks at 548 nm and 670 nm, corresponding to the crystal violet and methylene blue respectively. The presence of the 2 nm gold nanoparticles affected neither the dye peak intensity, shape, nor position compared to samples incorporated with dye only and the UV-Vis spectra of the dye/ nanogold-incorporated samples demonstrated no detectable absorbance in the visible region of the spectrum of the gold nanoparticles, as the small diameter of the nanoparticles used, is below the limit for surface plasmon resonance (4 nm) [23, 27]. It is also interesting to note that there appears to be little electronic interaction between the 2 dyes incorporated into the polymer, since the absorbance spectrum of the multi-dye silicone is effectively a 'sum' of the spectra of the individual dye incorporated silicones.

The UV-Vis absorbance spectra of gold-thiolate nanoparticles was measured within the range 300 - 800 nm and demonstrated absorption at $<$ 500 nm (Figure 20(a)). No peak correlating to surface plasmon resonance was noted, indicating that these nanoparticles are small and below the limit for surface plasmon resonance ($<$ 4 nm) [23, 27]. Nine parts acetone was added to the gold nanoparticle suspension and the solution was left at room temperature to ensure all precipitation was complete. It has been proposed that the observed pale yellow precipitation is the nanoparticle thiolate capping polymer. The UV-Vis absorbance spectra of the 9:1 acetone : gold nanoparticle suspension was measured and it was noted that the absorption edge at $<$ 500 nm was not evident. This indicates that this absorption correlated to the nanoparticle thiolate capping polymer, which precipitated off upon addition of acetone.

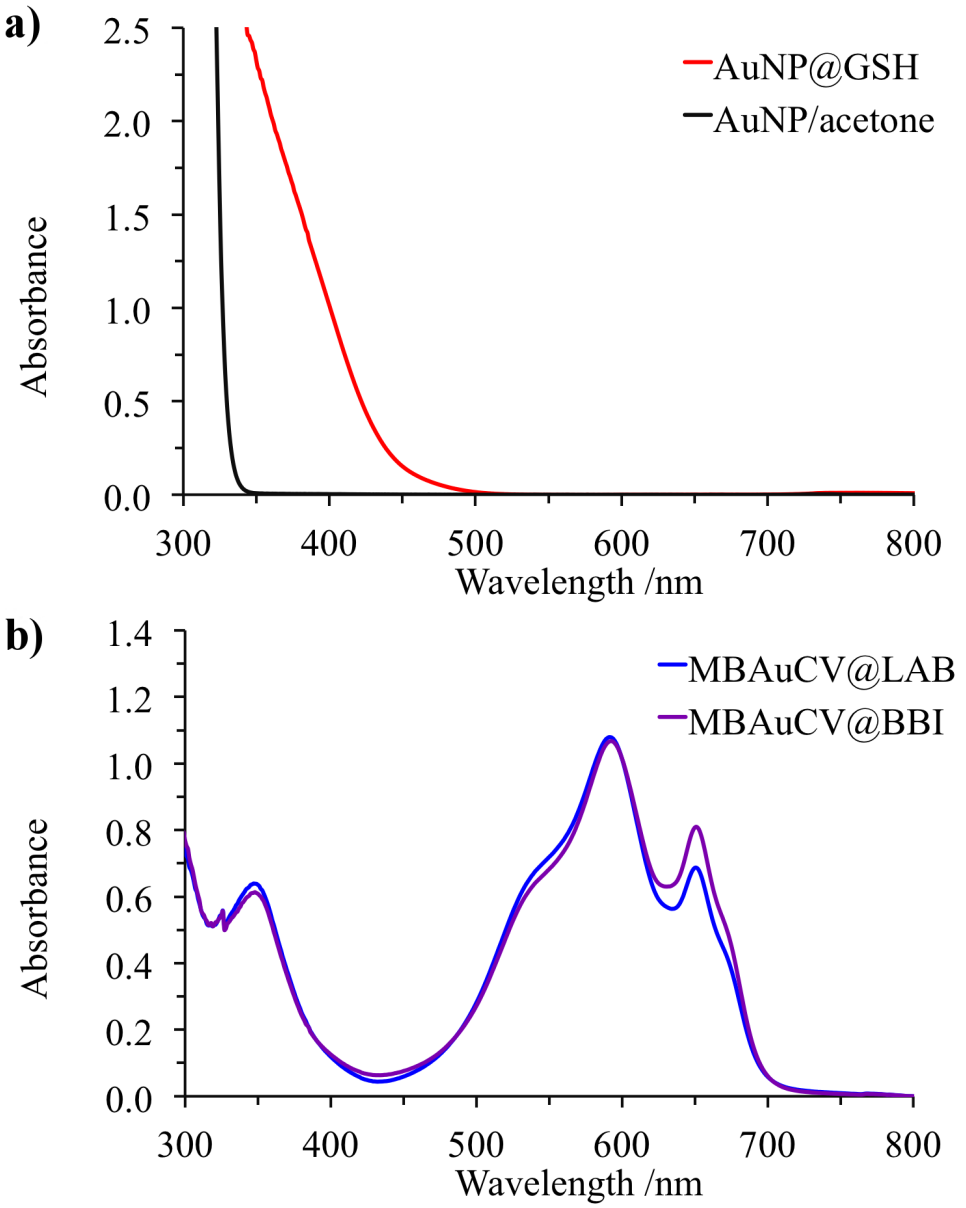

Figure 20: The UV-Vis absorbance spectra measured within the range 300 - 800 nm of: (a) Gold-thiolate nanoparticles dispersed in water (AuNP@GSH) and gold nanoparticles dispersed in 90 % acetone (AuNP/acetone) and (b) crystal violet-coated, methylene blue and gold nanoparticle-encapsulated silicone prepared using lab synthesised gold nanoparticles (MBAuCV@LAB) and commercially acquired gold nanoparticles (MBAuCV@BBI)

Medical grade silicone coated with crystal violet and encapsulated with methylene blue and gold nanoparticles were synthesised. These dark purple-coloured samples were prepared using either lab synthesised gold nanoparticles or commercially acquired gold nanoparticles (BBI). The UV-Vis absorbance spectra of both samples were measured within the range 300 - 800 nm (Figure 20(b)). It was found that the

type of gold nanoparticle affected neither the peak shape, nor peak position, with both samples absorbing strongly at 590 nm and 650 nm, showing characteristic absorption signals of the photosensitiser dyes crystal violet and methylene blue, respectively.

4.3.1.4 *ATR-FTIR Spectroscopy*

ATR-FTIR spectroscopy was used to measure the infrared absorbance spectra of the samples used for microbiological testing. The spectra (see Chapter 3, section 3.3.2.2) demonstrated no significant difference across the sample range, or, when compared to a control, untreated silicone sample, as the strong absorbance bands of the silicone substrate dominated over any signals due to the dye. The similarity of the spectra can be attributed to the low concentrations of dye present in these polymers. However, it can be commented that the similarity between the spectra indicates that the solvent treatment process did not cause any significant chemical change in the silicone polymer across the sample range.

4.3.2 *Microscopy*

4.3.2.1 *Transmission Electron Microscope*

TEM images of the commercially acquired 2 nm gold nanoparticles in solution, are shown in Figure 21(a). The TEM images indicate that the gold nanoparticles were spherical, mono-dispersed and nano-crystalline. By analysis of more than 1000 particles, the average size of the gold nanoparticles was calculated as 2.2 nm, with a narrow size distribution of 1.1 nm (Figure 21(c)). HR-TEM images of the gold nanoparticle showed lattice spacings of ~0.235 nm, correlating with the (111) plane of fcc gold (Figure 21(b)).

Flat nanoparticle-encapsulated silicone polymers were embedded vertically in paraffin blocks and 5 μm sections were cut using a microtome. The TEM images of these sections at the polymer edge, show the same crystalline nanostructures, roughly 2 nm in diameter (white

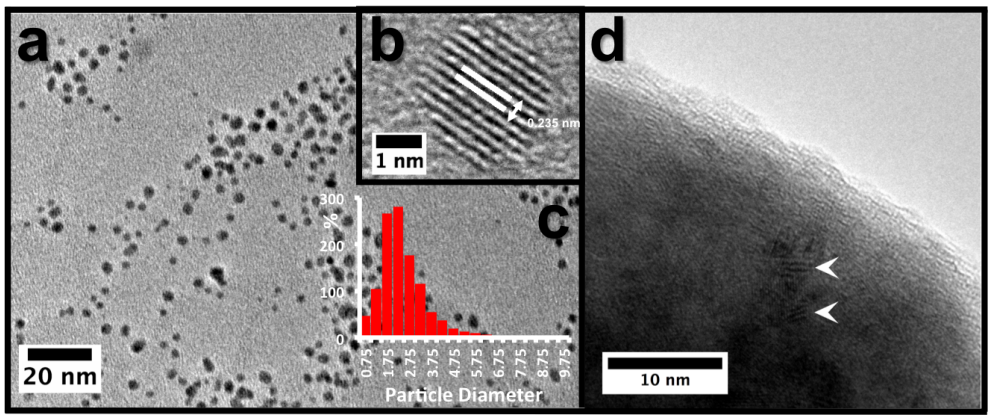

Figure 21: (a) TEM of commercially acquired gold nanoparticles, (b) HR-TEM of commercially acquired gold nanoparticle with lattice spacings, (c) histogram of particle size distribution of commercially acquired gold nanoparticles determined by TEM and (d) TEM of silicone polymer encapsulated with commercially acquired gold nanoparticles

arrows), confirming the presence of the gold nanoparticles in the silicone polymer (Figure 21(d)).

4.3.2.2 *Light Microscope*

A light microscope with an attached CCD camera was used to analyse the effects of exposing the silicone to an acetone swelling solution and the added effect of the incorporation of photosensitiser dyes at 40x magnification, to determine whether these treatments detrimentally affect the surface properties of the polymer. As observed in Figure 22(a), the untreated medical grade silicone sample presents a rough surface at this magnification. Exposure to a 90 % acetone dipping solution further roughens the polymer surface, with many additional surface features evident (Figure 22(b)). The acetone exposure induces polymer swelling, which is exploited to enable nanoparticle diffusion through the polymer matrix. When removed from the swelling solution, the residual solvent evaporates and the polymer shrinks. However, it is possible that the swelling treatment may disorder the polymer, resulting in the observed increase in surface roughness.

As detailed in Section 4.2.3, the photosensitiser dye crystal violet can be coated onto medical grade silicone using an aqueous dipping solution. From Figure 22(c), it is clear that the surface of the crystal violet-coated polymer is smooth compared to the acetone treated

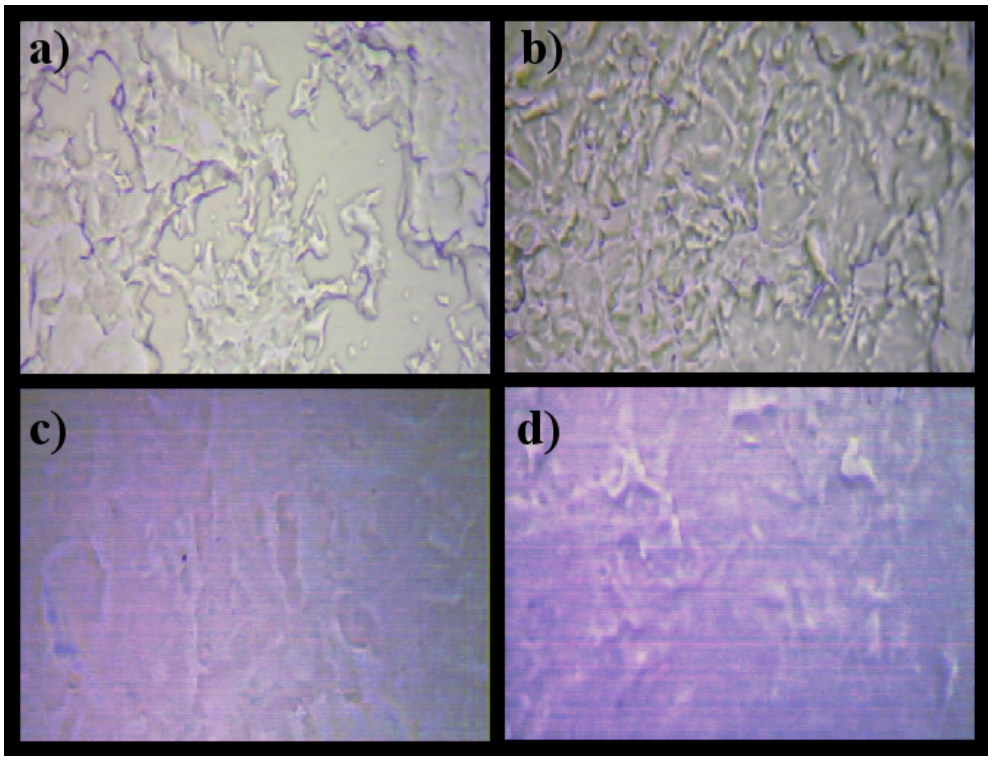

Figure 22: Images at 40x magnification of 1.1 cm x 1.1 cm silicone squares: (a) Untreated silicone, (b) acetone treated silicone, (c) crystal violet-coated silicone and d) methylene blue and gold nanoparticle-encapsulated, crystal violet-coated silicone. Note that images (c) and (d) are false coloured to differentiate between the non-dye embedded samples (a) and (b)

polymer, closely resembling the untreated silicone surface. This indicates that the uptake of crystal violet dye does not detrimentally affect the polymer surface. Surprisingly, despite solvent treatment used to incorporate the methylene blue and 2 nm gold nanoparticles, the crystal violet-coated, methylene blue and nanogold-encapsulated silicone surface is also similar to the untreated silicone surface, under 40x magnification (Figure 22(d)). This bodes well for potential clinical applications where these surfaces may be used in medical devices, as it is critical that the surface roughness properties of these devices are not altered, to prevent increased friction during device insertion and associated patient discomfort upon their use. It is also important that the antimicrobial incorporation process does not significantly increase polymer surface roughness for hospital touch surface applications. Smooth surfaces are key in a hospital environment since these hinder bacterial surface adhesion.

4.3.3 *Functional Properties*

4.3.3.1 *Dye Adherence Testing*

The stability of the photosensitiser dye adsorbed on the polymer surface, was tested to determine its suitability for clinical applications. The modified polymers were wiped rigorously with a 70 % alcohol wipe and no visual evidence of dye removal from the treated polymer surface was observed. This indicates that the modified polymers should be stable under standard hospital cleaning protocols. This test is crucial, since despite the potent antimicrobial nature of these polymers, it is anticipated that surfaces treated by this method will still undergo the regimented hospital cleaning protocol as an adjunct infection-control measure and thus, must be stable to robust wiping using an alcohol-based, anti-infective wipe.

4.3.3.2 *Wetting Properties*

The wetting properties of a range of untreated and treated silicone samples were measured under laboratory temperature and lighting conditions as detailed in Chapter 3. From the water contact angle measurement data (Table 3), it can be inferred that the untreated silicone presents a hydrophobic surface and the treatment of the

Table 3: Average water contact angle measurements (°) ± standard deviation, of water on a range of silicone polymers: untreated, solvent treated (control), methylene blue and 2 nm gold nanoparticle encapsulated (MBAu), crystal violet-coated (CV), crystal violet-coated, 2 nm gold nanoparticle encapsulated (CVAu) and crystal violet-coated, methylene blue and 2 nm gold nanoparticle encapsulated (CVMBAu)

Silicone Sample	**Water Contact Angle (°)**	±	**Standard Deviation**
Untreated	102	±	1.0
Control	101	±	1.5
MBAu	100	±	0.3
CV	100	±	0.5
CVAu	100	±	0.5
CVMBAu	102	±	0.8

polymers to incorporate dyes, dye-nanogold combinations or dye-dye-nanogold combinations effects negligible differences in the subsequent wetting properties of the surfaces.

Once a microorganism is within a critical distance of a surface (usually 1 nm), the net sum of the repulsive and attractive forces between the microorganism and the surface influences adhesion to the surface [35]. These forces include electrostatic and hydrophobic interactions, van der Waals forces and hydrodynamic forces [35]. Since bacteria and inert surfaces tend to be negatively charged, electrostatic interactions between these surfaces result in repulsion [35, 36]. It has been suggested that hydrophobic interactions may dominate the outcome of initial bacterial adhesion to abiotic surfaces [35], therefore it is crucial that surface modification treatments do not act to enhance surface hydrophobicity. The water contact angle measurements indicate that the polymer surface hydrophobicity is not adversely affected by the antimicrobial incorporation. This is beneficial in terms of the utilisation of this material in healthcare applications.

4.3.3.3 *Dye Photostability*

UV-Vis spectroscopy was employed to investigate the photostability of the dye incorporated silicone polymers upon exposure to a white light source - 8W GE lighting (3500 K) - commonly used in U.K. hospitals (for emission spectrum, see Figure 19(a)). The measured

Table 4: Recommended light intensities for different areas in U.K. healthcare environments [4, 31]

Environment	**Light Intensity /lx**
Operating theatre	10,000 - 100,000
A & E Examination Room	1,000
Ward corridors	$\leqslant$ 100
Typical dental chair*	250

* Measurement performed at UCLH Eastman Dental Hospital

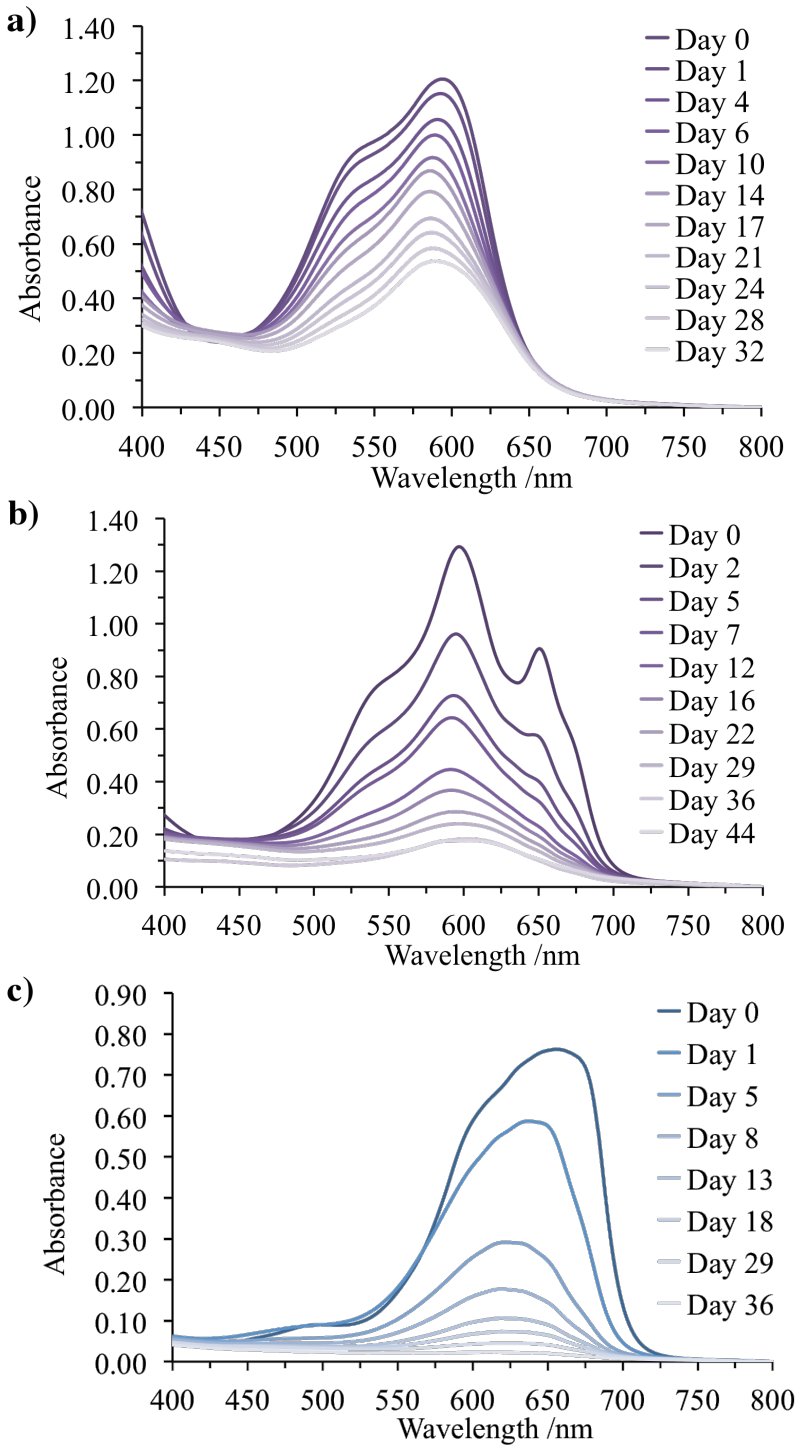

Figure 23: UV-Vis absorbance spectra measured in the range 400 - 800 nm of: (a) Crystal violet-coated nanogold encapsulated silicone, (b) crystal violet-coated, methylene blue and nanogold-encapsulated silicone and (c) methylene blue and nanogold-encapsulated silicone, using a simple dipping method. The samples were illuminated with a white light source emitting an average light intensity of 12,500 ± 250 lux at a distance of 16 cm from the samples

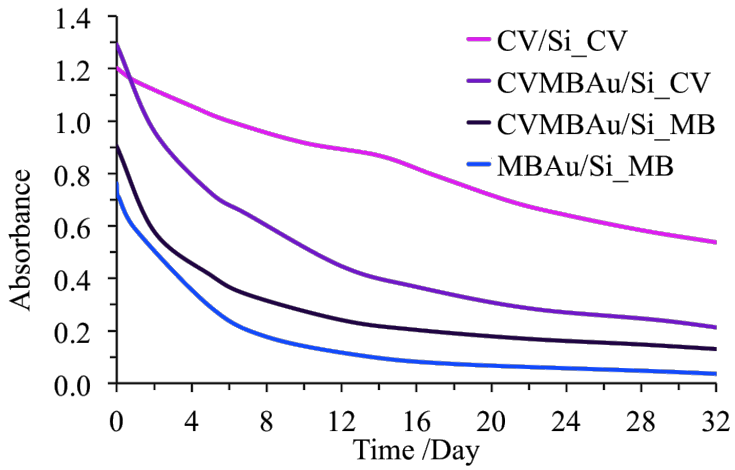

Figure 24: Rate of photodegradation of modified polymers upon exposure to white light illumination (32 days, 12,500 lx). The rate is displayed as a decrease in sample absorbance at the absorbance maxima, over time. Crystal violet has been abbreviated as CV and methylene blue has been abbreviated as MB. CV/Si_CV represents the crystal violet peak in the crystal violet-coated, nanogold encapsulated silicone sample, CVMBAu/Si_CV and CVMBAu/Si_MB represents the crystal violet and methylene blue peaks in the crystal violet-coated, methylene blue and nanogold-encapsulated silicone sample respectively and MBAu/Si_MB represents the methylene blue peak in the methylene blue and nanogold-encapsulated polymer

light intensity at the samples was ~12,500 lx at a distance of 16 cm from the light source. The absorbance of the illuminated samples was measured periodically within the range 400 - 800 nm (Figure 23). The lighting conditions used in this study were considered in relation to the brightness of various areas in U.K. healthcare environments, as recommended by the Department of Health (Table 4) [4] and were found to be ~125x more intense than those typically found in hospital corridors and wards, areas in which microbial contamination is prevalent. Under these intense irradiation conditions, the photodegradation of the crystal violet was ~51 % for the crystal violet-coated, nanogold-encapsulated silicone sample, ~94 % for the methylene blue and nanogold-encapsulated silicone sample and ~81 % for the crystal violet-coated, methylene blue and nanogold-encapsulated silicone sample, over the course of up to 29 days (Figure 23(a)-(c)).

The rate of dye photodegradation was determined by plotting the decrease in the UV-Vis absorbance of the samples at the dye peak maxima, against the illumination time (Figure 24). The graph

demonstrates that the rate of dye photodegradation in the multi-dye-nanogold sample far surpasses that of the same dye in the dye-nanogold only sample. It is clear from the figure that the rate of photodegradation of crystal violet in the crystal violet/nanogold sample is almost linear and there is greater photostability of the dye in this sample, compared to the crystal violet incorporated in the crystal violet/methylene blue/nanogold sample where there is a relatively smooth, exponential rate of degradation of the dye. It can be speculated that the discrepancy can be attributed to the presence of multiple dyes within the polymer interacting with each other upon photo-excitation. This leads to the formation of dye-dye bonds (Type I pathway), rather than undergoing a cyclic Type II photochemical pathway, wherein the dye molecule interacts with and transfers energy to molecular oxygen, generating singlet oxygen species, returning the dye molecule to its ground electronic state.

It should also be noted that the crystal violet-coated silicone samples were less susceptible to photodegradation than the methylene blue-encapsulated samples (> 90 % photodegradation, 18 days, Figure 24). Moreover, it was found that contrary to the methylene blue-encapsulated silicone samples (Figure 23(c)), there is only a very slight shift in the crystal violet absorbance maximum upon illumination for extensive time periods indicating that the photochemical activity is not effecting a substantial change in the photosensitiser structure. This minor 'right-shift' effect was evident in the crystal violet peak of both the crystal violet-coated, nanogold encapsulated silicone samples and the crystal violet-coated, methylene blue and nanogold-encapsulated silicone samples and became noticeable with an increase in illumination duration of > 30 days. Nevertheless, due to the high light intensities used in this study, the observed photodegradation should not pose a problem in practical clinical applications, for example in hospital wards and corridors which have less intense lighting conditions, as photodegradation will occur over a longer timescale (years).

It is anticipated that the degradation of these dyes correlates to the light-flux levels and thus, the samples tested indicate strong stability

and suitability for these antimicrobial surfaces to be employed in a clinical environment such as hospital wards and corridors. In these environments, it is expected that these photo-activated polymers would maintain potency for several years (based on light-flux levels used).

4.3.4 *Bactericidal Properties*

In this chapter, the antimicrobial activity of multi-dye, nanogold-encapsulated silicone sample systems are presented and compared to a series of other dye and dye-nanogold embedded silicones. The samples were tested against a Gram-positive bacterium and a Gram-negative bacterium, *S. epidermidis* and *E. coli*, respectively. The antimicrobial activity of these modified medical grade silicone polymers, was promoted by exposure of the samples to a white hospital light source; a compact fluorescent lamp, which emits light across the visible region of the spectrum and is similar to those commonly found in U.K. hospitals. In all experiments, a control sample set was maintained under dark conditions for the same period of time as the samples exposed to light and in a further experiment, a sample set was incubated under dark conditions for an extended time period. The antimicrobial activity of the following samples was compared to that of a control, solvent-treated silicone sample: (i) crystal violet-coated silicone (CV), (ii) crystal violet-coated, nanogold-encapsulated silicone (CVAu), (iii) methylene blue and nanogold encapsulated silicone (MBAu) and (iv) crystal violet-coated, methylene blue and nanogold-encapsulated silicone (CVMBAu).

Exposure of these samples to a white light source emitting an average light intensity of 3,750 $\pm$ 250 lux at a distance of 30 cm from the samples, resulted in the lethal photosensitisation of both bacteria, as demonstrated in Figure 25((a)-(c)). Under dark conditions for incubation times of 3 h, the MBAu sample exhibited no statistically significant kill of *S. epidermidis* when compared to the control silicone sample. However, all crystal violet-coated silicone samples demonstrated statistically significant ($P < 0.001$) bacterial kills compared to

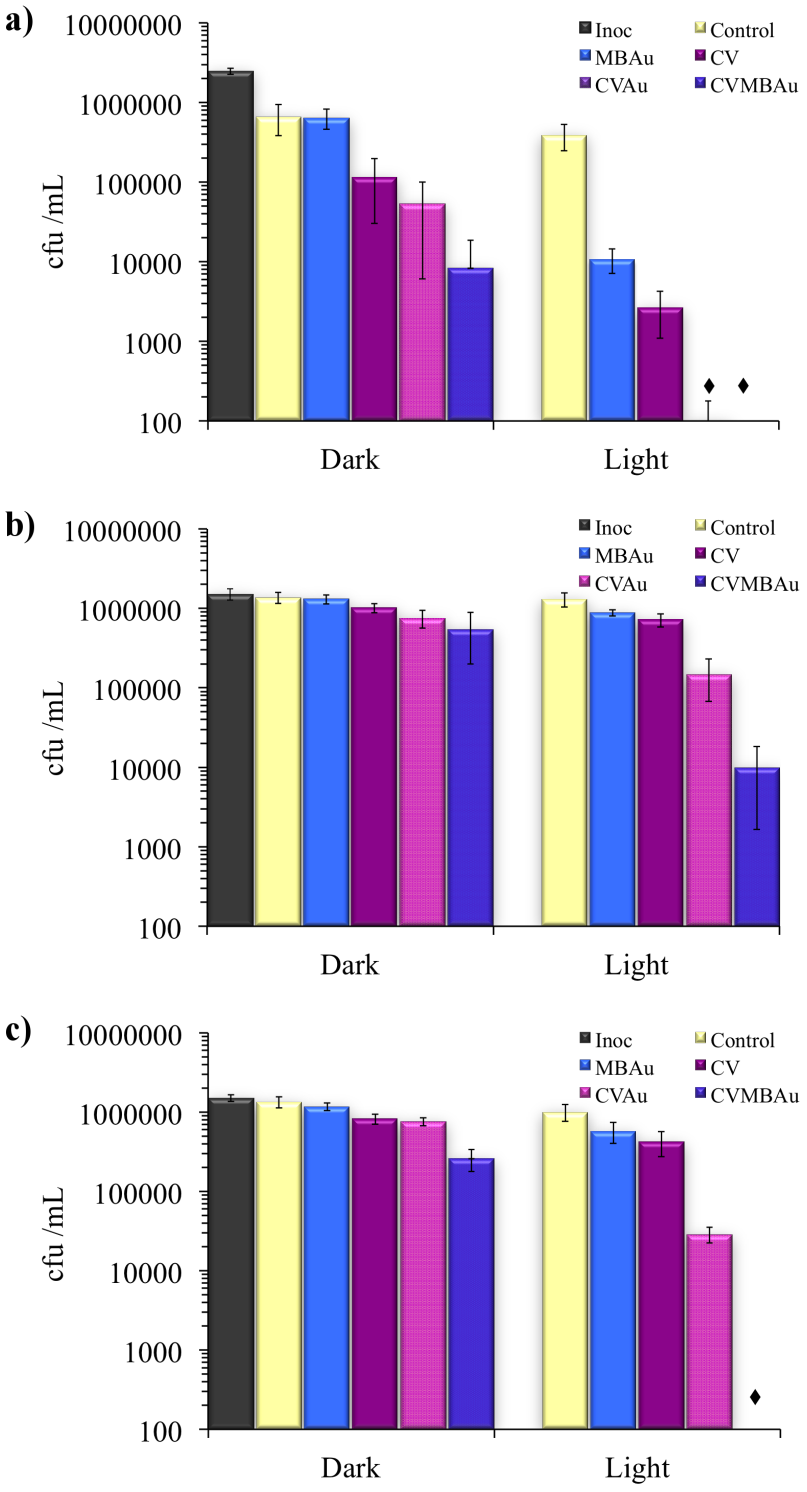

Figure 25: Viable counts of bacteria after incubation on modified silicone polymers exposed to white light illumination: (a) *S. epidermidis* (3 h illumination), (b) *E. coli* (3 h illumination) and (c) *E. coli* (6 h illumination). The white light source emitted an average light intensity of 3,750 ± 250 lux at a distance of 30 cm from the samples. The ♦ indicates that the bacterial numbers were reduced to below the detection limit of 400 cfu

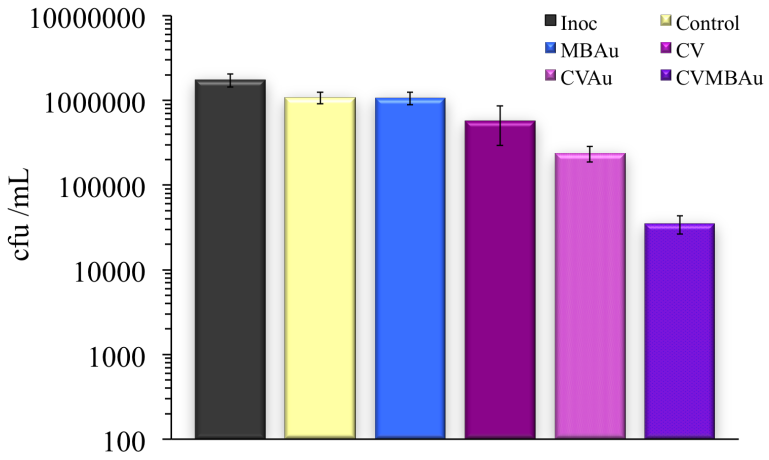

Figure 26: Viable counts of *E. coli* from the surface of samples incubated at 20 °C for 18 h under dark conditions. The ♦ indicates that the bacterial numbers were reduced to below the detection limit of 400 cfu

the control silicone sample, ranging from a 0.76 log reduction in bacterial numbers with CV alone to a 1.9 log kill with CVMBAu, within 3 hours of contact time in the dark (Figure 25(a)). Upon illumination with white light (3 h), all dye-incorporated samples demonstrated strong light-activated antimicrobial activity, with statistically significant kills compared to the same dye-incorporated samples stored in dark conditions for an equivalent time period ($P < 0.001$). The crystal violet-coated silicone sample types encapsulated with 2 nm gold nanoparticles exhibited the most efficacious light-activated activity against *S. epidermidis*, with bacterial numbers reduced below the detection limit within 3 h.

Microbiological testing also demonstrated that these novel photo-activated antimicrobial surfaces show significant antimicrobial activity against a Gram-negative bacterium, under dark conditions. When tested against *E. coli*, all crystal violet-coated silicone samples demonstrated statistically significant bactericidal activity against *E. coli* upon incubation in the dark for 3 hours (Figure 25(b); $P < 0.01$ (CV) and $P < 0.001$ (CVAu, CVMBAu)), with increased antimicrobial activity exhibited when incubated for 6 hours and 18 hours (Figure 25(c) and Figure 26). The efficacy of the bactericidal activity against *E. coli* demonstrated by these surfaces varied across the sample range. As with *S. epidermidis*, the CVMBAu sample resulted in the greatest

reduction in bacterial numbers of up to 1.49 log, when incubated for time periods of up to 18 hours in the dark. The CVAu sample also showed strong antimicrobial activity, resulting in up to 0.66 log kills against *E. coli* when in contact with the modified silicone surface for up to 18 hours. The MBAu sample demonstrated no statistically significant activity against *E. coli* despite an extended incubation in dark conditions, when compared to the control silicone sample.

The nanogold attributed enhancement in the lethal photosensitisation of Gram-negative bacteria on photosensitiser-incorporated silicone under conditions of white light illumination, was also examined. All modified silicone samples exhibited photo-activated bactericidal activity against *E. coli*. Although statistically significant kills were achieved in all cases for the treated silicone samples when compared to the corresponding samples under dark conditions ($P < 0.001$), the extent to which the lethal photosensitisation of *E. coli* was achieved by these surfaces varied greatly across the sample range tested. The modified sample that demonstrated the least bactericidal activity compared to the silicone control upon activation with a white hospital light source, was the methylene blue and nanogold-encapsulated silicone, with limited kills achieved even after 6 hour illumination. The CV sample demonstrated stronger photo-activity than the MBAu samples, although the presence of 2 nm gold nanoparticles significantly enhanced the bacterial kills achieved on the crystal violet-coated silicone surfaces, by a factor of > 1.15 log.

The novel multi-dye-nanogold silicone samples not only demonstrated potent bactericidal activity under dark conditions, but these samples also induced the lethal photosensitisation of *E. coli*, with bacterial numbers reduced by > 2.1 log upon 3 hours exposure to white light and reduction to below the detection limit within 6 hours of white light illumination. These multi-dye samples utilise a greater proportion of light emitted from the white light source, with sample absorbance within the region 475 - 700 nm (see Figure 19). Consequently, there is greater potential for the generation of ROS - the cytotoxic species that initiate multi-site attack against bacteria - since dye excitation can occur over a greater range of wavelengths

due to the multiple dyes incorporated in the silicone.

Contrary to previously synthesised materials, we have developed and reported here potent photobactericidal polymers that *also* demonstrate significant dark kill, predominantly against the Gram-positive bacterium, *S. epidermidis*, but also against the Gram-negative bacterium, *E. coli*. This has been achieved by incorporating the triarylmethane photosensitiser dye, crystal violet, into the nanogold or methylene blue and nanogold encapsulated silicone, by use of a novel two-step dipping strategy. Although the anti-infective properties of crystal violet were first discovered in the 1890s by Stilling, it was Churchman (1912) who noted the selective action of the dye against Gram-positive bacteria [37–40]. Crystal violet has since been used as a treatment for infected wounds and superficial skin infections, with clinical trials testing its efficacy as a treatment for MRSA infections [41, 42] and was an important topical antiseptic, before modern drugs replaced it [40]. The use of crystal violet as a treatment for skin conditions such as superficial wounds, fungal infections and infected scabies was recommended by the World Health Organisation for inclusion in 'The Interagency Emergency Health Kit' [43]. The photo-activated antimicrobial effect of crystal violet on *Porphyromonas gingivalis* has also been investigated using a rat model with a subcutaneous abscess, to determine the antimicrobial efficacy of this system in vivo, for potential applications in clinical periodontal therapy [42].

Results indicate that crystal violet coating the silicone samples significantly increases the susceptibility of the Gram-positive bacterium, *S. epidermidis*, within 3 hours. A statistically significant, but more limited increase in sensitivity was demonstrated by *E. coli*, although this effect required longer incubation times (18 hours). Interestingly, the results suggest that the encapsulation of gold nanoparticles into the silicone sample enhances not only the light-activated antimicrobial properties, but the inherent antimicrobial properties of crystal violet. It can be speculated that there may be an interaction between the dye molecules and the gold nanoparticles that enhance its antimicrobial action. A similar effect has recently been noted in the literature, with regard to antibiotics and gold nanoparticles, in which the binding

of antibiotics to spherical gold nanoparticles effects an enhancement in antimicrobial activity [44–46]. The results of this study show that this potential crystal violet-nanoparticle interaction also increases the sensitivity of the Gram-negative bacterium, *E. coli*, towards the dye (Figure 26). Following this reasoning, it can be further speculated that dye-dye interactions transpire, perhaps on the surface of the gold nanoparticles, since silicone samples embedded with methylene blue and gold nanoparticles in addition to crystal violet, consistently demonstrate greater efficacy in terms of their antimicrobial activity, compared to the sum kill of samples incorporated with only methylene blue and gold nanoparticles or crystal violet and gold nanoparticles.

The microbiological testing indicates that the crystal-violet incorporated samples outperform the methylene blue and nanogold-encapsulated samples under both dark conditions and white light illumination. It can be speculated that the increased efficacy in the photo-activated kill is due to the high concentration of crystal violet accumulated on the sample surfaces [27]. It has previously been estimated that the ROS, singlet oxygen, has a very short diffusion distance of around 0.2 microns within the polymer [27]. Consequently, in the case of the MBAu sample, since the dye is distributed relatively evenly throughout the polymer, the dye encapsulated within the polymer bulk is redundant with respect to the exhibited antimicrobial activity. Only dye embedded near the polymer surface will act in the photosensitisation of bacteria, as only the ROS generated near to the polymer surface, rather than that generated within the bulk, will act to photo-damage bacteria. With high concentrations of photosensitiser on the crystal violet-coated polymer surfaces, there is a greater probability of the generation of cytotoxic ROS within range of 'attack' against bacteria colonising the surface, subsequently contributing to the increased bacterial kills. It should also be noted that crystal violet at the polymer surface may also contribute to the dark kill exhibited by these samples, since the bacteria are in direct contact with high surface concentrations of the antimicrobial agent.

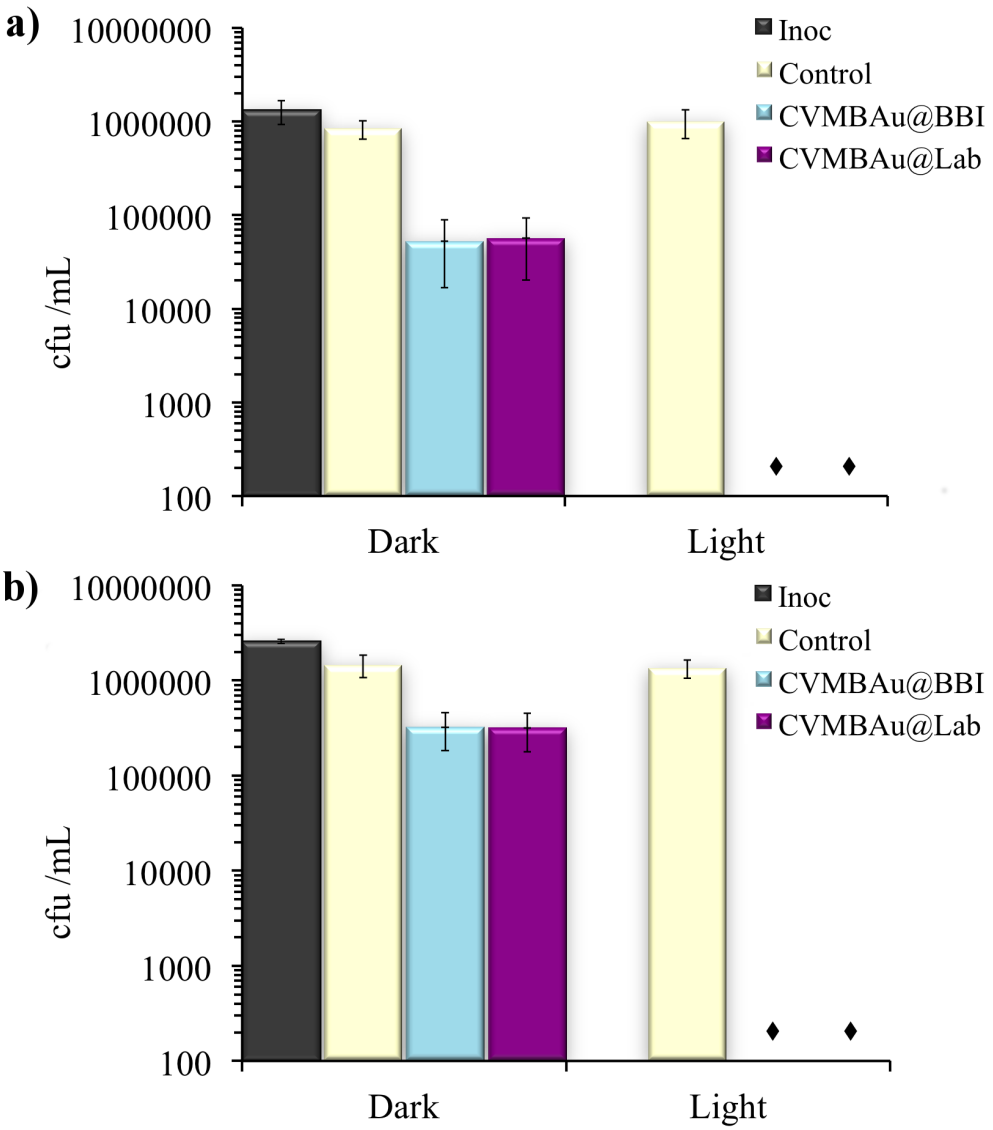

Figure 27: Viable counts of bacteria after incubation on modified silicone polymers exposed to white light illumination: (a) *S. epidermidis* (200 minutes illumination) and (b) *E. coli* (6 h illumination). The white light source emitted an average light intensity of 3,750 ± 250 lux at a distance of 30 cm from the samples. The ♦ indicates that the bacterial numbers were reduced to below the detection limit of 400 cfu

4.3.4.1 *Further Microbiological Testing*

The photo-enhanced antimicrobial activity of crystal violet-coated, methylene blue and nanogold encapsulated medical grade silicone prepared using lab synthesised gold nanoparticles (CVMBAu@Lab), was compared to that of crystal violet-coated, methylene blue and commercial gold nanoparticle-encapsulated silicone samples (CVMBAu@BBI). The antimicrobial efficacy of both samples was measured

relative to a solvent-treated control silicone polymer and all samples samples were tested against both a Gram-positive bacterium, *S. epidermidis* and a Gram-negative bacterium, *E. coli* using a white hospital light source to activate the photocatalytic kill mechanism. An additional sample set was stored under dark conditions, for the duration of illumination.

Microbiological testing indicated that both the CVMBAu@BBI samples and CVMBAu@Lab samples achieved significant kills against *S. epidermidis*, when stored under dark conditions for 200 minutes ($P < 0.001$). The CVMBAu@BBI sample reduced bacterial numbers by 1.20 log, whereas the CVMBAu@WP sample resulted in a 1.17 log decrease in bacterial numbers and it was found that there was no statistically significant difference in the antimicrobial activity of these two samples (Figure 27(a)). Exposure to a standard compact fluorescent hospital lamp induced the lethal photosensitisation of *S. epidermidis* within 200 minutes, reducing bacterial numbers to below the detection limit.

Similarly, when tested against *E. coli*, both samples demonstrated efficacious antimicrobial activity under dark conditions, decreasing viable bacterial numbers by 0.66 log within 6 hours ($P < 0.001$), with no statistically significant difference in the bactericidal activity between the samples (Figure 27(b)). White light illumination enhanced bacterial kills, resulting in the photo-activated reduction of bacterial numbers to below the detection limit on both surfaces ($P < 0.001$). Overall, it was observed that the use of lab synthesised gold nanoparticles did not inhibit, or impact on the potency of the lethal photosensitisation of bacteria on surfaces incorporated with this dye-dye-nanogold antimicrobial surface technology.

This comparative study of the photo-enhanced antimicrobial activity of crystal violet-coated, methylene blue and 2 nm gold nanoparticle-encapsulated silicone sections is of critical importance. The use of commercially acquired 2 nm gold nanoparticles hindered progress since the stability of gold nanoparticles in the purchased gold colloid was poor and nanoparticle precipitation was observed in

several batches of the gold nanoparticle suspension. Preliminary microbiological testing indicated that the antimicrobial efficacy of these samples was comparable to dye only-encapsulated silicone, with no synergistic enhancement in activity attributed to gold nanoparticles exhibited. Moreover, despite very low concentrations of gold nanoparticles used in the dipping solutions - 10 % nanogold in dipping solution, *ca.* 1 mL dipping solution per 1.21 cm^2 silicone sample - these nanoparticles presented some financial implications for the commercial viabilty of these surfaces, at a cost of £160.97 per 100 mL [47].

The gold-thiolate nanoparticles were synthesised at a cost of $<$ £10 per 100 mL - nanogold concentrations used 'as synthesised' - deeming this antimicrobial technology financially accessible for widespread use in a host of surface applications. Furthermore, these nanoparticles demonstrated stability in solution over prolonged periods of time, with no evidence of nanoparticle precipitation. Nevertheless, one concern regarding the use of these lab synthesised gold nanoparticles, was the presence of the fluorescent thiolate capping polymer. In PDT applications where it is imperative that the antimicrobial combination results in efficacious triplet state yields, the presence of a species that encourages gold nanoparticle fluorescence may be detrimental, as it can impact on the subsequent enhancement in the generation of the dye triplet state attributed to the nanogold. However, it was found that addition of acetone to the gold colloid effects the precipitation of thiolate-capping polymer, resulting in suspension of non-fluorescent gold nanoparticles. This was confirmed by UV-Vis spectroscopy of the gold nanocolloid with and without the presence of acetone, in addition to excitation to fluorescence of these solutions using a hand help UV lamp.

It is anticipated that these bactericidal surfaces can be employed in hospitals for use in touch surfaces, including but not limited to: tablet and mobile phone covers and screen protectors, computer keyboards, hand-dryers and paint films, to help maintain low bacterial levels and hence, potentially reduce the risk of the spread of infection. In addition, as detailed in Chapter 3, it is envisaged that this technology

can also be applied for use in medical devices such as catheters, however, a low power laser irradiation system will be required for these applications.

These novel samples demonstrate efficacious antimicrobial activity when tested against both Gram-positive and Gram-negative bacteria, commonly associated with nosocomial infection. Moreover, illumination with a white light source similar to that typically found in a hospital setting resulted in a strong enhancement in the antimicrobial activity. The intensity of the white light source used to activate the photobactericidal properties of these polymers was ~15x that typically found in hospital ward corridors and ~3x that found in Accident and Emergency examination rooms (see Table 4) [4, 31]. Consequently, the photobactericidal activity of these surfaces would be most efficacious in examination rooms where the light intensity is higher, however, it is anticipated that significant kills can still be achieved in areas of lower light intensity if the irradiation time is prolonged. Moreover, in these experiments, very high bacterial loads (~32,920 cfu /cm² *E. coli*, ~51,147 cfu /cm² *S. epidermidis*) were used to test the potency of these antimicrobial polymers, whereas on hospital surfaces, the bacterial loads on contaminated surfaces are considerably lower (up to an equivalent of 3,060 cfu /cm² with average values of < 100 cfu /cm²) [48–51].

4.4 CONCLUSIONS

This chapter outlines the development of potent light-activated antimicrobial surfaces that also demonstrate effective dark kill using polymers incorporated with multi-dye-nanogold combinations. Using a standard hospital white light source to activate the photobactericidal properties, these efficacious antimicrobial surfaces induced the lethal photosensitisation of *S. epidermidis* in just 3 hours and of *E. coli* in just 6 hours, with bacterial numbers reduced to below the detection limit. The multi-mechanism antimicrobial activity proves attractive for use in potential hospital surface applications, as low bacterial levels will be maintained under non-optimal lighting conditions (i.e.

at night, or when lights are dimmed), with a boost in antimicrobial activity achieved with increasing illumination intensity. The use of lab synthesised gold nanoparticles provides an inexpensive alternative to previously used commercial gold nanoparticles, without detracting from the efficacy of photobactericidal activity, increasing the viability of this antimicrobial strategy for use in both touch surfaces and indwelling devices.

Further work on these antimicrobial materials should include an examination of the efficacy of the bactericidal activity of these surfaces in a clinical environment. However, although these surfaces induce the lethal photosensitisation of high surface contamination levels of both Gram-positive and Gram-negative bacteria, the demonstrated dark kill levels are efficacious, but their activity can be improved. In the next chapter, an investigation into the development of 'dual-mechanism' antimicrobial surfaces will be pursued, in which novel antimicrobial dye-nanoparticle combinations will be incorporated into medical grade silicone. The aim of this study is to develop surfaces that achieve potent dark-activated antimicrobial activity against key hospital pathogens, that also demonstrate efficacious photosensitisation of bacteria.

REFERENCES

[1] S. Noimark, C. W. Dunnill, M. Wilson, and I. P. Parkin. "The role of surfaces in catheter-associated infections." In: *Chemical Society Reviews* 38 (2009), pp. 3435–3448.

[2] S. Noimark, C. W. Dunnill, and I. P. Parkin. "Shining light on materials - A self-sterilising revolution." In: *Advanced Drug Delivery Reviews* 65 (2013), pp. 570–580.

[3] K. Page, M. Wilson, and I. P. Parkin. "Antimicrobial surfaces and their potential in reducing the role of the inanimate environment in the incidence of hospital-acquired infections." In: *Journal of Materials Chemistry* 19 (2009), pp. 3819–3831.

[4] C. W. Dunnill, K. Page, Z. A. Aiken, S. Noimark, G. Hyett, A. Kafizas, J. Pratten, M. Wilson, and I. P. Parkin. "Nanoparticulate silver coated-titania thin films-Photo-oxidative destruction of stearic acid under different light sources and antimicrobial effects under hospital lighting conditions." In: *Journal of Photochemistry and Photobiology a-Chemistry* 220 (2011), pp. 113–123.

[5] Z. A. Aiken, G. Hyett, C. W. Dunnill, M. Wilson, J. Pratten, and I. P. Parkin. "Antimicrobial Activity in Thin Films of Pseudobrookite-Structured Titanium Oxynitride under UV Irradiation Observed for Escherichia coli." In: *Chemical Vapor Deposition* 16 (2010), pp. 19–22.

[6] C. W. Dunnill and I. P. Parkin. "Nitrogen-doped Tio_2 thin films: photocatalytic applications for healthcare environments." In: *Dalton Transactions* 40 (2011), pp. 1635–1640.

[7] C. W. Dunnill, Z. Ansari, A. Kafizas, S. Perni, D. J. Morgan, M. Wilson, and I. P. Parkin. "Visible light photocatalysts-N-doped Tio_2 by sol-gel, enhanced with surface bound silver nanoparticle islands." In: *Journal of Materials Chemistry* 21 (2011), pp. 11854–11861.

[8] C. W. Dunnill, Z. A. Aiken, J. Pratten, M. Wilson, and I. P. Parkin. "Sulfur- and Nitrogen-Doped Titania Biomaterials via APCVD." In: *Chemical Vapor Deposition* 16 (2010), pp. 50–54.

[9] K. Page, R. G. Palgrave, I. P. Parkin, M. Wilson, S. L. P. Savin, and A. V. Chadwick. "Titania and silver-titania composite films on glass-potent antimicrobial coatings." In: *Journal of Materials Chemistry* 17 (2007), pp. 95–104.

[10] *AcryMed Inc., SilvaGard^{TM} Technology Summary.* www.acrymed.com/pdf/SilvaGard%20Technical%20Summary.pdf. Accessed: 2013-07-22.

[11] *AgION Technologies Inc., AgION^{TM} Technology.* http://www.agion-tech.com. Accessed: 2013-07-22.

[12] C. D. Salgado, K. A. Sepkowitz, J. F. John, J. R. Cantey, H. H. Attaway, K. D. Freeman, P. A. Sharpe, H. T. Michels, and M. G. Schmidt. "Copper Surfaces Reduce the Rate of Healthcare-Acquired Infections in the Intensive Care Unit." In: *Infection Control and Hospital Epidemiology* 34 (2013), pp. 479–486.

[13] F. Marais, S. Mehtar, and L. Chalkley. "Antimicrobial efficacy of copper touch surfaces in reducing environmental bioburden in a South African community healthcare facility." In: *Journal of Hospital Infection* 74 (2010), pp. 80–82.

[14] A. Mikolay, S. Huggett, L. Tikana, G. Grass, J. Braun, and D. H. Nies. "Survival of bacteria on metallic copper surfaces in a hospital trial." In: *Applied Microbiology and Biotechnology* 87 (2010), pp. 1875–1879.

[15] T. J. Karpanen, A. L. Casey, P. A. Lambert, B. D. Cookson, P. Nightingale, L. Miruszenko, and T. S. J. Elliott. "The Antimicrobial Efficacy of Copper Alloy Furnishing in the Clinical Environment: A Crossover Study." In: *Infection Control and Hospital Epidemiology* 33 (2012), pp. 3–9.

[16] P. J. McCubbin, E. Forbes, M. M. Gow, and S. D. Gorham. "Novel self-disinfecting surface." In: *Journal of Applied Polymer Science* 100 (2006), pp. 381–389.

[17] P. J. McCubbin, E. Forbes, M. M. Gow, and S. D. Gorham. "Covalent attachment of quaternary ammonium compounds to a polyethylene surface via a hydrolyzable ester linkage: Basis for a controlled-release system of antiseptics from an inert surface." In: *Journal of Applied Polymer Science* 100 (2006), pp. 538–545.

[18] C. E. Edmiston, F. C. Daoud, and D. Leaper. "Is there an evidence-based argument for embracing an antimicrobial (triclosan)-coated suture technology to reduce the risk for surgical-site infections?: A meta-analysis." In: *Surgery* 154 (2013), pp. 89–100.

[19] D. L. Williams, K. D. Sinclair, S. Jeyapalina, and R. D. Bloebaum. "Characterization of a novel active release coating to prevent biofilm implant-related infections." In: *Journal of Biomedical Materials Research Part B: Applied Biomaterials* 101B (2013), pp. 1078–1089.

[20] S. Perni, J. Pratten, M. Wilson, C. Piccirillo, I. P. Parkin, and P. Prokopovich. "Antimicrobial Properties of Light-activated Polyurethane Containing Indocyanine Green." In: *Journal of Biomaterials Applications* 25 (2011), pp. 387–400.

[21] S. Perni, P. Prokopovich, C. Piccirillo, J. Pratten, I. P. Parkin, and M. Wilson. "Toluidine blue-containing polymers exhibit potent bactericidal activity when irradiated with red laser light." In: *Journal of Materials Chemistry* 19 (2009), pp. 2715–2723.

[22] S. Perni, C. Piccirillo, J. Pratten, P. Prokopovich, W. Chrzanowski, I. P. Parkin, and M. Wilson. "The antimicrobial properties of light-activated polymers containing methylene blue and gold nanoparticles." In: *Biomaterials* 30 (2009), pp. 89–93.

[23] S. Perni, C. Piccirillo, A. Kafizas, M. Uppal, J. Pratten, M. Wilson, and I. P. Parkin. "Antibacterial Activity of Light-Activated Silicone Containing Methylene Blue and Gold Nanoparticles of Different Sizes." In: *Journal of Cluster Science* 21 (2010), pp. 427–438.

[24] S. Perni, P. Prokopovich, I. P. Parkin, M. Wilson, and J. Pratten. "Prevention of biofilm accumulation on a light-activated antimicrobial catheter material." In: *Journal of Materials Chemistry* 20 (2010), pp. 8668–8673.

[25] S. Noimark, C. W. Dunnill, C. W. M. Kay, S. Perni, P. Prokopovich, S. Ismail, M. Wilson, and I. P. Parkin. "Incorporation of methylene blue and nanogold into polyvinyl chloride catheters; a new approach for light-activated disinfection of surfaces." In: *Journal of Materials Chemistry* 22 (2012), pp. 15388–15396.

[26] C. Piccirillo, S. Perni, J. Gil-Thomas, P. Prokopovich, M. Wilson, J. Pratten, and I. P. Parkin. "Antimicrobial activity of methylene blue and toluidine blue O covalently bound to a modified silicone polymer surface." In: *Journal of Materials Chemistry* 19 (2009), pp. 6167–6171.

[27] S. Noimark, M. Bovis, A. J. MacRobert, A. Correia, E. Allan, M. Wilson, and I. P. Parkin. "Photobactericidal polymers; the incorporation of crystal violet and nanogold into medical grade silicone." In: *RSC Advances* 3 (2013), pp. 18383–18394.

[28] S. Ismail, S. Perni, J. Pratten, I. Parkin, and M. Wilson. "Efficacy of a Novel Light-Activated Antimicrobial Coating for Disinfecting Hospital Surfaces." In: *Infection Control and Hospital Epidemiology* 32 (2011), pp. 1130–1132.

[29] A. J. T. Naik, S. Ismail, C. Kay, M. Wilson, and I. P. Parkin. "Antimicrobial activity of polyurethane embedded with methylene blue, toluidene blue and gold nanoparticles against Staphylococcus aureus; illuminated with white light." In: *Materials Chemistry and Physics* 129 (2011), pp. 446–450.

[30] V. Decraene, J. Pratten, and M. Wilson. "Assessment of the Activity of a Novel Light-Activated Antimicrobial Coating in a Clinical Environment." In: *Infection Control and Hospital Epidemiology* 29 (2008), pp. 1181–1184.

[31] V. Decraene, J. Pratten, and M. Wilson. "Cellulose acetate containing toluidine blue and rose bengal is an effective antimicrobial coating when exposed to white light." In: *Applied and Environmental Microbiology* 72 (2006), pp. 4436–4439.

[32] V. Decraene, J. Pratten, and M. Wilson. "Novel light-activated antimicrobial coatings are effective against surface-deposited Staphylococcus aureus." In: *Current Microbiology* 57 (2008), pp. 269–273.

[33] Z. Luo, X. Yuan, Y. Yu, Q. Zhang, D. T. Leong, J. Y. Lee, and J. Xie. "From aggregation-induced emission of Au(I)-thiolate complexes to ultrabright Au(0)@Au(I)-thiolate core-shell nanoclusters." In: *J Am Chem Soc* 134 (2012), pp. 16662–70.

[34] *White Light Source, Spectral Power Distribution*. http://www.gelighting.com/LightingWeb/emea/images/2D_Watt_Miser_DataSheet_tcm181-10576.pdf. Accessed: 2013-07-22.

[35] W. M. Dunne Jr. "Bacterial adhesion: Seen any good biofilms lately?" In: *Clinical Microbiology Reviews* 15 (2002), pp. 155–166.

[36] B. Carpentier and O. Cerf. "Biofilms and their consequences, with particular reference to hygiene in the food industry." In: *J. Appl. Bacteriol.* 75 (1993), pp. 499–511.

[37] J. W. Churchman. "The selective bactericidal action of gentian violet." In: *Journal of Experimental Medicine* 16 (1912), 221–U50.

[38] J. Stilling. "The aniline dyes as antiseptics, and their use in practice." In: *The Lancet* 136 (1890), pp. 965–966.

[39] J. Stilling. "The aniline dyes as antiseptics." In: *The Lancet* 137 (1891), pp. 872–873.

[40] "New and nonofficial remedies, 1939. Containing descriptions of the articles which stand accepted by the council on Pharmacy and Chemistry of the American Medical Association on January 1, 1939." In: *Chicago: American Medical Association* (1939).

[41] M. Saji, S. Taguchi, K. Uchiyama, E. Osono, N. Hayama, and H. Ohkuni. "Efficacy of gentian violet in the eradication of methicillin-resistant Staphylococcus aureus from skin lesions." In: *Journal of Hospital Infection* 31 (1995), pp. 225–228.

[42] K. Kawamoto, N. Senda, K. Shimada, K. Ito, Y. Hirano, and S. Murai. "Antibacterial Effect of Yellow He-Ne Laser Irradiation with Crystal Violet Solution on Porphyromonas gingivalis: An Evaluation Using Experimental Rat Model Involving Subcutaneous Abscess." In: *Lasers in Medical Science* 15 (2000), pp. 257–262.

[43] In: *World Health Organization; The interagency emergency health kit* (2006).

[44] H. Gu, P. L. Ho, E. Tong, L. Wang, and B. Xu. "Presenting Vancomycin on Nanoparticles to Enhance Antimicrobial Activities." In: *Nano Letters* 3 (2003), pp. 1261–1263.

[45] M. F. Zawrah and S. I. Abd El-Moez. "Antimicrobial Activities of Gold Nanoparticles against Major Foodborne Pathogens." In: *Life Science Journal-Acta Zhengzhou University Overseas Edition* 8 (2011), pp. 37–44.

[46] A. N. Grace and K. Pandian. "Antibacterial efficacy of aminoglycosidic antibiotics protected gold nanoparticles - A brief study." In: *Colloids and Surfaces a-Physicochemical and Engineering Aspects* 297 (2007), pp. 63–70.

[47] *Gold nanoparticles, 2 nm - Purchase price accurate as of 27.06.2014*. http : / / www . bbisolutions . com / products / 1377 - gold - nanoparticles-2nm. Accessed: 2013-07-22.

[48] M. G. Schmidt, I. Attaway Hubert H., S. E. Fairey, L. L. Steed, H. T. Michels, and C. D. Salgado. "Copper Continuously Limits the Concentration of Bacteria Resident on Bed Rails within the Intensive Care Unit." In: *Infection Control and Hospital Epidemiology* 34 (2013), pp. 530–533.

[49] M. G. Schmidt, H. H. Attaway, P. A. Sharpe, J. John Joseph, K. A. Sepkowitz, A. Morgan, S. E. Fairey, S. Singh, L. L. Steed, J. R. Cantey, K. D. Freeman, H. T. Michels, and C. D. Salgado. "Sustained Reduction of Microbial Burden on Common Hospital Surfaces through Introduction of Copper." In: *Journal of Clinical Microbiology* 50 (2012), pp. 2217–2223.

[50] F. Marais, S. Mehtar, and L. Chalkley. "Antimicrobial efficacy of copper touch surfaces in reducing environmental bioburden in a South African community healthcare facility." In: *Journal of Hospital Infection* 74 (2010), pp. 80–82.

[51] G. Hedin, J. Rynback, and B. Lore. "Reduction of bacterial surface contamination in the hospital environment by application of a new product with persistent effect." In: *Journal of Hospital Infection* 75 (2010), pp. 112–115.

5

WHITE LIGHT-ACTIVATED ANTIMICROBIAL POLYMERS; CRYSTAL VIOLET AND ZINC OXIDE NANOPARTICLE-ENCAPSULATED SILICONE

5.1 INTRODUCTION

Despite rigid hygiene protocols in place, the transfer of bacteria within hospital environments is a substantial issue and can lead to the contraction of HAIs. These infections are a significant financial burden to healthcare institutions, often markedly extending the length of hospital stay and causing additional discomfort and pain to the patient. The use of antimicrobial surfaces is an important infection-control strategy and can disrupt the cyclic transmission of bacteria in healthcare environments.

Chapter 4 describes the synthesis of potent white light-activated antimicrobial surfaces for use in hospital touch surface applications, as a strategy to decrease the incidence of associated infection. A simple two-step dipping process was used to incorporate crystal violet, methylene blue and 2 nm gold nanoparticles into medical grade silicone polymers and this method can easily be upscaled for commercial production. White hospital light illumination of these polymers achieved significant antimicrobial activity with > 4 log reductions in bacterial numbers within 6 hours when tested against *E. coli* and within 3 hours when tested against *S. epidermidis*. Moreover, for the first time, these light-activated antimicrobial surfaces demonstrated substantial kill against *E. coli* under dark conditions.

Although significant kills under dark conditions were documented in the previous chapter, these were achieved over an 18 hour time period. This chapter focuses on the development of 'dual-mechanism' antimicrobial surfaces that induce the lethal photosensitisation of bacteria and *also* demonstrate rapid, efficacious bactericidal activity

under dark conditions, such that low bacterial surface contamination levels can be effectively maintained in healthcare environments, even under low illumination conditions. Such surfaces would demonstrate versatile antimicrobial properties, with a minimal risk of the development of bacterial resistance, due to the multi-mechanism mode of bacterial attack. In this chapter, the development of these surfaces is described and was achieved through the incorporation of photosensitiser dyes in combination with nanoparticles with documented bactericidal properties, such as zinc oxide nanoparticles, into medical grade silicone.

Zinc oxide is a naturally occurring metal oxide; it is inexpensive, has a high thermal conductivity and a wide band gap (3.36 eV) lending itself to a large range of commercial applications from paint pigmentation to field effect transistors, gas sensors and in photovoltaics. Zinc oxide is generally considered to be safe and has widespread use as a food additive [1], in food packaging [2] and in skin ointments. In fact, it is commonly used to treat nappy rashes [3, 4] and also widely used in sunscreen products as it is an effective block of ultraviolet (UV) radiation [3, 5]. Recently, zinc oxide nanoparticles have attracted heightened research interest in terms of their bactericidal activity. They exhibit antibacterial properties against a range of both Gram-positive and Gram-negative bacteria through a cytotoxic mechanism, in addition to showing activity against high-temperature and -pressure resistant spores and fungal pathogens [6–10]. It has been suggested that the mechanism by which zinc oxide nanoparticles demonstrate antimicrobial activity may involve the accumulation of nanoparticles in the outer membrane or cytoplasm of bacterial cells, or may be attributed to the generation of ROS [10]. Reports have also indicated that zinc oxide nanoparticles may disrupt or damage bacterial cell membranes, resulting in the leakage of intracellular components, or cause oxidative stress [11, 12]. Zinc oxide nanoparticles also demonstrate an enhanced antimicrobial efficacy when compared to bulk zinc oxide [7, 9]. This can be attributed to the high surface area to volume ratio of nanoparticles [7]. Moreover, it has been observed that there exists a size dependency on the antimicrobial activity of the zinc oxide nanoparticles, with decreasing

nanoparticle size effecting greater bactericidal effectiveness [6, 9, 10].

Since nanoparticulate zinc oxide is insoluble in most solvents, in order to disperse the nanoparticles, large excesses of surfactant are often added. However, the presence of surfactant can reduce performance. To overcome these adverse effects and obviate the need for excess surfactant, a synthetic organometallic route to zinc oxide via hydrolysis of zinc alkyl groups in the presence of non-hydrolysable zinc carboxylates can be used [13, 14]. Recently, it has been noted that the use of zinc di(octyl) phosphinate surface groups enhances solubility of the nanoparticles, improving their catalytic performance in methanol synthesis [15]. The resultant small zinc oxide nanoparticles (3 - 4 nm) are easily dispersed in toluene and consequently, can be encapsulated into polymers using a simple swelling strategy.

In this chapter, the use of a two-stage dipping approach to incorporate zinc oxide nanoparticles in combination with a commercially available photosensitiser dye, crystal violet, into medical grade silicone, is reported. In addition to characterisation by UV-Vis absorbance spectroscopy and X-ray photoelectron spectroscopy (XPS), TEM was used to analyse the nanoparticle embedded polymer and demonstrated evidence of nanoparticle incorporation. The antimicrobial activity of the crystal violet-coated, nano zinc oxide-encapsulated polymer was tested against both Gram-negative and Gram-positive bacteria ubiquitous in healthcare settings and a white light source comparable to standard hospital lighting conditions was used to enhance the antimicrobial properties of the novel material. Significant kill was achieved against both bacteria under dark conditions, with a substantial enhancement in bactericidal activity demonstrated upon white light illumination.

5.2 EXPERIMENTAL

5.2.1 *Chemicals and Substrates*

The reagents used in materials synthesis were as follows: Crystal violet (Sigma, U.K.) and toluene (Fisher Scientific, U.K.). Diethyl zinc (Aldrich, U.K.) was used in nanoparticle synthesis. In common with many other organometallic compounds, it is pyrophoric and must be handled with appropriate precautions. Solvents used in nanoparticle synthesis were distilled from sodium, degassed by performing at least three freeze-pump thaw cycles and stored under nitrogen. In all synthetic work carried out, the water used was deionised (resistivity 15 MΩcm) and the substrate was medical grade flat silicone sheets (NuSil, Polymer Systems Technology Ltd., U.K.).

5.2.2 *Materials Synthesis*

5.2.2.1 *Preparation of Dipping Solutions*

Swelling solutions were prepared as specified. Di(octyl)phosphinic acid (DOPA-H) [15], zinc bis(di(octyl) phosphinate) ([$Zn(DOPA)_2$]) [16, 17] and di(octyl)phosphinic acid-capped zinc oxide nanoparticles (ZnO, 5:1 ZnO : DOPA-H) [18] that were synthesised as described in the literature [15–18] and were kindly provided by Mr Jonathan Weiner (Imperial College London, U.K.), were dispersed in toluene (1 mg/ mL) to prepare separate swelling solutions. The solutions were left for 24 h (RT) to ensure complete dissolution. A crystal violet dipping solution (aqueous, 0.001 mol dm^{-3}) was also prepared.

5.2.2.2 *Synthesis of Antimicrobial Polymers*

A series of samples, including the relevant controls, were prepared for antimicrobial testing. Medical grade silicone polymer squares (1.21 cm^2) were immersed in toluene swelling solutions (24 h) or aqueous swelling solutions (72 h) as described in Table 5:

Table 5: Dipping conditions for material preparation. Silicone samples were immersed in: Toluene (control), di(octyl)phosphinic acid in toluene (DOPA-H), zinc bis(di(octyl) phosphinate) in toluene ([$Zn(DOPA)_2$]), toluene dispersed di(octyl)phosphinic acid-capped zinc oxide nanoparticles (ZnO), 0.001 mol dm^{-3} crystal violet in water (CV) and ZnO nanoparticles followed by crystal violet (CVZnO)

Solution	**Control**	**DOPA-H**	**[$Zn(DOPA)_2$]**	**ZnO**	**CV**	**CVZnO**
Toluene	y	-	-	-	-	-
DOPA-H*	-	y	-	-	-	-
[$Zn(DOPA)_2$]*	-	-	y	-	-	-
nano ZnO*	-	-	-	y	-	y
0.001 M CV	-	-	-	-	y	y

* solution made up to concentration of 1 mg/ mL

The samples removed from the toluene solutions were air-dried for 48 h, whereas the samples removed from the aqueous solutions were air-dried for 24 h. All samples were subsequently washed and towel-dried, after which selected samples (see Table 5) were immersed in a crystal violet dipping solution (72 h). These samples were then air-dried, washed and towel-dried. Where possible, the samples were maintained under dark conditions both during and after synthesis.

5.2.3 *Materials Characterisation*

A PerkinElmer Lambda 25 UV-Vis spectrometer was used to measure the UV-Vis absorption spectra of the modified silicone polymers used for microbiology, within the range 250 - 1100 nm (full range not shown). The UV-Vis absorption spectra of: di(octyl)phosphinic acid-capped zinc oxide nanoparticles, di(octyl)phosphinic acid and bis(di(octyl) phosphinate) dispersed in separate toluene solutions, was also measured within this range.

X-ray diffraction (XRD) was carried out using an X'Pert Pro diffractometer (PANalytical B.V., The Netherlands) and X'Pert Data Collector software, version 2.2b. The instrument was used in the

theta/theta reflection mode, fitted with a nickel filter, 0.04 rad Soller slit, 10 mm mask, 1/4 ° fixed divergence slit, and 1/2 ° fixed antiscatter slit. The di(octyl)phosphinic acid-capped zinc oxide nanoparticle sample was analysed using a 0.0042 ° step size, at a scanning speed of 0.028 ° s^{-1}. A Bruker Platinum ATR-FTIR was used to measure the infrared transmittance spectra of di(octyl)phosphinic acid-capped zinc oxide nanoparticles, within the range 4000 - 400 cm^{-1} with an accumulation of 15 scans per sample. XPS was carried out using a Thermo K-Alpha spectrometer using monochromated Al Kα radiation. Di(octyl)phosphinic acid-capped zinc oxide nanoparticles and crystal violet-coated, zinc oxide nanoparticle-encapsulated silicone samples were analysed and survey scans were collected in the range 0 - 1200 eV. High resolution scans (0.1 eV) encompassing the principal peaks of Zn (2p), Si (2p), O (1s), N (1s) and C (1s) were collected at a pass energy of 50 eV. For all samples, high-resolution scans were calibrated to adventitious carbon at 284.8 eV.

Nanoparticles dispersed in toluene were drop-cast onto 300-mesh, holey carbon-coated copper or gold film TEM grids (Agar Scientific). A sample of the nanoparticle encapsulated polymer was cut by microtome to a thickness of *ca.* 5 μm and secured onto a TEM grid. Samples were imaged at an operating voltage of 200 kV on a JEOL JEM 2100F microscope. The HR-TEM images were recorded by an 80-300 TITAN (FEI) equipped with a monochromator, operated at 300 kV. Digital images were analysed for particle sizing using ImageJ software (version 1.46r, National Institutes of Health, U.S.A.).

5.2.4 *Functional Testing*

5.2.4.1 *Inductively Coupled Plasma - Optical Emission Spectroscopy*

Inductively Coupled Plasma - Optical Emission Spectroscopy (ICP-OES) was measured on a PerkinElmer Optima 2000 DV. ZnO embedded silicone samples (1.1 x 1.1 x 0.1 cm) were left immersed in deionised water (2 mL) for a set time period (1 day, 7 days, 21 days). Samples were diluted to 5 mL and the zinc concentration

was determined against a calibration curve prepared using Merck Certipur ICP multi element standard solution IV.

5.2.5 *Sample Photostability Testing*

Treated polymer samples were stored in a white light box for an extended duration. The samples were exposed to intense white lighting conditions using a white light source (General Electric 28 W Watt Miser^{TM} T5 2D compact fluorescent lamp) emitting an average light intensity of 6,200 $\pm$ 250 lux at a distance of 16 cm from the samples.

5.2.6 *Microbiological Investigation*

The following silicone elastomer samples (1.21 cm^2) were used in the microbiology experiments: (i) solvent treated silicone (control), (ii) crystal violet-coated silicone (CV), (iii) zinc oxide nanoparticle-encapsulated silicone (ZnO), (iv) di(octyl) phosphinic acid-encapsulated silicone (DOPA-H), (v) zinc bis(di(octyl) phosphinate-encapsulated silicone ([Zn(DOPA)$_2$]) and (vi) crystal violet-coated, zinc oxide nanoparticle-encapsulated silicone (CVZnO). These samples were tested against *S. aureus* NCTC 8325-4 and *E. coli* ATCC 25922. These organisms were stored at -70 ^{o}C in BHI broth containing 20 % (v/v) glycerol and propagated on either MSA or MAC agar for a maximum of two sub-cultures at intervals of two weeks.

BHI broth (10 mL) was inoculated with 1 bacterial colony and cultured in air at 37 ^{o}C for 18 h with shaking at 200 rpm. The bacterial pellet was recovered by centrifugation (21 ^{o}C, 1771 x*g*, 5 min), washed in PBS and centrifuged again to recover the bacteria, which were finally re-suspended in PBS (10 mL). The washed suspension was diluted 1000-fold to obtain the inoculum (~10^6 cfu /mL). The inoculum in each experiment was confirmed by plating ten-fold serial dilutions on agar for viable counts. Triplicates of each polymer sample type

were inoculated with 25 μL of the inoculum and covered with a sterile cover slip (22 mm x 22 mm). The samples were then irradiated for up to ~6 hours using a white light source (General Electric 28 W Watt Miser^{TM} T5 2D compact fluorescent lamp) emitting an average light intensity of 3,750 ± 250 lux at a distance of 30 cm from the samples. A further set of samples (in triplicate) was maintained in the dark for the duration of the irradiation time.

Post irradiation, the inoculated samples and cover slips were added to PBS (225 μL) and vortexed. The neat suspension and ten-fold serial dilutions were plated on the appropriate agar for viable counts. The plates were incubated aerobically at 37 ^{o}C for 24 h (*E. coli*) or 48 h (*S. aureus*). Each experiment contained 3 technical replicates and the experiment was reproduced three times. The Mann-Whitney U test was used to determine the significance of the following comparisons: (i) the activity of each of the modified polymers compared to the control silicone sample when both were incubated in the dark and (ii) the activity of each of the irradiated modified polymers compared to the same material incubated in the dark.

5.3 RESULTS

5.3.1 *Material Synthesis*

Silicone samples incorporated with dye- and dye-nanoparticle combinations were prepared using a simple dipping procedure (Figure 28(a)-(b)) [19]. Zinc oxide nanoparticles (Figure 28(c)) were encapsulated into medical grade silicone using a "swell-encapsulation" shrink strategy, which exploits the swelling of polymers induced by contact with certain organic solvents [19–21]. The silicone polymers were immersed into a 100 % toluene swelling solution made up to 1 mg/ mL of zinc oxide nanoparticles, prepared according to the previously published route [18]. Analogous to the mechanism by which dyes and gold nanoparticles are encapsulated into polymers [19–21], exposure of the silicone polymer to toluene induced considerable polymer swelling, enabling the diffusion of the zinc oxide

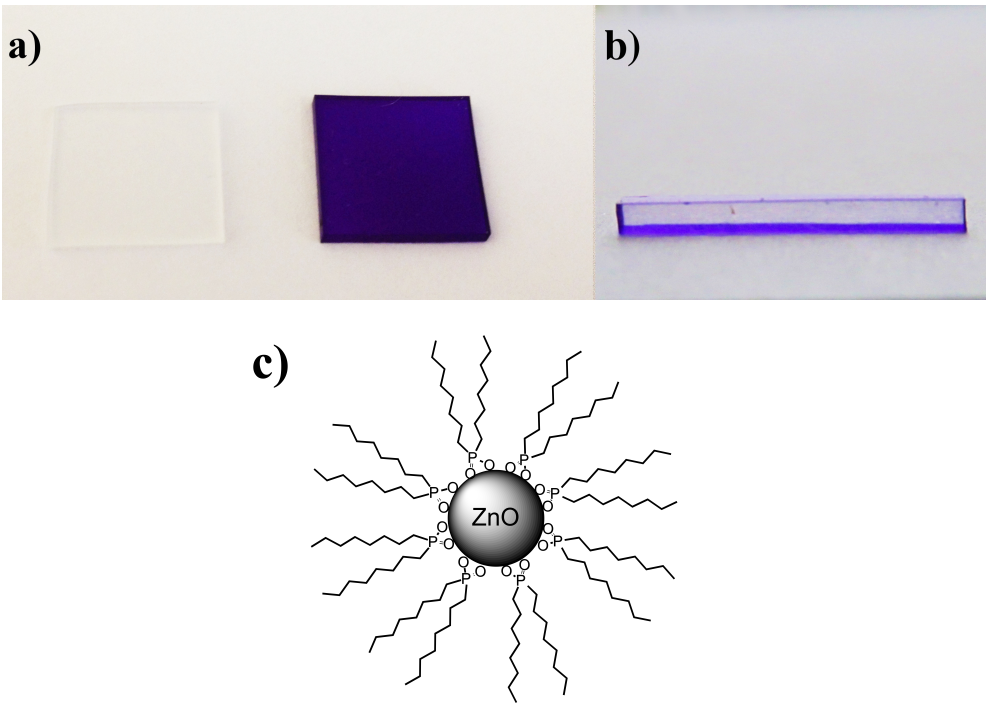

Figure 28: (a) Photograph of the zinc oxide nanoparticle-encapsulated silicone sample and the crystal violet-coated, zinc oxide nanoparticle-encapsulated silicone sample. (b) Cross sectional photograph of the zinc oxide nanoparticle-encapsulated, crystal violet-coated silicone sample. The sample dimensions are 1.1 x 1.1 x 0.1 cm. (c) Diagram to show zinc oxide nanoparticle with di(octyl)phosphinic acid capping ligands

nanoparticles through the silicone matrix. The resulting zinc oxide nanoparticle-encapsulated polymer was colourless in appearance.

Crystal violet was coated onto medical grade silicone and zinc oxide nanoparticle-encapsulated silicone by immersing the respective polymers in an aqueous crystal violet solution made up to 0.001 mol dm^{-3}, for 72 h (Figure 28). The mechanism of attachment is as yet unknown, but it has been found that it is a predominantly surface process at this concentration [19], with the purple dye adhering to the silicone surface and not distributed through the polymer bulk (see Figure 28(b)).

5.3.2 *Materials Characterisation*

5.3.2.1 *UV-Vis Absorbance Spectroscopy*

The UV-Vis absorbance spectra of toluene swelling solutions and selected treated silicone samples were measured within the range 250 - 1100 nm. The dispersed zinc oxide nanoparticle solution demonstrated a characteristic shoulder at 350 nm [15], whereas the capping agent solution and $[Zn(DOPA)_2]$ exhibited no significant absorption in this region (Figure 29(a)). Using a Tauc plot - a plot of $(ah\nu)^2$ against energy (eV), where 'a' is the absorbance of the zinc oxide nanoparticles [22] - the band onset of the nanoparticle suspension was estimated at 3.53 eV (Figure 29(a), inset), indicating that the zinc oxide nanoparticle is a UV photocatalyst (< 385 nm) and thus should not exhibit significant light-activated antimicrobial activity when illuminated with a white hospital lighting source.

UV-Vis absorbance spectroscopy was also used to examine some of the materials prepared for microbiological testing (Figure 29(b)). The zinc oxide nanoparticle-encapsulated silicone sample showed no UV-Vis absorbance signal at 350 nm, characteristic of the nanoparticles. This can be attributed to low nanoparticle concentrations in the polymer, in addition to the significant UV-Vis absorption signal of the silicone substrate in the region 250 - 350 nm. The UV-Vis

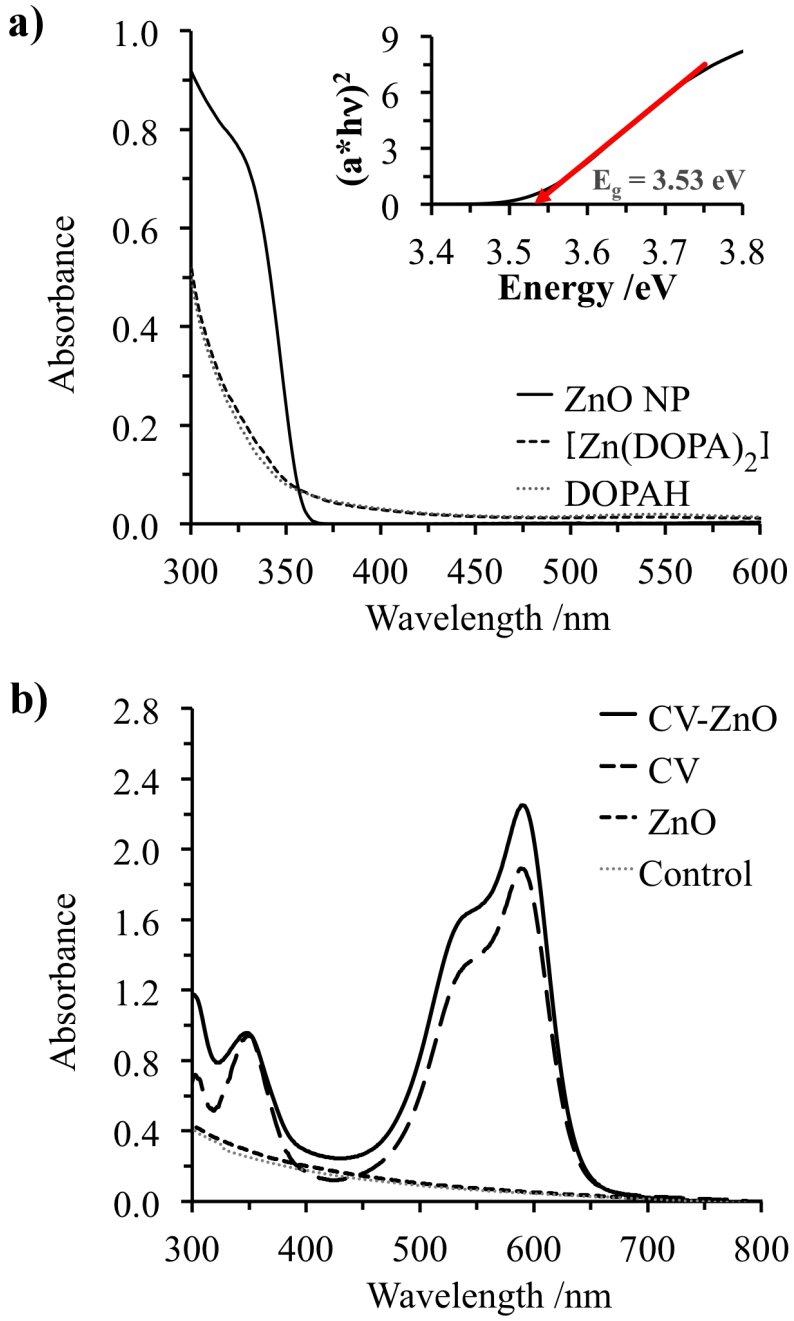

Figure 29: (a) UV-Vis absorbance spectra of toluene dispersed di(octyl)phosphinic acid-capped zinc oxide nanoparticles (ZnO NP), di(octyl)phosphinic acid in toluene (DOPA-H) and zinc bis(di(octyl) phosphinate) ([$Zn(DOPA)_2$]) in toluene. Inset: Tauc plot to determine band gap of di(octyl)phosphinic acid-capped zinc oxide nanoparticles. The band onset of the 3 - 4 nm zinc oxide nanoparticles was calculated as 3.53 eV. (b) UV-Vis absorbance spectra of modified samples used for microbiological testing: Solvent treated silicone (control), crystal violet coated-silicone (CV), zinc oxide nanoparticle encapsulated-silicone (ZnO) and crystal violet-coated, zinc oxide nanoparticle-encapsulated silicone (CV-ZnO)

absorbance signals of both the crystal violet coated- and crystal violet coated, zinc oxide nanoparticle-embedded silicone samples were similar in peak shape and position and characteristic of the crystal violet dye, with absorbance maxima at $\lambda \approx 590$ nm and a shoulder peak at $\lambda \approx 545$ nm. This indicates that the presence of the zinc oxide nanoparticles does not affect the position of spectral features, suggesting that there is no electronic interaction between the zinc oxide nanoparticles and crystal violet dye. Figure 29(b) also indicates that the concentration of crystal violet in the zinc oxide nanoparticle-embedded silicone is greater than that in the crystal violet coated-silicone. It can be speculated that this is due to the swelling treatment prior to dye coating, used to incorporate the zinc oxide nanoparticles, disordering the polymer surface and creating a greater surface area for uptake of the dye. This increased uptake of the dye may effect a more efficacious antimicrobial activity consequent to a greater concentration of bactericidal agent present.

5.3.2.2 *X-Ray Diffraction*

The di(octyl)phosphinic acid-capped zinc oxide nanoparticles were analysed using XRD and compared to a reference spectrum (Figure 30(a)). The nanoparticle sample examined corresponds to zinc oxide, with all the reference peaks correlating to that of the reference spectrum for the zinc oxide wurtzite structure. Two broad peaks were also present at *ca.* 12^{o} 2θ and 21^{o} 2θ. XRD analysis of the di(octyl)phosphinic acid showed a series of sharp peaks in this region (Figure 30(b)), confirming that these peaks can be attributed to amorphous DOPA-H on the surface of the zinc oxide nanoparticle.

5.3.2.3 *ATR-FTIR Spectroscopy*

The infrared transmittance spectra of the di(octyl)phosphinic acid-capped zinc oxide nanoparticles and the silicone encapsulated with the zinc oxide nanoparticles were obtained by ATR (Figure 31). The IR spectra of the zinc oxide nanoparticles showed sharp peaks at 1050 cm^{-1} and 1130 cm^{-1} and a broad band at 3400 cm^{-1} correlating to the P-O bonds and the O-H bond respectively, in the di(octyl)phosphinic

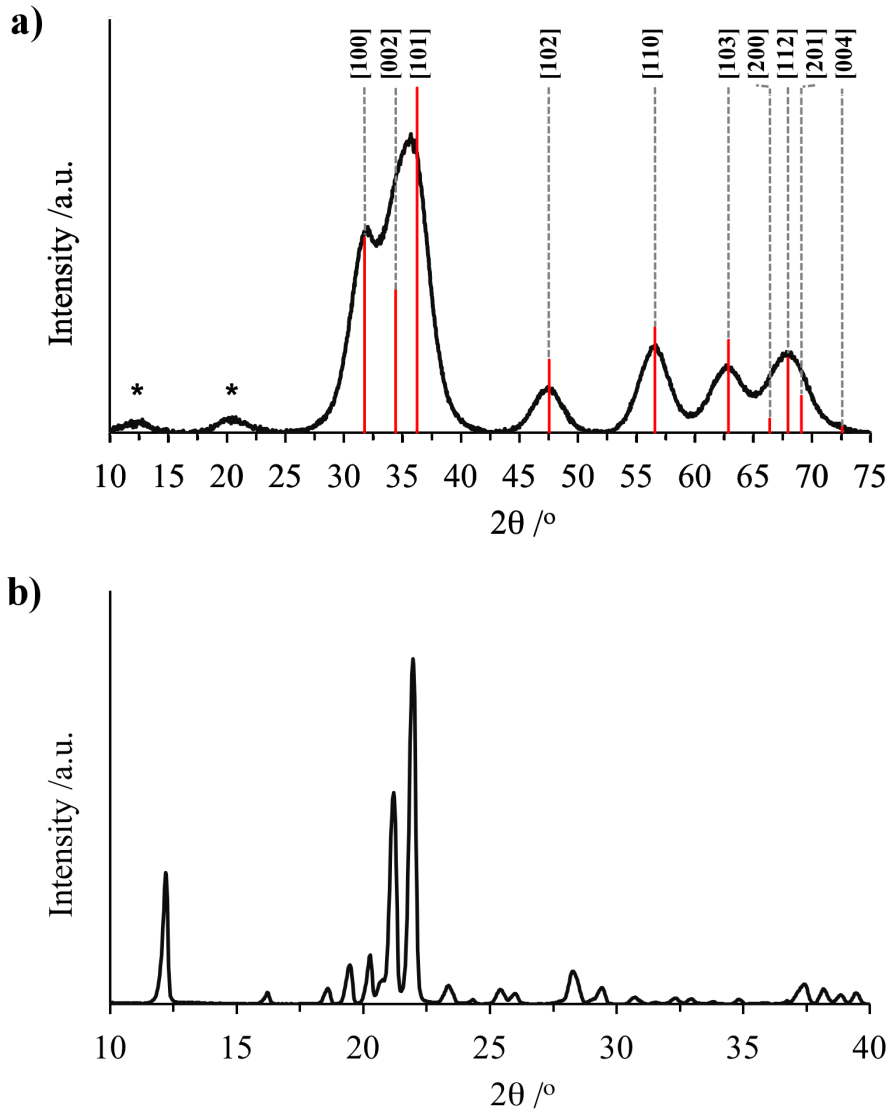

Figure 30: (a) XRD of di(octyl)phosphinic acid-capped zinc oxide nanoparticles. The red lines reference the zinc oxide nanoparticle peaks against the ZnO wurtzite structure (reference lines from PDF 036-1451, ICDD PDF4+ database). * indicates that these peaks are assigned to DOPA-H. (b) XRD of di(octyl)phosphinic acid

acid capping ligand (Figure 31(a)). A sharp peak at *ca.* 2900 cm^{-1} was also observed and corresponds to the long alkyl chain in the nanoparticle capping group. The IR spectrum of the silicone embedded with the zinc oxide nanoparticles was characteristic of the spectrum for the silicone polymer (Figure 31(b)). The spectrum showed no evidence of nanoparticle encapsulation and this can be attributed to the strong signal obtained for the silicone polymer, in addition to the low concentration of nanoparticles encapsulated within the polymer.

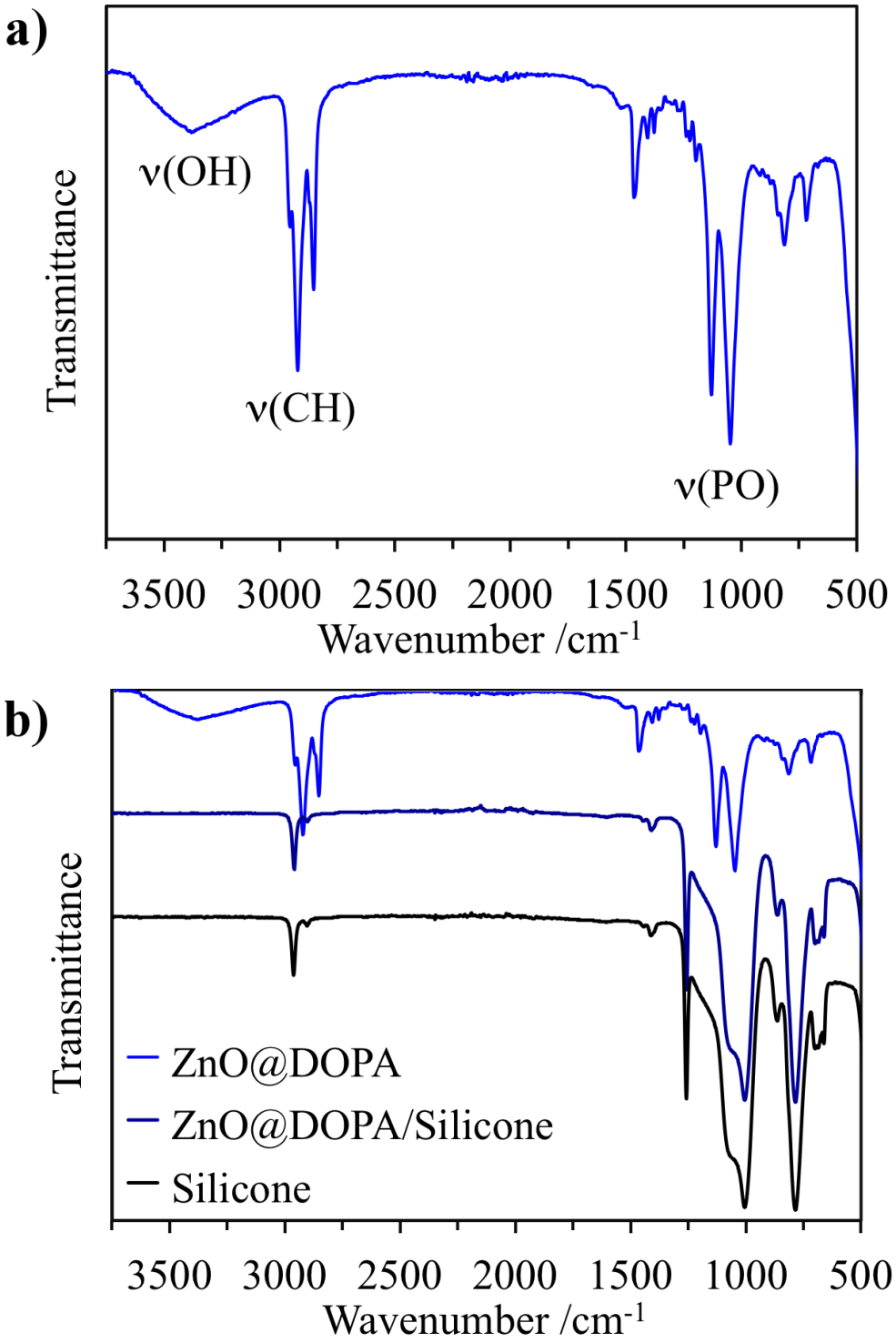

Figure 31: ATR-FTIR transmittance spectra measured within the range 4000 - 400 cm^{-1} of (a) di(octyl)phosphinic acid-capped zinc oxide nanoparticles and (b) silicone encapsulated with di(octyl)phosphinic acid-capped zinc oxide nanoparticles

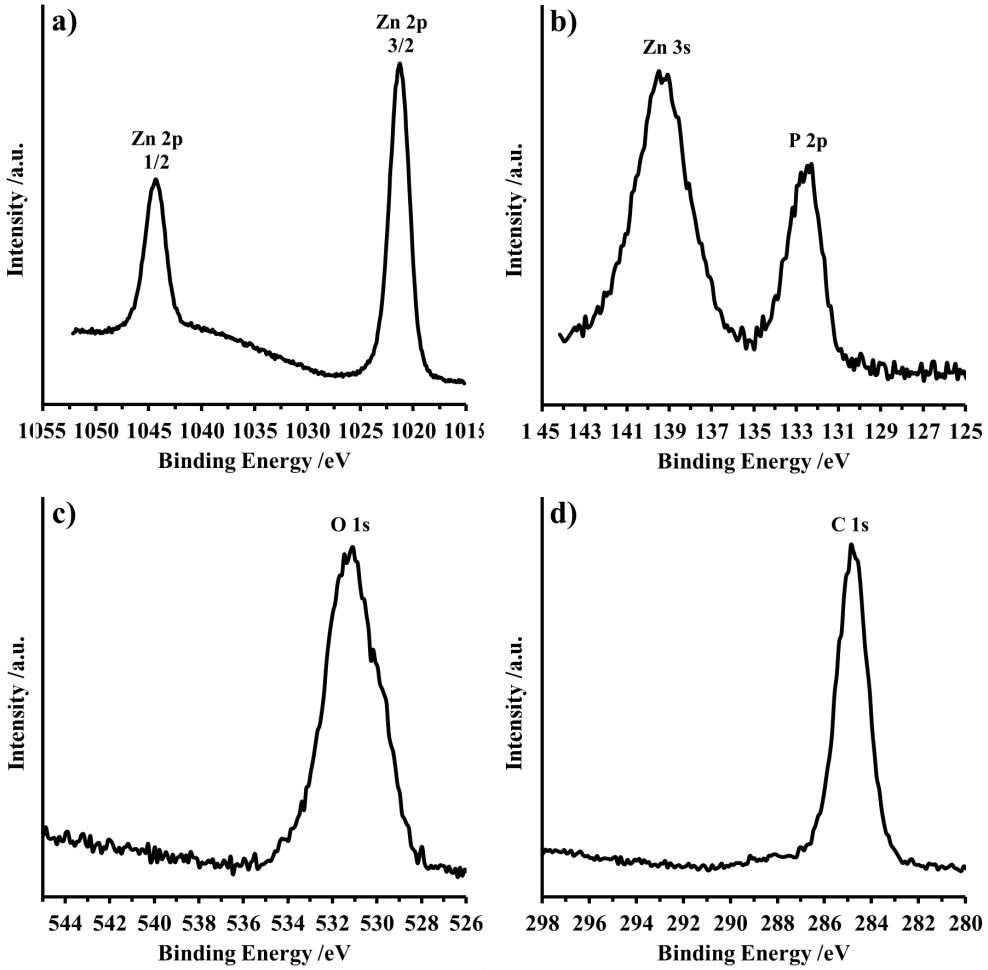

Figure 32: XPS spectra of di(octyl)phosphinic acid-capped zinc oxide nanoparticle to show (a) Zn scan, (b) P scan, (c) O scan and (d) C scan

5.3.2.4 *X-Ray Photoelectron Spectroscopy*

XPS of the di(octyl)phosphinic acid-capped zinc oxide nanoparticles showed a doublet in the Zn (2p) region corresponding to zinc in ZnO and an asymmetric peak in the P (2p) region, correlating to the overlapping P $2p_{3/2}$ and P $2p_{1/2}$ components typical of phosphorus in phosphate, as found in the nanoparticle capping ligand (Figure 32(a)-(b)). It should be noted that a Zn (3s) peak was observed in the P (2p) region and peaks in the O (1s) region and C (1s) region were also present (Figure 32(c)-(d)).

XPS of the crystal violet-coated, zinc oxide nanoparticle encapsulated silicone polymer showed evidence of nanoparticle encapsulation (Figure 33). As observed in the XPS spectra of the zinc oxide nanopar-

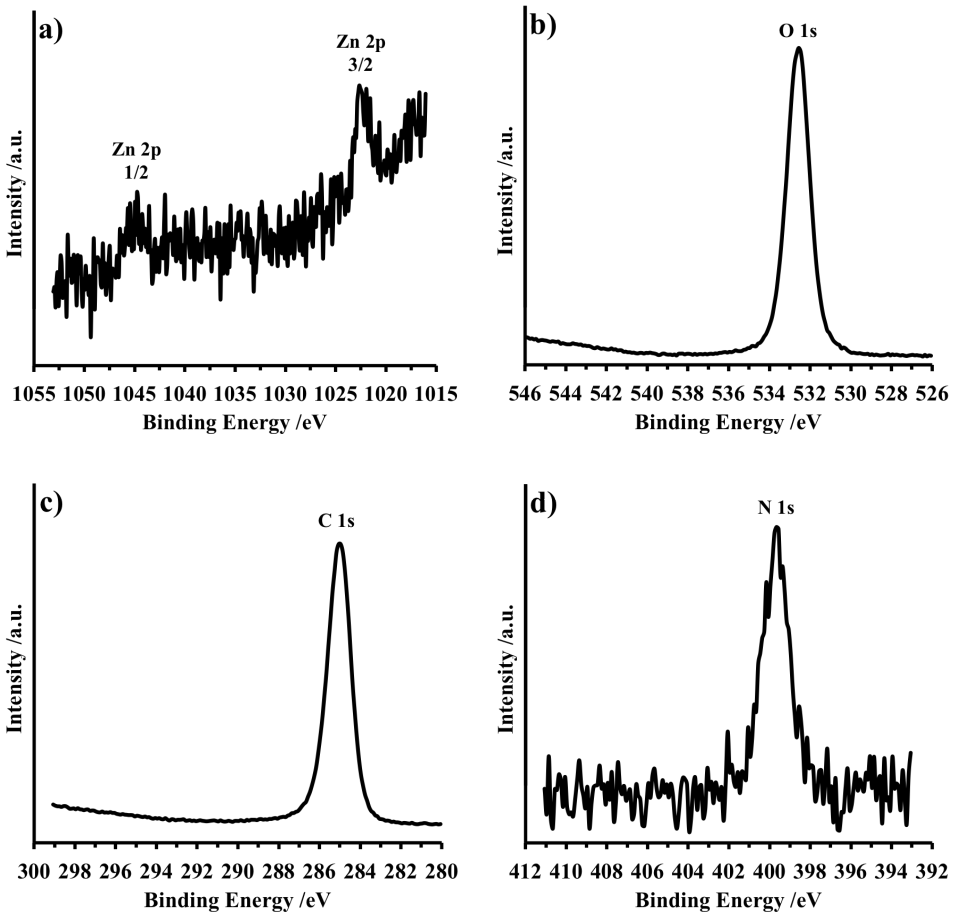

Figure 33: XPS spectra of crystal violet-coated, zinc oxide nanoparticle-encapsulated silicone to show (a) Zn scan, (b) O scan, (c) C scan and (d) N scan

ticles, a doublet in the Zn (2p) region corresponding to zinc in ZnO was identified, confirming the presence of zinc oxide nanoparticles within the polymer. Peaks in the O (1s) region, and C (1s) region Si (2p) region and N (1s) region were also present, correlating to the presence of the nanoparticle, polymer and crystal violet dye (N peak).

5.3.2.5 *Transmission Electron Microscopy*

The zinc oxide nanoparticle powder was dispersed in toluene to form a dilute solution and drop cast onto TEM grids. The TEM images (Figure 34) show well separated, small, spherical nanoparticles with no evidence of agglomeration. Size analysis showed an average nanoparticle diameter of 3.3 nm ($\pm$ 1.1 nm). HR-TEM images showed the particles to be crystalline with lattice spacings correlating

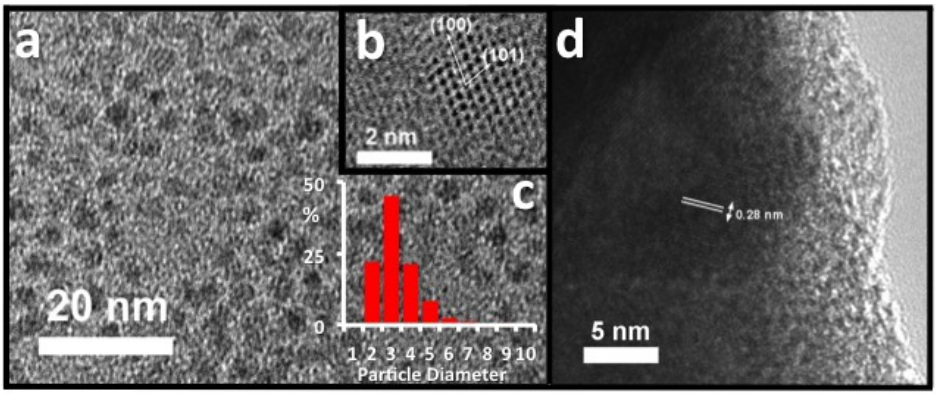

Figure 34: (a) TEM of zinc oxide nanoparticles with di(octyl) phosphinate capping ligands, (b) HR-TEM of zinc oxide nanoparticle with lattice spacings, (c) histogram of particle size distribution of zinc oxide nanoparticles as synthesised, determined by TEM and (d) TEM of silicone polymer encapsulated with zinc oxide nanoparticles with di(octyl) phosphinate capping ligands

with Wurtzite ZnO. Each nanoparticle was composed of a single crystalline domain, a result of the nucleation controlled growth and the prevention of oriented attachment by the strongly bound di(octy)phosphinate ligand.

TEM analysis of the zinc oxide nanoparticle embedded polymer edge demonstrated evidence of nanoparticle encapsulation, with visible crystallographic planes present (Figure 34(c)). Lattice spacings of 0.28 nm were observed correlating to the (100) plane of hexagonal ZnO.

5.3.3 *Functional Properties*

5.3.3.1 *Material Stability*

In order to elucidate the stability of the zinc oxide nanoparticles within the polymer, ICP-OES was used to determine whether zinc, either in nanoparticulate form or other zinc species, leached from the polymer under aqueous conditions. Samples of silicone embedded with zinc oxide nanoparticles were immersed in de-ionised water and the concentration of zinc that leached into solution was measured after 1 day, 7 days and 21 days. It was found that small traces of zinc

were released into solution (up to 0.0025 mg per zinc sample), but these leaching effects plateaued with time (Figure 35).

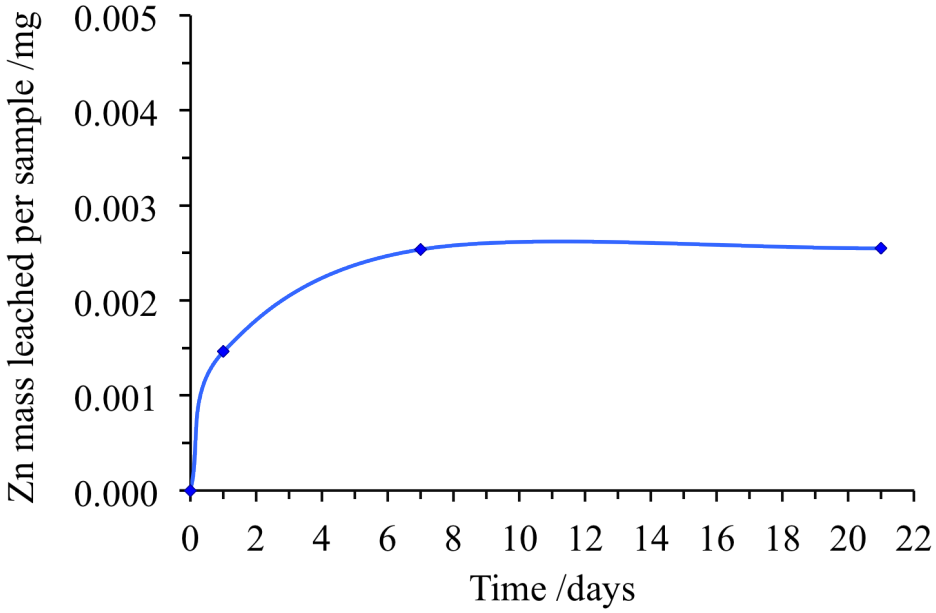

Figure 35: Leaching of zinc from ZnO encapsulated silicone polymer into de-ionised water at RT, determined by ICP-OES, measured as function of time (days)

5.3.3.2 *Material Photostability*

UV-Vis spectroscopy was used to examine the photostability of crystal violet and crystal violet-coated, zinc oxide nanoparticle-encapsulated silicone polymers upon exposure to a white light source. The samples were illuminated and the dye absorbance was measured periodically within the range 400 - 750 nm (Figure 36). As in the previous Chapter (Section 4.3.3.3), the white light source - 8 W GE lighting (3500 K) - was similar to that commonly used in U.K. hospitals and the lighting intensity used in this investigation was considered in relation to the brightness of various areas in U.K healthcare environments, as recommended by the Department of Health (Table 4) [22]. In this study, the lighting intensity used, ~6,200 lx, was ~62x more intense than that typical of hospital corridors and wards (*ca.* 200 lx) [22].

Under these intense lighting conditions, the crystal violet-coated silicone sections demonstrated suitable photostability (Figure 36(a)-

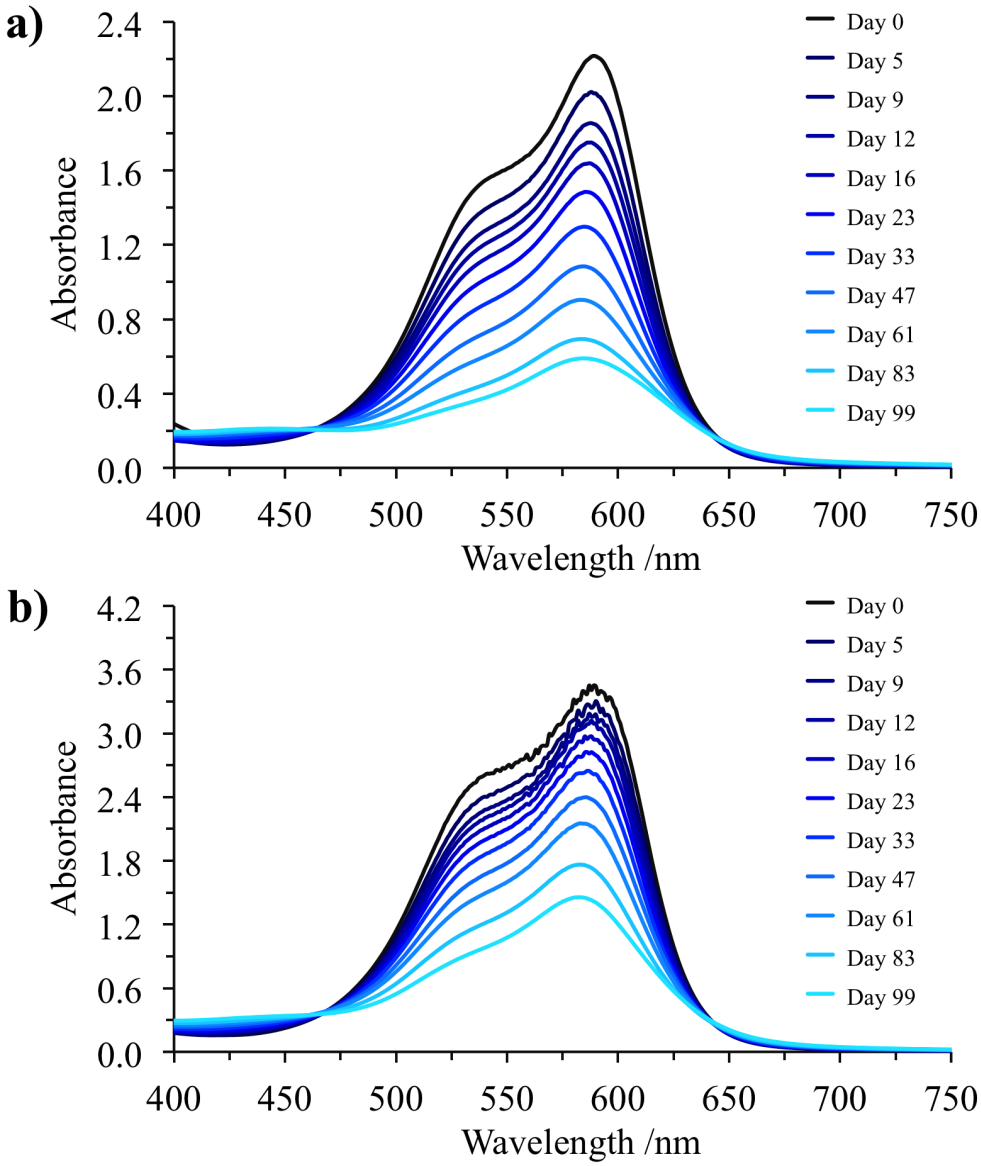

Figure 36: UV-Vis absorbance spectra measured in the range 400 - 750 nm of (a) crystal violet-coated silicone and (b) crystal violet-coated, zinc oxide nanoparticle-encapsulated silicone. The samples were illuminated with a white light source emitting an average light intensity of 6,200 ± 250 lux at a distance of 16 cm from the samples

(b)). The rate of dye photodegradation was determined by plotting the decrease in the UV-Vis absorbance of the samples at the dye peak maxima, against the illumination time (Figure 37). The rate of photodegradation of both the crystal violet-coated silicone and crystal violet-coated, zinc oxide nanoparticle-encapsulated silicone is linear in form, showing a smooth, gradual decrease in dye intensity as a function of illumination time. The photodegradation of the

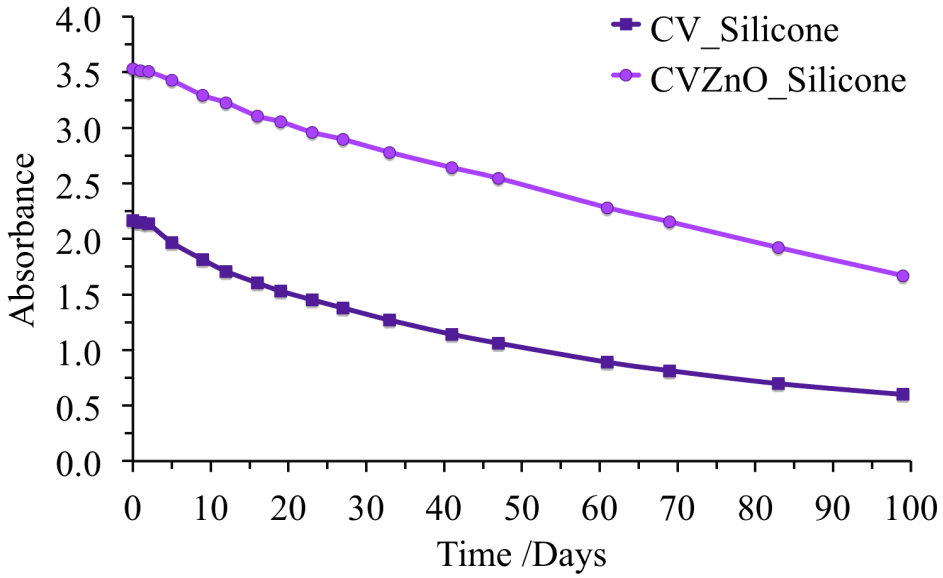

Figure 37: Rate of photodegradation of modified polymers upon exposure to white light illumination (99 days, 6,200 lx). The rate is displayed as a decrease in sample absorbance at the crystal violet absorbance maxima, over time. Crystal violet has been abbreviated as CV and the zinc oxide nanoparticles have been abbreviated as ZnO. CV_Silicone represents the crystal violet peak in the crystal violet-coated silicone sample and CVZnO_Silicone represents the crystal violet peak in the crystal violet-coated, zinc oxide nanoparticle-encapsulated silicone sample

crystal violet-coated silicone polymers was *ca.* 72 % over a period of 99 days. Over the same period of time, the crystal violet-coated, zinc oxide-encapsulated polymer resulted in a 52 % photodegradation of the crystal violet dye, suggesting that the presence of the nanoparticles may stabilise the dye with respect to photodegradation.

It is expected that the rate of dye photodegradation linearly correlates with the lighting intensities used in the investigation. Previously (Chapter 4, Section 4.3.3.3) it was noted that over a period of 29 days, a 50 % photodegradation of crystal violet was observed for the crystal violet-coated, 2 nm gold nanoparticle-encapsulated silicone, upon illumination with a 12,500 lx light source. Here, the crystal violet-coated, zinc oxide nanoparticle samples demonstrate an apparent enhanced photostability, indicating a 27 % photodegradation of crystal violet within 47 days, using a 6,200 lx white light source. It is possible to draw conclusions about the relative photostability of the two dye-nanoparticle systems, by accounting for the light intensity

received at the sample over a specific time period. However, it should be noted that a more rigorous comparison of the photostability of the two dye-nanoparticle systems explored in these chapters can only be achieved by investigating the photostabilities of the respective samples in a direct study, using the same illumination source.

The crystal violet-coated, zinc oxide-encapsulated samples demonstrate strong photostability over a prolonged time period using intense illumination conditions. These samples demonstrate suitability for use as photo-activated antimicrobial surfaces in healthcare environments, where the lighting conditions in hospital wards and corridors are *ca.* 62x less intense than that investigated in this study. It is anticipated that under ambient lighting conditions, these samples should maintain potency for several years.

5.3.4 *Microbiological Testing*

The antimicrobial activity of a series of modified medical grade silicone samples was determined using representative Gram-positive and Gram-negative bacteria, *S. aureus* and *E. coli*, respectively, both of which are commonly found in healthcare environments. For each experiment, a set of samples were illuminated with a white hospital light source (28 W), emitting an average light intensity of 3,750 lux at a distance of 30 cm from the samples, whilst a parallel set were stored under dark conditions for the same duration. Although the white light intensity used in this investigation is approximately three times that found in a typical A & E examination room [22], the microbial loads used in these experiments are far greater than those typically found in a clinical environment (~45,529 cfu cm^{-2} used in this investigation, compared to $\leqslant$ 3,060 cfu cm^{-2} with average values of < 100 cfu cm^{-2} in a clinical environment [23–27]).

The light-activated and intrinsic bactericidal activities of the following samples were tested: (i) solvent-treated silicone, (ii) crystal violet-coated silicone (CV), (iii) di(octyl) phosphinic acid-capped zinc oxide nanoparticle-encapsulated silicone (ZnO), (iv)

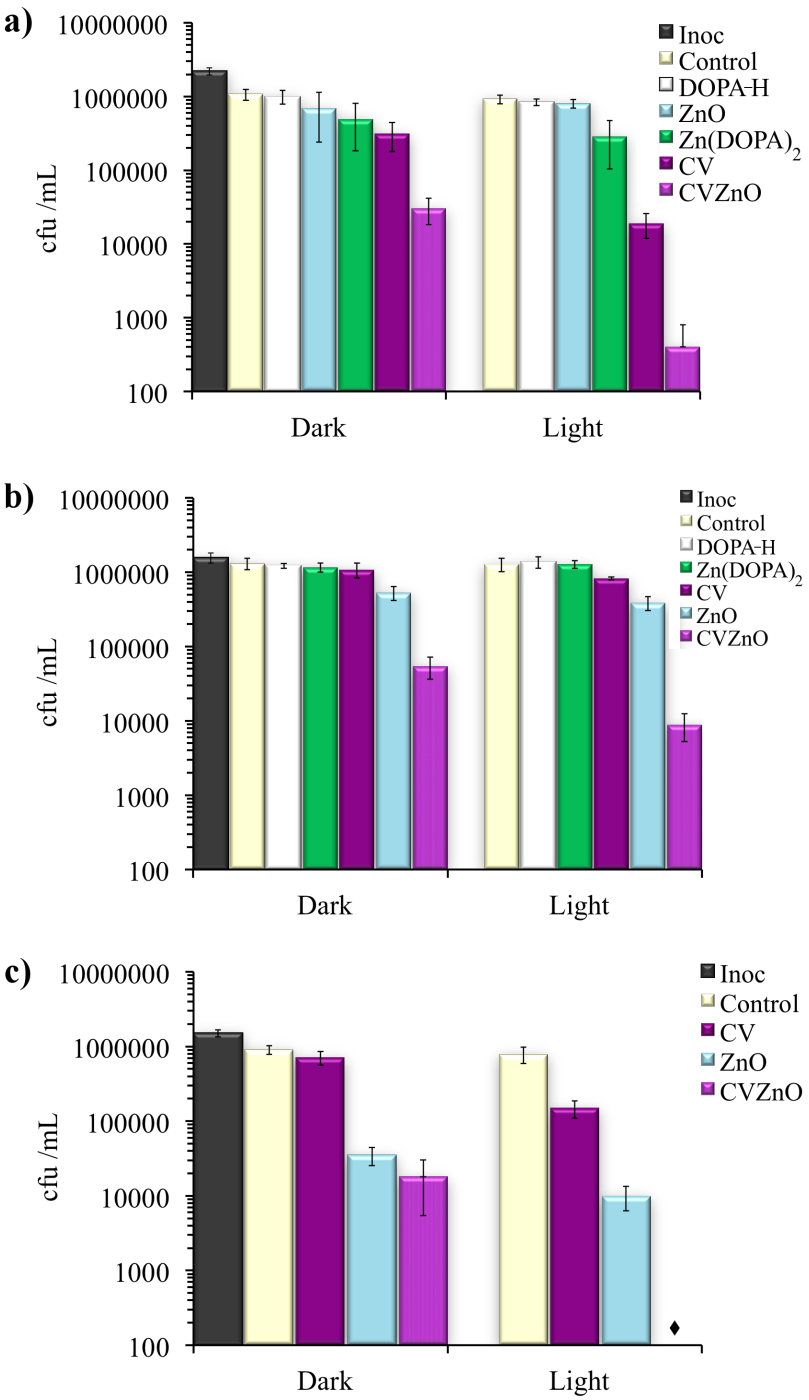

Figure 38: Graph to show the viable counts of bacteria after incubation on modified silicone polymers exposed to white light illumination: (a) *S. aureus* (1 h illumination), (b) *E. coli* (3 h illumination) and (c) *E. coli* (6 h illumination). The white hospital lighting source emitted an average light intensity of 3,750 ± 250 lux at a distance of 30 cm from the samples. DOPA refers to di(octyl)phosphinic acid, the nanoparticle capping ligand. The ♦ indicates where the bacterial counts were reduced to below the detection limit of 400 cfu

di(octyl)phosphinic acid encapsulated silicone (DOPA-H), (v) zinc bis(di(octyl) phosphinate-encapsulated silicone ([Zn(DOPA)$_2$]) and (vi) crystal violet-coated, di(octyl) phosphinic acid-capped zinc oxide nanoparticle encapsulated silicone (CVZnO). This range of samples was tested to deduce whether it was the ZnO nanoparticle, free capping agent or the ZnO-bound capping agent, that contributed to the antimicrobial activity. Samples were also coated with crystal violet dye to establish whether this enhances bacterial kills and if there exists a similar synergistic enhancement in the antimicrobial activity as previously established with crystal violet, methylene blue and gold nanoparticle combinations encapsulated into medical grade polymers [19–21, 23].

Figure 38 shows the antimicrobial efficacy of a range of treated silicone samples when inoculated with either *S. aureus* or *E. coli* for up to 6 hours (Figure 38). Under dark conditions (1 h incubation at 20 ^{o}C), neither the ZnO sample, nor the DOPA-H sample demonstrated significant activity against *S. aureus*. However, the [Zn(DOPA)$_2$] sample induced a statistically significant reduction in staphylococcal numbers ($P < 0.001$) in the dark. The CVZnO sample significantly reduced the number of viable *S. aureus* on the sample surface ($P < 0.001$), with enhanced bacterial kills compared to the sample containing CV alone. This can be attributed to the higher concentration of crystal violet at the sample surface, due to the pre-swelling treatment in toluene used to encapsulate the ZnO nanoparticles. Illumination of these samples using a standard hospital lighting source for just 1 hour, resulted in the lethal photosensitisation of *S. aureus* on the CV sample (1.69 log kill), with a marked increase in antimicrobial activity on the CVZnO sample ($P < 0.001$, 3.36 log kill).

A correlation has been noted in the literature between the decreasing size of the zinc oxide nanoparticle and its bactericidal efficacy [6, 9, 10]. In this study, small 3 - 4 nm ZnO nanoparticles were incorporated into the polymer. These polymers exhibited antimicrobial activity against *E. coli*, with a statistically significant reduction in bacterial numbers (1.41 log) following incubation for 6 hours in the dark ($P < 0.001$, Figure 38). ICP-OES studies indicated that small traces of

zinc species leached from the polymer when left in aqueous solution for extended periods. However, previous research has shown that leached Zn^{2+} ions are unlikely to contribute to the antimicrobial activity [10].

Illumination of the ZnO sample resulted in enhanced antimicrobial activity with a 1.9 log reduction in bacterial numbers for the same incubation duration. No antimicrobial activity was observed on the DOPA-H and [$Zn(DOPA)_2$] samples either under dark conditions or with white light illumination for 3 hours. CV samples demonstrated a limited, but statistically significant bactericidal activity when tested against *E. coli* (0.72 log kill, 6 h illumination). This discrepancy between the efficacy of PDT against Gram-positive bacteria and Gram-negative bacteria can be attributed to differences in their cell wall structures [19]. Gram-negative bacteria have both inner and outer phospholipid bilayer cell membranes, whereas Gram-positive bacteria have only a single inner phospholipid bilayer cellular membrane surrounded by peptidoglycan, which acts as an ineffective barrier against PDT. It has also been noted that the inherent bactericidal efficacy of crystal violet against Gram-negative bacteria is more limited [19]. However, the dual-combination CVZnO sample exhibited potent photobactericidal activity against *E. coli*, with bacterial numbers reduced by 2.16 log within 3 hours of white light illumination and by at least 4.25 log within 6 hours (below detection limit, $P < 0.001$). This suggests a synergistic effect in the activity of the triarylmethane dye when ZnO nanoparticles are present, as an enhancement in bacterial kill was noted, that surpassed the kills expected if they were caused by an additive effect.

Overall, the results indicate that the ZnO samples demonstrate a stronger bactericidal efficacy against the Gram-negative bacterium, *E. coli*, than the Gram-positive bacterium, *S. aureus*. Conversely, the CV samples exhibit a more efficacious antimicrobial activity against *S. aureus*. Crystal violet is known to exhibit antimicrobial activity against Gram-positive bacteria and is used in the treatment of superficial wounds and some skin infections [28–32]. Consequently, this novel ZnO-dye combination creates an antimicrobial surface on

medical grade silicone, effective against both *E. coli* and *S. aureus*. The CVZnO sample demonstrates superior antimicrobial efficacy, inducing the lethal photosensitisation of both *S. aureus* and *E. coli*, with high reductions in viable bacterial numbers achieved after only 1 hour and 6 hours illumination, respectively. Moreover, significant kills were also observed under dark conditions and importantly, a highly significant reduction in *E. coli* numbers (1.70 log) was recorded with CVZnO after 6 hours incubation. These samples achieved a 1.16 log greater reduction in bacterial numbers when tested against *E. coli* under dark conditions (6 hours), compared to the dual photosensitiser dye-gold nanoparticle system described in the previous chapter. It is clear that the antimicrobial activity of the novel zinc oxide nanoparticle, dye-coated silicone samples is more efficacious than other dye-nanoparticle samples investigated, however, the photobactericidal activity demonstrated by these samples is comparable to that demonstrated by a previously tested multi-dye-nanogold-encapsulated silicone (Chapter 4), with both samples reducing bacterial numbers to below the detection limit within 6 hours illumination.

To validate the antimicrobial efficacy of these surfaces, the exhibited photobactericidal activity of these surfaces was compared to other antimicrobial systems published in the literature. Limited data has been published on the development of photobactericidal polymers. One system details the synthesis of protoporphyrin- and zinc protoporphyrin-grafted nylon fibres using a white light source of intensities ranging from 10,000 - 60,000 lux, to activate the antimicrobial properties [33]. When tested against *S. aureus* these samples induced the lethal photosensitisation of bacteria within 30 minutes, reducing bacterial numbers to 5.6 % on the zinc protoporphyrin sample at a light fluence of 40,000 lx [33], however, no antimicrobial activity was observed when tested against *E. coli* at this light fluence [33].

Other visible light photo-active antimicrobial surfaces include titania, silver-loaded titania, nitrogen-doped titania and silver-loaded nitrogen-doped titania thin films, on glass surfaces [22, 34]. Titania coatings demonstrated negligible antimicrobial activity upon irradi-

ation with white light for 12 h, when tested against EMRSA-16 [22]. Titania is a UV-active photocatalyst and so, this poor photo-activity can be attributed to the limited proportion of UV light present in the white light source [22]. Silver-doped titania-coatings demonstrated an enhanced photocatalytic effect, reducing bacterial numbers by *ca.* 2.5 log [22]. Moreover, when tested against *E. coli*, silver-doped titania samples demonstrated efficacious bacterial kills, even under dark conditions, reducing bacterial numbers to below the detection limit within 6 hours [22]. Silver-loaded nitrogen-doped titania samples demonstrated enhanced light-activated kill rates, reducing bacterial levels to below the detection limit within 5 hours at a light fluence of 1,000 lx, although less efficacious antimicrobial acitivity was noted under dark conditions [34]. When tested against MRSA however, these samples only effected a 2 log reduction in bacterial numbers upon irradiation for 5 hours [34]. Copper surfaces have also attracted much attention in terms of their efficacious antimicrobial activity, with thin films of copper and copper oxide on glass surfaces reducing bacterial numbers to below the detection limit within 30 minutes and 1 hour, when tested against *E. coli* and *S. aureus* respectively, in a laboratory investigation [35]. The use of copper surfaces in hospital touch surface applications, has also effected a significant reduction in microbial surface contamination levels in clinical trials [24, 25], impacting on the incidence of hospital-acquired infections [36].

Some of these antimicrobial systems demonstrate poor antimicrobial efficacy compared with the crystal violet-coated zinc oxide nanoparticle encapsulated silicone reported here [22, 33]. However, other systems exhibited comparable, or enhanced antimicrobial activity [34, 35]. The use of thin film antimicrobial coatings, or copper surfaces however, presents a substantial financial burden to healthcare institutions. Existing furnishings would have to be replaced with the antimicrobial equivalent and U.K. hospitals that are part of the Private Finance Initiative scheme would also be required to pay an upfront '30 year lifetime cost' for new furnishing installations. The use of an antimicrobial polymer that can be retrofit onto existing furnishings presents a promising, inexpensive alternative for use as

an infection-control mechanism.

It is anticipated that this crystal violet-zinc oxide-polymer technology can be utilised to develop antimicrobial surfaces for use, chiefly in healthcare environments, but also in everyday applications such as keyboards, mobile phone and tablet covers and kitchen surfaces. Although this novel material has been developed for use in touch surfaces rather than implanted medical devices, it is crucial that these surfaces are non-toxic and contact with them does not effect adverse reactions. With the widespread use of zinc oxide nanoparticles in the cosmetics and food industry, their toxicity has been extensively studied in a number of reports. The toxicity of nanoparticles depends on a number of factors including their size, shape, route of administration and dosage [37]. Nano zinc oxide is generally believed to be safe, with investigations concluding that zinc oxide nanoparticle penetration through the skin is negligible and through other routes of administration zinc oxide only showed toxic effects at high doses (> 100 μg/mL) [38–40]. Similarly, crystal violet poses a low toxicity risk and was used as a topical antiseptic before its use was superseded by modern drugs [41]. The World Health Organisation also recommended its inclusion in the 'Interagency Emergency Health Kit' [42] and clinical trials have investigated its efficacy as a potential treatment against MRSA [43, 44]. Consequently, the use of this antimicrobial combination in these novel dual mechanism antimicrobial surfaces, should not present a risk to users and should maintain low surface bacterial levels, reducing the likelihood of the spread of infections in a hospital environment.

5.4 CONCLUSION

Highly efficacious antimicrobial surfaces encapsulated with 3 - 4 nm zinc oxide nanoparticles and coated with crystal violet dye, have been synthesised using a straightforward and simple two stage dipping process. These materials demonstrated strong photostability upon extensive illumination with a white hospital light source. For the first time, TEM analysis was used as a technique to confirm the incorporation of nanoparticles into the silicone polymer, with

visible lattice spacings matching those as determined from TEM micrographs of the drop cast nanoparticle suspension.

These efficacious antimicrobial materials present ideal surfaces for use in healthcare environments and demonstrated strong bactericidal activity via a novel-dual mechanism approach, utilising PDT in combination with the inherent antimicrobial properties of zinc oxide nanoparticles. The resultant polymer, a potent bactericidal surface, achieved a 3.4 log reduction in bacterial numbers within an hour, when tested against Gram-positive bacteria and reduced bacterial numbers to below the detection limit within 6 hours against Gram-negative bacteria, upon illumination with a white light source. Significant kills against both Gram-positive and Gram-negative bacteria were also achieved under dark conditions within the same time period.

The principal aim of this thesis is to detail the development of potent antimicrobial polymers that utilise multiple mechanisms of bacterial attack to maintain low surface bacterial contamination levels in healthcare environments. Up to this point, there has been a strong emphasis on the development of photobactericidal polymers incorporated with photosensitiser dyes and nanoparticles. However, to advance materials development, an understanding of the underpinning photophysics is key. The next chapter presents an investigation into the photochemical properties of photosensitiser dye- and photosensitiser dye and nanoparticle-encapsulated polymers, to gain insight into the mechanism of the photobactericidal activity demonstrated.

REFERENCES

[1] M. J. Salgueiro, M. Zubillaga, A. Lysionek, R. Caro, R. Weill, and J. Boccio. "Fortification strategies to combat zinc and iron deficiency." In: *Nutrition Reviews* 60 (2002), pp. 52–58.

[2] M. Cushen, J. Kerry, M. Morris, M. Cruz-Romero, and E. Cummins. "Nanotechnologies in the food industry - Recent developments, risks and regulation." In: *Trends in Food Science & Technology* 24 (2012), pp. 30–46.

[3] J. Pasquet, Y. Chevalier, E. Couval, D. Bouvier, G. Noizet, C. Morlière, and M.-A. Bolzinger. "Antimicrobial activity of zinc oxide particles on five micro-organisms of the Challenge Tests related to their physicochemical properties." In: *International Journal of Pharmaceutics* 460 (2014), pp. 92–100.

[4] A. Arad, D. Mimouni, D. Ben-Amitai, A. Zeharia, and M. Mimouni. "Efficacy of Topical Application of Eosin Compared with Zinc Oxide Paste and Corticosteroid Cream for Diaper Dermatitis." In: *Dermatology* 199 (1999), pp. 319–322.

[5] S. R. Pinnell, D. Fairhurst, R. Gillies, M. A. Mitchnick, and N. Kollias. "Microfine Zinc Oxide is a Superior Sunscreen Ingredient to Microfine Titanium Dioxide." In: *Dermatologic Surgery* 26 (2000), pp. 309–314.

[6] L. L. Zhang, Y. H. Jiang, Y. L. Ding, M. Povey, and D. York. "Investigation into the antibacterial behaviour of suspensions of ZnO nanoparticles (ZnO nanofluids)." In: *Journal of Nanoparticle Research* 9 (2007), pp. 479–489.

[7] P. Nagarajan and V. Rajagopalan. "Enhanced bioactivity of ZnO nanoparticles - an antimicrobial study." In: *Science and Technology of Advanced Materials* 9 (2008), p. 035004.

[8] E. Hoseinzadeh, M.-Y. Alikhani, M.-R. Samarghandi, and M. Shirzad-Siboni. "Antimicrobial potential of synthesized zinc oxide nanoparticles against gram positive and gram negative bacteria." In: *Desalination and Water Treatment* (2013), pp. 1–8.

[9] A. A. Tayel, W. F. El-Tras, S. Moussa, A. F. El-Baz, H. Mahrous, M. F. Salem, and L. Brimer. "Antibacterial action of zinc oxide nanoparticles against foodborne pathogens." In: *Journal of Food Safety* 31 (2011), pp. 211–218.

[10] K. R. Raghupathi, R. T. Koodali, and A. C. Manna. "Size-Dependent Bacterial Growth Inhibition and Mechanism of Antibacterial Activity of Zinc Oxide Nanoparticles." In: *Langmuir* 27 (2011), pp. 4020–4028.

[11] Y. Liu, L. He, A. Mustapha, H. Li, Z. Q. Hu, and M. Lin. "Antibacterial activities of zinc oxide nanoparticles against Escherichia coli O157:H7." In: *Journal of Applied Microbiology* 107 (2009), pp. 1193–1201.

[12] Y. Xie, Y. He, P. L. Irwin, T. Jin, and X. Shi. "Antibacterial Activity and Mechanism of Action of Zinc Oxide Nanoparticles against Campylobacter jejuni." In: *Applied and Environmental Microbiology* 77 (2011), pp. 2325–2331.

[13] M. Shaffer, C. Williams, K. Orchard, N. Jones, and J. Weiner. *Process for producing nanoparticles*. WO Patent App. PCT/GB2013/051,175. 2013. URL: http://www.google.com/patents/WO2013164650A2?cl=en.

[14] K. L. Orchard, M. S. P. Shaffer, and C. K. Williams. "Organometallic Route to Surface-Modified ZnO Nanoparticles Suitable for In Situ Nanocomposite Synthesis: Bound Carboxylate Stoichiometry Controls Particle Size or Surface Coverage." In: *Chemistry of Materials* 24 (2012), pp. 2443–2448.

[15] N. J. Brown, J. Weiner, K. Hellgardt, M. S. P. Shaffer, and C. K. Williams. "Phosphinate stabilised ZnO and Cu colloidal nanocatalysts for CO2 hydrogenation to methanol." In: *Chemical Communications* 49 (2013), pp. 11074–11076.

[16] H. D. Gillman and J. L. Eichelberger. "Inorganic coordination polymers. XXII. Manganese(II), cobalt(II), nickel(II), copper(II), and zinc(II) bis[bis(N-phenylaminomethyl)phosphinates]. Effects of coordinating side groups." In: *Inorganica Chimica Acta* 24 (1977), pp. 31–34.

[17] V. Crescenzi, V. Giancotti, and A. Ripamonti. "Inorganic Coordination Polymers. Cobalt(II) and Zinc (II) Di-n-butylphosphinates1." In: *Journal of the American Chemical Society* 87 (1965), pp. 391–392.

[18] F. Wang, R. Tang, and W. E. Buhro. "The Trouble with TOPO; Identification of Adventitious Impurities Beneficial to the Growth of Cadmium Selenide Quantum Dots, Rods, and Wires." In: *Nano Letters* 8 (2008), pp. 3521–3524.

[19] S. Noimark, M. Bovis, A. J. MacRobert, A. Correia, E. Allan, M. Wilson, and I. P. Parkin. "Photobactericidal polymers; the incorporation of crystal violet and nanogold into medical grade silicone." In: *RSC Advances* 3 (2013), pp. 18383–18394.

[20] S. Perni, C. Piccirillo, J. Pratten, P. Prokopovich, W. Chrzanowski, I. P. Parkin, and M. Wilson. "The antimicrobial properties of light-activated polymers containing methylene blue and gold nanoparticles." In: *Biomaterials* 30 (2009), pp. 89–93.

[21] S. Perni, C. Piccirillo, A. Kafizas, M. Uppal, J. Pratten, M. Wilson, and I. P. Parkin. "Antibacterial Activity of Light-Activated Silicone Containing Methylene Blue and Gold Nanoparticles of Different Sizes." In: *Journal of Cluster Science* 21 (2010), pp. 427–438.

[22] C. W. Dunnill, K. Page, Z. A. Aiken, S. Noimark, G. Hyett, A. Kafizas, J. Pratten, M. Wilson, and I. P. Parkin. "Nanoparticulate silver coated-titania thin films-Photo-oxidative destruction of stearic acid under different light sources and antimicrobial effects under hospital lighting conditions." In: *Journal of Photochemistry and Photobiology a-Chemistry* 220 (2011), pp. 113–123.

[23] S. Noimark, E. Allan, and I. P. Parkin. "Light-activated antimicrobial surfaces with enhanced efficacy induced by a dark-activated mechanism." In: *Chemical Science* 5 (2014), pp. 2216–2223.

[24] M. G. Schmidt, I. Attaway Hubert H., S. E. Fairey, L. L. Steed, H. T. Michels, and C. D. Salgado. "Copper Continuously Limits the Concentration of Bacteria Resident on Bed Rails within

the Intensive Care Unit." In: *Infection Control and Hospital Epidemiology* 34 (2013), pp. 530–533.

[25] M. G. Schmidt, H. H. Attaway, P. A. Sharpe, J. John Joseph, K. A. Sepkowitz, A. Morgan, S. E. Fairey, S. Singh, L. L. Steed, J. R. Cantey, K. D. Freeman, H. T. Michels, and C. D. Salgado. "Sustained Reduction of Microbial Burden on Common Hospital Surfaces through Introduction of Copper." In: *Journal of Clinical Microbiology* 50 (2012), pp. 2217–2223.

[26] F. Marais, S. Mehtar, and L. Chalkley. "Antimicrobial efficacy of copper touch surfaces in reducing environmental bioburden in a South African community healthcare facility." In: *Journal of Hospital Infection* 74 (2010), pp. 80–82.

[27] G. Hedin, J. Rynback, and B. Lore. "Reduction of bacterial surface contamination in the hospital environment by application of a new product with persistent effect." In: *Journal of Hospital Infection* 75 (2010), pp. 112–115.

[28] J. W. Churchman. "The selective bactericidal action of gentian violet." In: *Journal of Experimental Medicine* 16 (1912), 221–U50.

[29] J. Stilling. "The aniline dyes as antiseptics, and their use in practice." In: *The Lancet* 136 (1890), pp. 965–966.

[30] J. Stilling. "The aniline dyes as antiseptics." In: *The Lancet* 137 (1891), pp. 872–873.

[31] M. Saji, S. Taguchi, K. Uchiyama, E. Osono, N. Hayama, and H. Ohkuni. "Efficacy of gentian violet in the eradication of methicillin-resistant Staphylococcus aureus from skin lesions." In: *Journal of Hospital Infection* 31 (1995), pp. 225–228.

[32] K. Kawamoto, N. Senda, K. Shimada, K. Ito, Y. Hirano, and S. Murai. "Antibacterial Effect of Yellow He-Ne Laser Irradiation with Crystal Violet Solution on Porphyromonas gingivalis: An Evaluation Using Experimental Rat Model Involving Subcutaneous Abscess." In: *Lasers in Medical Science* 15 (2000), pp. 257–262.

[33] J. Bozja, J. Sherrill, S. Michielsen, and I. Stojiljkovic. "Porphyrin-based, light-activated antimicrobial materials." In: *Journal of Polymer Science Part a-Polymer Chemistry* 41 (2003), pp. 2297–2303.

[34] C. W. Dunnill, Z. Ansari, A. Kafizas, S. Perni, D. J. Morgan, M. Wilson, and I. P. Parkin. "Visible light photocatalysts-N-doped Tio_2 by sol-gel, enhanced with surface bound silver nanoparticle islands." In: *Journal of Materials Chemistry* 21 (2011), pp. 11854–11861.

[35] I. A. Hassan, I. P. Parkin, S. P. Nair, and C. J. Carmalt. "Antimicrobial activity of copper and copper(i) oxide thin films deposited via aerosol-assisted CVD." In: *Journal of Materials Chemistry B* 2 (2014), pp. 2855–2860.

[36] C. D. Salgado, K. A. Sepkowitz, J. F. John, J. R. Cantey, H. H. Attaway, K. D. Freeman, P. A. Sharpe, H. T. Michels, and M. G. Schmidt. "Copper Surfaces Reduce the Rate of Healthcare-Acquired Infections in the Intensive Care Unit." In: *Infection Control and Hospital Epidemiology* 34 (2013), pp. 479–486.

[37] A. Nel, T. Xia, L. Madler, and N. Li. "Toxic potential of materials at the nanolevel." In: *Science* 311 (2006), pp. 622–627.

[38] T.-K. Hong, N. Tripathy, H.-J. Son, K.-T. Ha, H.-S. Jeong, and Y.-B. Hahn. "A comprehensive in vitro and in vivo study of ZnO nanoparticles toxicity." In: *Journal of Materials Chemistry B* 1 (2013), pp. 2985–2992.

[39] R. J. Vandebriel and W. H. De Jong. "A review of mammalian toxicity of ZnO nanoparticles." In: *Nanotechnology, Science and Applications* 5 (2012), pp. 61 –71.

[40] K. M. Reddy, K. Feris, J. Bell, D. G. Wingett, C. Hanley, and A. Punnoose. "Selective toxicity of zinc oxide nanoparticles to prokaryotic and eukaryotic systems." In: *Nanotechnology, Science and Applications* 90 (2007).

[41] C. A. M. Association. "New and nonofficial remedies, 1939. Containing descriptions of the articles which stand accepted by the council on Pharmacy and Chemistry of the American Medical Association on January 1, 1939." In: (1939).

[42] W. H. Organization. “The interagency emergency health kit 2006.” In: (2012).

[43] M. Saji, S. Taguchi, K. Uchiyama, E. Osono, N. Hayama, and H. Ohkuni. “Efficacy of gentian violet in the eradication of methicillin-resistant Staphylococcus aureus from skin lesions.” In: *Journal of Hospital Infection* 31 (1995), pp. 225–228.

[44] K. Kawamoto, N. Senda, K. Shimada, K. Ito, Y. Hirano, and S. Murai. “Antibacterial Effect of Yellow He-Ne Laser Irradiation with Crystal Violet Solution on Porphyromonas gingivalis: An Evaluation Using Experimental Rat Model Involving Subcutaneous Abscess.” In: *Lasers in Medical Science* 15 (2000), pp. 257–262.

6

PHOTOEXCITATION OF PHENOTHIAZINE AND TRIARYLMETHANE PHOTOSENSITISER DYES ENCAPSULATED IN MEDICAL GRADE SILICONE

6.1 INTRODUCTION

This thesis has detailed the development of novel photosensitiser and nanoparticle-encapsulated polymers, that exhibit efficacious antimicrobial activity against key pathogens associated with HAIs through a light-activated mechanism. It has also been noted in Chapters 3 and 4, that the photobactericidal activity of photosensitiser dyes is significantly enhanced through interactions between the dye molecule and 2 nm gold nanoparticles. This synergistic enhancement has been observed in polymers incorporated with either methylene blue [1, 2] or crystal violet [3, 4]. It is critical that the photochemistry of these dye- and dye-nanoparticle-encapsulated polymers is explored, to gain an understanding of the photochemical mechanism by which antimicrobial activity is achieved, such that this technology can be refined to develop more potent antimicrobial polymers.

As detailed in the literature and in previous chapters, photobactericidal polymers pose as attractive candidates for use as an infection-control strategy in healthcare environments. These polymers can be synthesised by incorporating photosensitiser dye molecules and nanoparticles into polymers, using a simple dipping approach. Photosensitisers used include methylene blue, toluidine blue O and crystal violet and these dye-incorporated polymers have induced the lethal photosensitisation of both Gram-positive and Gram-negative bacteria, with samples demonstrating strong antimicrobial efficacy under both laser irradiation and also, under standard hospital lighting conditions [1–11]. The utilisation of this photochemical kill approach reduces the risk of bacterial resistance, consequent to the non-site-specific mode of attack. The photosensi-

tiser dyes used in this strategy are cheap and commercially available and the method of incorporation is easy to upscale on an industrial level. Consequently, these novel polymers are ideal candidates for use as antimicrobial surfaces in hospitals, as a means to help decrease the risk of infection.

The polymers demonstrate antimicrobial activity predominantly by a light-activated mechanism: photosensitiser dyes immobilised in the polymers absorb light, resulting in the transition of an electron from the delocalised π orbital in the dye molecule, to a π^* antibonding orbital; an excited singlet state. This electron can then undergo an intersystem crossing, such that the dye molecule is in the slightly lower energy, longer-lived excited triplet state [12, 13]. The triplet state molecule can return to its ground state by undergoing a variety of radiative or radiationless processes, including phosphorescence, intersystem crossing and vibrational relaxation [13].

The triplet state dye molecule can also undergo two categories of photochemical processes, termed a 'Type I' and 'Type II' mechanism. The Type I mechanism involves one-electron redox processes that occur between the excited triplet state dye molecule and any molecule with the appropriate redox potential; in this context, proteins, unsaturated lipids, DNA etc. on the target cell [14]. The Type II mechanism involves an energy transfer process between the excited triplet state dye molecule and molecular oxygen in the vicinity, resulting in the generation of singlet oxygen species [14]. Highly electrophilic, singlet oxygen rapidly reacts with electron-rich substrates such as unsaturated hydrocarbons, amines, sulfides and phenols which are abundant in cell membrane proteins, lipids and in DNA [15–18].

Electronically excited triplet state photosensitiser molecules can undergo both types of photochemical pathways and the efficacy of each mechanism is dependent upon the triplet state energy level, the triplet photosensitiser oxidation-reduction potentials, in addition to the surrounding substrate and oxygen concentrations and their corresponding reaction rates with the excited triplet state dye [14]. Collectively, the two photoprocesses result in the generation of a

wide range of cytotoxic ROS upon photo-excitation, including singlet oxygen and superoxide radicals, which subsequently generate superoxide anions and hydroxyl radicals [12, 14]. It is these generated ROS which initiate a non-site specific attack against bacteria in the vicinity, damaging bacterial intracellular proteins, cellular membranes and DNA, hence reducing the risk of the development of resistance to this antimicrobial strategy [12].

In this chapter, the photochemical properties of these polymers are examined, in order to gain insight into the mechanism of photobactericidal activity demonstrated. Low temperature time-resolved electron paramagnetic resonance (TR-EPR) spectroscopy was used to compare and investigate the properties of the photoexcited triplet states of a series of dye-incorporated polymers. Subsequently, time-resolved near infrared singlet oxygen (TRNIR-$^1O_2$) phosphorescence experiments were carried out (emitted at 1270 nm), to determine whether the photo-excited triplet states undergo a 'Type II' photochemical pathway. These techniques were also used to investigate the photochemical properties of a crystal violet and nanogold-incorporated polymer, to gain an understanding into the enhanced light-activated antimicrobial activity noted when 2 nm gold nanoparticles are present (refer to Chapters 3 and 4).

6.2 EXPERIMENTAL

6.2.1 *Chemicals and Substrates*

The reagents used in materials synthesis were as follows: Methylene blue hydrate (Riedel-de Haën, U.K.), crystal violet (Sigma, U.K.), acridine orange (hemi-acetate zinc salt, Fisher, U.K.), toluidine blue O (Sigma, U.K.), malachite green (oxalate salt, Sigma, U.K.), 2 nm gold nanoparticles (kindly provided by Mr William Peveler) and acetone (VWR, U.K.). In all synthetic work carried out, the water used was deionised (resistivity 15 MΩcm). For the TR-EPR experiments, the substrate was commercially available 100 % silicone Foley catheters: BRILLANT AquaFlate 2 way, 10 cc silicone catheter with an opposed eye, (12 Fr, 4 mm diameter, Rüsch). For the extended TRNIR-$^1O_2$ phosphorescence experiments, the substrate was medical grade flat silicone sheets (NuSil, Polymer Systems Technology Ltd., U.K.).

6.2.2 *Materials Synthesis and Characterisation*

6.2.2.1 *Polymer Synthesis for Singlet Oxygen Measurements*

Liquid MED-4950 (Polymer Systems Technology Ltd) was combined with a crosslinking agent (Polymer Systems Technology Ltd) in a 1:1 ratio and an excess (4 - 5 g) was spread into a channel on a clean glass surface. The system was centrifuged for 5 minutes (1100 rpm, 60 mbar vacuum) and any excess was removed. The polymer was cured at 150 ^oC for 6 minutes after which it was allowed to cool and subsequently, was cut into 1 cm x 3 cm strips.

6.2.2.2 *Polymer Modification*

Methylene blue, toluidine blue O and acridine orange were incorporated into the silicone catheter polymer using a 'swell-encapsulation-shrink technique'. The silicone catheters were immersed in a 9:1 acetone : water swelling solution made up to a concentration of 0.002 moldm^{-3} dye. The samples were allowed to swell in the dark

under room temperature conditions for 24 h, after which they were removed and air-dried in the dark (24 h). Residual dye was removed by gently washing the samples in water and the towel-dried samples were stored under dark conditions.

Crystal violet and malachite green were incorporated into the silicone catheter polymer using a simple dipping process [3]. The silicone samples were immersed in dye solutions (0.002 moldm^{-3}) made up in water for 24 h, after which they were removed and air-dried under dark conditions (24 h). Residual dye was washed off using water and the samples were towel-dried and stored under dark conditions.

6.2.2.3 *Polymer Modification For Extended Photochemical Investigations*

For crystal violet and nanoparticle incorporation into silicone catheter samples or medical grade flat sheets, samples were immersed in a 9:1 acetone : nanogold swelling solution for 72 hours. The samples were subsequently air-dried, washed and towel-dried, after which they were immersed in a crystal violet solution (0.001 moldm^{-3}) for 72 h. Residual dye was washed off using water and the samples were towel-dried and stored under dark conditions.

6.2.2.4 *Materials Characterisation*

A PerkinElmer Lambda 25 UV-Vis Spectrometer was used to measure the UV-Vis absorption spectra of the modified silicone polymers, within the range 400 - 750 nm.

6.2.3 *Photochemical Activity Investigations*

6.2.3.1 *Time-resolved Electron Paramagnetic Resonance Spectroscopy*

A Bruker E580 pulsed EPR spectrometer operating at X-band frequencies (9 - 10 GHz / 0.3 T) was used to record the time-resolved EPR spectra of acridine orange-, crystal violet-, malachite green-, methylene blue- and toluidine blue O- incorporated silicone catheter

samples, under aerobic conditions and in the air-equilibrated solid phase. TR-EPR spectra of crystal violet-coated and crystal violet-coated, 2 nm gold nanoparticle-encapsulated silicone catheter samples were also recorded under the same conditions. A Surelite broadband OPO system within the operating range 410 - 2550 nm, pumped by a Surelite I-20 Q-switched Nd:YAG laser with 2nd and 3rd harmonic generators (20 Hz, pulse length: 5 ns) was used to achieve a pulsed laser excitation at a wavelength within the range of the dye absorption, with the energy at the sample approximately 10 mJ per pulse. An Oxford Instruments CF935O flow cryostat was used to cool the sample using liquid helium and an Oxford Instruments ITC 503 temperature controller was employed to control the temperature (50 K). EPR spectra were simulated using the EasySpin toolbox [19] in MATLAB^{TM}.

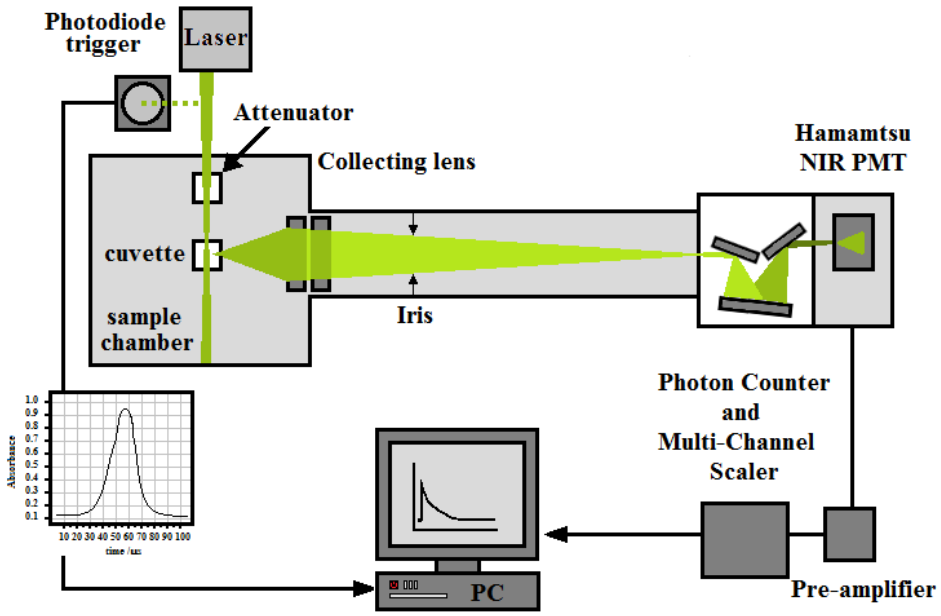

Figure 39: Experimental setup of the luminescence spectroscopy used for the time-resolved detection of near infrared singlet oxygen phosphorescence

6.2.3.2 *Singlet Oxygen Measurements*

The singlet oxygen studies were carried out in the air-equilibrated solid phase and as shown in Figure 39. A thermoelectrically cooled photomultiplier (H10330-45, Hamamatsu Photonic Ltd.) was used for the detection of singlet oxygen at 1270 nm ($^1O_2$ quantum efficiency: 3 %, rise time: 0.5 ns). A range of lenses from the cuvette, in addition to a long-pass and a band-pass filter centred at 1270 nm (Infrared Engineering Ltd.) on the cuvette holder, were used to detect the $^1O_2$ phosphorescence signal. A Nd:YAG laser (Lumanova, GmbH), operating at 532 nm (repetition rate: 3kHz, pulse length: 2ns) was used to irradiate the acridine orange-, crystal violet-, crystal violet and nanogold-, malachite green-, methylene blue- and toluidine blue O- incorporated silicone samples that were placed in a 1 cm square quartz cuvette. A PC-mounted multiscaler board (model MSA-300, Becker-Hickl, Germany) with a pre-amplifier (Becker-Hickl) was used as the photon counting system and provided a resolution of 5 nm/ channel. The time-resolved $^1O_2$ phosphorescence measurements were executed by the multiscalar board (100,000 laser pulses over a 30 s integration time). After the $^1O_2$ phosphorescence of the samples was measured, the data was analysed using the curve fitting tool in MATLAB^{TM}.

6.3 RESULTS AND DISCUSSION

6.3.1 *Material Synthesis and Characterisation*

Commercially available catheters were used for the TR-EPR experiments whereas a laboratory prepared, or commercially available medical grade silicone flat sheets were used for the singlet oxygen measurements. This discrepancy is consequent to the requirements of the different experimental apparatus.

Simple dipping processes were used to incorporate a range of photosensitiser dyes into the silicone substrates. The phenothiazine dyes: methylene blue (MB), toluidine blue O (TBO) and acridine orange (AO) were incorporated into the polymers using a "swell-encapsulation-shrink" technique, in which the polymers were immersed into 90 % acetone dipping solutions. Exposure to the organic solvent causes the polymer to swell, enabling the dye molecules to diffuse through the polymeric matrix. Upon removal from the swelling solution, the residual solvent evaporates and the polymer shrinks back to its previous dimensions, leaving dye molecules trapped within its matrix [1, 2, 6–8]. Conversely, the triarylmethane dyes crystal violet (CV) and malachite green (MG) were incorporated into the polymers using aqueous-based dye solutions due to the high affinity of the dyes for the polymer, such that polymer swelling was unnecessary. These dipping processes facilitated a good polymer uptake of the various dyes (Figure 40). The "swell-encapsulation-shrink" technique resulted in the uniform encapsulation of dye throughout the bulk, whereas the aqueous-based dipping strategy results in polymers with a strong surface dye uptake and minimal dye diffusion through the polymer bulk [3, 4].

A set of samples were also prepared for extended photochemical characterisation experiments, to determine the effects of nanoparticle incorporation on the embedded dye triplet state production and subsequent singlet oxygen yields. A two-step dipping method was used to incorporate crystal violet or, crystal violet and gold nanoparticles into medical grade silicone catheters and flat polymer

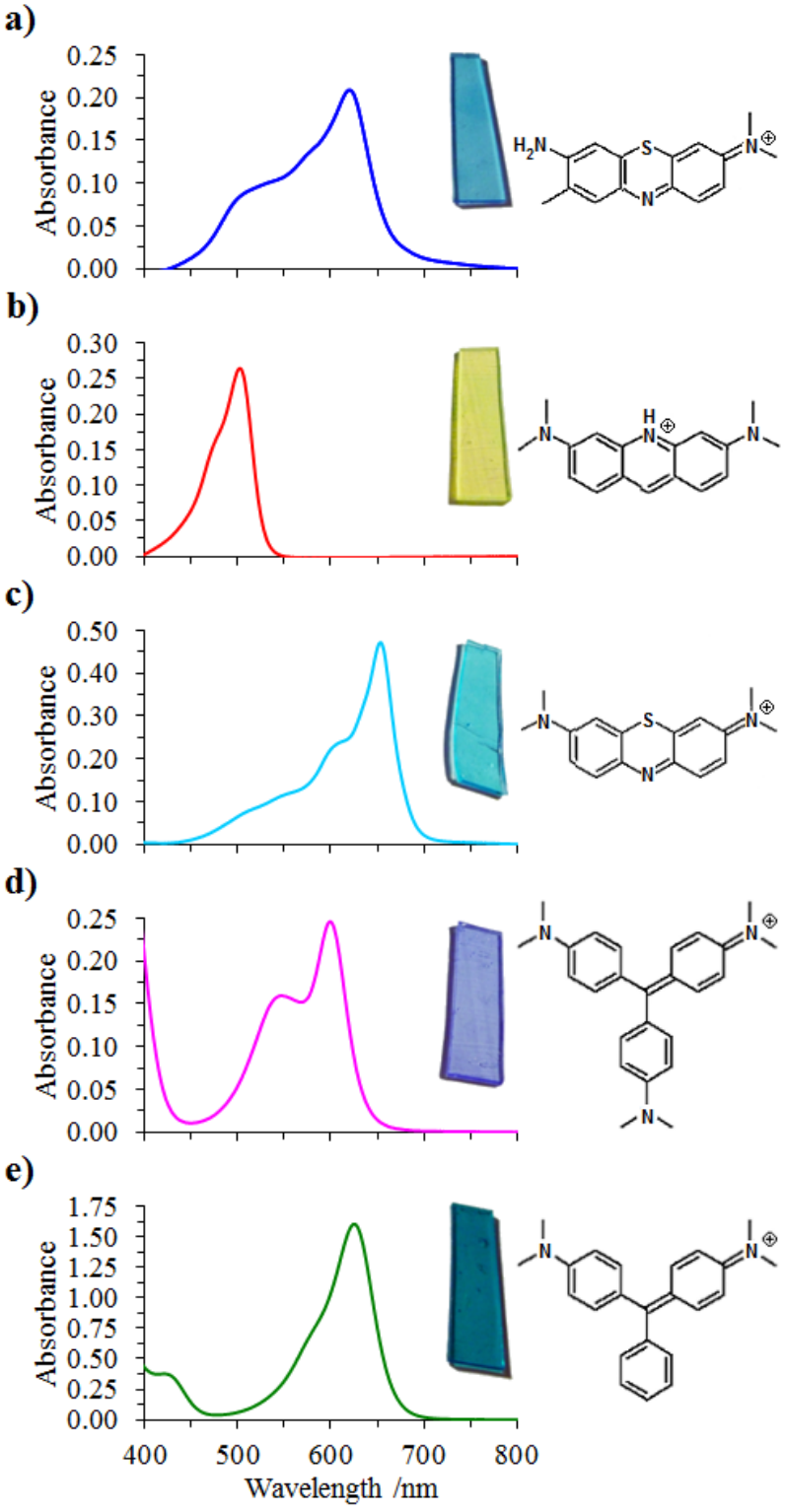

Figure 40: UV-Vis absorbance spectra of silicone incorporated with: (a) toluidine blue O (TBO), (b) acridine orange (AO), (c) methylene blue (MB), (d) crystal violet (CV) and (e) malachite (MG), measured within the range 400 - 750 nm

sheets. Crystal violet-coated samples were pre-treated with a solvent dipping step (9:1 acetone : water solution) to ensure that all samples were exposed to the same dipping treatment, to standardise the incorporation of dye in the subsequent step. Crystal violet and nanoparticle-incorporated samples were prepared by immersion of the polymer into a 9:1 acetone : nanogold swelling solution. The nanoparticle-encapsulated samples were subsequently dipped in a crystal violet solution for dye incorporation. The resultant crystal violet coated-silicone samples were encapsulated with 2 nm gold nanoparticles (CVAu sample).

The UV-Vis absorbance spectra of the dye incorporated silicone polymers, prepared by immersion in dye solutions for 24 h, were measured within the range 400 - 750 nm. All the dye-incorporated silicones demonstrated strong absorption in the visible region of the spectrum (Figure 40), with absorption signals characteristic of the dye molecules. With the exception of the acridine orange-embedded polymer, the dye-encapsulated samples demonstrate strong absorbance bands at longer wavelengths, typically near or in the 'red region' of the spectrum. Toluidine blue O-encapsulated silicone demonstrates a maximum absorbance at 620 nm with shoulder peaks at $\lambda \approx 578$ nm and $\lambda \approx 510$ nm. The UV-Vis absorbance signal of acridine orange-encapsulated silicone exhibits a peak maximum at 502 nm, with a lower wavelength, small shoulder peak at $\lambda \approx 475$ nm; whereas the signal for methylene blue-encapsulated silicone shows a sharp absorbance maximum at $\lambda \approx 653$ nm, with a shoulder peak at ~610 nm. The spectrum also suggests second and third shoulder peaks at ~548 nm and ~509 nm respectively.

The final two spectra are those of the triarylmethane dyes, crystal violet and malachite green. The crystal violet-encapsulated sample demonstrates a strong absorbance at $\lambda \approx 600$ nm, with a sharp shoulder peak at 547 nm. The absorbance spectrum for the malachite green-encapsulated sample shows an intense peak at 625 nm, with a shoulder at 582 nm and overall, this sample absorbs more strongly than the other samples examined. It should be noted that the UV-Vis absorbance spectra of the photosensitiser dyes in solution were

comparable in form to their polymer-embedded analogues, however, across all dyes studies, there was a shift in peak position, which can be attributed to interactions between the dye molecule and its immediate environment.

6.3.2 *Photosensitiser Dye-Encapsulated Silicone*

6.3.2.1 *Time-Resolved Electron Paramagnetic Resonance Spectroscopy of Photosensitiser Dye Encapsulated-Polymers*

Suitable dyes for consideration in the development of photobactericidal polymers should exhibit: i) strong absorption in the visible region of the electromagnetic spectrum, ii) a high intersystem crossing yield for efficient production of the corresponding triplet state and iii) a long triplet lifetime to allow for the reaction with surrounding molecules such as molecular oxygen. Here, low temperature TR-EPR spectroscopy was used to detect paramagnetic species upon photoexcitation of medical grade silicone embedded with either phenothiazine (methylene blue, acridine orange, toluidine blue O) or triarylmethane (crystal violet, malachite green) photosensitiser dyes, under aerobic conditions (see Figure 40 for structures).

TR-EPR allows the determination of the zero-field splitting (ZFS) parameters of the dye triplet state and the values of non-equilibrium populations of the triplet sublevels. The ZFS parameters - *D* and *E* - describe the magnetic dipolar interaction between the two unpaired electrons (Figure 41). These parameters are directly related to the singly occupied molecular orbitals and in turn, correlate to the electron density on the excited state and they depend on the conformation and the protonation state of the dye. The ZFS parameter *D* is a measure of the dipolar spin-spin interaction and it is proportional to the inverse third power of the average distance between the unpaired triplet electrons. Therefore it provides an estimate of the extent of the electron delocalisation in the excited state molecule. The ZFS parameter *E* depends on the deviation of the spin-spin interaction from axial symmetry and it is related to

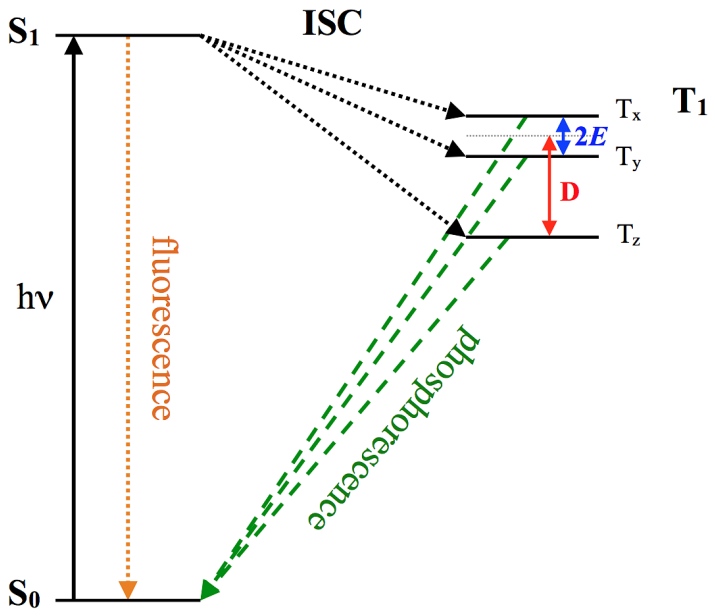

Figure 41: Adapted from Chapter 2, a Jablonski diagram representing processes upon photoexcitation of a photosensitiser dye. The ground state photosensitiser molecule (S_0) absorbs a photon of energy and is promoted to an excited singlet state (S_1). The excited singlet state molecule can undergo various photoprocesses, including the radiative release of energy (fluorescence) or intersystem crossing (ISC) to the excited triplet state (T_1), which is split into three triplet sublevels, T_x, T_y, T_z. The triplet state molecule can release energy as radiation (phosphorescence) or undergo further photoprocesses. Shown also are D and E, the zero field splitting parameters, which describe the magnetic dipolar interaction between the two unpaired electrons

molecular shape and symmetry. Non-equilibrium populations of the spin sublevels characterise the photophysical path leading to the triplet state formation which, in the present case, is the intersystem crossing from the excited singlet state.

The spectra obtained (Figure 42) show that the TR-EPR signals of dyes with analogous molecular structures are comparable in form and typical of spin-polarised (i.e. non-Boltzmann populated) triplet states of aromatic molecules, but they differ in detail and intensity. The spectrum of each of the five samples was simulated using EasySpin software in MATLAB^{TM} to obtain the relative populations of the three triplet sublevels $p_x : p_y : p_z$ and $|D|$ and $|E|$. Note that the modulus is given since the sign of the ZFS parameters cannot be directly derived from the TR-EPR spectra. An isotropic g value equal to the free electron g value ($g_x : g_y : g_z = 2.0023$) was used in the

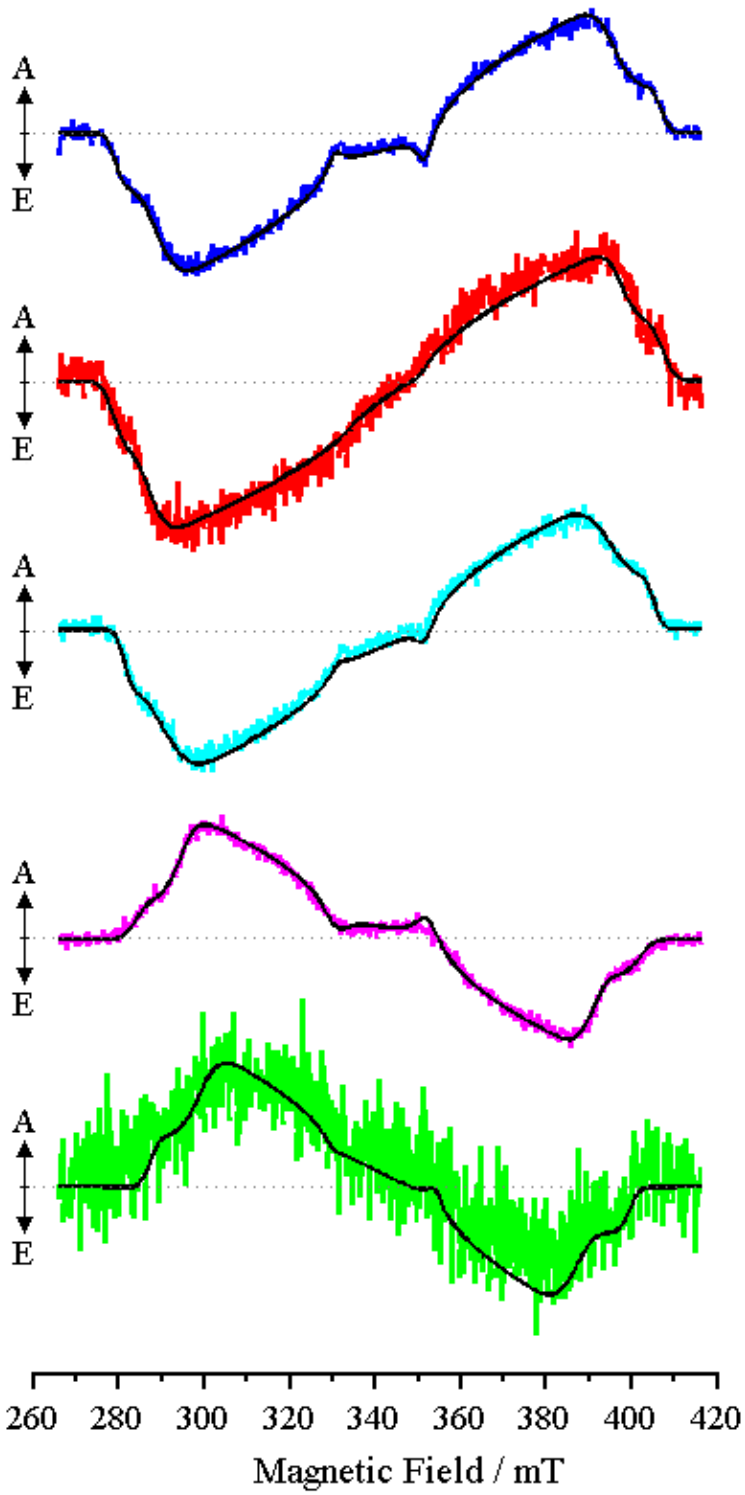

Figure 42: Low temperature TR-EPR spectra of silicone catheters encapsulated with: TBO (blue), AO (red), MB (cyan), CV (fuschia) and MG (green), under aerobic conditions. The simulated spectra are superimposed onto the experimental data (black line). A and E stand for absorption and emission, respectively

simulations.

The triplet states of the phenothiazine dyes and the triarylmethane dyes have similar ZFS parameters (see Table 6). Interestingly, this suggests that in the latter dye group, the spin density is mostly localised over adjacent rings rather than spread over the entire molecule. Moreover, the similarity between the ZFS parameters within members of the same dye group implies that chemical variability has little influence on the distribution of the unpaired triplet electrons within the delocalised system. However, the relative sublevel populations give inverse polarisation patterns for the phenothiazine dyes compared to the triarylmethane dyes (see Table 6). This inversion can be rationalised in two alternative ways: either the change in the molecular geometry - planar as opposed to propeller-like - influences the sign of the ZFS parameters (they have been assumed to be both positive in the simulations), or it changes the population rates without affecting the sign of ZFS parameters.

Inspection of Figure 42 shows that the quality (signal-to-noise ratio, S/N) of the spectra largely varies within both dye groups, despite similarities in triplet sublevel populations (Table 6). This variability can be accounted for as follows: i) some dyes have lowered triplet yield (i.e. intersystem crossing efficiency) or ii) the intersystem crossing process for these dyes is more isotropic, leading to a less polarised spin system. Within the phenothiazine dye group, acridine orange displays the worst S/N and it should be noted that compared to the other two phenothiazine dyes examined, acridine orange is the only dye lacking a sulphur atom in its structure. From quantum mechanical considerations, it is known that 'heavy atoms' significantly enhance the intersystem crossing efficiency. The above mentioned considerations hold for malachite green, which within the triarylmethane dye group, displays the worst S/N. In effect, malachite green lacks a nitrogen atom in its structure compared to crystal violet. Since the signal intensity in TR-EPR spectra depends on differences in triplet sublevel populations and only relative populations can be extracted from spectra simulation, spectra with a similar shape may share relative sublevel population differences, whilst the net

	TR-EPR Parameters		TRNIR-$^1O_2$ Phosphorescence Signal Analysis		
	Relative Populations $[p_x : p_y : p_z]$	ZFS Parameters $\lvert D\rvert, \lvert E\rvert$ (MHz)	τ_1 (µs)	τ_2 (µs)	Φ_Δ Normalised
TBO	0.81 : 0.19 : 0	1790, 400	49.08 ± 0.03	2.28 ± 0.02	1.00
AO	0.68 : 0.32 : 0	1800, 430	49.52 ± 0.07	1.80 ± 0.09	0.85
MB	0.76 : 0.24 : 0	1738, 390	49.59 ± 0.08	1.69 ± 0.04	0.56
CV	0 : 0.46 : 0.54	1650, 350	40.00 ± 0.12	0.78 ± 0.15	0.10
MG	0 : 0.40 : 0.60	1570, 300	-	-	0.01

Table 6: TR-EPR parameters and TRNIR-$^1O_2$ phosphorescence analysis (1270 nm)

polarisation (absolute populations) can be different. Therefore, it is difficult to assess whether a more isotropic intersystem crossing process is responsible for the observed S/N in acridine orange and malachite green.

6.3.2.2 *Singlet Oxygen Measurements*

Illumination of the dye incorporated polymers effects interesting photochemical consequences. As confirmed using low temperature TR-EPR spectroscopy, laser excitation results in the promotion of the polymer-embedded dye molecule to an excited triplet state. One photochemical pathway that the triplet state dye molecule undergoes is a 'Type II' photoprocess, whereby molecular oxygen in the vicinity collides with the immobilised triplet state molecule. Energy transfer occurs between the triplet excited state of the encapsulated dye and an O_2 molecule, relaxing the dye molecule to its ground state and concurrently generating singlet oxygen species ($^1O_2$). The reaction is feasible since O_2 has a triplet ground state, with low-lying excited states and thus, low energy (22 kcal mol^{-1}) is needed to produce the highly oxidative species, singlet oxygen [13]. A minor proportion of these $^1O_2$ molecules decay by emission of a photon at 1270 nm and this $^1O_2$ phosphorescence can be used to gain information about the kinetics of $^1O_2$ production and decay [15].

To establish whether the dye-embedded silicone samples examined in this study undergo a 'Type II' photoprocess, the samples were excited at 532 nm and the production of $^1O_2$ was measured through the time-resolved detection of near infrared $^1O_2$ phosphorescence, emitted at 1270 nm. Equation 2 can be used to describe the key factors that determine the concentration of singlet oxygen concentration, $[O_2(a^1\Delta_g)]$ [15]:

$$[O_2(a^1\Delta_g)]_t = [^3sens^*]_0 \frac{k_\Delta^{O_2}\,[^3O_2]}{k_d^T + k_q^{O_2}\,[^3O_2]} \frac{\tau_\Delta}{\tau_T - \tau_\Delta} (e^{-t/\tau_T} - e^{-t/\tau_\Delta}) \quad (2)$$

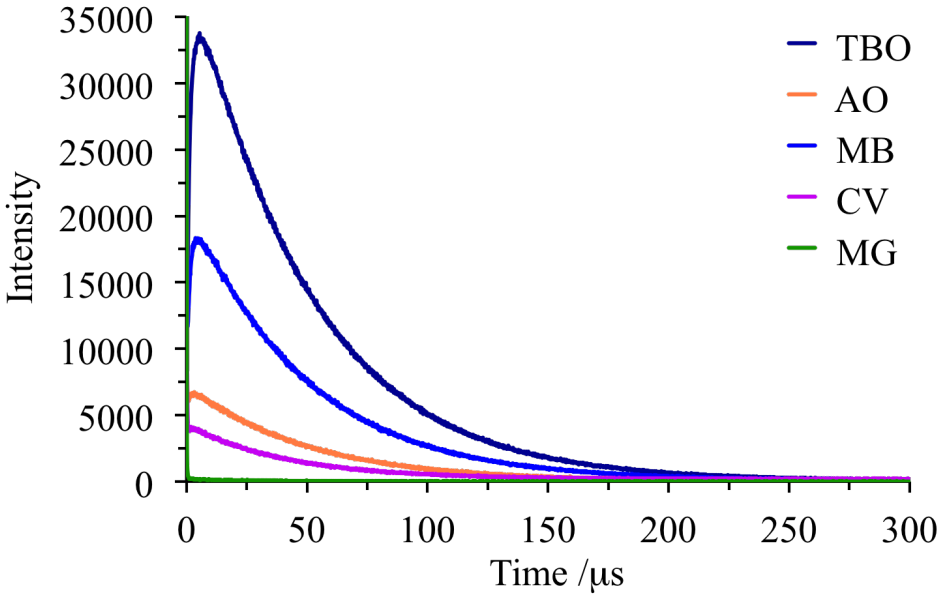

Figure 43: The time-resolved near infrared phosphorescence of the singlet oxygen, emitted at 1270 nm, of photosensitiser dyes embedded in a silicone polymer. TBO (black line), MB (blue line), CV (purple line), AO (orange line) and MG (green line)

Where $k_{\Delta}^{O_2}$ is the rate constant of energy transfer between the excited triplet state of the photosensitiser and molecular oxygen, k_d^T is the rate constant of the photosensitiser's triplet state decay by oxygen-independent processes, $k_q^{O_2}$ is the rate constant for the photosensitiser's triplet state decay by quenching with molecular oxygen, τ_T is the photosensitiser triplet state lifetime and τ_Δ is the O_2 ($a^1\Delta_g$) lifetime [15].

As dictated by Equation 2 and shown in Figure 43, [O_2 ($a^1\Delta_g$)] is zero at time t = 0, after which the signal grows to a maximum, correlating to a steep rise in $^1O_2$ production upon laser excitation of the silicone encapsulated dye, preceding a more gentle decay. $^1O_2$ is a transient species; it rapidly reacts with other molecules and this results in a decrease in the $^1O_2$ signal as a function of time. Analysis of the data demonstrates that the $^1O_2$ signal detected can be broken down into two main components with lifetimes τ_1 and τ_2. Using equation 2, it can be suggested that τ_1 corresponds to collisional quenching of $^1O_2$ with other species such as the polymer matrix (τ_Δ), whereas the latter component with a shorter lifetime, τ_2, correlates to the $^1O_2$ rise time, which is proportional to the decay of the dye triplet state and mainly

determined by quenching by molecular oxygen (τ_T). The calculated lifetimes, τ_1 and τ_2 are similar across the samples investigated, although both τ_1 and τ_2 are comparatively shorter for the crystal violet sample (Table 6). It should also be noted that in contrast to crystal violet samples, Table 6 shows comparable τ_2 for the samples where the dye is embedded, suggesting the $^1O_2$ quenching mechanism may be similar i.e. quenching within the polymeric matrix.

The TRNIR-$^1O_2$ measurements also provide information on the relative $^1O_2$ production of the dye-incorporated polymers under air-equilibrated solid phase conditions. Using the integrated signal for the time-resolved detection of near infrared $^1O_2$ phosphorescence, in addition to the UV-Vis absorbance data, the relative singlet oxygen quantum yields were calculated using equation 3:

$$I = \kappa \text{ x } P \text{ x } \Phi_\Delta \text{ x } (1 - 10^{-A}) \tag{3}$$

Where I is the time-integrated $^1O_2$ phosphorescence peak intensity, κ and P are constants that have been equated to '1', Φ_Δ is the $^1O_2$ quantum yield and A is the UV-Vis absorbance peak intensity. The calculated Φ_Δ indicated that the photosensitiser dye toluidine blue O, generates the greatest number of $^1O_2$ molecules per photon absorbed by the photosensitiser molecule. The calculated Φ_Δ were normalised against this value and it was found that:

$$\Phi_{\Delta TBO} > \Phi_{\Delta AO} > \Phi_{\Delta MB} > \Phi_{\Delta CV} > \Phi_{\Delta MG}$$

The TRNIR-$^1O_2$ phosphorescence experiments enable us to gain key information about the photoprocesses upon laser excitation, in addition to consolidating findings obtained through TR-EPR measurements. Overall, these findings are in strong agreement with observations attained through low temperature TR-EPR measurements. In particular, the TRNIR-$^1O_2$ phosphorescence measurements indicate that the photo-excited malachite green sample $^1O_2$ yields

are negligible. This finding is analogous to that determined from the TR-EPR measurements, which show poor malachite green triplet state S/N. Note that the UV-Vis absorbance signal of the malachite green sample was at least 3x greater than that observed for the other dyes investigated. TRNIR-$^1O_2$ phosphorescence measurements of a range of samples of varying malachite green concentration, indicated that the poor $^1O_2$ yield noted was not a concentration effect, potentially attributable to dimerisation of the embedded dye, since all malachite green-embedded samples examined - synthesised by varying the polymer exposure time to the malachite green dipping solution - exhibited negligible $^1O_2$ yields.

One discrepancy however, is the unusually high calculated acridine orange $^1O_2$ quantum yield, which is in contrast to the poor TR-EPR signal obtained for the same sample. It can be hypothesised that the high $^1O_2$ yield is related to better energy coupling with molecular oxygen orbitals, resulting in efficient $^1O_2$ production upon photo-excitation, despite poor triplet state yields. It should be noted that as shown in Figure 40, the acridine orange first excited singlet state has the highest energy among the considered molecules. Alternatively, it can be suggested that the poor TR-EPR acridine orange triplet signal can be attributed to small population differences between the triplet sub-levels, rather than reflect on the triplet state generation upon photo-excitation.

TRNIR-$^1O_2$ phosphorescence measurements for the phenothiazine and triarylmethane photosensitiser dyes in solution, showed a differing trend in $^1O_2$ quantum yields compared to polymer-embedded dyes:

$$\Phi_{\Delta TBO} > \Phi_{\Delta MB} > \Phi_{\Delta AO} > \Phi_{\Delta MG} \approx \Phi_{\Delta CV}$$

Here, acridine orange shows a poor $^1O_2$ quantum yield relative to that found in the polymer investigation. It can be hypothesised that when free in solution, triplet state deactivation pathways such as vibrational relaxation, or collisional quenching by other substrate molecules may become favourable, resulting in a more limited

$^1O_2$ generation. Alternatively, although not explored within the constraints of this investigation, it should also be noted that the dye triplet state generation in solution phase may not be comparable to that in solid phase. In solution, interactions between dye molecules may occur, for example, π-stacking effects and dimerisation, that may hinder triplet state production and subsequently lead to reduced $^1O_2$ quantum yields. Moreover, upon photo-excitation, rotor molecules such as crystal violet can form twisted intramolecular charge transfer (TICT) states, rather than undergo intersystem crossing into the triplet state [20], resulting in negligible observed $^1O_2$ yields (Φ_Δ(CV) normalised = 0). However, as noted earlier, polymer-encapsulation of crystal violet results in comparatively enhanced $^1O_2$ yields and this can be attributed to the viscosity dependent behaviour of the formation of TICT states [20].

Overall, the TR-EPR studies and TRNIR-$^1O_2$ phosphorescence measurements indicate that photosensitiser dyes such as toluidine blue O or methylene blue are ideal candidates for light-activated antimicrobial agents, as they yield efficient triplet-state production and $^1O_2$ generation. However, one drawback associated with the use of these dyes is as follows. As noted in Chapter 3, the diffusion distance of $^1O_2$ is very short (< 1 micron). Since the phenothiazine dye-polymer incorporation strategy results in the uniform dispersion of dye through the polymer bulk, rather than a controlled surface dye uptake - unlike in the case of crystal violet - the relative surface dye concentration is low. Subsequently, it can be suggested that the photo-generation of ROS at the polymer surface is limited compared to crystal violet-encapsulated samples, where the ROS is generated predominantly at the sample surface. This may provide insight as to why despite poor $^1O_2$ quantum yields upon photo-excitation, crystal violet samples result in enhanced bacterial kills compared to methylene blue samples in microbiological testing.

6.3.3 *Photosensitiser Dye and Gold Nanoparticle-Encapsulated Silicone*

6.3.3.1 *Time-Resolved Electron Paramagnetic Resonance Spectroscopy of Photosensitiser Dye and Nanoparticle Encapsulated-Polymers*

Potent photobactericidal surfaces have been developed by incorporating photosensitiser dyes into medical grade polymers [6, 8]. Microbiological testing observations indicate that this light-activated antimicrobial activity can be further enhanced by the additional incorporation of 2 nm gold nanoparticles. The resultant dye-nanoparticle-incorporated surfaces achieve the lethal photosensitisation of bacteria under both laser and white light illumination conditions, reducing bacterial numbers to below the detection limit [1–4]. Using TR-EPR as a tool to investigate the mechanism of photochemical activity, it was established that the incorporation of 2 nm gold nanoparticles into methylene blue-encapsulated PVC catheters, resulted in a 38 % increase in the dye triplet state production [7]. Here, TR-EPR spectroscopy was used to detect photo-generated paramagnetic species present in CV- and CVAu-encapsulated silicone catheters following laser excitation (~590 nm) and determine whether a similar enhancement in triplet state production is observed for this dye. Both samples were prepared using a standardised protocol, to ensure there were no differences in crystal violet concentration.

TR-EPR spectra recorded under aerobic conditions of CV- and CVAu-encapsulated silicone catheters at 50 K, showed signals typical of spin-polarised triplet states of aromatic molecules, comparable in detail (Figure 44(a)), but differing in intensity (Figure 44(b)). The spectra of both samples were simulated using an isotropic g value equal to the free electron g value ($g_x : g_y : g_z$ = 2.00232), ZFS parameters $|D|$ = 1650 MHz and $|E|$ = 350 MHz and relative populations $p_x : p_y : p_z$ = 0 : 0.46 : 0.54, indicating that the triplet states are localised on the same species, crystal violet. Note that despite differences in crystal violet concentrations in the two TR-EPR studies, the parameters used to simulate the CV- and CVAu-encapsulated catheters were as reported in Table 6 (Section 6.3.2.1).

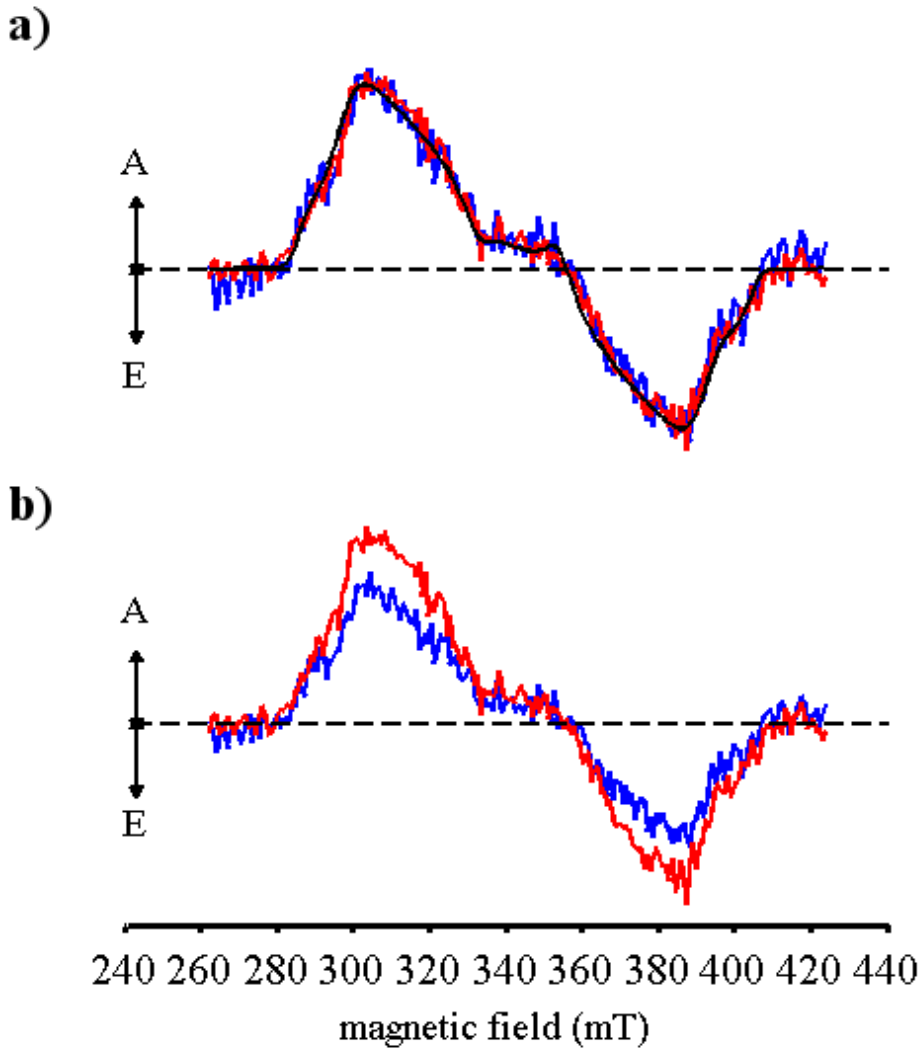

Figure 44: Low temperature TR-EPR spectra of CV (blue) and CVAu (red) encapsulated silicone catheters showing: (a) peaks aligned with simulated spectra superimposed onto the experimental data (black line) and (b) scales aligned for a direct comparison of signal intensity. A and E stand for absorption and emission, respectively

Despite no change in the ZFS parameters or relative populations of the triplet state sublevels - suggesting that electronic structure of the triplet state was unchanged - the presence of 2 nm gold nanoparticles resulted in a significant increase in intensity of the crystal violet triplet state signal (40 %). This triplet state enhancement, attributed to the presence of 2 nm gold nanoparticles, is comparable to that

reported previously for methylene blue and nanogold-encapsulated PVC catheters [7] and indicates that this effect is not observed for phenothiazine dyes only.

6.3.3.2 *Singlet Oxygen Measurements - Crystal Violet and Crystal Violet and Gold Nanoparticle-Incorporated Silicone*

To determine whether the increased dye triplet state production, correlates to enhanced $^1O_2$ yields, TRNIR-$^1O_2$ phosphorescence measurements of CV- and CVAu-encapsulated silicone were recorded under air-equilibrated solid phase conditions (Figure 45). Results indicated that the presence of 2 nm gold nanoparticles increased the $^1O_2$ quantum yield of crystal violet samples (Φ_Δ(CV) = 0.83, when normalised against Φ_Δ(CVAu)), although both τ_1 (42.79 and 43.65) and τ_2 (1.41 and 1.99) are similar for the CV- and CVAu- silicone samples.

The TR-EPR studies and TRNIR-$^1O_2$ phosphorescence measurements corroborate findings from microbiological testing that indicate that the 2 nm gold nanoparticles effects a synergistic enhancement on the

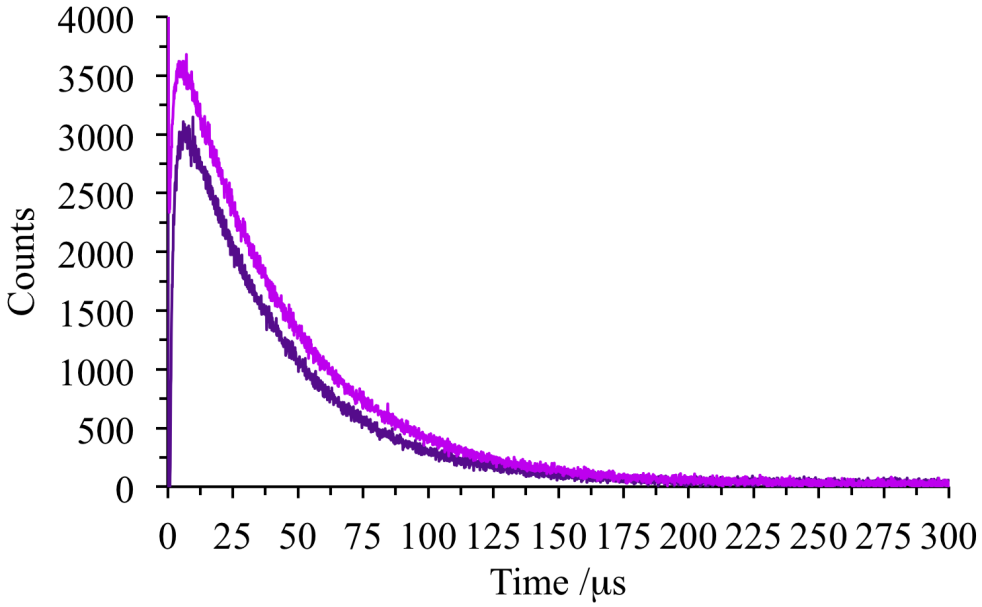

Figure 45: The time-resolved near infrared phosphorescence of the singlet oxygen, emitted at 1270 nm of CV (dark purple line) and CVAu (violet line) encapsulated silicone polymer

photochemical activity of the photosensitiser dye, crystal violet. These studies demonstrate that the observed increased triplet state production correlates to a greater concentration of the photo-generated ROS $^1O_2$, ultimately achieving the observed enhanced bacterial kills, compared to dye only-encapsulated polymers [3, 4].

It should also be noted that the increased photochemical activity of the dye, associated with interactions between the dye and gold nanoparticles, has further implications. It can be rationalised that increased dye triplet state production in the presence of gold nanoparticles means that lower concentrations of dye can be used to achieve the significant lethal photosensitisation of bacteria, compared to dye-only embedded silicones. This may be beneficial in medical device applications where concerns may arise regarding toxicity of high concentrations of dye present on the device surface in contact with patient epithelial cells.

6.4 CONCLUSION

TR-EPR and TRNIR-$^1O_2$ phosphorescence studies provided insight into the underpinning photochemical mechanism of dye- and dye-nanogold encapsulated silicone polymers. The latter demonstrated that with the exception of malachite green, which overall exhibits poor photochemical activity, the triplet states of a range of phenothiazine and triarylmethane dyes are deactivated by a Type II photochemical pathway, resulting in the generation of the highly reactive species, $^1O_2$.

The photochemical characterisation also shed light onto the underlying photophysical mechanism effecting an enhancement in bacterial kills upon light-activation, as observed in the microbiological testing. The spectroscopic techniques demonstrated that crystal violet-gold nanoparticle interactions result in signficant enhancements in dye triplet state production and subsequently, greater $^1O_2$ yields. The findings confirm that the additional incorporation of 2 nm gold nanoparticles aids and increases the efficacy of the lethal photo-

sensitisation of bacteria induced by the dye embedded in the polymer.

Using this knowledge, more effective photobactericidal polymers can be developed with light-activated antimicrobial functionality. The modification process can be manipulated to incorporate antimicrobial agents that achieve bacterial kills via multiple mechanisms, potentially targeting both Type I and Type II triplet state deactivation pathways, such that greater kills can be achieved by the photogeneration of a wide range of ROS. These design tactics will result in the development of polymers with enhanced rates of bactericidal activity. Optimisation by the current empirical approach is not effective as a long-term strategy and a mechanistic understanding is critical to underpin future advances in the development of bactericidal surfaces for use in healthcare technologies. Moreover, the strategic design of nanoparticles such that the modified surfaces exhibit additional antimicrobial functionality under dark conditions is also key, in the development of more potent antimicrobial surfaces for healthcare environments and this will be explored further in the next chapter.

REFERENCES

[1] S. Perni, C. Piccirillo, J. Pratten, P. Prokopovich, W. Chrzanowski, I. P. Parkin, and M. Wilson. "The antimicrobial properties of light-activated polymers containing methylene blue and gold nanoparticles." In: *Biomaterials* 30 (2009), pp. 89–93.

[2] S. Perni, C. Piccirillo, A. Kafizas, M. Uppal, J. Pratten, M. Wilson, and I. P. Parkin. "Antibacterial Activity of Light-Activated Silicone Containing Methylene Blue and Gold Nanoparticles of Different Sizes." In: *Journal of Cluster Science* 21 (2010), pp. 427–438.

[3] S. Noimark, M. Bovis, A. J. MacRobert, A. Correia, E. Allan, M. Wilson, and I. P. Parkin. "Photobactericidal polymers; the incorporation of crystal violet and nanogold into medical grade silicone." In: *RSC Advances* 3 (2013), pp. 18383–18394.

[4] S. Noimark, E. Allan, and I. P. Parkin. "Light-activated antimicrobial surfaces with enhanced efficacy induced by a dark-activated mechanism." In: *Chemical Science* 5 (2014), pp. 2216–2223.

[5] S. Perni, P. Prokopovich, I. P. Parkin, M. Wilson, and J. Pratten. "Prevention of biofilm accumulation on a light-activated antimicrobial catheter material." In: *Journal of Materials Chemistry* 20 (2010), pp. 8668–8673.

[6] S. Perni, P. Prokopovich, C. Piccirillo, J. Pratten, I. P. Parkin, and M. Wilson. "Toluidine blue-containing polymers exhibit potent bactericidal activity when irradiated with red laser light." In: *Journal of Materials Chemistry* 19 (2009), pp. 2715–2723.

[7] S. Noimark, C. W. Dunnill, C. W. M. Kay, S. Perni, P. Prokopovich, S. Ismail, M. Wilson, and I. P. Parkin. "Incorporation of methylene blue and nanogold into polyvinyl chloride catheters; a new approach for light-activated disinfection of

surfaces." In: *Journal of Materials Chemistry* 22 (2012), pp. 15388–15396.

[8] S. Perni, J. Pratten, M. Wilson, C. Piccirillo, I. P. Parkin, and P. Prokopovich. "Antimicrobial Properties of Light-activated Polyurethane Containing Indocyanine Green." In: *Journal of Biomaterials Applications* 25 (2011), pp. 387–400.

[9] A. J. T. Naik, S. Ismail, C. Kay, M. Wilson, and I. P. Parkin. "Antimicrobial activity of polyurethane embedded with methylene blue, toluidene blue and gold nanoparticles against Staphylococcus aureus; illuminated with white light." In: *Materials Chemistry and Physics* 129 (2011), pp. 446–450.

[10] C. Piccirillo, S. Perni, J. Gil-Thomas, P. Prokopovich, M. Wilson, J. Pratten, and I. P. Parkin. "Antimicrobial activity of methylene blue and toluidine blue O covalently bound to a modified silicone polymer surface." In: *Journal of Materials Chemistry* 19 (2009), pp. 6167–6171.

[11] S. Ismail, S. Perni, J. Pratten, I. Parkin, and M. Wilson. "Efficacy of a Novel Light-Activated Antimicrobial Coating for Disinfecting Hospital Surfaces." In: *Infection Control and Hospital Epidemiology* 32 (2011), pp. 1130–1132.

[12] S. Noimark, C. W. Dunnill, and I. P. Parkin. "Shining light on materials - A self-sterilising revolution." In: *Advanced Drug Delivery Reviews* 65 (2013), pp. 570–580.

[13] I. J. MacDonald and T. J. Dougherty. "Basic principles of photodynamic therapy." In: *Journal of Porphyrins and Phthalocyanines* 5 (2001), pp. 105–129.

[14] C. S. Oliveira, R. Turchiello, A. J. Kowaltowski, G. L. Indig, and M. S. Baptista. "Major determinants of photoinduced cell death: Subcellular localization versus photosensitization efficiency." In: *Free Radical Biology and Medicine* 51 (2011), pp. 824–833.

[15] A. Jimenez-Banzo, X. Ragas, P. Kapusta, and S. Nonell. "Time-resolved methods in biophysics. 7. Photon counting vs. analog time-resolved singlet oxygen phosphorescence detection." In: *Photochemical & Photobiological Sciences* 7 (2008), pp. 1003–1010.

[16] A. Michaeli and J. Feitelson. "Reactivity of singlet oxygen toward amino-acids and peptides." In: *Photochemistry and Photobiology* 59 (1994), pp. 284–289.

[17] J. L. Ravanat, P. Di Mascio, G. R. Martinez, M. H. G. Medeiros, and J. Cadet. "Singlet oxygen induces oxidation of cellular DNA." In: *Journal of Biological Chemistry* 275 (2000), pp. 40601–40604.

[18] X. S. Zhang, B. S. Rosenstein, Y. Wang, M. Lebwohl, and H. C. Wei. "Identification of possible reactive oxygen species involved in ultraviolet radiation-induced oxidative DNA damage." In: *Free Radical Biology and Medicine* 23 (1997), pp. 980–985.

[19] S. Stoll and A. Schweiger. "EasySpin, a comprehensive software package for spectral simulation and analysis in EPR." In: *J. Magn. Reson.* 178 (2006), pp. 42–55.

[20] M. A. Haidekker and E. A. Theodorakis. "Environment-sensitive behavior of fluorescent molecular rotors." In: *Journal of Biological Engineering* 4 (2010).

7

UV-LIGHT-ACTIVATED ANTIMICROBIAL POLYMERS: FUNCTIONALISED GOLD-TITANIA AND TITANIA NANOPARTICLE-ENCAPSULATED SILICONE

7.1 INTRODUCTION

The development of light-activated antimicrobial polymers for use in healthcare applications to decrease the incidence of HAIs, has been examined in this thesis. These photobactericidal polymers, synthesised through the incorporation of photosensitiser dyes and nanoparticles into medical grade silicone, have been developed for both medical device applications (Chapter 3, laser light-activation) and hospital touch surface applications (Chapters 4 and 5, white light-activation) and the mechanism of light-activated antimicrobial activity has been examined using spectroscopic techniques (Chapter 6). This chapter focuses on the development of versatile antimicrobial surfaces that achieve rapid kills under both dark and UVA illumination conditions, for both medical device and hospital touch surface applications.

Photosensitiser dye-nanoparticle antimicrobial technology has demonstrated great potential, for use in antimicrobial surfaces in both medical devices [1–6] and hospital touch surface applications [7–11]. Although these surfaces rapidly kill both Gram-positive and Gram-negative bacteria under laser-activation conditions, upon white light-activation, similar kills are achieved over far longer time periods (Chapters 3 - 5). One drawback associated with the use of these surfaces is that it is difficult to achieve rapid kills over large areas; laser technology is not practical for use in the sterilisation of large touch surfaces commonly found in hospital environments. This chapter details the development of potent antimicrobial surfaces incorporated with oleic acid-functionalised titania and gold-doped titania nanoparticles, that achieve rapid bacterial kills in both UVA

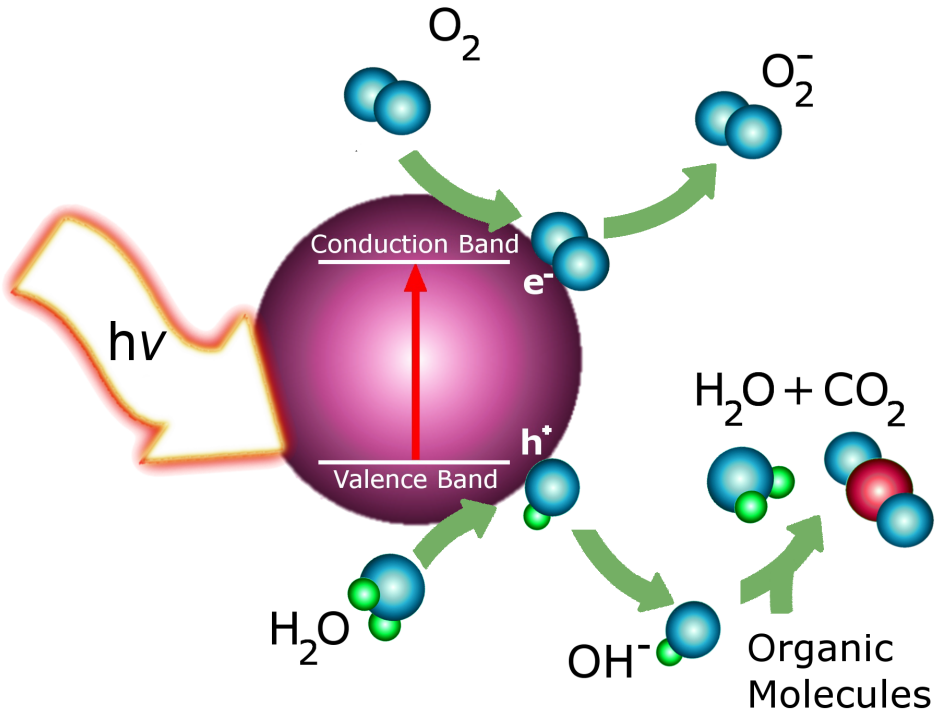

Figure 46: Schematic of the mechanism of the photocatalytic properties of TiO_2 adapted from [12]

illuminated and dark conditions. In cases where devices are frequently used and rapid surface sterilisation is preferable, polymers incorporated with UV-activated photocatalytic nanoparticles may prove more suitable.

Titania, TiO_2, is inexpensive, robust and is widely used in range of applications including: as a white pigment, in cosmetics and sunscreen and as a 'builder' in vitamin tablets [13]. It is also an efficient photocatalyst under UV irradiation conditions [13, 14] and this well established property has been exploited in the development of self-cleaning windows and for drinking water sterilisation [12, 15–18]. Due to its wide band gap (3.2 eV for anatase TiO_2), in order to activate its photocatalytic properties, < 385 nm irradiation is required. A schematic of the photocatalytic properties of TiO_2 is shown in Figure 46 and is detailed as follows: Upon absorption of photons of energy greater than the band gap energy, a valence band electron is promoted to the semiconductor conduction band producing electron-hole pairs [13, 14]. These electron-hole pairs can

interact with adsorbed water and molecular oxygen at the surface of TiO_2, forming highly reactive radical species such as $HO_2^{\cdot}$, HO_2^{-}, $OH^{\cdot}$ and superoxide anions [14, 19]. The photo-generated radicals subsequently participate in redox reactions for the degradation of organic pollutants and the killing of bacteria and viruses [20–23]. Similar to other light-activated antimicrobial agents, for example photosensitiser dyes, the species photogenerated on the TiO_2 surface have an active role in the destruction of bacterial cell outer membranes, resulting in leakage of cell minerals, proteins and genetic material, ultimately leading to cell death [22–26].

The modification of TiO_2 with gold nanoparticles, Au/TiO_2 systems, has been widely studied for environmental applications, for example water splitting [27] and the degradation of organic dye pollutants [28–30]. It has been proposed previously for similar systems that the presence of gold results in improved charge separation and combined with plasmon induced properties, these Au/TiO_2 systems are potentially efficient as visible-active photocatalysts [31–33]. However, there has been little research into the development of Au/TiO_2 materials for antimicrobial surface applications. In one laboratory investigation, gold-capped TiO_2 nanoparticle solutions synthesised using a sol-gel route exhibited an enhanced antimicrobial activity compared to TiO_2 nanoparticle solutions under room lighting conditions, achieving the photo-destruction of Gram-negative bacteria at a slighly lower nanoparticle concentration (*E. coli*) [34]. Conversely, conflicting observations have been noted when Au/TiO_2 systems have been tested against Gram-positive bacteria, although these experiments were carried out using different irradiation conditions [34, 35]. Fu *et al* [34] reported similar inhibition rates in the growth of *Bacillus megaterium* for both TiO_2 nanoparticle and Au/TiO_2 nanoparticle systems, whereas in the case of the latter, under UVA-irradiation it was observed that the antimicrobial activity of the Au/TiO_2 nanoparticle system was reduced compared to that of the pure TiO_2, in the killing of *Bacillus subtilis* [35].

This chapter details the development of novel UV-activated photobactericidal polymers, prepared by using a "swell-encapsulation-shrink"

strategy to incorporate TiO_2 and Au/TiO_2 nanoparticles into commercially available medical grade silicone. Raman, XRD, XPS and TEM were used to characterise the TiO_2 and Au/TiO_2 nanoparticles and the relative photocatalytic activity of these nanoparticles was compared by investigating their efficacy in the photo-destruction of stearic acid, upon exposure to UV-irradiation. Using a UVA source (365 nm) to activate the photobactericidal properties of the materials, the antimicrobial activity of TiO_2 nanoparticle- and Au/TiO_2 nanoparticle-encapsulated silicone polymers was tested against *S. aureus* and *E. coli*, representative Gram-positive and Gram-negative bacteria commonly found in hospital environments. Unprecedented kills were achieved when these surfaces were tested against *S. aureus*, with bacterial numbers reduced by at least 3 log within 15 minutes, under dark conditions. Although only a limited 'dark kill' effect was observed when these samples were tested against *E. coli*, UVA illumination for 95 minutes reduced bacterial numbers to below the detection limit. To our knowledge, this is the first report of bacterial kill under dark conditions from a titanium dioxide modified silicone polymer and this demonstrated antimicrobial activity can be attributed to the surface functionalisation of the nanoparticles used.

7.2 EXPERIMENTAL

7.2.1 *Chemicals and Substrates*

The reagents used in materials synthesis were as follows: Toluene (Fisher Scientific, U.K.), titanium (IV) oxysulfate (Sigma-Aldrich, U.K.), free hydrated sulphuric acid (Aldrich, U.K.), potassium hydroxide (Fisher Scientific, U.K.), chloroauric acid (Alfa Aesar, U.K.), oleic acid (Aldrich, U.K.) and triethylamine (Sigma-Aldrich, U.K.). Unless otherwise specified, in all synthetic work carried out, the water used was deionised (resistivity 15 MΩcm) and the substrate was medical grade flat silicone sheets (NuSil, Polymer Systems Technology Ltd., U.K.).

7.2.2 *Materials Synthesis*

7.2.2.1 *Synthesis of TiO_2 nanoparticles*

TiO_2 nanoparticles were kindly provided by Professor Jawwad Darr and produced using a continuous hydrothermal flow synthesis (CHFS) route. The pilot scale CHFS system used is as detailed in the literature [36, 37]. The precursors were carried into a confined jet reactor under controlled-flow conditions, by four industrial diaphragm type chemical dosing pumps (Milton Roy, Primeroyal K). In the reactor, the precursors were mixed concurrently with supercritical water, at temperature and pressure conditions of 400 ^{o}C and 24.1 MPa respectively. Type K thermocouples were used to monitor the temperature of the system at different points. The actual temperature at the reactor point, in the mixing of supercritical water and the precursor solutions, was 307 ^{o}C. A custom built electrical heater arrangement (Watlow Cast X 2000, maximum thermal output 24 kW) was used to reach supercritical conditions for the water and a back-pressure regulator in the system (BPR, Swagelok KHB series), was adjusted using a PID algorithm, to maintain pressure conditions.

In the TiO_2 nanoparticle synthesis each of the precursors, titanium(IV) oxysulfate ($TiOSO_4$, 0.2 M) with free hydrated sulphuric acid and potassium hydroxide (KOH, 0.4 M) were pumped separately at 150 mL min^{-1} into a T-piece, before meeting the flow of supercritical water. The flow-rate of supercritical water was adjusted to 300 mL min^{-1}. The formed TiO_2 nanoparticles were rapidly quenched and cooled using an external cooling system (outer jacket through which water flowed at 100 L min^{-1} and an inlet temperature of 15 ^{o}C). The nanoparticles were collected as a slurry, centrifuged and washed three times with deionised water (10 MΩ) until the pH was neutral. The nanoparticles were subsequently dried in a freeze-drier (Virtis Genesis 35XL) by slowly heating under vacuum (100 mTorr) from -60 to 25 ^{o}C over a period 24 h.

7.2.2.2 *Deposition of gold nanoparticles on TiO_2*

Gold nanoparticles were deposited onto the titania following a procedure adapted from the literature, by Mr Joseph C. Bear [38]. Chloroauric acid ($HAuCl_4$, 30 mg), 1 % sodium citrate solution (30 mL) and de-ionised water (120 mL) were refluxed for 4 h at 110 ^{o}C. 50 ml of the purple gold colloid was subsequently stirred with 1 g of TiO_2 nanoparticles and sodium chloride (5.8 g, NaCl) was added suddenly, resulting in the precipitation of Au metal onto the TiO_2 particles. The purple precipitate (Au/TiO_2) was then filtered, repeatedly washed with de-ionised water (10 MΩ), centrifuged and lyophilized.

7.2.2.3 *Functionalisation of TiO_2 and Au/TiO_2 nanoparticles*

TiO_2 and Au/TiO_2 nanoparticles were functionalised following a procedure adapted from the literature, by Mr Joseph C. Bear [39]. TiO_2 or Au/TiO_2 nanoparticles (1 g) were heated to 80 ^{o}C in excess oleic acid (120 mmol, 38.1 mL) over a period of 24 hours, with a catalytic amount of triethylamine (8 mmol, 1.12 ml) added to encourage ester formation between the titanol groups on the nanoparticle surface and the oleic acid. The nanoparticles were subsequently precipitated with ethanol and centrifuged at 2500 x*g*, before dispersion in toluene. Note

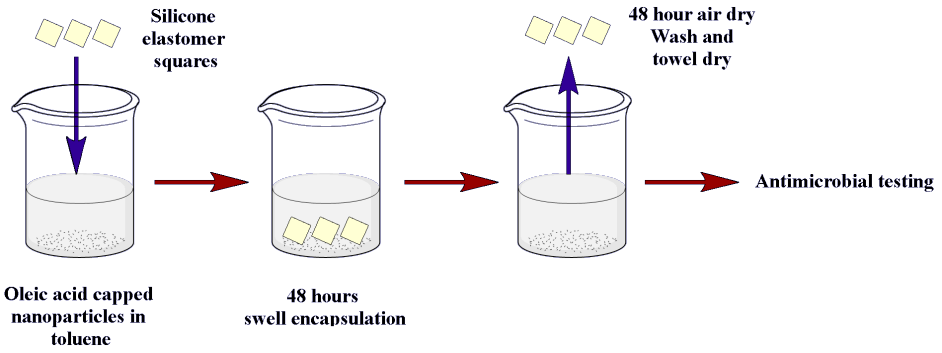

Figure 47: Schematic to show preparation of TiO_2 and Au/TiO_2 encapsulated silicone samples

that the nanoparticles were precipitated and re-dispersed in toluene three times, to remove excess surfactant.

7.2.2.4 *Preparation of Antimicrobial Polymers*

A series of silicone samples were prepared for microbiological testing. Swelling solutions were prepared in which oleic acid functionalised-TiO_2 or Au/TiO_2 nanoparticles were dispersed in toluene. The toluene-based swelling solutions were made up to a concentration of 20 mg/ mL nanoparticles. Medical grade silicone polymer coupons (1.21 cm^2) were immersed in toluene, oleic acid functionalised TiO_2 nanoparticles dispersed in toluene or Au/TiO_2 nanoparticles dispersed in toluene and allowed to swell for 48 h. The samples were subsequently removed from the toluene swelling solutions, air-dried (48 h), washed and towel-dried. Where possible, the samples were maintained under dark conditions. An overview of the materials synthesis is presented in Figure 47.

7.2.3 *Materials Characterisation*

A PerkinElmer Lambda 25 UV-Vis spectrometer was used to measure the UV-Vis absorption spectra of the toluene-based nanoparticle swelling solutions and the modified silicone polymers used for microbiology, within the range 250 - 1100 nm (full range not shown). Samples for TEM were prepared by drop-casting a suspension of

nanoparticles in hexane solvent onto a 400 Cu mesh holey carbon film TEM grid (Agar Scientific Ltd). Samples were imaged using a JEOL 2100 HR-TEM with a LaB_6 source, operating at an acceleration voltage of 200 kV with an Oxford Instruments XMax EDX detector, running AZTEC software. TEM images were recorded on a Gatan Orius CCD.

XRD was performed using a Bruker-Axs D8 (GADDS) diffractometer. The instrument operates with a Cu X-ray source, monochromated ($K\alpha_1$ and $K\alpha_2$) and a 2D area X-ray detector with a resolution of 0.01^{o}. TiO_2- and Au/TiO_2-nanoparticulate films were analysed with a glancing incident angle (θ) of 5^{o}. The diffraction patterns obtained, were compared with ICDD database standards. Raman spectra of TiO_2 and Au/TiO_2 nanoparticles and nanoparticle-embedded polymers were obtained using a Renishaw Raman System 1000, calibrated using a Silicon standard. XPS was carried out using a Thermo Scientific K-alpha spectrometer with monochromated Al $K\alpha$ radiation, a dual beam charge compensation system and constant pass energy of 50 eV (spot size 400 μm). Survey scans were collected in the range 0 - 1200 eV. High-resolution scans (0.1 eV) were used for the principal peaks of Ti (2p), O (1s), Au (4f) and C (1s) and all spectra were calibrated against adventitious carbon (C1s, 284.8 eV).

7.2.4 *Functional Properties*

7.2.4.1 *Wetting properties*

Equilibrium water contact angle measurements (~ 5 μL) on: untreated silicone, solvent treated (control) silicone, TiO_2-encapsulated silicone and Au/TiO_2-encapsulated silicone, were recorded using an FTA 1000 Drop Shape Instrument at room temperature conditions. The contact angle measurement for each sample type was taken to be the average value over $\geqslant 5$ measurements, using a droplet of de-ionised water dispensed by gravity from a gauge 27 needle and the samples were photographed side on. The data was analysed using SURFTENS

software (V. 4.5).

7.2.4.2 *Photocatalytic testing of the TiO_2 and Au/TiO_2 nanoparticles*

The photo-activity of the functionalised titania nanoparticles and functionalised gold-modified-titania nanoparticles was determined by the photo-oxidation of a model organic pollutant, octadecanoic (stearic) acid. TiO_2 or Au/TiO_2 nanoparticle films (0.8 mg) were prepared by drop-casting a concentrated solution of nanoparticles made up in toluene onto a borosilicate glass substrate, after which the samples were allowed to dry such that the residual solvent evaporated. A thin layer of stearic acid solution in chloroform (0.05 M) was subsequently dip-coated onto the coated-glass substrate samples. The samples were then irradiated using a blacklight-blue (BLB) lamp (*Vilber Lourmat*, 365 nm, 2 x 8 W, 1.2 mW cm^{-2}) and the photodegradation of the acid was monitored using a Perkin Elmer RX-I Fourier transform infrared (FTIR) spectrometer.

7.2.5 *Microbiological Testing*

The following silicone elastomer samples (1.21 cm^2) were used in the microbiology experiments: (i) solvent treated silicone (control), (ii) oleic acid functionalised-TiO_2 encapsulated silicone (TiO_2) and (iii) gold deposited, oleic acid functionalised-TiO_2 encapsulated medical grade silicone (Au/TiO_2). Immediately prior to microbiological testing, all samples were pre-irradiated for 18 hours using a 365 nm UV light source (BLB, Vilber Lourmat, 365 nm) emitting an average light intensity of 1.8 mW cm^{-2} at a distance of 10 cm from the samples, after which they were maintained under dark conditions (24 h). The samples were subsequently tested against *S. aureus* 8325-4 and *E. coli* ATCC 25922. These organisms were stored at -70 ^{o}C in BHI broth containing 20 % (v/v) glycerol and propagated on either MSA or MAC agar for a maximum of two sub-cultures at intervals of two weeks.

BHI broth (10 mL) was inoculated with 1 bacterial colony and cultured in air at 37 °C for 18 h with shaking at 200 rpm. The bacterial pellet was recovered by centrifugation (21 °C, 1771 x*g*, 5 min), washed in PBS and centrifuged again to recover the bacteria, which were finally re-suspended in PBS (10 mL). The washed suspension was diluted 1000-fold to obtain the inoculum (~10^6 cfu /mL). The inoculum in each experiment was confirmed by plating ten-fold serial dilutions on agar for viable counts. Triplicates of each polymer sample type were inoculated with 20 μL of the inoculum and covered with a sterile cover slip (22 x 22 mm). The samples were then irradiated for the required time period using a 365 nm UV light source emitting an average light intensity of 1.8 mW cm^{-2} at a distance of 10 cm from the samples. A further set of samples (in triplicate) was maintained in the dark for the duration of the irradiation time.

Post irradiation, the inoculated samples and cover slips were added to PBS (180 μL) and vortexed. The neat suspension and ten-fold serial dilutions were plated on the appropriate agar for viable counts. The plates were incubated aerobically at 37 °C for 24 h (*E. coli*) or 48 h (*S. aureus*). Each experiment contained 3 technical replicates and the experiment was reproduced three times. The Mann-Whitney U test was used to determine the significance of the following comparisons: (i) the activity of each of the modified polymers compared to the control silicone sample when both were incubated in the dark and (ii) the activity of each of the irradiated modified polymers compared to the same material incubated in the dark.

7.3 RESULTS AND DISCUSSION

7.3.1 *Materials Synthesis*

7.3.1.1 *Nanoparticle Synthesis and Functionalisation*

A CHFS route was used to synthesise titania nanoparticles and subsequently, using a modified Turkevich synthesis, gold addition was achieved on the titania nanoparticles. The latter synthetic route relies on the formation of gold on the added nanoparticle surface, after precipitation with salt. The presence of titania nanoparticles provides a lower energy surface on which the gold can grow, rather than undergoing Ostwald ripening as they are precipitated. Due to the presence of citrate ligands on the Turkevich synthesised gold, the nanoparticles are stabilised by electrostatic interactions and thus, because of a lowering of surface charge, they are susceptible to salt flocculation.

The titania and gold-modified-titania nanoparticles were functionalised according to the method proposed in the literature [39]. The functionalisation step was achieved to add sterically stabilising oleic acid to the nanoparticle surface. Some of the oleic acid added, weakly binds to the nanoparticle via Van der Waals interactions and the remainder undergoes esterification reactions with titanol groups present on the nanoparticle surface.

7.3.1.2 *Materials Synthesis*

Silicone samples were embedded with TiO_2 nanoparticles or Au/TiO_2 nanoparticles using a simple one-step "swell-encapsulation-shrink" strategy, as used to incorporate a range of photosensitiser dyes and nanoparticles into medical grade polymers [1–8]. Medical grade silicone coupons were immersed in toluene swelling solutions made up to a concentration of 20 mg/ mL of titania or Au/TiO_2 nanoparticles for a period of 48 hours. The toluene induced substantial polymer swelling, enabling the diffusion of the nanoparticles through the polymer bulk. Upon removal from the swelling solution, the titania-

modified samples were allowed to air-dry for at least 48 hours prior to washing, to ensure complete evaporation of residual solvent and the solvent-treated polymers shrunk to their previous dimensions over this time period.

It should be noted that contrary to previous work involving the incorporation of dyes and nanoparticles into medical grade polymers [1–8], some of which has been detailed in previous chapters, here, the encapsulation of neither the TiO_2 nanoparticles, nor the Au/TiO_2 nanoparticles impacted on polymer colouration. This is an attractive property in terms of future commercialisation of this technology for antimicrobial surface technology applications, where strong material colouration may be detrimental.

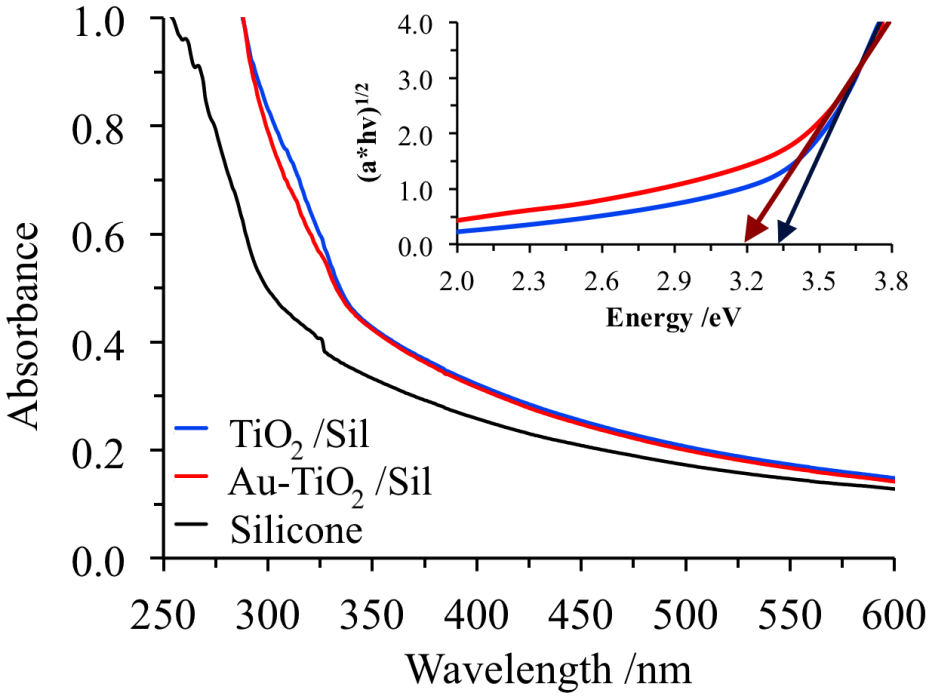

Figure 48: UV-Vis absorbance spectra of a toluene treated silicone polymer (black line), a TiO_2-encapsulated silicone polymer (blue line) and a Au/TiO_2-encapsulated silicone polymer (red line). Inset: Tauc plot constructed using nanoparticle solution data to determine band gap of TiO_2 nanoparticles (blue line) and Au/TiO_2 nanoparticles (red line). The band onset of the TiO_2 nanoparticles was calculated as 3.33 eV and the band onset of Au/TiO_2 nanoparticles was calculated at 3.18 eV

7.3.2 *Materials Characterisation*

7.3.2.1 *UV-Vis Absorbance Spectroscopy*

UV-Vis absorbance spectroscopy was used to examine the toluene dispersed TiO_2 and Au/TiO_2 nanoparticle solutions, as well as the nanoparticle-encapsulated silicone polymers (Figure 48). Using the UV-Vis data of the toluene dispersed TiO_2 and Au/TiO_2 nanoparticles, a Tauc plot was constructed - $(ah\upsilon)^{1/2}$ as a function of photon energy $h\upsilon$, where 'a' is the absorbance of the nanoparticles [40] - to estimate the nanoparticle band onset. The data indicates that the deposition of gold onto the modified-titania nanoparticle shifts the band onset towards the visible region of the spectrum (3.18 eV for Au/TiO_2 compared to 3.33 eV TiO_2).

The UV-Vis absorbance spectra of the TiO_2- and Au/TiO_2-encapsulated silicone polymers were recorded and compared to the absorbance spectrum of an untreated control silicone polymer. The absorbance spectra provide evidence of nanoparticle encapsulation within the polymer, since as demonstrated by Figure 48, the band edge of the TiO_2 and Au/TiO_2-encapsulated silicone polymers is noticeably red shifted, with respect to that of the control silicone polymer.

7.3.2.2 *Transmission Electron Microscopy*

The TiO_2 and Au/TiO_2 nanoparticle powders were dispersed in hexane to form a dilute solution and drop cast onto TEM grids. The TEM images (Figure 49) showed polydisperse populations of crystalline nanoparticles, dominated by anatase titania in both the case of the TiO_2 and Au/TiO_2 nanoparticle samples. Size analysis showed an average nanoparticle diameter of 11 ± 4.7 nm for the TiO_2 nanoparticles and 11 ± 4.4 nm for the Au/TiO_2 nanoparticles. HR-TEM images showed the particles to be highly crystalline, with lattice spacings of 0.34 nm and 0.33 nm (49(b) and 49(d)). Using the Bragg equation (see XRD data, Section 7.3.2.3), it was determined that

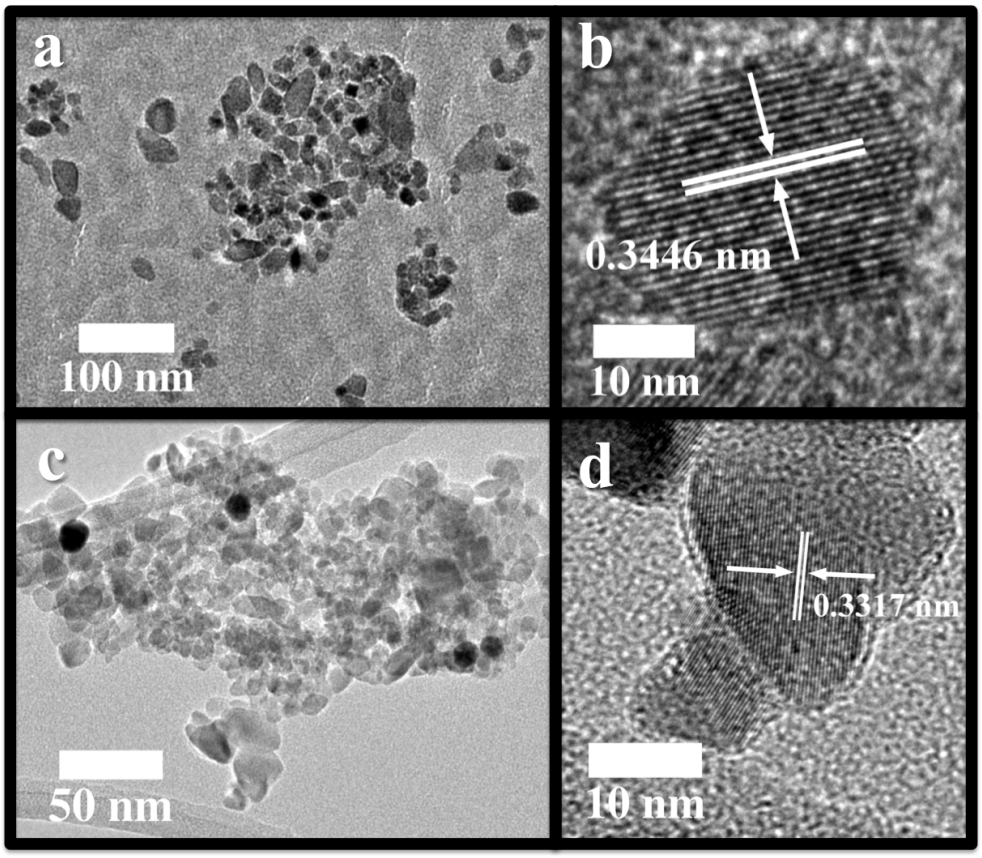

Figure 49: (a) TEM of oleic acid functionalised TiO_2 nanoparticles, (b) HR-TEM of oleic acid functionalised TiO_2 nanoparticles, (c) TEM of Au/TiO_2 nanoparticles and (d) HR-TEM of Au/TiO_2 nanoparticles

Table 7: Energy-dispersive X-ray spectroscopy data for TiO_2 and Au/TiO_2 samples

Sample	Element	Line Type	k factor	Wt%	σ Wt%	Atomic %
TiO_2	O	K series	1.181	47.29	0.32	72.87
	Ti	K series	0.635	52.71	0.32	27.13
Au/TiO_2	O	K series	1.181	51.61	0.64	77.00
	Ti	K series	0.635	45.45	0.61	22.65
	Au	M series	1.012	2.94	0.60	0.36

these lattice spacings correspond to the (101) planes of anatase titania.

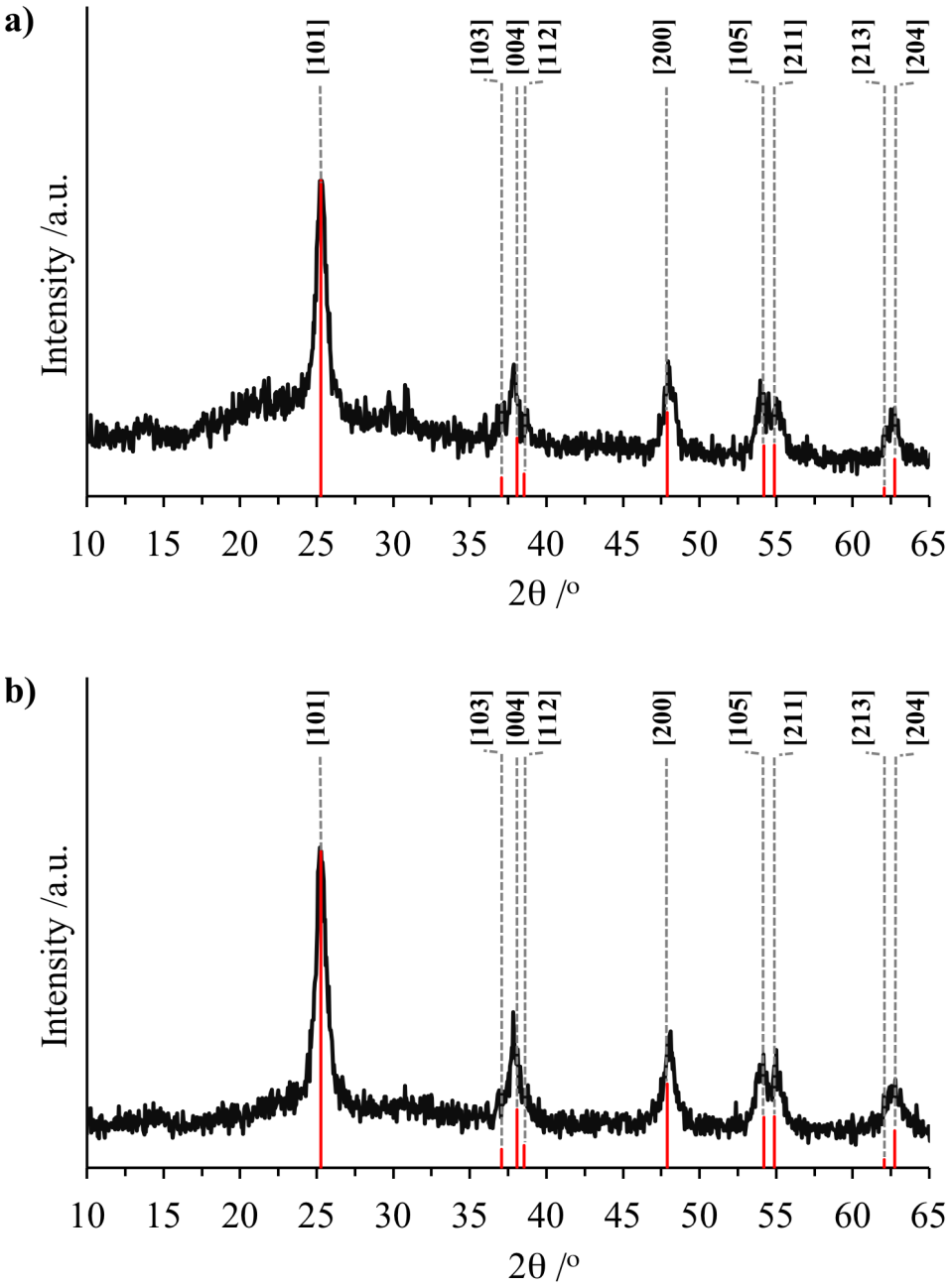

Figure 50: X-Ray diffraction pattern of: (a) TiO_2 and (b) Au/TiO_2 showing distinctive peaks of anatase TiO_2. Reference lines from ICSD collection code: 154610

TEM analysis also indicated that the size and shape of the TiO_2 nanoparticles are unaltered by neither the gold deposition, nor the oleic acid functionalisation processess. It can be suggested that in the case of the former, this is possibly due to the small quantities of Au (*ca.* 0.36 %, Table 7) that is surface bound.

7.3.2.3 *X-Ray Diffraction*

The TiO_2 and Au/TiO_2 nanoparticle samples were analysed using XRD (Figure 50). The XRD data supported the TEM analysis and the diffraction pattern showed prominent peaks at 25.3, 37.9, 48.0, 54.1, 55.0 and 62.4° 2θ, corresponding to anatase TiO_2 (ICSD collection code: 154610). The Scherrer equation [41] was used to estimate the size of individual nanoparticles, by correlating the particle linear dimension with the diffraction pattern peak breadth:

$$L = \frac{K \lambda}{B \cos \theta} \tag{4}$$

where *L* is the particle linear dimension, *K* is the Scherrer constant, *B* is a measure of the peak broadening, full-width at half-maximum (FWHM) and λ represents the wavelength of the incoming X-rays [42]. Using the Scherrer equation (Equation 4), the average nanoparticle diameter was estimated as 11.1 nm for the TiO_2 nanoparticles and 10.0 nm for the Au/TiO_2 nanoparticles. It should be noted that these approximated values are in good agreement to those obtained by TEM analysis (11.2 nm and 10.9 nm, respectively). The peak broadness compared to that of bulk anatase TiO_2, can be attributed to the small crystallite size. It should also be highlighted that as expected, the deposition of gold onto the TiO_2 nanoparticle surface effected no discernible change in XRD peak positions.

TiO_2- and Au/TiO_2 nanoparticle-encapsulated polymer samples were also analysed using XRD. Analysis of the measured diffraction patterns showed no difference between that of the control silicone samples and either nanoparticle-encapsulated sample. It can be suggested that this is due to the low quantities of nanoparticles present in the polymer, such that the encapsulated nanoparticle concentrations are below that detectable using XRD.

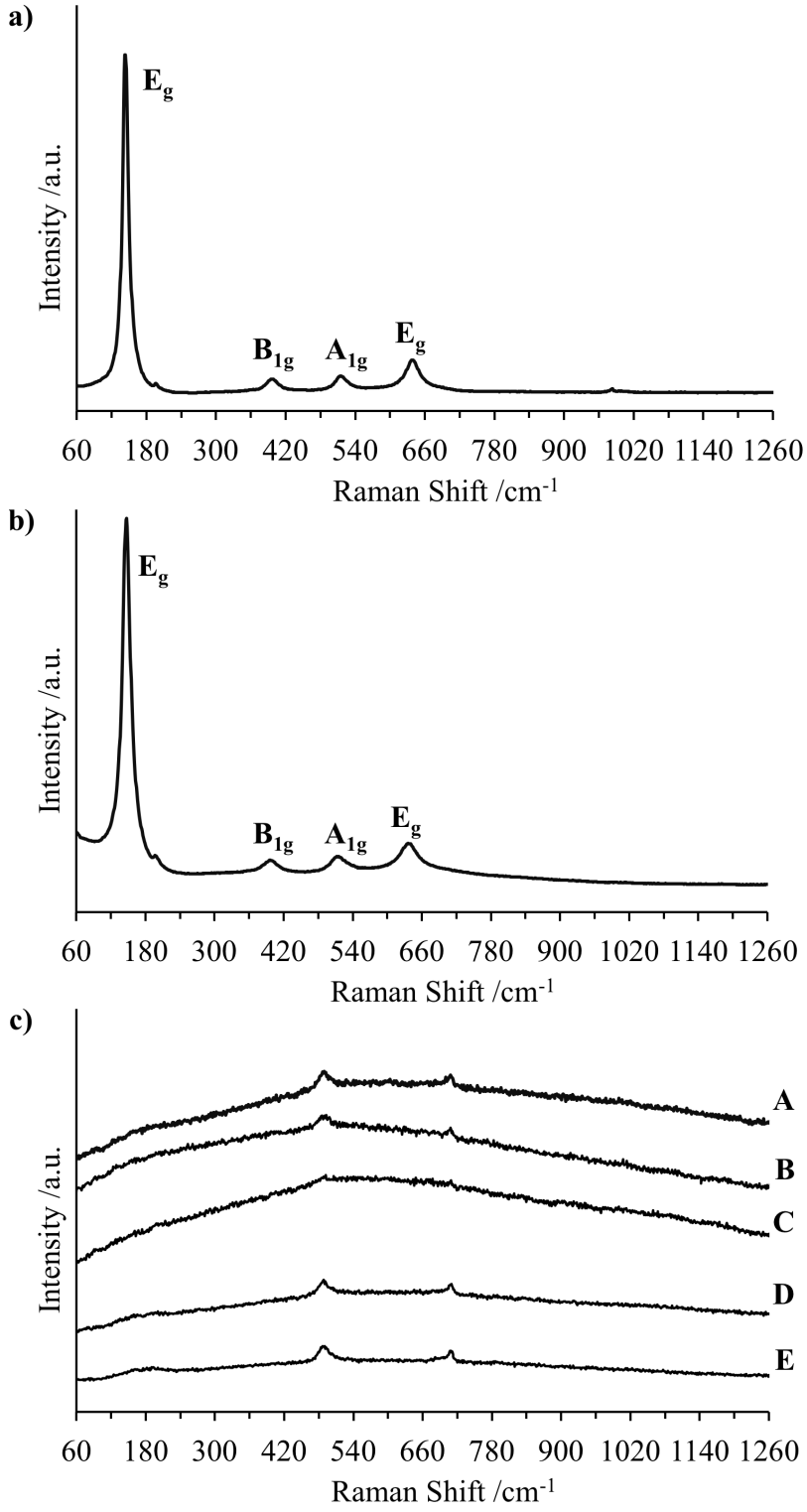

Figure 51: Raman spectra of the (a) TiO_2 and (b) Au/TiO_2 nanoparticle samples [43]. (c) Raman spectra of: A) control solvent-treated silicone, B) TiO_2-encapsulated silicone, C) TiO_2-encapsulated silicone irradiated with UV light (365 nm, 18 h), d) Au/TiO_2-encapsulated silicone and e) Au/TiO_2-encapsulated silicone irradiated with UV light (365 nm, 18 h)

7.3.2.4 *Raman Spectroscopy*

Raman spectroscopy was used to analyse the TiO_2 and Au/TiO_2 nanoparticle samples. Both measured nanoparticle spectra showed characteristic Raman signals for titania at 146.7 and 636.7, 396 and 512.5 cm^{-1} and these peaks can be assigned as the E_g, B_{1g} and A_{1g} modes of the anatase phase [43]. As expected, no discernible shift in Raman peak was noted between the TiO_2 and Au/TiO_2 nanoparticle samples, as the gold is deposited on the nanoparticle surface. Moreover, no characteristic peak for gold was observed in the spectrum of the Au/TiO_2 sample (Figure 51(b)).

Raman spectra of TiO_2- and Au/TiO_2-encapsulated silicone were measured and compared to that of a control silicone sample. No significant difference was noted across the sample range and the spectra were comparable to that of the control silicone sample. The polymer samples were exposed to UV irradiation (365 nm, 18 h) and the Raman spectra were re-measured. It was found that the spectra were comparable and this indicates that neither the UV-irradiation, nor the presence of the photo-active nanoparticle, photodegrade the silicone polymer.

7.3.2.5 *X-Ray Photoelectron Spectroscopy*

XPS of both the TiO_2 and Au/TiO_2 nanoparticle samples (Figures 52 and 53) showed a doublet in the Ti (2p) region corresponding to titanium in TiO_2. An oxygen peak in the O (1s) region corresponding to oxygen in TiO_2 was also observed. XPS of the Au/TiO_2 sample

Table 8: Nanoparticle composition data from XPS measurements for titanium (Ti), oxygen (O) and gold (Au) content

Sample	**Sample Description**	**Ti Content (atom %)**	**O Content (atom %)**	**Au Content (atom %)**
TiO_2	Unmodified TiO_2	22.4	62.05	-
Au/TiO_2	Gold-doped TiO_2	20.54	53.24	0.51

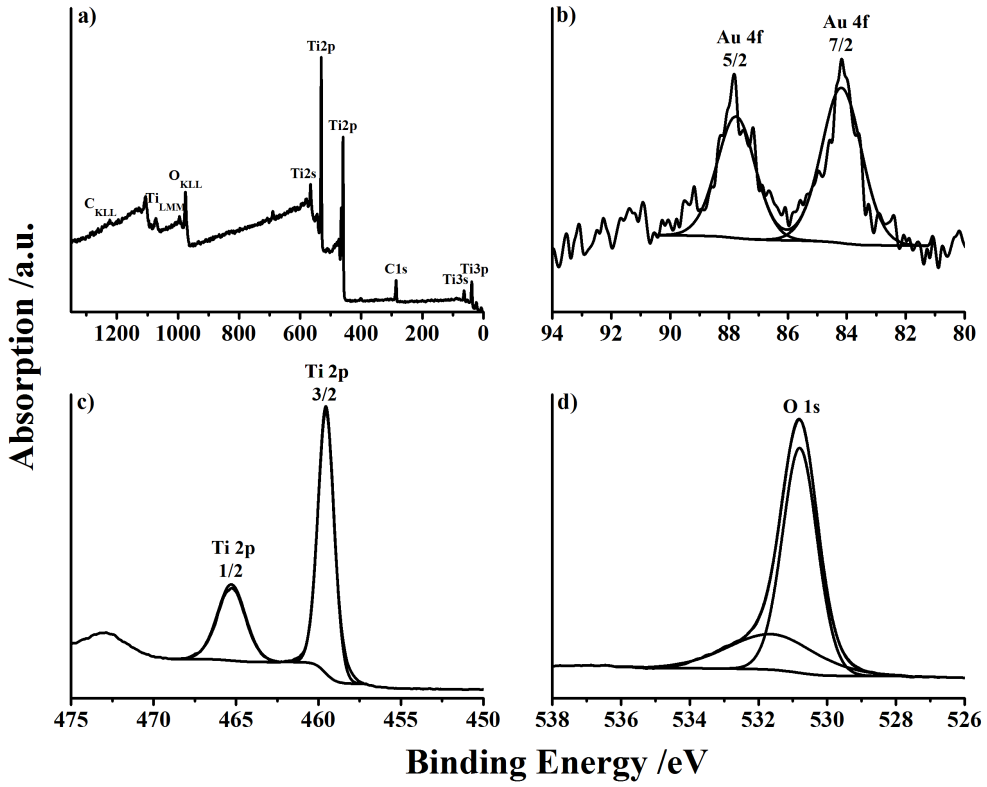

Figure 52: Fitted XPS spectra of Au/TiO_2 nanoparticle powder sample. (a) Labelled survey scan, (b) Au 4f scan, (c) Ti 2p scan and (d) O 1s scan

confirmed the presence of low quantities of gold (*ca.* 0.5 %), with determined values in close approximation to composition values obtained by Energy-dispersive X-ray spectroscopy (EDX). Comparing Figure 52(c) - (d) with Figure 53(a) - (b), it is noteworthy that there is no shift in the binding energies and chemical environments of the Ti 2p and O 1s in the two nanoparticle powder samples.

XPS of both TiO_2 and Au/TiO_2 nanoparticle-encapsulated silicone samples showed evidence of nanoparticle encapsulation, with a doublet in the Ti (2p) region corresponding to titanium in TiO_2, with a slight right shift in binding energy compared to the nanoparticle powder samples. However, due to the low concentration of gold present in the nanoparticle encapsulated polymer, it was not possible to confirm the presence of gold in the Au/TiO_2 nanoparticle-encapsulated sample.

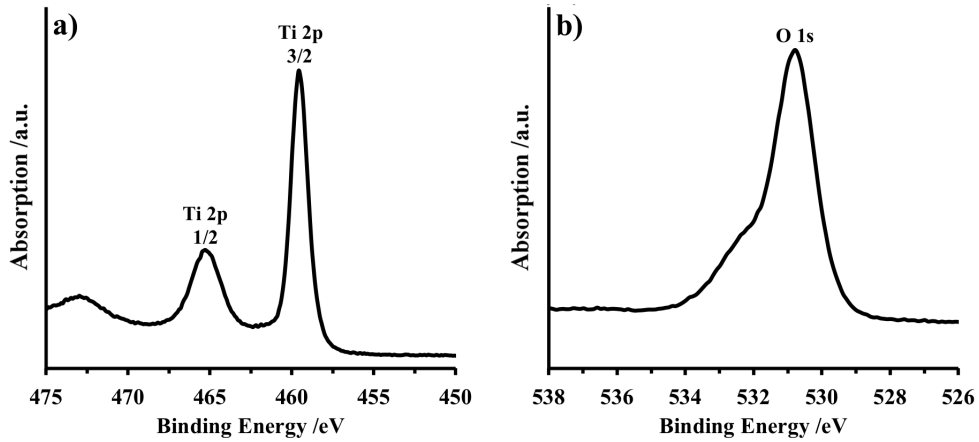

Figure 53: XPS spectra of TiO_2 nanoparticle powder sample. (a) Ti 2p scan and (b) O 1s scan

7.3.3 *Functional Properties*

7.3.3.1 *Wetting Properties*

The wetting properties of a range of untreated and nanoparticle-modified silicone samples were measured under laboratory temperature and lighting conditions. The water contact angle measurements indicate that the polymer itself presents a highly hydrophobic surface (120 °) and the water contact angle is reduced through the encapsulation of TiO_2 or Au/TiO_2 nanoparticles (90 °). However, it should be noted that no photo-activated polymer hydrophilicity was observed on the nanoparticle-encapsulated samples upon irradiation with a 365 nm UV lamp. It can be suggested that this is because the nanoparticles do not form a thin film at the polymer surface, rather they are dispersed throughout the polymer matrix and therefore impact on the hydrophilicity of the polymer, rather than the UV-activated hydrophilicity.

7.3.3.2 *Photocatalytic Activity*

TiO_2 and Au/TiO_2 nanoparticle films were prepared by drop-casting a concentrated solution of nanoparticles onto a glass substrate and the comparative photoactivity of these films was evaluated through their efficacy to photodegrade stearic acid, a model organic pollutant, under 365 nm UV irradiation conditions. The use of stearic acid as a

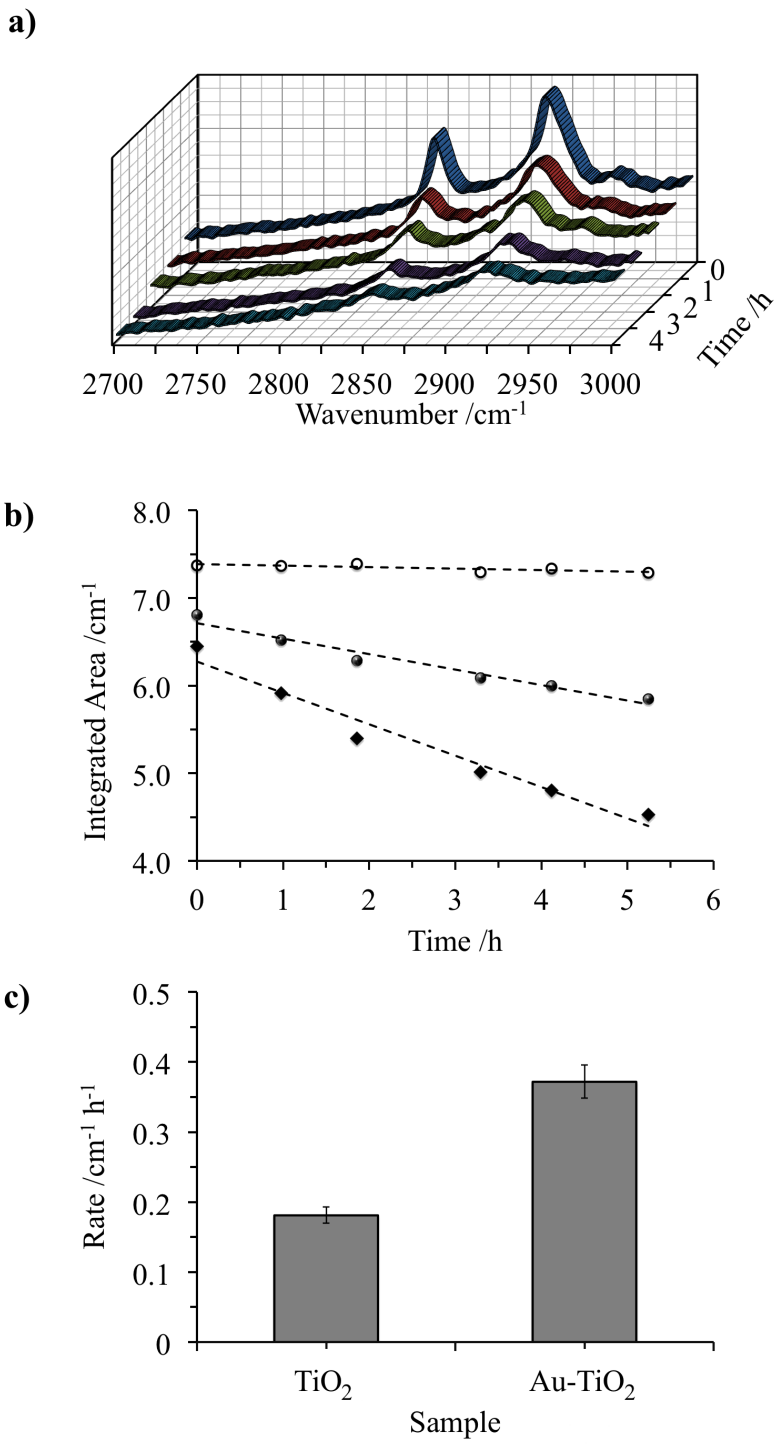

Figure 54: (a) IR spectra of stearic acid upon UVA illumination (1.2 mW cm^{-2}) on a TiO_2 drop-cast film. (b) Integrated areas obtained during illumination of TiO_2 (full circles), Au/TiO_2 (full diamonds) and plain glass control (open circles) films. (c) Photo-activity rates (given as rate over irradiance) of TiO_2 and Au/TiO_2 films obtained during UVA irradiation (BLB 365 nm)

preferred method to assess the activity of photocatalytic materials is based on a number of reasons including: (i) its high stability under UV irradiation in the absence of a photocatalytic surface, (ii) the ease of deposition of stearic acid films from methanol or chloroform solutions, (iii) simple photodestruction kinetics (zero-order) such that film thickness is not a critical factor when evaluating photo-activity of surfaces and (iv) the photodestruction of stearic acid can easily be monitored spectroscopically [44].

The overall oxidation reaction can be summarised as follows:

$$CH_3(CH_2)_{16}CO_2H \; + \; 26\, O_2 \overset{TiO_2(h) \geqslant E_{bg}}{\longrightarrow} 18\, CO_2 \; + \; 18\, H_2O \qquad (5)$$

and here, the photodestruction of stearic acid as a function of time, on TiO_2 and Au/TiO_2 nanoparticle films, was monitored using IR absorption spectroscopy, following the disappearance of typical C-H bands at 2958, 2923 and 2853 cm^{-1} (Figure 54(a)). These peaks are attributed to the asymmetric in-plane C-H stretches in the stearic acid CH_3 group and both the asymmetric and symmetric C-H stretches in the stearic acid CH_2 groups, respectively [44]

Using a conversion factor from the literature based on the integrated area of the IR spectrum, where:

$$1\ cm^{-1} \; \equiv \; 9.7\ x\ 10^{15}\ molecules\ cm^{-2}$$

the number of stearic acid molecules that have been degraded can be estimated [44]. The photoactivity rates are estimated from linear regression of the initial 20 - 30 % degradation steps (zero-order kinetics regime) of the curves of the integrated areas (Figure 54(b)). Preliminary photocatalytic tests of drop-cast films of the TiO_2 and Au/TiO_2 powders indicate that the Au/TiO_2 nanoparticle thin films showed an enhanced photo-activity under 365 nm UV irradiation regimes (Figure 54(c)).

The increased activity of TiO_2-based systems containing noble metal nanoparticles is typically explained in terms of an efficient charge

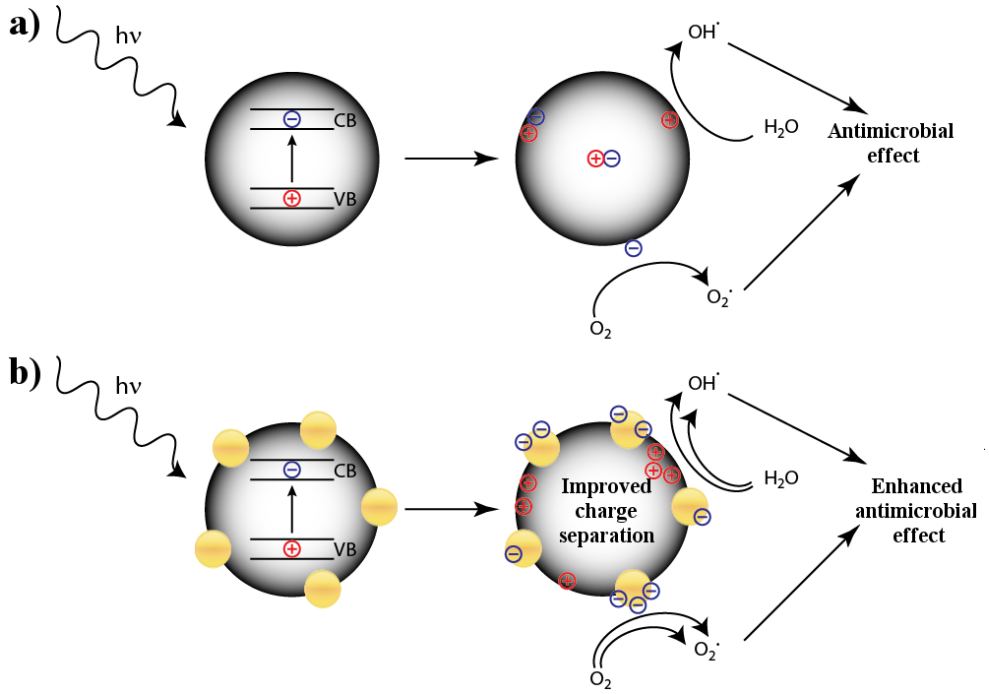

Figure 55: Proposed mechanism of photocatalytic antimicrobial activity of (a) TiO_2 encapsulated silicone sample and (b) Au/TiO_2 encapsulated silicone sample

separation as shown in Figure 55 [35, 45], although conflicting accounts regarding the mechanism of improved charge separation have been commented on in the literature [31]. It has been proposed that the photocatalysed charge separation enhancement mechanisms may differ depending on the excitation wavelength used, for example UV-light irradiation compared to visible-light irradiation [27, 46]. For UV-activation, literature accounts suggest that the presence of the gold deposited on the TiO_2 nanoparticles can promote interfacial charge transfer and due to the difference in the work functions of the titania and gold, the conduction band electrons in the former, may be attracted by the latter, hindering electron-hole pair recombination (See Figure 55) [35, 47]. It has also been reported that the gold-titania contact is a Schottky junction and this junction 'forces' electrons and holes generated within this region, to move in opposite directions [35, 45]. After photo-excitation, electrons migrate to the metal, which traps the electrons at the metal surface and provides a host for additional active sites for photocatalysed reactions with targeted reactants [45, 48] The hole diffuses to the surface of the TiO_2 nanoparticle, where it can react to oxidise organic species [48]. Through facilitating the transfer

of photo-generated electrons and holes to the surfaces of the metal and semiconductor respectively, the metal suppresses electron-hole recombination and increases the photocatalytic efficiency of the TiO_2 [35, 45].

7.3.4 *Photobactericidal Activity*

The light-activated antimicrobial activity of TiO_2 nanoparticle- and Au/TiO_2 nanoparticle encapsulated medical grade silicone samples was tested against representative Gram-positive and Gram-negative bacteria commonly found in healthcare environments, *S. aureus* and *E. coli*, respectively. Prior to microbiological testing, the samples were pre-irradiated with a 365 nm UV lamp for 18 hours to photodegrade any residual organic precursor material on the sample surfaces, after which they were stored under dark conditions for 24 hours. In the microbiology assays, the samples were irradiated using a 365 nm UV lamp emitting an average of 1.8 mW cm^{-2}, at a distance of 10 cm from the samples. A further sample set was maintained in the dark for the duration of the experiment to determine whether antimicrobial activity is due to a photocatalysed effect, or can be attributed to intrinsic bactericidal properties of the modified titania surfaces.

The antibacterial properties of silicone samples encapsulated with either TiO_2 nanoparticles or Au/TiO_2 nanoparticles was compared to that of a control, solvent treated silicone sample. Interestingly, both the TiO_2 nanoparticle- and Au/TiO_2 nanoparticle-encapsulated silicone demonstrated strong antimicrobial activity under dark conditions when tested against *S. aureus*, reducing bacterial numbers to below the detection limit ($P < 0.001$, Figure 56(a)). Consequently, no additional photocatalysed antimicrobial effects could be established. TiO_2 is a photo-activated antimicrobial agent and therefore, the potent bactericidal activity observed under dark conditions was surprising. Since it has been noted that oleic acid can inhibit the growth of Gram-positive bacteria including *S. aureus* [49], it can be speculated that the intrinsic antibacterial activity of both the TiO_2- and Au/TiO_2-silicone samples, may be attributed to the oleic

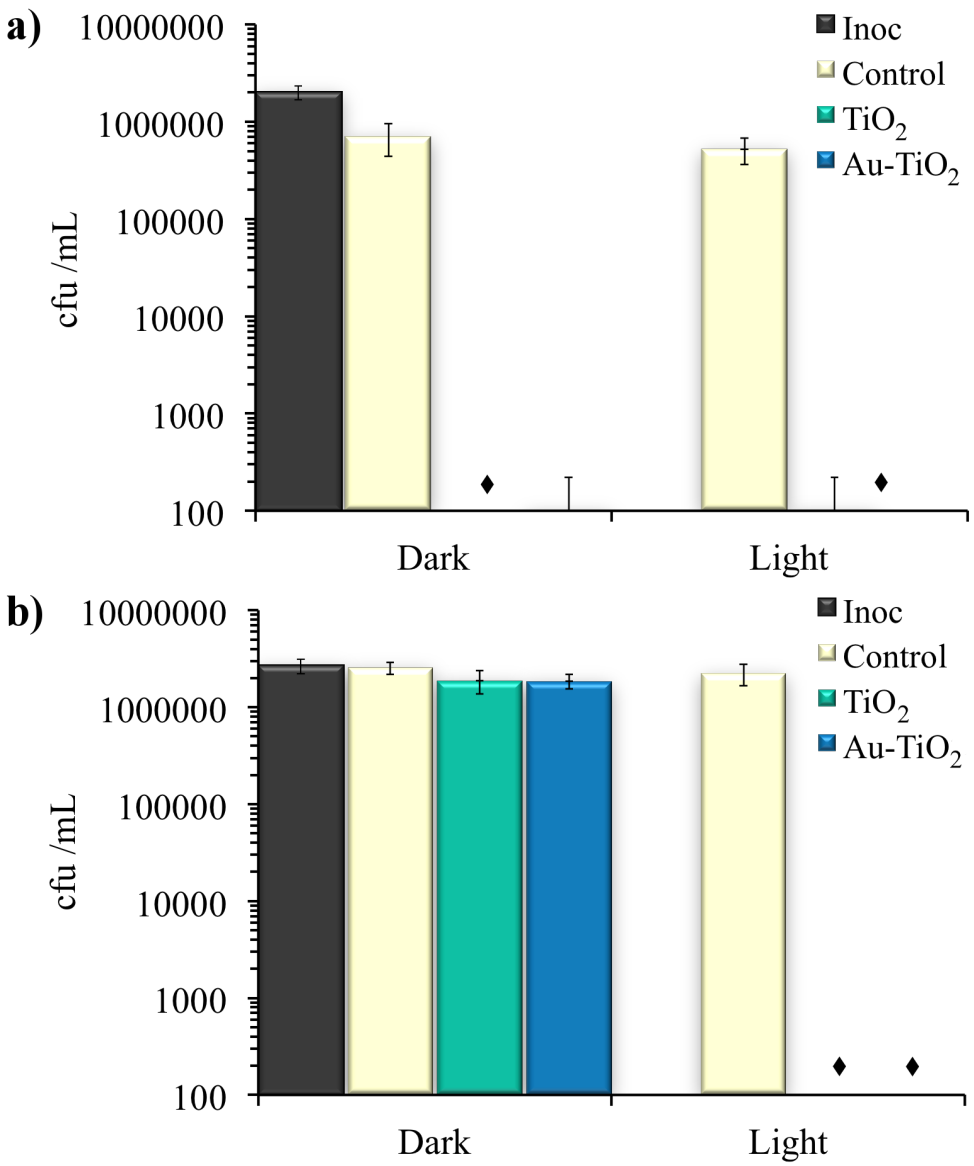

Figure 56: Viable counts of bacteria (colony forming units (cfu) /mL) after incubation on modified silicone polymers exposed to UV irradiation (365 nm): (a) *S. aureus* (15 min illumination) and (b) *E. coli* (95 min illumination). The UV source emitted an average light intensity of 1.8 ± 0.1 mW cm^{-2} at a distance of 10 cm from the samples. The ♦ symbols indicate that the bacterial numbers were reduced to below the detection limit of 500 cfu /mL

acid nanoparticle capping agent. Further experiments to test the antimicrobial activity of a range of oleic acid-capped nanoparticles and non-oleic acid-capped TiO_2 and Au/TiO_2 nanoparticles, would be of benefit in elucidating the mechanism of dark kill observed in this investigation.

When tested against *E. coli* under dark conditions, as shown in Figure 56(b), both the TiO_2-encapsulated silicone and the Au/TiO_2-encapsulated silicone samples exhibited limited antimicrobial activity and these effects were not highly significant ($P < 0.01$). These results suggest that the bactericidal properties of the capping agent are not as effective against this bacterium, as indicated in the literature [49]. However, when both the TiO_2- and Au/TiO_2-encapsulated silicone samples were exposed to 365 nm UV irradiation, they induced the lethal photosensitisation of *E. coli*, reducing viable bacterial numbers to below the detection limit within 95 minutes (3.7 log kill, $P < 0.001$).

TiO_2 is a UV-activated photocatalyst and generates mobile electron-hole pairs upon absorption of photons with energy greater than that of its band gap energy. The electron-hole pair can migrate to the nanoparticle surface where the electrons reduce molecular oxygen in the environs, generating superoxide anions and the positive holes interact with adsorbed water, generating hydroxyl radicals. The photo-generated radical species can subsequently react further, resulting in the production of a wide range of radicals. These radicals, including ROS, can initiate a non-site specific attack against bacteria near the surface, oxidising organic matter and ultimately, photo-destroying bacterial cellular membranes and components. Moreover, due to the multi-site attack mechanism, the emergence of bacterial resistance to this antimicrobial strategy is unlikely. This is a highly desirable property in antibacterial surfaces developed for applications in healthcare settings.

In this study, it was not possible to determine whether the deposition of gold onto the titania nanoparticle enhanced its photocatalytic activity. Rapid kills of both Gram-positive and Gram-negative bacteria, *S. aureus* and *E. coli*, were achieved on both the TiO_2 nanoparticle- and Au/TiO_2 nanoparticle-encapsulated sample, with viable bacterial numbers reduced by at least 3 log. Further microbial investigations involving white light activation or shorter illumination times, may shed light onto whether the presence of gold shifts the TiO_2 nanoparticle towards visible light photocatalysis, or improves the antimicrobial efficacy over that of TiO_2 alone. Moreover, microbial

testing on surfaces incorporated with a range of oleic acid-capped nanoparticles may be of interest, to further investigate whether the antimicrobial activity under dark conditions can be attributed to the nanoparticle capping group. It would also be advantageous in further investigations to study organisms with known antibiotic resistance or recent clinical isolates.

7.4 CONCLUSION

This chapter details the development of a new class of potent UV-activated antimicrobial polymers, developed by incorporating TiO_2 nanoparticles or Au/TiO_2 nanoparticles into medical grade silicone. The nanoparticles were incorporated using a simple "swell-encapsulation-shrink" strategy. Dissimilar to other antimicrobial polymers detailed in this thesis involving the incorporation of both dyes and nanoparticles into medical grade silicone, the encapsulation of TiO_2 nanoparticles or Au/TiO_2 nanoparticles did not affect polymer colouration, a highly desirable property from a commercial viewpoint.

These modified silicone polymers induced the lethal photosensitisation of *E. coli* within 95 minutes, with bacterial numbers reduced to below the detection limit. Moreover, these surfaces achieved rapid kills of *S. aureus*, resulting in > 3 log kills (below detection limit) within 15 minutes, via a non-light-activated mechanism. It should be noted that these samples demonstrate the most efficacious antimicrobial activity under dark conditions against the Gram-positive bacterium, *S. aureus*, reported in this thesis. However, under the lighting conditions used in this investigation, no enhancement in the photo-activated antimicrobial activity was observed on the Au/TiO_2 nanoparticle-encapsulated polymer compared to the TiO_2 nanoparticle-encapsulated silicone.

Overall, this thesis has detailed the development of a series of potent photobactericidal polymers, activated by a range of lighting conditions. These UVA-activated antimicrobial polymers are simple to

develop, achieve rapid kills over very short time scales and can be utilised for both touch surface applications and medical device applications, provided suitable light delivery systems can be designed. It may be possible to achieve UV-light delivery for medical device applications using a hollow core optical fibre. Moreover, their antimicrobial effectiveness under dark conditions may help maintain low bacterial numbers when the surfaces are not illuminated, increasing their attractiveness as candidates for antimicrobial polymers. It is hopeful that the use of these polymers in healthcare applications may help decrease hospital surface contamination and reduce the incidence of HAIs.

REFERENCES

[1] S. Perni, C. Piccirillo, J. Pratten, P. Prokopovich, W. Chrzanowski, I. P. Parkin, and M. Wilson. "The antimicrobial properties of light-activated polymers containing methylene blue and gold nanoparticles." In: *Biomaterials* 30 (2009), pp. 89–93.

[2] S. Perni, C. Piccirillo, A. Kafizas, M. Uppal, J. Pratten, M. Wilson, and I. P. Parkin. "Antibacterial Activity of Light-Activated Silicone Containing Methylene Blue and Gold Nanoparticles of Different Sizes." In: *Journal of Cluster Science* 21 (2010), pp. 427–438.

[3] S. Perni, P. Prokopovich, C. Piccirillo, J. Pratten, I. P. Parkin, and M. Wilson. "Toluidine blue-containing polymers exhibit potent bactericidal activity when irradiated with red laser light." In: *Journal of Materials Chemistry* 19 (2009), pp. 2715–2723.

[4] S. Perni, J. Pratten, M. Wilson, C. Piccirillo, I. P. Parkin, and P. Prokopovich. "Antimicrobial Properties of Light-activated Polyurethane Containing Indocyanine Green." In: *Journal of Biomaterials Applications* 25 (2011), pp. 387–400.

[5] S. Noimark, C. W. Dunnill, C. W. M. Kay, S. Perni, P. Prokopovich, S. Ismail, M. Wilson, and I. P. Parkin. "Incorporation of methylene blue and nanogold into polyvinyl chloride catheters; a new approach for light-activated disinfection of surfaces." In: *Journal of Materials Chemistry* 22 (2012), pp. 15388–15396.

[6] S. Noimark, M. Bovis, A. J. MacRobert, A. Correia, E. Allan, M. Wilson, and I. P. Parkin. "Photobactericidal polymers; the incorporation of crystal violet and nanogold into medical grade silicone." In: *RSC Advances* 3 (2013), pp. 18383–18394.

[7] S. Noimark, E. Allan, and I. P. Parkin. "Light-activated antimicrobial surfaces with enhanced efficacy induced by a dark-activated mechanism." In: *Chemical Science* 5 (2014), pp. 2216–2223.

[8] A. J. T. Naik, S. Ismail, C. Kay, M. Wilson, and I. P. Parkin. "Antimicrobial activity of polyurethane embedded with methylene blue, toluidene blue and gold nanoparticles against Staphylococcus aureus; illuminated with white light." In: *Materials Chemistry and Physics* 129 (2011), pp. 446–450.

[9] V. Decraene, J. Pratten, and M. Wilson. "Cellulose acetate containing toluidine blue and rose bengal is an effective antimicrobial coating when exposed to white light." In: *Applied and Environmental Microbiology* 72 (2006), pp. 4436–4439.

[10] V. Decraene, J. Pratten, and M. Wilson. "Novel light-activated antimicrobial coatings are effective against surface-deposited Staphylococcus aureus." In: *Current Microbiology* 57 (2008), pp. 269–273.

[11] M. Wilson. "Light Activated Antimicrobial Coating for the Continuous Disinfection of Surfaces." In: *Infection Control and Hospital Epidemiology* 24 (2003), pp. 782–784.

[12] S. Noimark, C. W. Dunnill, and I. P. Parkin. "Shining light on materials - A self-sterilising revolution." In: *Advanced Drug Delivery Reviews* 65 (2013), pp. 570–580.

[13] M. R. Hoffmann, S. T. Martin, W. Y. Choi, and D. W. Bahnemann. "Environmental applications of semiconductor photocatalysis." In: *Chemical Reviews* 95 (1995), pp. 69–96.

[14] A. Mills and S. LeHunte. "An overview of semiconductor photocatalysis." In: *Journal of Photochemistry and Photobiology a-Chemistry* 108 (1997), pp. 1–35.

[15] A. Mills, R. H. Davies, and D. Worsley. "Water-purification by semiconductor photocatalysis." In: *Chemical Society Reviews* 22 (1993), pp. 417–425.

[16] A. Mills, N. Elliott, I. P. Parkin, S. A. O'Neill, and R. J. H. Clark. "Novel TiO2 CVD films for semiconductor photocatalysis." In: *Journal of Photochemistry and Photobiology a-Chemistry* 151 (2002), pp. 171–179.

[17] S. A. O'Neill, I. P. Parkin, R. J. H. Clark, A. Mills, and N. Elliott. "Atmospheric pressure chemical vapour deposition of titanium dioxide coatings on glass." In: *Journal of Materials Chemistry* 13 (2003), pp. 56–60.

[18] A. Mills, G. Hill, M. Crow, and S. Hodgen. "Thick titania films for semiconductor photocatalysis." In: *Journal of Applied Electrochemistry* 35 (2005), pp. 641–653.

[19] S. Noimark, C. W. Dunnill, M. Wilson, and I. P. Parkin. "The role of surfaces in catheter-associated infections." In: *Chemical Society Reviews* 38 (2009), pp. 3435–3448.

[20] L. K. Adams, D. Y. Lyon, and P. J. J. Alvarez. "Comparative ecotoxicity of nanoscale TiO2, SiO2, and ZnO water suspensions." In: *Water Research* 40 (2006), pp. 3527–3532.

[21] I. Ditta, A. Steele, C. Liptrot, J. Tobin, H. Tyler, H. Yates, D. Sheel, and H. Foster. "Photocatalytic antimicrobial activity of thin surface films of TiO2, CuO and TiO2/CuO dual layers on Escherichia coli and bacteriophage T4." In: *Applied Microbiology and Biotechnology* 79 (2008), pp. 127–133.

[22] J. C. Yu, W. K. Ho, J. Lin, K. Y. Yip, and P. K. Wong. "Photocatalytic activity, antibacterial effect, and photoinduced hydrophilicity of TiO2 films coated on a stainless steel substrate." In: *Environmental Science & Technology* 37 (2003), pp. 2296–2301.

[23] K. Sunada, Y. Kikuchi, K. Hashimoto, and A. Fujishima. "Bactericidal and detoxification effects of TiO2 thin film photocatalysts." In: *Environmental Science & Technology* 32 (1998), pp. 726–728.

[24] D. M. Blake, P. C. Maness, Z. Huang, E. J. Wolfrum, J. Huang, and W. A. Jacoby. "Application of the photocatalytic chemistry of titanium dioxide to disinfection and the killing of cancer cells." In: *Separation and Purification Methods* 28 (1999), pp. 1–50.

[25] Z. X. Lu, L. Zhou, Z. L. Zhang, W. L. Shi, Z. X. Xie, H. Y. Xie, D. W. Pang, and P. Shen. "Cell damage induced by photocatalysis of TiO2 thin films." In: *Langmuir* 19 (2003), pp. 8765–8768.

[26] X. Wei, Z. Yang, S. L. Tay, and W. Gao. "Photocatalytic TiO2 nanoparticles enhanced polymer antimicrobial coating." In: *Applied Surface Science* 290 (2014), pp. 274–279.

[27] C. G. Silva, R. Juarez, T. Marino, R. Molinari, and H. Garcia. "Influence of Excitation Wavelength (UV or Visible Light) on the Photocatalytic Activity of Titania Containing Gold Nanoparticles for the Generation of Hydrogen or Oxygen from Water." In: *Journal of the American Chemical Society* 133 (2011), pp. 595–602.

[28] S. Padikkaparambil, B. Narayanan, Z. Yaakob, S. Viswanathan, and S. M. Tasirin. "Au/TiO2 Reusable Photocatalysts for Dye Degradation." In: *International Journal of Photoenergy* 2013 (2013), p. 10.

[29] G. K. Naik, P. M. Mishra, and K. Parida. "Green synthesis of Au/TiO2 for effective dye degradation in aqueous system." In: *Chemical Engineering Journal* 229 (2013), pp. 492–497.

[30] Z. Bian, T. Tachikawa, P. Zhang, M. Fujitsuka, and T. Majima. "Au/TiO2 superstructure-based plasmonic photocatalysts exhibiting efficient charge separation and unprecedented activity." In: *J Am Chem Soc* 136 (2014), pp. 458–65.

[31] Y. Tian and T. Tatsuma. "Mechanisms and applications of plasmon-induced charge separation at TiO2 films loaded with gold nanoparticles." In: *Journal of the American Chemical Society* 127 (2005), pp. 7632–7637.

[32] K. Kimura, S.-i. Naya, Y. Jin-nouchi, and H. Tada. "TiO2 Crystal Form-Dependence of the Au/TiO2 Plasmon Photocatalyst's Activity." In: *Journal of Physical Chemistry C* 116 (2012), pp. 7111–7117.

[33] M. J. Uddin, F. Cesano, D. Scarano, F. Bonino, G. Agostini, G. Spoto, S. Bordiga, and A. Zecchina. "Cotton textile fibres coated by Au/TiO2 films: Synthesis, characterization and self

cleaning properties." In: *Journal of Photochemistry and Photobiology a-Chemistry* 199 (2008), pp. 64–72.

[34] G. F. Fu, P. S. Vary, and C. T. Lin. "Anatase TiO2 nanocomposites for antimicrobial coatings." In: *Journal of Physical Chemistry B* 109 (2005), pp. 8889–8898.

[35] L. Armelao, D. Barreca, G. Bottaro, A. Gasparotto, C. Maccato, C. Maragno, E. Tondello, U. L. Stangar, M. Bergant, and D. Mahne. "Photocatalytic and antibacterial activity of TiO2 and Au/TiO2 nanosystems." In: *Nanotechnology* 18 (2007), p. 375709.

[36] C. J. Tighe, R. I. Gruar, C. Y. Ma, T. Mahmud, X. Z. Wang, and J. A. Darr. "Investigation of counter-current mixing in a continuous hydrothermal flow reactor." In: *Journal of Supercritical Fluids* 62 (2012), pp. 165–172.

[37] R. I. Gruar, C. J. Tighe, and J. A. Darr. "Scaling-up a Confined Jet Reactor for the Continuous Hydrothermal Manufacture of Nanomaterials." In: *Industrial & Engineering Chemistry Research* 52 (2013), pp. 5270–5281.

[38] A. Mills. "Platinisation of semiconductor particles." In: *Journal of the Chemical Society-Chemical Communications* (1982), pp. 367–368.

[39] C. R. Crick, J. C. Bear, A. Kafizas, and I. P. Parkin. "Superhydrophobic Photocatalytic Surfaces through Direct Incorporation of Titania Nanoparticles into a Polymer Matrix by Aerosol Assisted Chemical Vapor Deposition." In: *Advanced Materials* 24 (2012), pp. 3505–3508.

[40] C. W. Dunnill, K. Page, Z. A. Aiken, S. Noimark, G. Hyett, A. Kafizas, J. Pratten, M. Wilson, and I. P. Parkin. "Nanoparticulate silver coated-titania thin films-Photo-oxidative destruction of stearic acid under different light sources and antimicrobial effects under hospital lighting conditions." In: *Journal of Photochemistry and Photobiology a-Chemistry* 220 (2011), pp. 113–123.

[41] P. Scherrer. "Bestimmung der Größe und der inneren Struktur von Kolloidteilchen mittels Röntgenstrahlen." In:

Nachrichten von der Gesellschaft der Wissenschaften zu Göttingen, Mathematisch-Physikalische Klasse 26 (1918), pp. 98–100.

[42] A. L. Patterson. "The Scherrer formula for x-ray particle size determination." In: *Physical Review* 56 (1939), pp. 978–982.

[43] W. F. Zhang, Y. L. He, M. S. Zhang, Z. Yin, and Q. Chen. "Raman scattering study on anatase TiO2 nanocrystals." In: *Journal of Physics D: Applied Physics* 33 (2000), pp. 912–916.

[44] A. Mills and J. Wang. "Simultaneous monitoring of the destruction of stearic acid and generation of carbon dioxide by self-cleaning semiconductor photocatalytic films." In: *Journal of Photochemistry and Photobiology A: Chemistry* 182 (2006), pp. 181–186.

[45] X. Zhang, Y. L. Chen, R.-S. Liu, and D. P. Tsai. "Plasmonic photocatalysis." In: *Reports on Progress in Physics* 76 (2013), p. 046401.

[46] E. Kowalska, R. Abe, and B. Ohtani. "Visible light-induced photocatalytic reaction of gold-modified titanium(iv) oxide particles: action spectrum analysis." In: *Chem. Commun.* (2009), pp. 241–243.

[47] I. M Arabatzis, T Stergiopoulos, D Andreeva, S Kitova, S. G Neophytides, and P Falaras. "Characterization and photocatalytic activity of Au/TiO2 thin films for azo-dye degradation." In: *Journal of Catalysis* 220 (2003), pp. 127–135.

[48] A. L. Linsebigler, G. Lu, and J. T. Yates. "Photocatalysis on TiO2 Surfaces: Principles, Mechanisms, and Selected Results." In: *Chemical Reviews* 95 (1995), pp. 735–758.

[49] F. Dilika, P. D. Bremner, and J. J. Meyer. "Antibacterial activity of linoleic and oleic acids isolated from Helichrysum pedunculatum: a plant used during circumcision rites." In: *Fitoterapia* 71 (2000), pp. 450–452.

8

CONCLUSIONS AND FUTURE WORK

8.1 CONCLUSIONS

The prevalence of HAIs, often caused by multi-drug resistant bacteria, highlights the necessity of the development of efficacious infection-prevention strategies. One approach to reduce the spread of infection is the use of self-sterilising surfaces to help both decrease the risk of infection upon use of medical devices such as catheters and also to disrupt the cycle of transmission of bacteria in healthcare environments.

This thesis detailed the development of potent antimicrobial polymers that demonstrate an enhanced efficacy induced by a light-activated bactericidal mechanism. A novel approach was used, exploiting the concept of PDT. The advantage of this strategy for use in healthcare applications is two-fold. Firstly, the overuse of antibiotics and other antiseptics has resulted in the emergence of bacterial resistance to a host of antimicrobial strategies. These polymers however, induce the lethal photosensitisation of bacteria through the generation of a range of ROS that initiate a non-site specific attack against bacteria in the vicinity, decreasing the likelihood of the emergence of bacterial resistance to this approach. Secondly, whereas other bactericidal surfaces lose effectiveness consequent to the build-up of dirt obscuring the antimicrobial properties, these surfaces are self-cleaning in that the photo-generated species oxidise organic matter contaminating the polymer surface, thus maintaining the anti-infective efficacy. Further work focused on the development of materials that harnessed a dual-mechanism bacterial kill strategy, through the incorporation of both photo-active antimicrobials and intrinsically antimicrobial nanoparticles or other moieties, for the development of antimicrobial surfaces that demonstrate bactericidal activity under dark conditions

with enhanced kills upon light-activation.

Using a simple synthetic technique, a range of antimicrobial polymers were developed for medical device applications such as urinary catheters, in addition to hospital touch surface applications. For medical device applications, the antimicrobial activity was activated using either a 635 nm laser (crystal violet-coated, methylene blue and 2 nm gold nanoparticle-encapsulated silicone), or a UVA source (oleic acid functionalised titania- or gold-doped titania nanoparticle-encapsulated silicone). These surfaces demonstrated rapid, potent light-activated antimicrobial activity when tested against both Gram-positive and Gram-negative bacteria. Moreover, the oleic acid functionalised titania- and gold-doped titania nanoparticle-encapsulated silicone polymers achieved significant kills in the dark, when tested against *S. aureus*, reducing bacterial numbers by > 4 log.

Antimicrobial silicone surfaces, activated using a white hospital light source, were also developed for hospital touch surface applications, utilising the multi-dye-nanogold surface technology as well as a novel antimicrobial combination of crystal violet and 3 nm zinc oxide nanoparticles. Both materials induced the lethal photosensitisation of key causative pathogens for HAIs. Moreover, for the first time, significant dark kill was observed against *both* Gram-positive and Gram-negative bacteria, highlighting the development of versatile, 'dual-mechanism' antimicrobial polymers for potential use in health-care environments to decrease the risk of infection.

The development of a range of potent photobactericidal surfaces has been examined and therefore, an in-depth investigation into the photochemical properties of dye- and dye-nanoparticle encapsulated polymers, is of critical importance to gain insight into the mechanism of photobactericidal activity demonstrated. This was achieved using TR-EPR spectroscopy and TRNIR-$^1O_2$ phosphorescence measurements. These studies indicated that the presence of small 2 nm gold nanoparticles enhance dye triplet state production and subsequently lead to increased $^1O_2$ generation upon photo-activation. These findings facilitate an understanding of the

underlying photophysics, providing key information on enhancements observed in microbiological kills when antimicrobial surfaces with incorporated dye-nanogold combinations were tested. The use of a logical synthetic strategy that involves an extensive investigation into the photochemical properties of dye-nanoparticle encapsulated polymers, is crucial for future work in the design of more potent photobactericidal materials that achieve rapid bacterial kills.

8.2 FUTURE WORK

Future work should focus on the use of TR-EPR spectroscopy as a tool to optimise the light-activated activity of these surfaces. Singlet oxygen production measurements in combination with CW-EPR spectroscopy should also be utilised to investigate the mechanism of photochemical activity, through examining the photo-generated radical generation of these surfaces. In addition, further work should include a strong emphasis on the synthesis of novel antimicrobial nanoparticles and the utilisation of an understanding of the underpinning photophysics to advance materials development. These materials should be tested against clinical strains of bacteria, spore-forming bacteria such as *C. difficile* and viruses. The materials developed will be of strong commercial interest for use in both hospital touch surfaces and in invasive medical devices, to help maintain low bacterial contamination levels on hospital surfaces, reducing the risk of associated infection.

One aim of future investigations is to optimise the photobactericidal activity of polymers that utilise multiple mechanisms of bacterial attack, to reduce bacterial contamination levels in healthcare environments. Dissimilar to prior research, the design approach should be a strategic one, with a strong emphasis on the synthesis of new antimicrobial nanoparticles and the use of an understanding of the underlying photophysics to optimise the light-activated antimicrobial properties of materials developed. In surfaces developed based on dye-gold interactions, the gold nanoparticles used should be functionalised with antimicrobial ligands, for example, oleic acid,

to maximise antimicrobial activity exhibited under dark conditions. In addition, TR-EPR should be used to optimise gold nanoparticle polymer loading such that surfaces that generate optimal triplet state production can be subsequently tested against bacteria.

Work achieved on the incorporation of antimicrobial zinc oxide nanoparticles in combination with photosensitisers into medical grade polymers, indicates that there exist dye-nanoparticle synergic interactions, with indications of advantageous implications on the exhibited photostability of the dye, although as yet, this has not been investigated using TR-EPR. These polymers demonstrate one of the most effective antimicrobial activities we have reported to date, with substantial activity under dark conditions, in addition to the reduction of bacterial numbers to below the detection limit upon white light illumination. It is critical that the photochemical mechanism is explored such that this technology can be refined to achieve more potent antimicrobial polymers. Moreover, it is important to explore the incorporation of this antimicrobial technology into further polymers, for example, for use in paints, such that existing surfaces can be modified to exhibit bactericidal functionality.

In addition to investigating the properties of the photo-excited triplet states, CW-EPR in combination with a spin-trap should be executed, to enable an examination of the photo-generated radical distribution. These investigations will provide insight into whether the presence of different nanoparticles impact on the photochemical mechanism the triplet state dye undergoes, to be exact, whether the presence of nanoparticles result in dye triplet state quenching by molecular oxygen or substrate radicals. Polymers incorporated with photosensitisers in combination with: gold nanoparticles, zinc oxide nanoparticles, titania nanoparticles, copper nanoparticles and so forth, should be investigated. This knowledge can be used to promote the generation of a wide range of ROS to target bacteria more effectively.

Further work should be focused on facilitating vital research into the understanding of the photochemical mechanisms of the

light-activated antimicrobial activity of dye-nanoparticle embedded polymers. Using this knowledge, more effective bactericidal polymers can be developed with antimicrobial functionality under both dark and light conditions. The modification process can be manipulated to incorporate antimicrobial agents that achieve bacterial kills via multiple mechanisms, including both dark-kills and kills achieved by the photo-generation of a wide range of ROS. These design tactics will result in the development of polymers with enhanced rates of bactericidal activity. The simple synthetic technique used to develop these surfaces can be easily up-scaled for commercial production and also enables this antimicrobial technology to be used in a wide range of polymers for healthcare applications. Optimisation by the current empirical approach is not effective as a long-term strategy and a mechanistic understanding is critical to underpin future advances in the development of bactericidal surfaces, for use in healthcare technologies.